JOURNAL OF RESEARCH

OF THE U.S. GEOLOGICAL SURVEY

JANUARY–FEBRUARY 1975
VOLUME 3, NUMBER 1

Scientific notes and summaries of investigations in geology, hydrology, and related fields

U.S. DEPARTMENT OF THE INTERIOR

UNITED STATES DEPARTMENT OF THE INTERIOR
ROGERS C. B. MORTON, Secretary
GEOLOGICAL SURVEY
V. E. McKelvey, Director

For sale by the Superintendent of Documents, U.S. Government Printing Office, Washington, DC 20402. Order by SD Catalog No. JRGS. Annual subscription rate $18.90 (plus $4.75 for foreign mailing). Single copy $3.15. Make checks or money orders payable to the Superintendent of Documents.

Send all subscription inquiries and address changes to the Superintendent of Documents at the above address.

Purchase orders should not be sent to the U.S. Geological Survey library.

Library of Congress Catalog-card No. 72-600241.

The Journal of Research is published every 2 months by the U.S. Geological Survey. It contains papers by members of the Geological Survey and their professional colleagues on geologic, hydrologic, topographic, and other scientific and technical subjects.

Correspondence and inquiries concerning the Journal (other than subscription inquiries and address changes) should be directed to the Journal of Research, Publications Division, U.S. Geological Survey, National Center 321, Reston, VA 22092.

Papers for the Journal should be submitted through regular Division publication channels.

The Secretary of the Interior has determined that the publication of this periodical is necessary in the transaction of the public business required by law of this Department. Use of funds for printing this periodical has been approved by the Director of the Office of Management and Budget through February 11, 1975.

GEOGRAPHIC INDEX TO ARTICLES

See "Contents" for articles concerning areas outside the United States and articles without geographic orientation.

JOURNAL OF RESEARCH

of the

U.S. Geological Survey

Vol. 3 No. 1 Jan.–Feb. 1975

CONTENTS

Abbreviations ---------- II

GEOLOGIC STUDIES

Possible extension of mineral belts, northern part of Coeur d'Alene district, Idaho ---------- *G. B. Gott and J. M. Botbol* 1
Ore grade, metal production, and energy ---------- *N. J Page and S. C. Creasey* 9
The megaspore genus *Henrisporites* from the Cretaceous of Massachusetts ---------- *R. H. Tschudy* 15
Quantitative determination of dawsonite in Green River shale by powder-sample X-ray diffraction: effect of grinding ---------- *E-an Zen and J. G. Hammarstrom* 21
Notes on the origin of Colluma Crater, Bolivia ---------- *Sam Rosenblum, R. J. Anderson, Ismael Montes de Oca, and Edgar Delgadillo* 31
K-Ar age of the Similkameen batholith and Kruger Alkalic Complex, Washington and British Columbia ---------- *K. F. Fox, Jr., C. D. Rinehart, and J. C. Engels* 39
Radiocarbon dates indicate rates of graben downfaulting, San Jacinto Valley, Calif ---------- *B. E. Lofgren and Meyer Rubin* 45
Stratigraphic relationships within the Baraga Group of Precambrian age, central Upper Peninsula, Mich ---------- *W. F. Cannon and J. S. Klasner* 47
The Nectarian System, a new lunar time-stratigraphic unit ---------- *D. E. Stuart-Alexander and D. E. Wilhelms* 53
Geometry and growth of the White Sands dune field, New Mexico ---------- *E. D. McKee and R. J. Moiola* 59
A proposed glacial history of the Henrys Lake basin, Idaho ---------- *I. J. Witkind* 67

HYDROLOGIC STUDIES

Recurrent geothermally induced debris avalanches on Boulder Glacier, Mount Baker, Wash ---------- *David Frank, Austin Post, and J. D. Friedman* 77
Changes in concentration of certain constituents of treated waste water during movement through the Magothy aquifer, Bay Park, N.Y ---------- *H. F. H. Ku, John Vecchioli, and S. E. Ragone* 89
Mobilization of iron in water in the Magothy aquifer during long-term recharge with tertiary-treated sewage, Bay Park, N.Y ---------- *S. E Ragone, H. F. H. Ku, and John Vecchioli* 93
Norman Creek, a source of recharge to Maramec Spring, Phelps County, Mo ---------- *E. E. Gann and E. J. Harvey* 99
Water-quality changes during a salmon run in an interior Alaskan stream ---------- *J. W. Nauman and D. R. Kernodle* 103
Combining estimates of low-flow characteristics of streams in Massachusetts and Rhode Island ---------- *G. D. Tasker* 107
Adjustment of logarithmic flood-frequency statistics for gaged California streams to minimize the time sampling error ---------- *S. E. Rantz and J. R. Crippen* 113
Pyrrolidone—a new solvent for the methylation of humic acid ---------- *R. L. Wershaw, D. J. Pinckney, and S. E. Booker* 123

Recent publications of the U.S. Geological Survey ---------- Inside of back cover

ABBREVIATIONS

acre-ft ---- acre-foot
alt -------- altitude
avg ------- average
B.P. ------ before present
°C -------- degree Celsius
cal ------- calorie
cm ------- centimetre
cm^2 ------- square centimetre
COD ------ chemical oxygen demand
cP -------- centipoise
D -------- debye unit
d --------- day
diam ----- diameter
DO ------- dissolved oxygen
Eh ------- oxidation-reduction potential
eq -------- equation
ERTS ---- Earth Resources Technology Satellite
ft -------- foot
ft^2 -------- square foot
ft-c ------- foot-candle
g --------- gram
gal ------- gallon
h --------- hour
in. ------- inch
J --------- joule
K -------- kelvin
kg ------- kilogram
km ------- kilometre
km^2 ------- square kilometre
kV -------- kilovolt
kWh ------ kilowatt-hour
l ---------- litre
lb -------- pound
lm -------- lumen
log ------- logarithm (common)
M -------- molarity, molar (concentration)
m -------- metre
m^2 -------- square metre
mA ------- milliampere
MBAS ---- methylene blue active substance
mg ------- milligram
Mgal ----- million gallons
mi -------- mile
mi^2 ------- square mile
min ------- minute
Ml ------- million litres
ml -------- millilitre
mm ------- millimetre
mo ------- month
mol ------- mole
m.y. ------ million years
μcal ------ microcalorie
μm ------- micrometre
μmho ----- micromho
N --------- normality
NASA ---- National Aeronautics and Space Administration
nm ------- nanometre
P.d.t. ----- Pacific daylight time
pH ------- measure of hydrogen ion activity
ppm ------ part per million
s --------- second
(s) ------- solid
W -------- watt
w/v ------ weight per volume
yd -------- yard
yr -------- year

Any trade names and trademarks found in this publication are used for descriptive purposes only and do not constitute endorsement by the U.S. Geological Survey.

Jour. Research U.S. Geol. Survey
Vol. 3, No. 1, Jan.–Feb. 1975, p. 1–7

POSSIBLE EXTENSION OF MINERAL BELTS, NORTHERN PART OF COEUR D'ALENE DISTRICT, IDAHO

By GARLAND B. GOTT and JOSEPH M. BOTBOL,

Denver, Colo., Reston, Va.

Abstract.—The ore deposits in the northern part of the Coeur d'Alene district are located within rocks of the Belt Supergroup that have been intruded by Cretaceous quartz monzonites. Lead-zinc-silver replacement veins constitute most of the deposits. The geometry of the district has been modified by post-ore faulting along the Osburn, Dobson Pass, and other faults. The original position of the Gem stocks, before their separation from the Dago Peak stocks by the Dobson Pass fault, can be approximately reconstructed by moving the truncated stocks and associated geochemical dispersion patterns back into matching positions. The known mineral belts are defined by dispersion patterns of both lead and the Pb:Zn ratio. Similar dispersion patterns of lead and the Pb:Zn ratio northwest of the original position of the Gem stocks suggest that the mineral belts extend into that area.

The ore deposits in the Coeur d'Alene district of northern Idaho (lat 47°28′ to 47°35′ N., long 115°45′ to 116°00′ W.) are largely lead-zinc-silver replacement veins in highly folded Precambrian Belt Supergroup quartzites, siltites, and argillites. Within the Coeur d'Alene district the exposed Belt Supergroup rocks range in thickness from 6,250 to 8,540 m (20,500–28,000 ft) where the top has been eroded and the bottom is not exposed. These rocks have been intruded by Cretaceous quartz monzonites (fig. 1). Galena, sphalerite, and tetrahedrite are the most important ore minerals, and chalcopyrite is probably present in most, if not all, ore deposits. Siderite is an abundant gangue mineral, and pyrite is ubiquitous.

The geometry of the Coeur d'Alene district has been modified by post-ore faulting along the Osburn, Dobson Pass, and other faults (Hobbs and others, 1965). Movement along the normal, westward-dipping Dobson Pass fault has offset the roots of the monzonite intrusions, known as the Gem stocks, from their cupola which is represented by the Dago Peak stocks and parts of numerous lead-zinc-silver veins (Fig. 3). The eastward fault block has been the locus of mining of lead-zinc-silver ores since mining began in the district. As a result of the mining activity, several mineral belts have been delineated (Fryklund, 1964, pl. 2*A*; Crosby, 1969) and are shown in figure 2. These belts have not been proved to continue beyond the Dobson Pass fault. However, inasmuch as the mineral belts appear to be older than the Dobson Pass fault, their extension northwestward into the area west of the Dobson Pass fault is a reasonable possibility.

Acknowledgments.—We are greatly indebted to Susan Truesdell and Reinhardt Leinz for the analyses of lead and zinc in the Denver laboratories of the U.S. Geological Survey. We are also indebted to J. B. Cathrall for his assistance in sample collection and to T. M. Billings, both for sample collection and for retrieval and manipulation of computerized data.

GEOCHEMICAL DATA

The writers and others of the U.S. Geological Survey recently have made geochemical investigations in the Coeur d'Alene district that involves the collection and analysis of several thousand rock and soil samples. The analytical data pertaining to the rock samples have not yet been evaluated; the discussion that follows is, therefore, based on the analyses of soil samples. The soil-sample localities within the area discussed in this paper are shown in figure 2. Contours shown in figures 4 and 5 are based on the lead and zinc data determined by atomic absorption methods.

The A horizon of the soil is only 2.5–5 cm (1–2 in) thick in most places within the Coeur d'Alene district. This horizon was not sampled because of the possibility of contamination resulting from mining activity. Orientation studies of several dozen soil profiles indicate that, except in the Kellog area 11 km (7 mi) to the west, soil samples collected in the Coeur d'Alene district from depths greater than about 15 cm (6 in.) below the A horizon are free from contamination. All samples from the area discussed in this report, therefore, were collected at or below this depth.

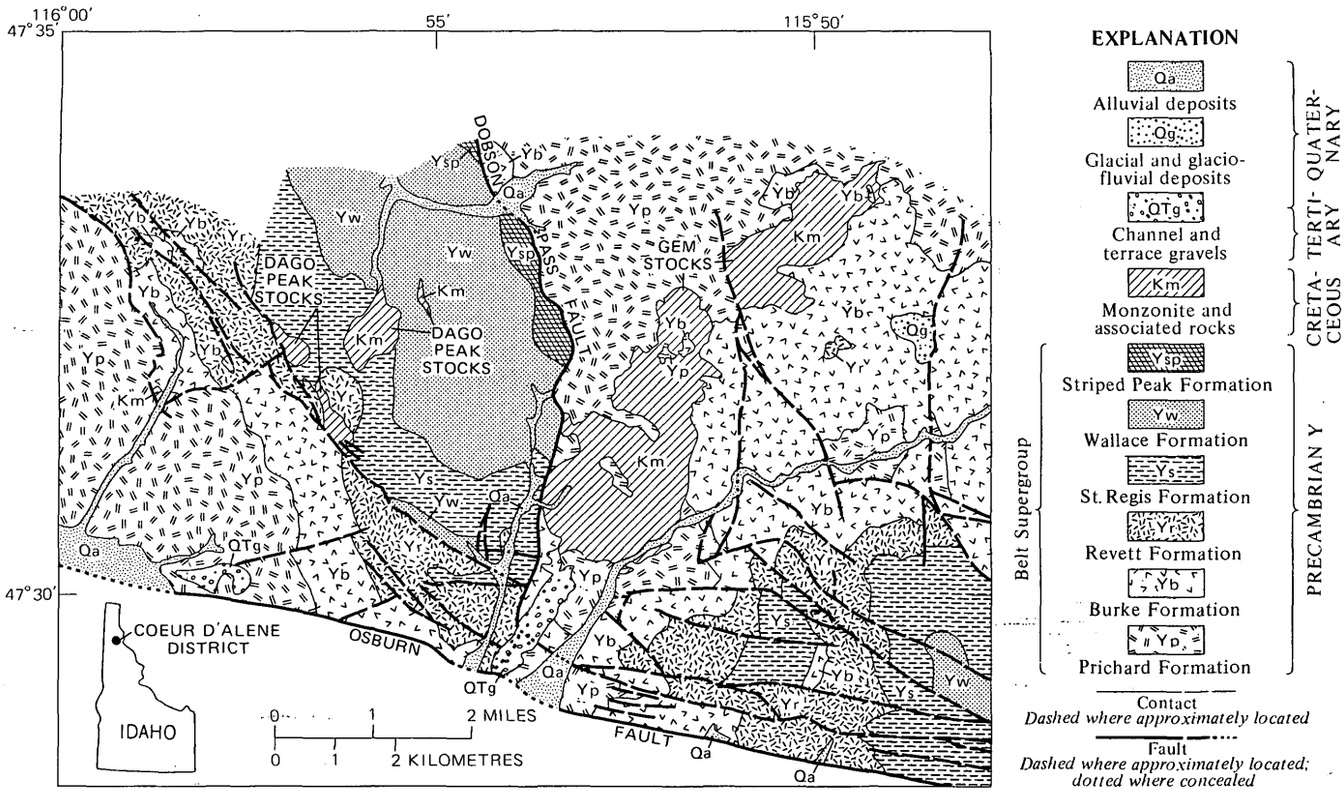

FIGURE 1.—Generalized geologic map of the Coeur d'Alene district (modified from Hobbs and others, 1965, pls. 3–5).

A computer-implemented graphics technique has been used to illustrate the geochemical relationships. The original analytical data were expanded to include ratios of the more common sulfide-forming elements. All data were then gridded to a rectangular coordinate system with mesh points 305 m (1,000 ft) apart.

In accordance with the computer graphics technique, the original data points are transposed to grid coordinates or mesh points by drawing a circle of arbitrary size around each mesh point and shifting the coordinates of data points within each circle to the coordinates of the mesh point. When the coordinates are shifted, each point is weighted according to its distance from the mesh point; as a result, close-lying data points have more influence than outlying data points on the final value to be used at the mesh point. After data points have been weighted and projected to a mesh point, the multiplicity of values created at the mesh point is removed by averaging. The extent of interpolation between mesh points is determined by the radius of the search circle drawn around each mesh point. The larger the radius of the circumscribed circle, the larger is the number of data points represented by a single value. Thus, larger circle sizes have a smoothing effect on the resulting geochemical surface. For the illustrations presented here, a circle of radius 305 m (1,000 ft) was used.

The computed geochemical values were plotted at coordinate intersections on an x-y flatbed plotter equipped with a 127- by 152-cm (50 by 60 in) table. All contouring of isoconcentration was done manually to permit interpretation of stratigraphic and structural discontinuities and, in areas of low sample density, to allow extrapolation beyond the bounds set in the gridding program.

KNOWN MINERAL BELTS

The generalized boundaries of the known mineral belts as shown in figure 2 have been taken from Fryklund (1964, pl. 2*A*). The mineral belts pertinent to this paper are the Gem-Gold Hunter belt, the Rex-Snowstorm belt, the Tamarack-Marsh subbelt, the Carlisle-Hercules belt, and the Sunset belt. The belts are nearly parallel to each other and trend about N. 65° W. They range in width from about 900 to 1,500 m (3,000–5,000 ft). Their boundaries are obscure and are generally determined by the outermost mineralized

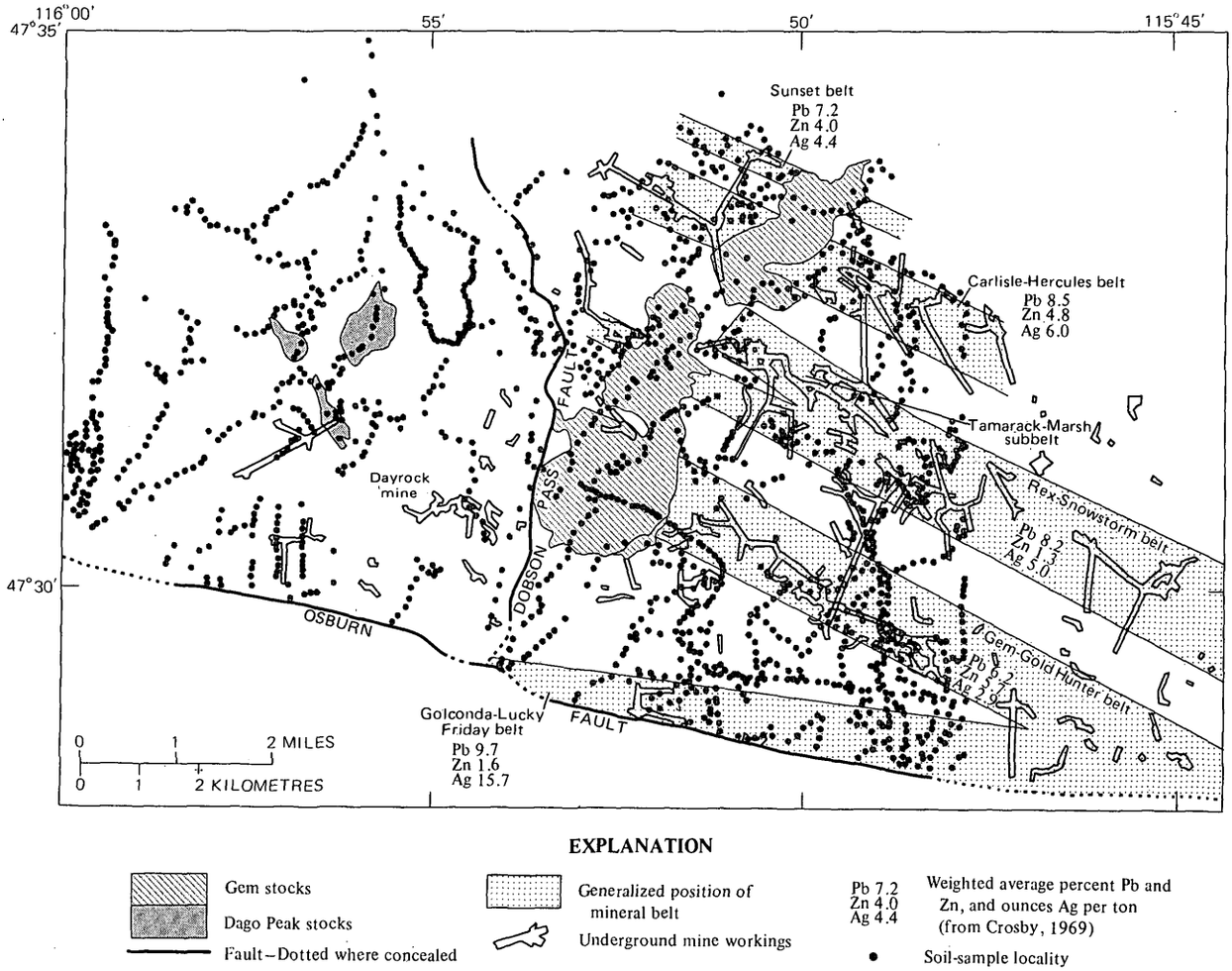

FIGURE 2.—Location of mineral belts (modified from Fryklund, 1964, pl. 2A) weighted average percent lead and zinc and ounces per ton silver (Crosby, 1969), some underground workings, Dago Peak and Gem stocks, and soil-sample localities.

structures. The mineral belts cross fold structures, lithology, and the various formations of the Belt Supergroup. The ore shoots that constitute the ore bodies are fracture controlled and, in general, trend parallel or subparallel to the mineral belts.

These mineral belts have been the center of mining activity since ore was first discovered in the district in 1885. Crosby (1969) gives the tonnage of lead-zinc-silver ore mined through 1967, from all the mineral belts north of the Osburn fault, as 54,301,376 tons with a weighted average of 7.2 percent lead, 4.0 percent zinc, and 4.4 ounces silver per ton. The extent of this mining activity can be seen from some of the underground workings, generalized from the mapping by

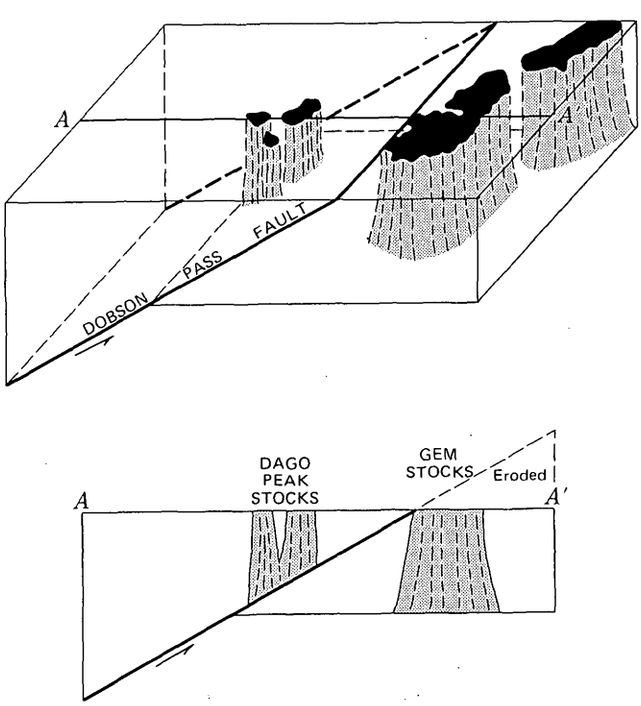

FIGURE 3.—Block diagram showing offset of Gem stocks from Dago Peak stocks.

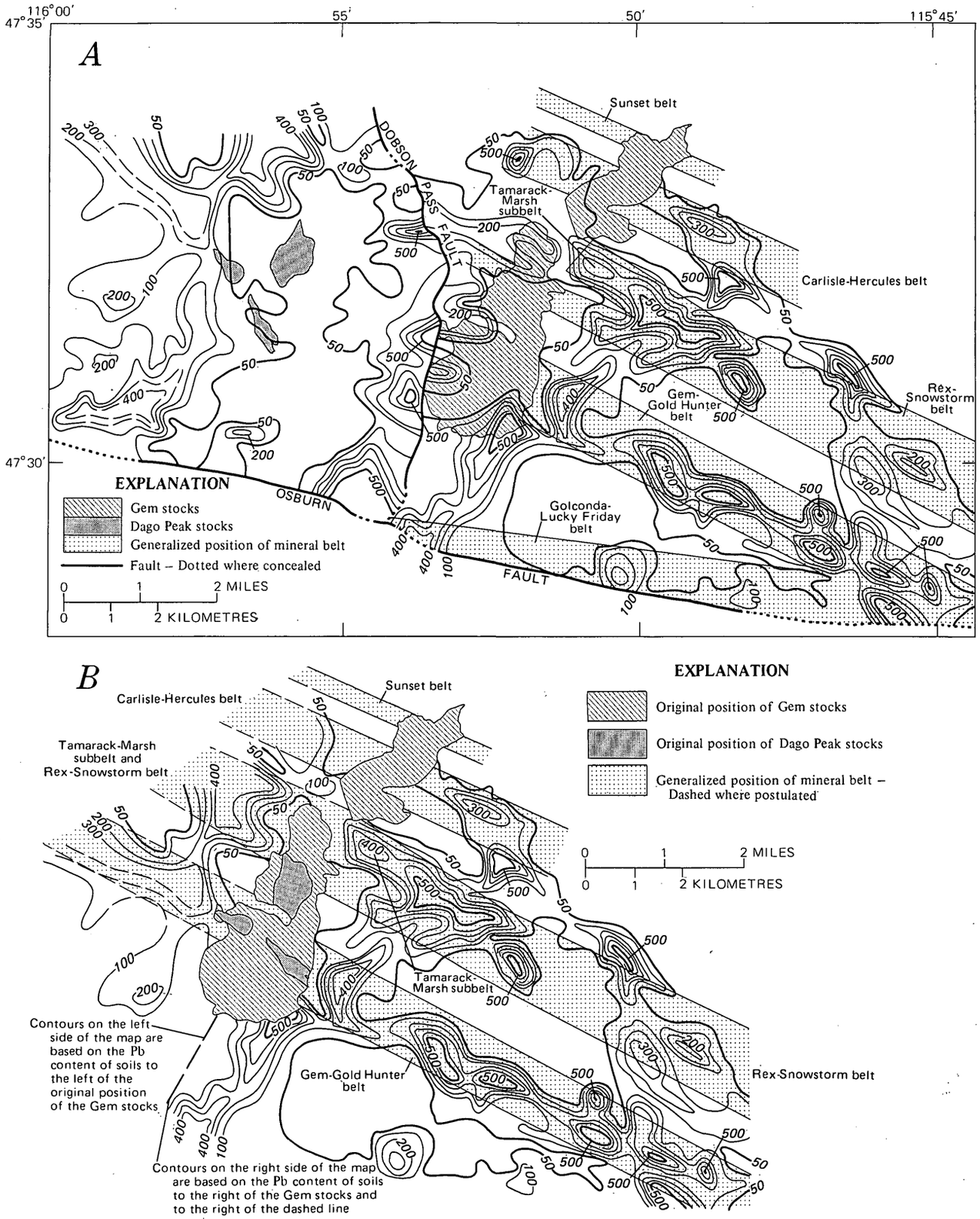

FIGURE 4.—Map showing present distribution of lead (*A*) and diagram showing dispersion pattern of lead restored to its pre-Dobson Pass fault position (*B*). Contours are at 50, 100, 200, 300, 400 and 500 ppm Pb; dashed where projected.

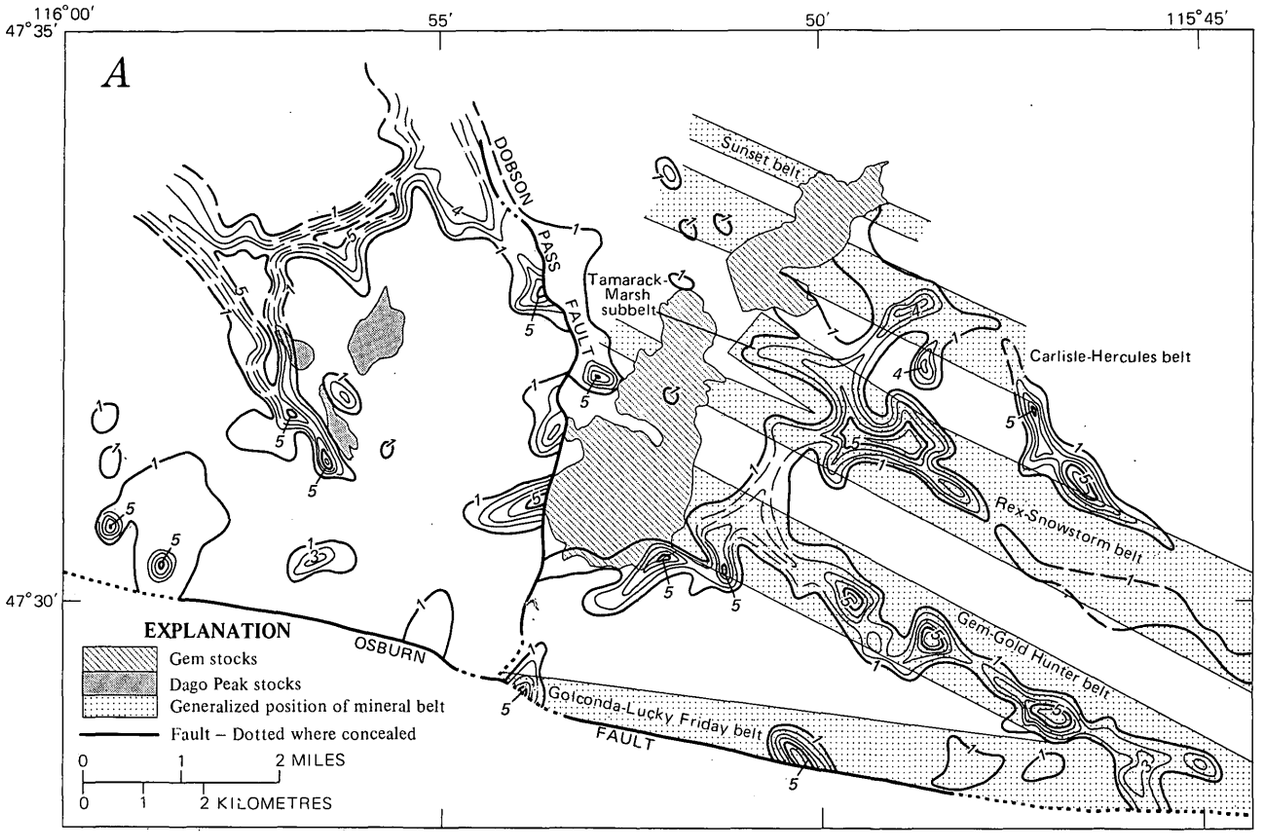

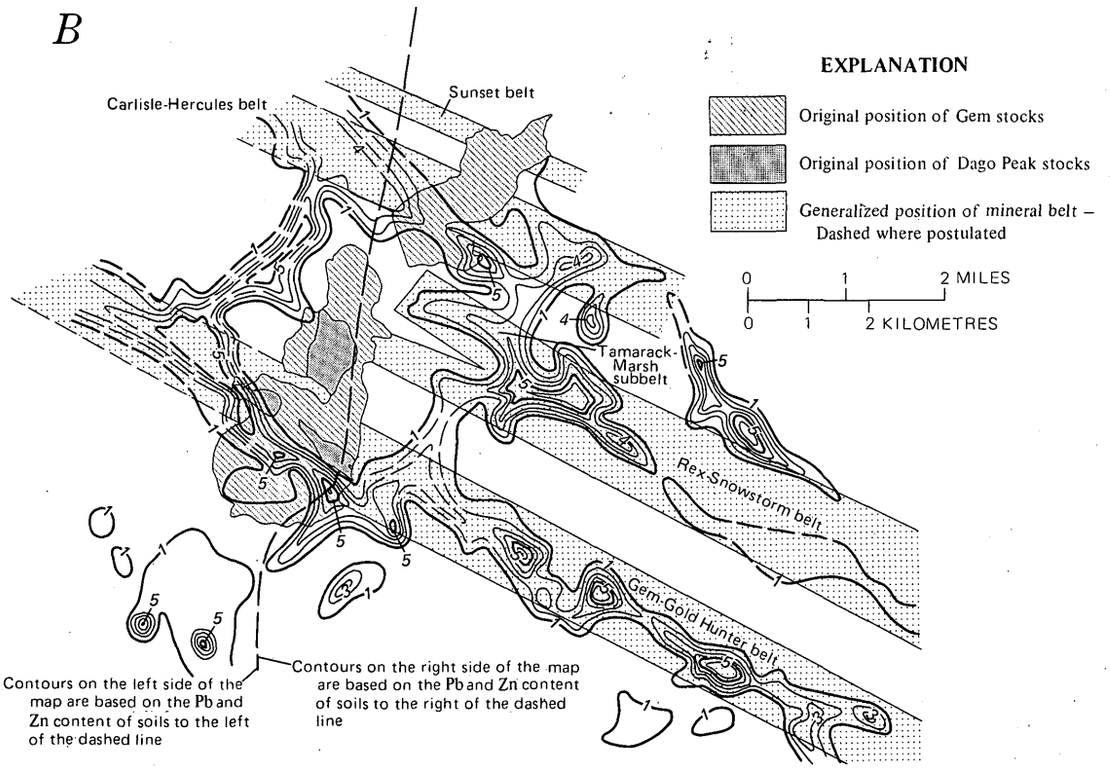

FIGURE 5.—Map showing present Pb:Zn dispersion pattern (*A*) and diagram showing Pb:Zn dispersion pattern restored to its pre-Dobson Pass fault position (*B*). Contour interval is 1; not contoured above 6; dashed where projected.

Hobbs, Griggs, Wallace, and Campbell (1965, pls. 3–5), as plotted in figure 2.

The mineral belts are characterized by a dominance of lead over zinc. The data given by Crosby (1969; fig. 2) show that within the various mineral belts the Pb:Zn ratio of the ores ranges from about 1:1 to 6:1. The soil samples collected over these mineral belts have a similar Pb:Zn ratio which ranges from 1:1 to greater than 6:1. In contrast, the median values for lead and zinc of all soil samples collected from the Coeur d'Alene district as a whole are 43 and 95 ppm respectively.

The known mineral belts in this area are in part defined by the geochemical distribution of lead, silver, zinc, copper, and antimony, but are best defined from the data resulting from the analysis of soil samples according to the distribution of lead and the Pb:Zn ratio. Lead and the Pb:Zn ratio (figs. 4 and 5) well define the Gem–Gold Hunter belt and the Tamarack-Marsh subbelt and partly define the Rex-Snowstorm and Carlisle-Hercules belts. Insufficient samples were collected to determine whether or not the Sunset belt could be defined.

INTERPRETIVE EXTENSIONS OF THE MINERAL BELTS

The rocks in the area east of the Dobson Pass fault have been more dissected than have the rocks on the western side. On the eastern side of the fault, favorable host rocks in the Prichard, Burke, Revett, and St. Regis Formations have been exposed. In contrast, on the western side of the fault, parts of the Striped Peak and Wallace Formations, and the upper part of the St. Regis Formation overlie the older rocks. Termination of the mineral belts against the post-ore Dobson Pass fault gives reason for speculation that these belts continue in the favorable host rocks at depth beneath the Wallace Formation and the upper part of the St. Regis Formation west of the fault. This speculation encouraged an attempt to approximate the original geologic structure by removal of the Dobson Pass fault on the premise that this restoration of the original structure would reveal evidence indicating whether the mineral belts do extend beyond the fault.

According to Hobbs, Griggs, Wallace, and Campbell (1965, p. 83–86 and pl. 4), the Dobson Pass fault dips about 30° W. and has a normal displacement of about 4,270 m (14,000 ft) and a probable net slip displacement of about 5.6 km (3.5 mi). This implies that before displacement along the fault the Gem stocks were attached to the Dago Peak stocks—stocks now exposed 2.4–4.8 km (1.5–3 mi) west of the trace of the Dobson Pass fault. Truncation of the Dago Peak–Gem stocks and eastward displacement of the footwall block moved the Gem stocks into their present position, leaving the Dago Peak Cupola in the hanging wall to the west.

In accordance with this interpretation, restoration of the geologic structure prior to Dobson Pass faulting (figs. 4*B*, 5 *B*) can be accomplished by sliding the part of the map that is east of the fault under the western part of the map, fitting the Gem stocks under the Dago Peak stocks, and matching the details of the geochemistry to their best fit. The best fit obtained by this procedure required a western translation of about 5.6 km (3.5 mi) and a 21° clockwise rotation of the Gem stocks from their present position (fig. 4*A*). The outlines of the south stock and that part of the north stock occurring west of the Dobson Pass fault were then traced on the map in their approximate original positions (fig. 4*B*.)

This restoration brings the lead and the Pb:Zn dispersion patterns that currently define all or parts of the known mineral belts into juxtaposition with similar lead-dominant dispersion patterns which occur on opposing sides of the restored Gem stocks (figs. 4*B* and 5*B*). Strong dispersion patterns of lead west of the original position of the Gem stocks, shown in figure 4*B*, match the Gem–Gold Hunter belt and the combined Rex-Snowstorm–Tamarack-Marsh belts. A somewhat weaker dispersion pattern corresponds to the Carlisle-Hercules belt.

The Pb:Zn dispersion patterns west of the original position of the Gem stocks (fig. 5*B*) correspond to extensions of the Gem–Gold Hunter belt and the Carlisle-Hercules belt. However, because of an increase in zinc in that area, these patterns do not indicate an extension of the Rex-Snowstorm belt or the Tamarack-Marsh subbelt.

In addition to these northwest-trending dispersion patterns that correspond, in part, to the known mineral belts, northeast-trending dispersion patterns of lead and Pb:Zn are also present. These patterns conform to the shape and orientation of the south Gem stock. This conformity suggests that these patterns may have resulted from the migration of the metals from the northwest-trending mineral belts as a result of heat that was still emanating from the stock.

The anomalously high lead northwest of the Dago Peak stocks occurs along the strike of the Revett and Wallace Formations, and, if present, lead-rich strata in these formations probably would account for the distribution patterns shown in figures 4 and 5. Numerous deposits of the stratiform type have been observed within the Belt Supergroup in recent years. For example, Clark (1971) described strata-bound copper deposits in the Revett Formation, which are overlain by a lead-rich zone in the Idaho-Montana area north

of the Coeur d'Alene district. According to Harrison (1972) strata-bound copper, in concentrations as high as ore grade, occurs throughout most of the formations of the Belt Supergroup over a wide geographic area. The presence of strata-bound lead in the lead-rich zones northwest of the Dago Peak stocks would negate the postulation that these zones represent the extensions of vein deposits included within the mineral belts present southeast of the Gem stocks. The distribution patterns of lead in the soils throughout the Coeur d'Alene district, however, suggest that concentrations in the range of 400–500 ppm or more have been derived from deposits that are structurally controlled. By analogy, therefore, the dispersion patterns of lead and Pb:Zn in the area northwest of the Dago Peak stocks have probably been derived from vein deposits similar to those in the known mineral belts rather than from stratiform deposits.

This interpretation permits the conclusion that the dispersion patterns northwest of the Dago Peak stocks (figs. 4*B* and 5*B*) represent extensions of the mineral belts. The dominance of lead over zinc, which characterizes the dispersion patterns northwest of the Dago Peak stocks as well as patterns in the known mineral belts, suggests that the dispersion patterns beyond the original position of the Gem stocks define extensions of the mineral belts.

A simple dichotomy at the Dobson Pass fault influences the interpretation of the position of mineral belts west of the fault trace: the mineral belts in the hanging-wall block have been truncated by the fault, whereas the mineral belts in the footwall block are structurally continuous across the trace of the fault and have been rotated about 20° in a counterclockwise direction. There would, therefore, be a divergence in the alinement of the belts in the two blocks depending on the precise amount of rotation in the footwall block. For this reason the projected extensions of the mineral belts shown in Figures 4*B* and 5*B* would apply only to the hanging-wall block.

REFERENCES CITED

Clark, A. L., 1971, Strata-bound copper sulfides in the Precambrian Belt Supergroup, northern Idaho and northwestern Montana, *in* International association of genesis of ore deposits, Tokyo-Kyoto Mtg., 1970, Papers and Proc. (IAGOD volume): Soc. Mining Geologists Japan, Spec. Issue 3, p. 261–267.

Crosby, G. M., 1969, A preliminary examination of trace mercury in rocks, Coeur d'Alene district, Idaho, *in* International geochemical exploration symposium: Colorado School Mines Quart., v. 64, no. 1, p. 169–194.

Fryklund, V. C., Jr., 1964, Ore deposits of the Coeur d'Alene district, Shoshone County, Idaho, *with a section on* The bleached rock in the Coeur d'Alene district, by P. L. Weis: U.S. Geol. Survey Prof. Paper 445, 103 p.

Harrison, J. E., 1972, Precambrian Belt Basin of northwestern United States—Its geometry, sedimentation, and copper occurrences: Geol. Soc. America Bull., v. 83, no. 5, p. 1215–1240.

Hobbs, S. W., Griggs, A. B., Wallace, R. E., and Campbell, A. B., 1965, Geology of the Coeur d'Alene district, Shoshone County, Idaho: U.S. Geol. Survey Prof. Paper 478, 139 p.

Jour. Research U.S. Geol. Survey
Vol. 3, No. 1, Jan.–Feb. 1975, p. 9–13

ORE GRADE, METAL PRODUCTION, AND ENERGY

By NORMAN J PAGE and S. C. CREASEY, Menlo Park, Calif.

Abstract.—Recent resource estimates have been stimulated by national concern over present and pending shortages of energy and mineral resources. Although some believe that the resource base of a commodity is the total amount in the crust, the energy consumption for mining and milling under present technology suggests that grades of the metallic ores have a lower limit when production is assumed to be for common usages. The tonnage required to mine and mill ores to obtain one unit of metal is a hyperbolic function of the grade, and as the tonnage increases hyperbolically, so does the energy consumed. For copper, the hyperbolic relation suggests that deposits with grades below about 0.20–0.25 percent Cu will not be mined to produce metal for common electrical and construction uses. Although the energy used to mine and mill a unit of metal differs from one metal to another, all show the hyperbolic increase in energy consumption as grade decreases.

National concern over present and pending shortages of energy and mineral resources has stimulated a rash of statements on resource estimates and resource positions from both private and government sectors of our society. At least two independent mineral-resources surveys by prestigious groups have been completed recently (Malenbaum, 1973; Brobst and Pratt, 1973). The resource summations of these independent surveys are difficult to compare because of different views on the restrictions, if any, that should be placed on what are classed as resources. Some (Govett and Govett, 1972, p. 285) hold that the resource base of a commodity is the total amount within all the Earth's crust. Pragmatists, however, hold that such figures are not only meaningless but misleading because they promise resources that will not be available to society within the predictable future.

There is much merit in computing resource figures on the basis of known technology and much merit in using restrictions to resources where such restrictions can be defined with sufficient precision that they cannot be eliminated by present technology or by predictable economics. One restriction that may be placed on resources of selected metals is the energy necessary to mine, mill, smelt, and refine the ore material to produce the metal in a form usable by man. The hard resources, the ones that will be used by society, are strongly dependent on factors other than mere existence of material at some place with some grade and in some form. Also, consideration of energy requirements to extract and process a few ores, although based on limited data, demonstrates that low-grade resources, types of resource occurrences for exploitation, and eventual substitution of one metal for another may be ultimately determined by availability of the required energy.

Normally, mining geologists and engineers evaluate metal extraction and processing in terms of costs for drilling, blasting, loading, hauling, and labor (for example, Eng. and Mining Journal, 1968) or in terms of equipment, supplies, and power. Relation of all the mining costs directly to energy cycles is beyond the scope of this report, but the primary energy cycles developed by Bravard, Flora, and Portal (1972) involved in the utilization of selected metals are an initial and important factor in such an evaluation. No claim or inference that our present treatment of energy requirements can be converted into the total cost of producing a unit of metal is intended.

Our data are based on energy requirements for current established mining, milling, smelting, and refining methods. Until these techniques are replaced, they represent the most efficient methods known for production of metals from their ores. Evaluation of assumptions about the amount of energy needed for undeveloped or theoretical methods of mining, milling, smelting, and refining such as chemical leaching or use of breeder reactors is speculative, and metal resources calculated from such energy uses are therefore equally speculative, not only as to amount but also whether they exist at all.

ENERGY CONSUMPTION AS A FUNCTION OF ORE GRADE

Brobst and Pratt (1973, p. 8) recognized that an important factor in considering progressively lower grades of ores for processing is the relation between the amount of energy required and the particular grade. Consideration of data presented by Bravard, Flora, and Portal (1972), who were concerned with

the energy expenditures of recycling versus the refining of metals, shows that there is indeed a relation between the energy requirement and grade of material processed. Because the mill concentrates used in a large number of smelting and refining processes have a fixed or narrow range of mineral compositions, the energy requirement for a particular smelting and refining process is basically fixed, remains constant, and is independent of the initial grade of ore used. But the energy required for mining and milling of the ore to obtain the concentrate is a function of the grade of the ore. The tonnage of ore necessary to produce 1 ton of metal from different grades of material shows a hyperbolic increase as the grade decreases (fig. 1).

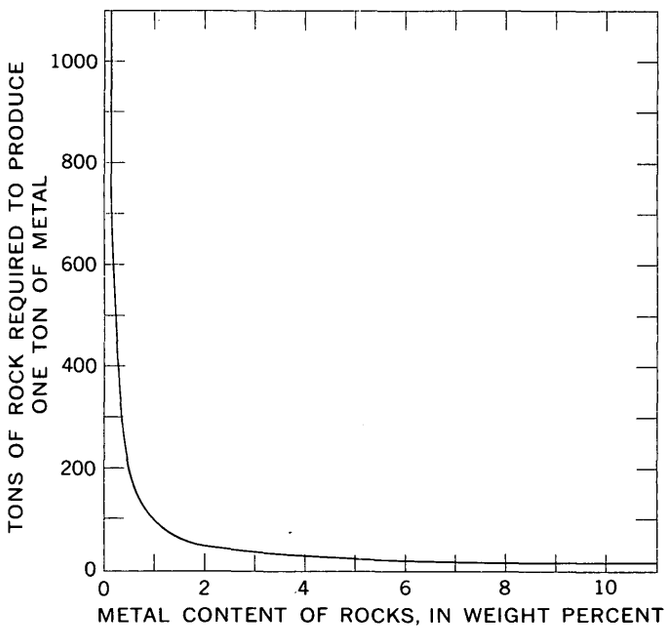

FIGURE 1.—Relation between ore grade and ore tonnage required to produce 1 ton of metal.

Obviously, the energy required to mine and mill different grades of ore by a particular technique increases as a function of the tonnage of ore necessary to produce 1 ton of metal and is the product of the energy required to mine and mill 1 ton of rock and the number of tons of rock necessary at that particular grade.

If we let E_T represent the total energy necessary to process 1 ton of metal from its ore, E_m the energy to mine and mill 1 ton of ore, E_s the energy to smelt and refine the concentrate to produce a ton of metal, T the tonnage of rock needed to recover 1 ton of metal, and g the grade of the ore, then $E_T = (E_m \cdot T) + E_s$, and $T = 1/g$. Therefore $E_T = (E_m/g) + E_s$ where E_m and E_s are constants. For most metals and mineral products, the constants E_m and E_s are not readily available and for many metals and processes probably have not been evaluated.

APPLICATION TO SELECTED METALLIC RESOURCES

Figure 2 shows an evaluation of the equation

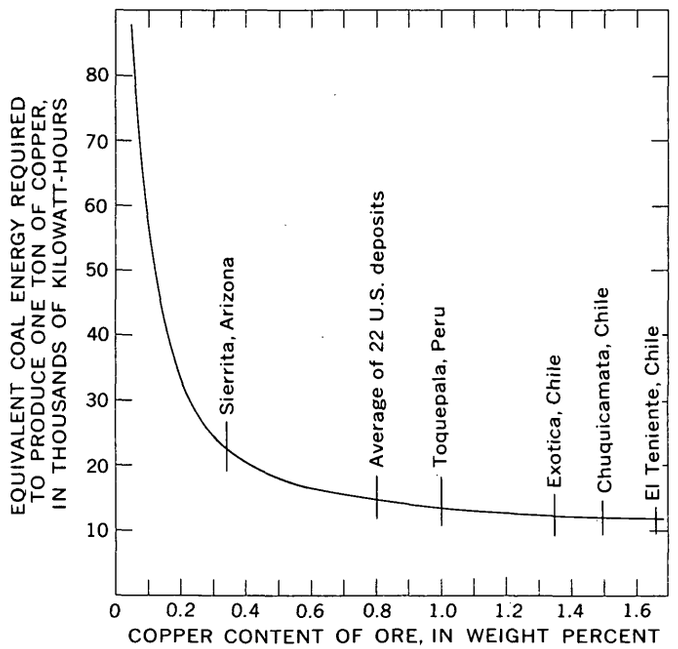

FIGURE 2.—Equivalent coal energy requirements for different grades of copper sulfide ores. Grades of some copper deposits are shown; data from Cox, Schmidt, Vine, Kirkemo, Tourtelot, and Fleischer (1973) and Beall and Haddon (1969).

$E_T = (E_m/g) + E_s$ for copper sulfide deposits mined by open-pit methods; energy is expressed as equivalent coal energy in kilowatt-hours (kWh), and the constants and calculations are based on Bravard, Flora, and Portal's (1972) data. The value of E_m, 47.975 kWh per ton of ore, includes energy for blasting, transporting the ore, crushing, grinding, flotation, lime calcination, and limestone crushing, all of which are dependent on ore grade. The value of E_s is 8715 kWh per ton of metal and is not dependent on grade. The hyperbolic shape of this relation (fig. 2) suggests that deposits with grades below about 0.20–0.25 percent Cu will not be mined to produce metal for common electrical and construction uses because of the sharply increasing amount of energy necessary to produce a unit of the metal. In other words, the energy consumption per unit of metal for low-grade ore is extremely high.

The term E_m/g in the equation $E_T=(E_m/g)+E_s$ shows that a 10-fold decrease in grade results in a 10-fold increase in the energy necessary to mine and mill enough ore to produce 1 ton of copper (E_m/g). The significance, however, of a 10-fold increase in energy depends on the amount of energy relative to the other agents required to produce the ton of copper, or stated in another way, a 10-fold increase of a very small amount of energy is still not much energy. An informative procedure for such a comparison is to reduce all production factors to cost. On this basis, the cost of the primary energy (electrical power and fuel) for mining and milling at the Silver Bell open-pit copper deposit in Pima County, Ariz., is 30 percent of the total cost of mining and milling ore containing 0.9 percent copper (Hardwick, 1963). This percentage figure does not include secondary energy costs, such as the energy requried to build mining and milling equipment, to produce other supplies, and to supply labor. Even so, a 10-fold decrease in grade would result in a 300 percent increase in the cost of mining and milling considering only the cost of primary energy, assuming that the energy is available and at the same unit price. Energy is not a trivial part of the production of metals.

Examination of other metals, their ore grades, and energy requirements shows similar relations. Preliminary mining and milling constants for iron, aluminum, and titanium from various natural sources were estimated from the data of Bravard, Flora, and Portal (1972). In order to derive E_m, the mining and milling part of each process is assumed to be a direct function of grade for iron, titanium, and bauxite sources. In addition, for clay and anorthosite aluminum sources a mining value of bauxite and open-pit copper were added, respectively. Table 1 lists the E_m and E_s estimated values for processes and respective metals. Plots of the energy requirements for recovery of these metals at various grades (fig. 3) show that (1) recovery of different metals has as much as about a two-hundred variation in energy requirements (compare iron and titanium), (2) each metal has an independent fixed energy requirement for smelting and refining, and (3) as the grade in any particular source of metal decreases, the total energy to recover the metal increases at first gradually until the energy for mining and milling approaches that for smelting and refining, after which the total energy required increases rapidly as the mining and milling demands become larger than the smelting demands.

Other metals for which the energy requirement data are unavailable must have grade-energy relations as expressed by the formulas or such as those in figure 3. The mining and milling methods for disseminated molybdenum deposits are virtually the same as for disseminated copper ores. The energy consumption for mining and milling of these molydenum ores, therefore, must be close to that for the copper ores. Similarly, the energy consumed in smelting and refining of sulfide nickel ores may not differ significantly from that for sulfide copper ores.

TABLE 1.—*Calculated energy constants for smelting and refining* (E_s) *and milling and mining* (E_m)

[Constants based on data from Bravard, Flora, and Portal, 1972]

Metal, source, and grade	Calculated energy constants	
	E_s (kilowatt-hour per ton of metal)	E_m (kilowatt-hour per ton of ore)
Aluminum:		
Bauxite, 50 percent Al_2O_3	38,774	5,302.5
Clay by bauxite mining techniques, 30 percent Al_2O_3.	38,500	9,216.6
Anorthosite by porphyry copper open-pit mining method, 30 percent Al_2O_3.	38,500	11,455.6
Iron:		
High-grade hematite, 58.5 percent Fe.	4,209	38.685
Magnetic taconite, 32.5 percent Fe.	4,209	145.275
Nonmagnetic taconite, 28 percent Fe.	4,209	297.97
Specular hematite, 38 percent Fe.	4,209	351.88
Iron laterite	4,209	988.8
Copper, in 1-percent sulfide ores	8,715	47.975
Titanium, 1.4 percent TiO_2, in ilmenite beach sands.	148,357.5	65.765

CONCLUSIONS

The energy required to produce a unit of metal can be used to determine a lower limit on the grade of ores used to calculate potential resources. This grade restriction can be evaluated and the figure used as a limiting factor in the search for low-grade minerals that might be mined in the predictable future. Further refinement of this concept would involve considering the energy requirements along similar lines as Bravard, Flora, and Portal (1972) for the mining, milling, smelting, and refining of different metallic and industrial minerals. Given this refinement, evaluation of resources would then have a practical lower limit in terms of grade for a particular mineral commodity.

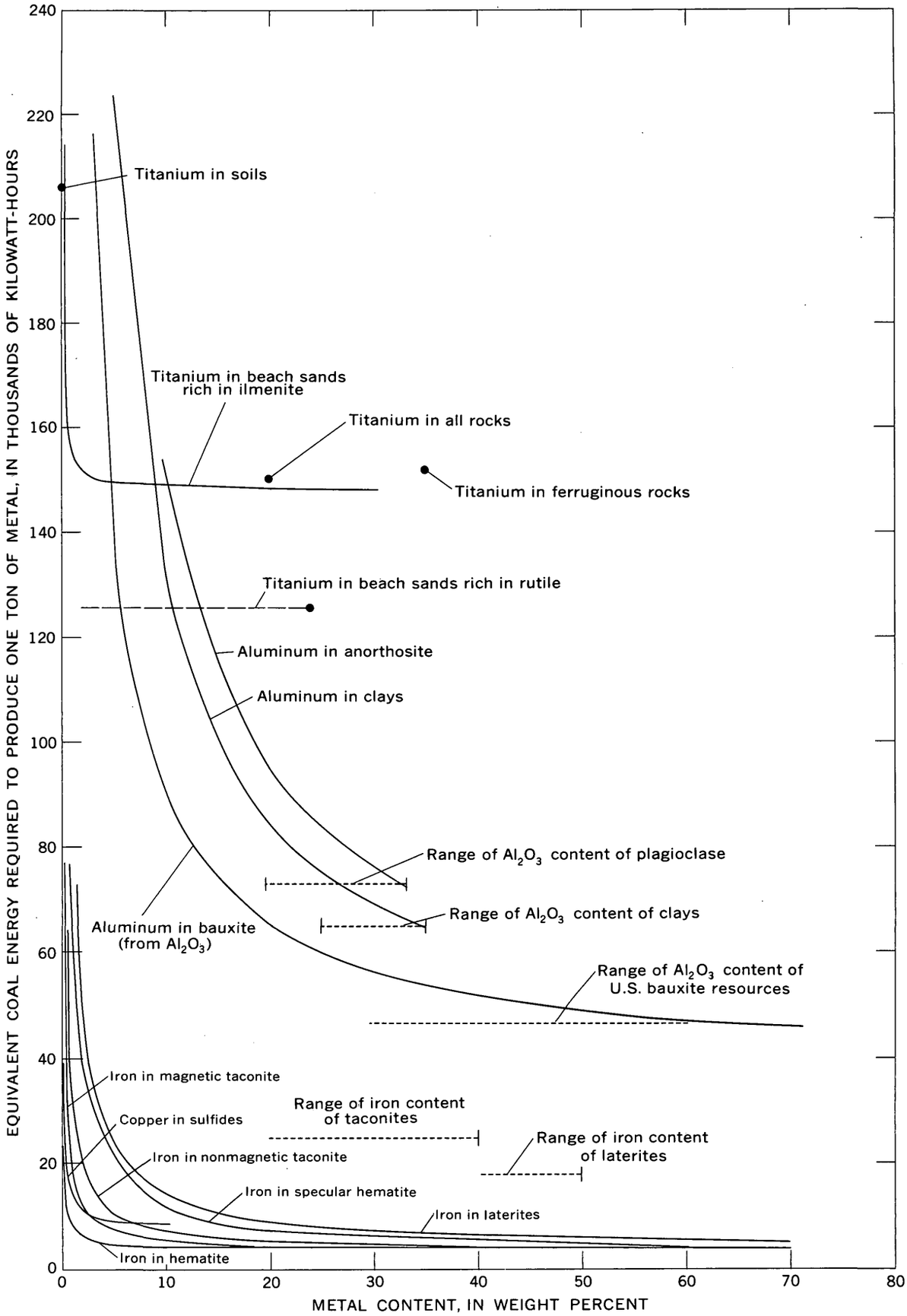

FIGURE 3.—Energy requirements for recovery of iron, titanium, and aluminum at different grades from various sources.

REFERENCES CITED

Beall, J. V., and Haddon, W. F., 1969 Copper in the Andes: Mining Eng., November, p. 59–60.

Bravard, J. C., Flora, H. B., and Portal, Charles, 1972, Energy expenditures associated with the production and recycle of metals: Oak Ridge Natl. Lab.-Natl. Sci. Found.-Environmental Program, p. 1–87.

Brobst, D. A., and Pratt, W. P., eds., 1973, United States mineral resources: U.S. Geol. Survey Prof. Paper 820, 722 p.

Cox, D. P., Schmidt, R. G., Vine, J. D., Kirkemo, Harold, Tourtelot, E. B., and Fleischer, Michael, 1973, Copper, *in* Brobst, D. A., and Pratt, W. P., eds., United States mineral resources: U.S. Geol. Survey Prof. Paper 820, p 163–190

Engineering and Mining Journal, 1968, E/MJ 1968 guidebook: Eng. and Mining Jour., v. 169, no. 6, p. 153–204.

Govett, G. J. S., and Govett, M. H., 1972, Mineral resources supplies and the limits of economic growth: Earth-Sci. Rev., v. 8, p. 275–290.

Hardwick, W. R., 1963, Open pit copper mining and concentrating methods and costs, Silver Bell unit, American Smelting and Refining Co., Pima County, Arizona: U.S. Bur. Mines Inf. Circ. 8153, 72 p.

Malenbaum, Wilfred, 1973, Materials requirements in the United States and abroad in the year 2000—A research project: Natl. Comm. on Materials Policy, p. 1–40.

Jour. Research U.S. Geol. Survey
Vol. 3, No. 1, Jan.–Feb. 1975, p. 15–20

THE MEGASPORE GENUS *HENRISPORITES* FROM THE CRETACEOUS OF MASSACHUSETTS

By ROBERT H. TSCHUDY, Denver, Colo.

Abstract.—A new megaspore species belonging to the genus *Henrisporites* was found in Cretaceous (probably Cenomanian) rocks from Massachusetts. Megaspores of *Paxillitriletes dakotaensis* (Hall) Hall and Nicolson were found in the same rocks. This paper discusses the occurrence of these two megaspores in North America and describes *Henrisporites angustus* n. sp. from Massachusetts.

The genus *Henrisporites* was first proposed by Potonié (1956) for megaspore species recovered from Wealden rocks, species which had previously been included in the genus *Triletes* by Dijkstra (1951). Potonié included two of Dijkstra's species, *affinis* and *undulatus*, in the new genus. I find no other reference to the genus until 1968 when three new species were proposed for inclusion in the genus *Henrisporites* by Binda and Srivastava (1968). These species were based upon specimens of silicified megaspores isolated from the Knee Hills Tuff (Maestrichtian) of western Canada. Some of the morphological characteristics of these new species prompted emendation of the genus by Binda and Srivastava (1968) in order that the species could be included. The only other reference to *Henrisporites* that I find is that of Gunther and Hills (1972), who listed *Henrisporites* megaspores from the Brazeau Formation of western Canada and assigned them to the previously established species *H. affinis* and *H. undulatus*. These megaspores were found in the Belly River equivalent at the base of the Brazeau Formation and are of Campanian age. At present only five species have been assigned to the genus *Henrisporites*. I am here proposing a sixth species.

Acknowledgments.—I thank Imogene Doher for isolating some of the megaspores and calling my attention to them; also, Kathryn Dieterich for isolating additional megaspores and for photographing the specimens.

MATERIAL AND METHODS

The rock sample was provided by Mr. J. V. A. Trumbull of the U.S. Geological Survey. It was from the westernmost exposure of a 2-ft (0.6-m) bed of lignitic clay about 7 ft (2.1-m) above mean sea level. The clay is overlain by Pleistocene gravel on the southern shoreline of Nonamesset Island, Mass., about 1½ mi (2.5 km) southwest of the town of Woods Hole. The sample was assigned USGS paleobotany locality D3727.

The lignitic clay was broken up and treated with 52 percent hydrofluoric acid for about 4 h, then subjected to Schulze solution for about 6 min. The succeeding treatment with 10 percent potassium hydroxide dissolved the humates and freed the palynomorphs. The megaspores were then picked from the washed coarse residue, dehydrated in alcohol and alcohol-xylene, and mounted in canada balsam.

TYPE AND ILLUSTRATED SPECIMENS

All specimens illustrated in this report are preserved on slides deposited in the paleobotanical collections of the U.S. Geological Survey, Denver, Colo. All illustrated specimens are within black inked circles marked directly on the slides; they may also be located on the slides by the mechanical-stage coordinates given in the figure captions. In order that other workers may convert their mechanical-stage readings to those recorded for specimens included in this report, the coordinates for the center point of a 1- by 3-in. standard microscope slide are 108.0 and 12.3 mm (designated as 108.0×12.3). The method of accurately locating the center of a standard microscope slide is described by Tschudy (1966, p. D78). If the slide label is placed to the left, the vertical coordinates decrease toward the near edge of the slide and the horizontal coordinates decrease toward the right edge of the slide.

In addition to slides of illustrated specimens, color photographs are available from the U.S. Geological Survey laboratory, Denver, Colo., on a limited-time loan basis.

AGE OF THE SAMPLE

The palynomorph assemblage that accompanied the megaspores consisted of abundant well-preserved small

spores, conifer pollen, and a very few angiosperm pollen grain types. The most common angiosperm pollen grain present probably can be assigned to *Tricolpopollenites minutus* Brenner. Another, much less common, type can be assigned to *Tricolporopollenites* cf. *T. triangulus* Groot, Penny, and Groot. The former is apparently restricted to the Patapsco formation of Maryland (Brenner, 1963) and the latter was found in both the Raritan and Magothy Formations (Groot and others, 1961). Doyle (1969) and Wolfe and Pakiser (1971) found *Tricolporopollenites* cf. *T. triangulus* in the lower Raritan and in the Patapsco-Raritan transition zone in the Atlantic Coastal Plain region. The paucity of angiosperm pollen taxa and the presence of tricolporate pollen are suggestive of the early Late Cretaceous (no younger than Cenomanian). The presence in the sample of a few specimens of *Complexiopollis* cf. *C. funiculus* (Tschudy, 1973) is also suggestive of the early Late Cretaceous. The presence of megaspores of *Paxillitriletes dakotaensis* (Hall) Hall and Nicolson in this material is of particular interest. *P. dakotaensis* has been reported only from the top of the Dakota Sandstone of Iowa (Cenomanian age). This taxon was originally described by Hall (1963) as *Thomsonia dakotaensis* and more recently transferred to the new genus *Paxillitriletes* by Hall and Nicolson (1973); they found the generic name *Thomsonia* Mädler (1954) invalid as it was clearly a later homonym of *Thomsonia* Wallich (1830), an extant angiosperm.

The available evidence all points to an early Late Cretaceous, probably Cenomanian, age for the sample.

SYSTEMATIC DESCRIPTIONS

Genus *HENRISPORITES* (Potonié) Binda and Srivastava, 1968, emend.

Type species.—*Henrisporites* (al. *Triletes*) *affinis* (Dijkstra, 1951 [Netherlands] Meded. Geol. Stichting, new ser., no. 5, p. 13, pl. 2, fig. 4) nov. comb.

Diagnosis.—(From Potonié, 1956, p. 68) genotype 440 μm (according to the illustration), trilete zonate megaspores, equatorial outline subtriangular to triangular, Y-marks reaching to the equatorial outline of the zona, clearly higher than broad, often much higher (*undulatus*), contact areas and distal side sparsely occupied by coni to spinae whose lengths in the genotype are about 1–1½ times their breadths at their bases. Auriculae may be developed by elongation of the Y-marks (*undulatus* as well as *affinis*), remainder of exine wrinkled.

Potonié (1956) included two of Dijkstra's species, *affinis* and *undulatus*, in this new genus.

The genus was emended by Binda and Srivastava (1968, Micropaleontology, v. 14, no. 1, p. 106) as follows:

Diagnosis.—"Megaspores trilete, zonate; amb subtriangular to triangular; tetrad mark reaching the equatorial outline of the zona; arms higher than their breadth, sometimes very high; proximal and distal surfaces with sparse granulate to spinate ornamentation."

Binda and Srivastava (1968, p. 106) emended the genus to include "* * * all zonate trilete megaspores having a raised tetrad mark, granulate to spinate ornamentation, and exine with or without wrinkles." This emendation was considered necessary in order for the genus to accommodate some of the silicified megaspores found in the Knee Hills Tuff. Binda and Srivastava (1968) proposed the new species *H. granulatus*, *H. elkwaterensis*, and *H. sheilae*.

Henrisporites angustus n. sp.

Figures 1, 2

Holotype.—Locality D3727 (fig. 2*a*).

Paratypes.—Locality D3727 (fig. 2*b–f*).

Diagnosis.—Shape of megaspores subtriangular in polar view, spherical to gabled spherical in equatorial view. Rims of trilete laesurae membranous; membranes with somewhat irregular margins, prominent, probably consisting of two fused membranes (acrolameliae—Tschudy, 1966), one on either side of the laesurae. Acrolamellae 40–70 μm high, smooth or with small surface verrucae or reduced spines. Zona subequatorial on the proximal hemisphere, narrow, threadlike in ap-

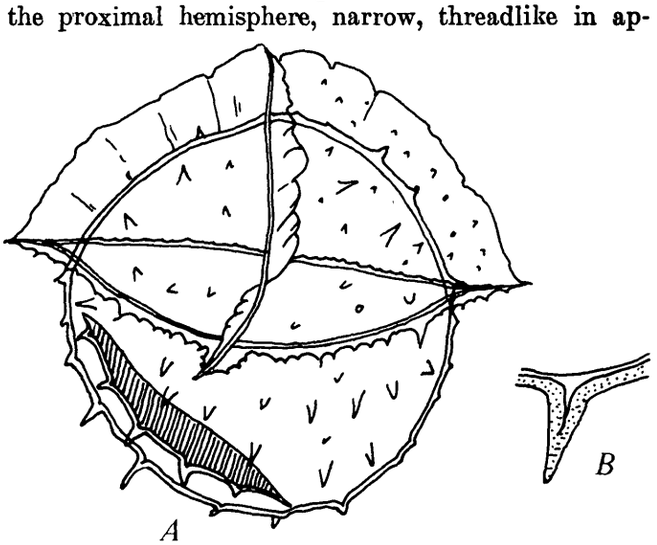

FIGURE 1.—Diagram of *Henrisporites angustus*. Magnification of approximately × 200. *A*, Variation in sculpture of acrolamellae is shown; left side—almost smooth, right side—with small coni; note the subequatorial narrow zona with irregular, somewhat fimbriate margin. *B*, Single spine showing hollow nature and development from ektexine; inner, very thin endexine also shown.

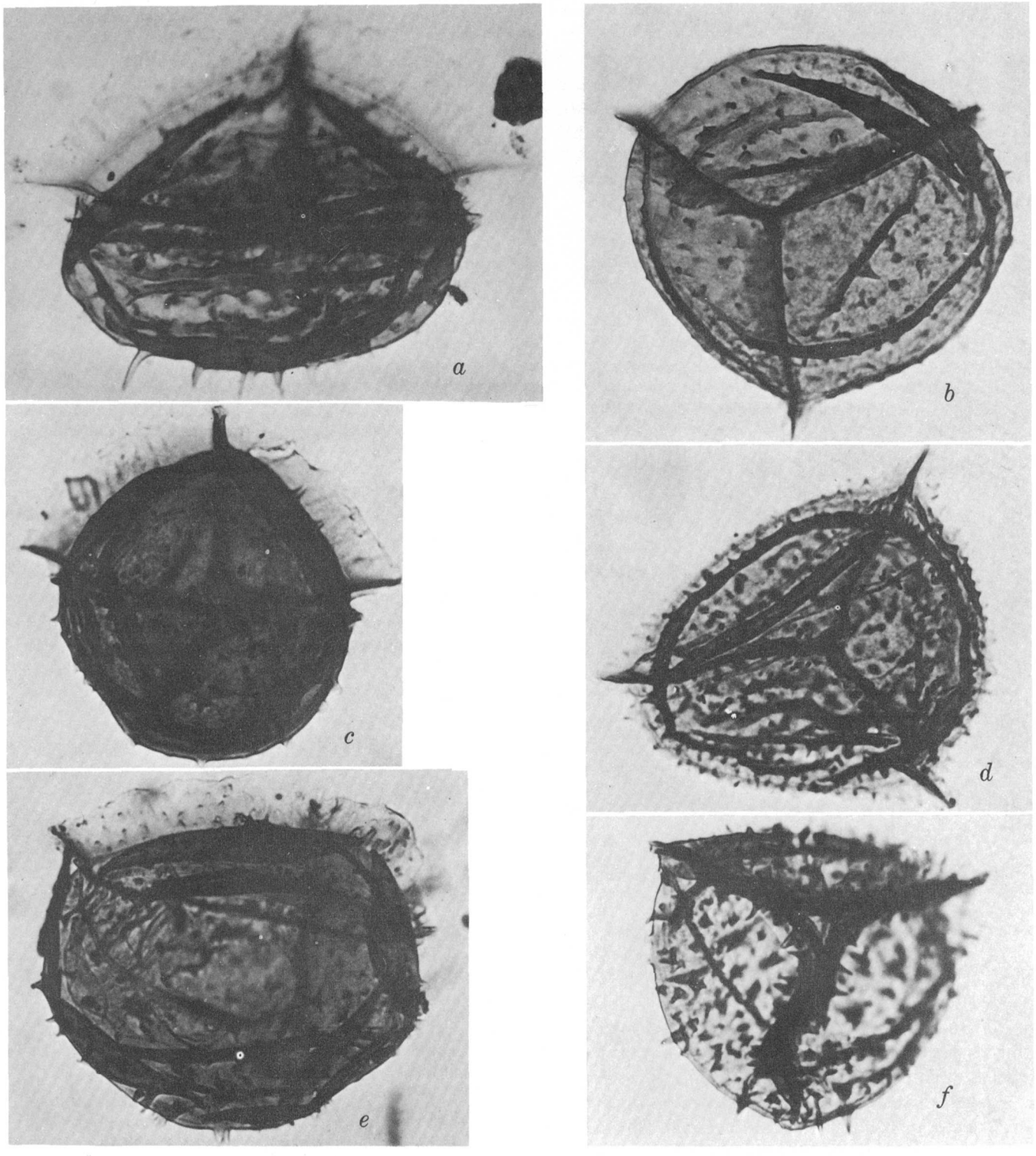

FIGURE 2.—*Henrisporites angustus* Tschudy n. sp. Megaspores from Massachusetts. Magnification × 200.

a. Holotype. Locality D3727, slide 4, coordinates 110.8×21.0, equatorial view.

b. Paratype. Locality D3727, slide mega 4, coordinates 112.5×3.6, polar proximal view

c. Paratype. Locality D3727, slide mega 4, coordinates 103.4×7.8, equatorial view.

d. Paratype. Locality D3727, slide mega 1, coordinates 111.2×20.4, polar proximal view. Note small auriculae with somewhat fimbriate outline as extensions of the zone at contact with the triradiate lamellae.

e. Paratype. Locality D3727, slide mega 1, coordinates 110.5×3.0, equatorial view. Note small coni on acrolamella and wrinkled ektexine.

f. Paratype. Locality D3727, slide mega 5, coordinates 103.1×10.5, polar proximal view. Note abundant spines and open laesurae at the pole.

pearance, 7–11 μm wide, often with somewhat toothed outline. Triangular small auriculae developed on the zona at the confluence of the trilete extensions. Wall two layered, commonly wrinkled; ektexine up to 4 μm thick; endexine very thin, about 1 μm thick. Surface granulate to scabrate with scattered coni or spinae up to 40 μm long; spines hollow at bases and developed from ektexine. Diameter 240–350 μm, average 296 μm (100 specimens measured).

Remarks.—*Henrisporites angustus* n. sp. can be distinguished from *H. affinis* and *H. undulatus* principally by its much narrower zona. Furthermore, *H. affinis* possesses a wrinkled reticulate distal surface. In *H. undulatus* the distal surface is densely covered with spinae or hairlike appendages. *H. angustus* can be readily distinguished from the three species proposed by Binda and Srivastava (1968) by its much more prominent acrolamellae, and by its conspicuous elongate spines.

Gunther and Hills (1972) figured specimens of *Henrisporites*, which they assigned to the species *H. affinis* and *H. undulatus*. The photographs of these specimens show very wide, prominent equatorial flanges and so are excluded from *H. angustus*.

Affinity.—The probable affinity of the genus *Henrisporites* is with the family Selaginellaceae.

Genus *PAXILLITRILETES* Hall and Nicolson, 1973, nom. nov.

1954. *Thomsonia* Mädler, Geol. Jahrb., v. 70, p. 150, pl. 5, fig. 15.

1973. *Paxillitriletes* Hall and Nicolson, Taxon, v. 22, no. 2/3, p. 319.

Type species.—*Paxillitriletes* (al. *Thomsonia*) *reticulata* Mädler, 1954.

***Paxillitriletes dakotaensis* (Hall) Hall and Nicolson, 1972**

Figure 3

1963. *Thomsonia dakotaensis* Hall, Pollen et spores, v. 5, no. 2, p. 438, pl. 91, figs. 37–39.

1973. *Paxillitriletes dakotaensis* (Hall). Hall and Nicolson, Taxon, v. 22, no. 2/3, p. 319.

Remarks.—Of the dozen or so species previously reported, only *Paxillitriletes dakotaensis* and *P. midas* possess prominent robust distal projections. However, *P. midas* is much smaller (diameter of spore body 250–450 μm, mean 380 μm) and only rarely do the spores bear prominent distal appendages. The original description of *P. dakotaensis* was based upon observations and photographs taken by reflected light. The following notes, based on observation and photographs taken by transmitted light, may serve to clarify some of the characteristics of the species, but they are not intended as an emendation.

Description.—Trilete, spherical to subtriangular megaspores possessing a subequatorial flange or zona on the proximal hemisphere and broad auriculae opposite the ends of the laesurae; zona with an irregular, somewhat fimbriate margin, 20–50 μm wide between auriculae; auriculae generally rounded at their tips but occasionally slightly notched or dissected (200 μm long by about 240 μm wide). Laesurae extend to the subequatorial flange or zona and are bordered on each side by one row (rarely more than one row) of cylindrical to strap-shaped, pointed or blunt projections; projections 200–250 μm long and 15–35 μm broad, sometimes recurved at their tips. Distal surface with scattered similar cylindrical projections, sometimes hook shaped at their tips; projections up to 140 μm long and up to 50 μm wide, often slightly constricted at their bases; projections on distal hemisphere commonly more robust than the projections adjacent to the leasurae. Diameter of spores 480–720 μm (according to Hall, 1963); 420–610 μm, average 520 μm not including auriculae, in our material (10 undistorted spores measured). Wall two layered, ektexine about 11μm thick, endexine about 1 μm thick. Sculpture of proximal and distal surface reticulate; at the juncture of adjacent muri, short irregular spinelike processes 6–25 μm long are developed.

FIGURE 3.—*Paxillitriletes dakotaensis* (Hall) Hall and Nicolson. Megaspores from Massachusetts. Magnification × 100 unless otherwise indicated.

a. Locality D3727, slide mega 6, coordinates 116.0×3.7. Proximal polar view showing auriculae, narrow zona, and strap-shaped appendages adjacent to the laesurae.

b. Same specimen as that in *a*. Distal polar view showing distal coarse outgrowths of the ektexine.

c. Locality D3727, side mega 6, coordinates 113.7×12.2. Partial equatorial view showing many distal outgrowths as well as partially eroded appendages adjacent to the laesurae.

d. Locality D3727, slide mega 7, coordinates 94.8×13.6. Note elongate strap-shaped appendages adjacent to the laesurae, as well as the narrow zona.

e. Locality D3727, slide 4, coordinates 108.2×16.1: magnification × 200. Note reticulation of proximal surface and small spines developed at junctures of muri.

f. Locality D3727, slide mega 6, coordinates 101.5×4.3; magnification × 200. Distal surface with small spines at junctures of muri. Note granular surface sculpture.

g. From same specimen as that in *f*; magnification × 500. A single distal outgrowth with granular structure and constricted base. A small surface spine is visible at the left of the base of projection.

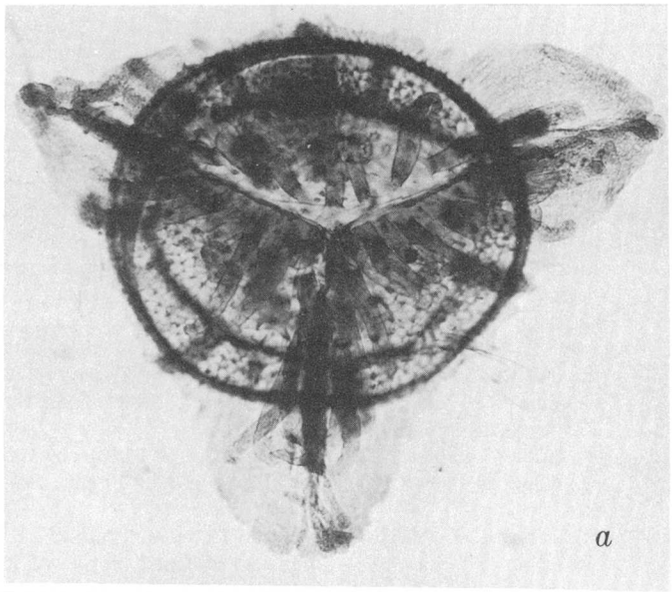

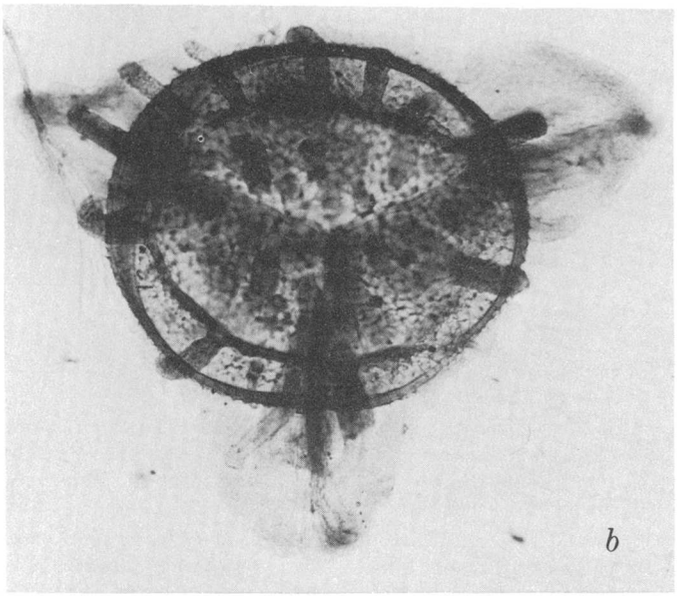

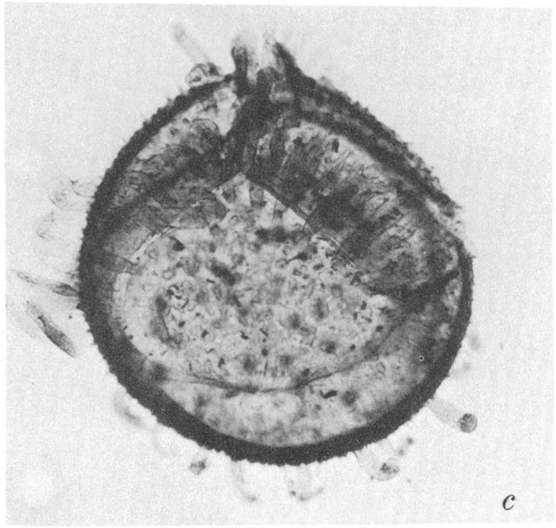

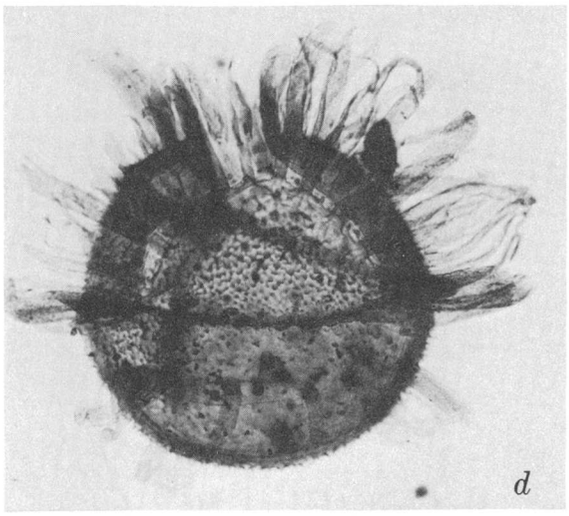

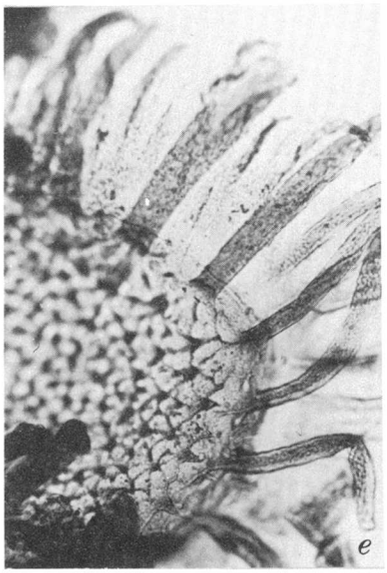

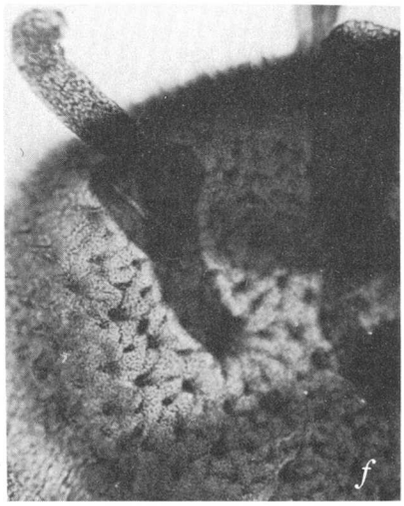

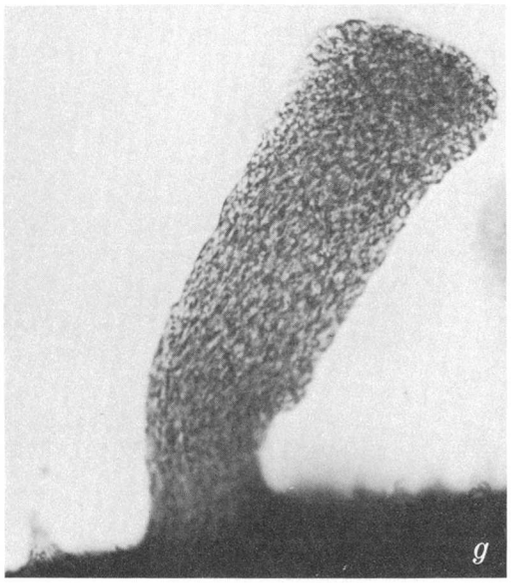

PAXILLITRILETES

REFERENCES CITED

Brenner, G. J., 1963, The spores and pollen of the Potomac Group of Maryland: Maryland Dept. Geology, Mines and Water Resources Bull. 27, 215 p.

Binda, P. L., and Srivastava, S. K., 1968, Silicified megaspores from Upper Cretaceous beds of southern Alberta, Canada: Micropaleontology, v. 14, no. 1, p. 105–113.

Dijkstra, S. J,. 1951, Wealden megaspores and their stratigraphical value: [Netherlands] Meded. Geol. Stitching, new ser., no. 5, p. 7–21.

Doyle, J. A., 1969, Cretaceous angiosperm pollen of the Atlantic Coastal Plain and its evolutionary significance: Arnold Arboretum Jour., v. 50, no. 1, p. 1–35.

Groot, J. J., Penny, J. S. and Groot, C. R,. 1961, Plant microfossils and age of the Raritan, Tuscaloosa and Magothy formations of the eastern United States: Palaeontographica v. 108, ser. B, nos. 3–6, p. 121–140.

Gunther, P. R., and Hills, L. V., 1972, Megaspores and other palynomorphs of the Brazeau Formation (Upper Cretaceous), Nordegg area, Alberta: Geoscience and Man, v. 4, p. 29–48.

Hall, J. W., 1963, Megaspores and other fossils in the Dakota Formation (Cenomanian) of Iowa, (U.S.A.): Pollen et Spores, v. 5, no. 2, p. 425–443.

Hall, J. W., and Nicolson, D. H., 1973, *Paxillitriletes*, a new name for fossil megaspores hitherto invalidly named *Thomsonia:* Taxon, v. 22, no. 2/3, p. 319–320.

Mädler, K. A., 1954, *Azolla* aus dem Quartär und Tertiär sowie ihre Bedeutung für die Taxionomie älterer Sporen: Geol. Jahrb., v. 70, p. 143–155 [1955].

Potonié, Robert, 1956, Sporites, Part 1 *of* Synopsis der Gattungen der Sporae dispersae: Geol. Jahrb. Beihefte, v. 23, 103 p.

Tschudy, R. H., 1966, Associated megaspores and microspores of the Cretaceous genus *Ariadnaesporites* Potonié, 1956, emend., *in* Geological Survey research 1966: U.S. Geol. Survey Prof. Paper 550–D, p. D76–D82.

——— 1973, *Complexiopollis* pollen lineage in Mississippi embayment rocks: U.S. Geol. Survey Prof. Paper 743–C, 15 p.

Wolfe, J. A., and Pakiser, H. M., 1971, Stratigraphic interpretations of some Cretaceous microfossil floras of the Middle Atlantic States, *in* Geological Survey research 1971: U.S. Geol. Survey Prof. Paper 750–B, p. B35–B47.

Jour. Research U.S. Geol. Survey
Vol. 3, No. 1, Jan.–Feb. 1975, p. 21–30

QUANTITATIVE DETERMINATION OF DAWSONITE IN GREEN RIVER SHALE BY POWDER-SAMPLE X-RAY DIFFRACTION: EFFECT OF GRINDING

By E-AN ZEN and JANE G. HAMMARSTROM, Reston, Va.

Abstract.—In an effort to evaluate the method of quantitative analysis by X-ray diffraction as a means of determining dawsonite abundances in Green River oil shale, we performed a series of grinding experiments. Weighed mixtures of dawsonite + quartz and dawsonite + quartz + shale were ground for preset lengths of time, and the following X-ray diffraction peaks were measured for intensity: dawsonite (110) at 15.6 2θ and (211)(002) at 32.1° 2θ, and quartz (100) at 20.9° 2θ and (101) at 26.6° 2θ. Heights and areas were measured. Intensity ratios were plotted as functions of grinding time with a calculated probable error. Intensity ratios generally decrease as grinding time increases. The intensity of the 15.6° peak, $D_{15.6°}$, is most affected, and the most drastic reduction occurs during the first 20 min of grinding. The $D_{32.1°}$ peak is least sensitive to grinding but is subject to interference by other minerals in the shale. We conclude that the X-ray diffraction method is not well adapted to the routine quantitative determination of dawsonite in oil shale of the Green River Formation.

The discovery of significant quantities of dawsonite, $NaAlCO_3(OH)_2$, in the Parachute Creek Member of the Green River Formation, Piceance Basin, northwestern Colorado, is of considerable interest because dawsonite is potentially a source of readily recoverable aluminum. Many reports on the geology, mineralogy, chemistry, and technology of these dawsonite-bearing rocks already exist (for example, Smith and Milton, 1966; Hay, 1966; Hite and Dyni, 1967; Dyni and Hite, 1968; Young and Smith, 1970; Trudell and others, 1970). A detailed study of the Parachute Creek Member was recently made by Brobst and Tucker (1973).

Dyni and Hite (1968) and Huggins, Green, and Turner (1973) used the powder-sample X-ray diffraction method to determine dawsonite quantitatively in the shales of the Green River Formation. These authors as well as Brobst and Tucker (1973) recognized that the intensities of dawsonite diffraction peaks depend not only on the amount of dawsonite present but also on the extent of grinding of the sample. We now report the results of a systematic study of the effect of grinding on dawsonite diffraction peak intensities; these results show that grinding of a sample causes drastic changes in dawsonite peak intensities. Serious errors can result in the estimate of dawsonite abundances by X-ray diffraction methods in the oil shale of the Green River Formation.

SAMPLES

Samples used for the study were dawsonite, quartz, and two samples of oil shale from the Green River Formation.

The dawsonite comes from near Kanaskat Junction, Cumberland quadrangle, King County, Wash. (fig. 1). It occurs in the marginal zone of an andesite sill that intruded coal beds of the Eocene-Oligocene Puget Group (Vine, 1969) and appears to have formed through contact reaction between the magma and the coal bed. The geology and mineralogy of the andesite sill were described by Vine (1969, p. 35).

The X-ray pattern of a typical dawsonite separate is given in figure 2*C*. Figure 2*D* shows a trace of dawsonite from Olduvai Gorge, Africa (Hay, 1966, p. 42), for comparison. As the dawsonite in the Green River shale occurs as paper-thin laminae, it could not be concentrated for experimental use. However, the X-ray peak qualities (height-width ratios) of the dawsonite from Washington and from the Green River shale (fig. 2*C*, *B*) show that they are closely comparable.

One sample of Green River shale used was from Colorado and consisted mainly of quartz, dolomite, and feldspar as well as an easily detectable amount of dawsonite. The second sample of Green River shale is dawsonite free and came from the 1,247- to 1,255-ft (374.1- to 376.5-m) level, Texas Gulf Sulfur mine, near Green River, Wyo. It is a paper-thin oil shale containing dolomite, quartz, mica, and feldspar; an X-ray pattern (fig. 2*A*) shows absence of dawsonite or other minerals whose peak positions might interfere with our study. The oil-shale samples were homogenized for experimental use by grinding.

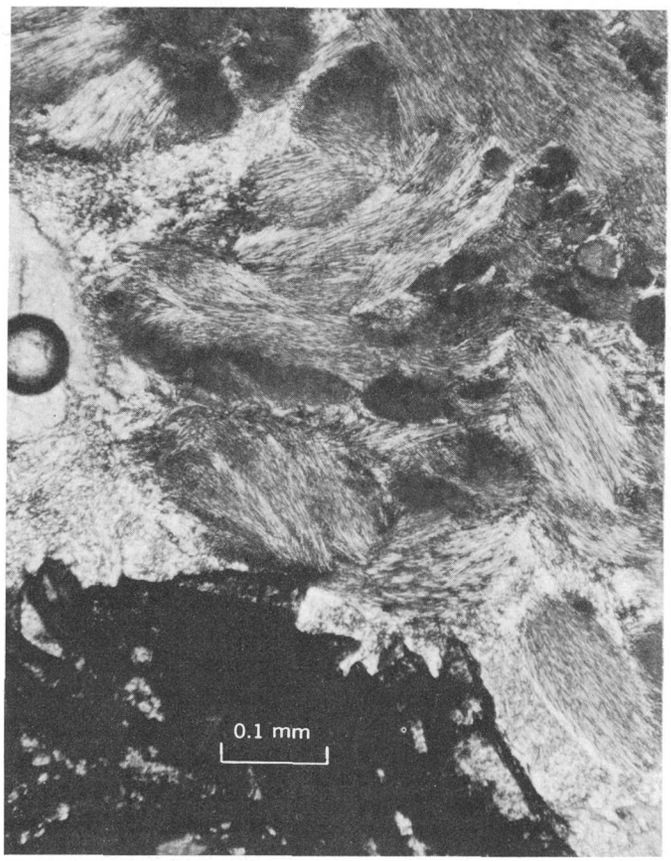

FIGURE 1.—Photomicrograph of dawsonite from Kanaskat Junction, King County, Wash. Closeup of a cluster of fibrous dawsonite with crossed polarizers to show the fabric of the fibers.

The quartz used in the experiments is a water-clear single crystal of unknown origin.

PROCEDURE

Weighed amounts of the component minerals and rocks were mixed and hand ground under acetone in a porcelain mortar. Although the particle size of the starting material varied somewhat from run to run, the maximum particle size for all components of a given run was constant and is stated later for individual runs.

After it had been ground the preset length of time, the sample was generally a compact mass. It was fluffed up by sieving through a screen sufficiently coarse to prevent sample loss and then prepared for X-ray study by use of a small handpress and standard Norelco aluminum sample holder. A pressure of about 12–15 bars was applied to the press for each sample. The prepared mount was inspected for surface smoothness and evenness of the sample level against the holder before use.

Several types of experiments were made. First, mixtures of dawsonite and quartz in fixed ratios were studied for the effect of grinding on relative peak intensities. Second, known amounts of both minerals were added to a known amount of homogenized sample of dawsonite-free oil shale. As the shale already contained some X-ray-detectable quartz, the total proportions of quartz in such mixtures were undefined; however, because the relative amount of quartz to dawsonite was constant for a given series of runs, the relative intensities of diffraction peaks are meaningful quantities. Finally, a sample of Colorado Green River oil shale containing dawsonite and quartz was prepared for X-ray study by the same procedure used for the synthetic mixtures.

A single Norelco diffraction goniometer and recording unit (copper radiation and nickel filter) was operated at 35 kV and 20 mA for all the experiments. The goniometer was periodically alined. Each mount was repeatedly measured, and each individual scan was completed in less than an hour; therefore, instrumental drifts are considered negligible.

The sample was first scanned at 1°/min goniometer speed and ½-in./min chart speed to record the 15.6° and 32.1° 2θ dawsonite peaks and the 20.9° and 26.6° 2θ quartz peaks. The sample holder was then shifted to two different positions on the goniometer head to see if significant differences in relative peak intensities resulted. If the sample was judged insufficiently homogenized by this procedure, it was broken up and remixed by very light grinding until a scan of the mount resulted in relative peak intensities that were not position-dependent (fig. 3). Detailed measurements then began.

The four peaks of dawsonite and quartz were traced at ¼°/min scanning speed and recorded at ½ in./min chart speed. A time constant of 4 s was used; this reduces the noise but does not significantly affect the peak shape at the scanning speed used. The scale factor was adjusted to obtain maximum intensities without any peak going off the chart. Each peak was traced at three different positions of the sample holder in the goniometer head. Enough background was recorded on either side of each peak to establish a baseline for measurement.

Peak intensities above the baseline were measured in two ways: (1) Peak heights were directly observed in chart-paper units, and (2) integrated intensities were measured planimetrically as areas. A typical set of measurements (table 1) demonstrates the reproducibility of planimeter measurements for a given peak. After several complete runs were measured both ways and showed consistent results, the tedious planimetric method was dropped for the sake of efficiency.

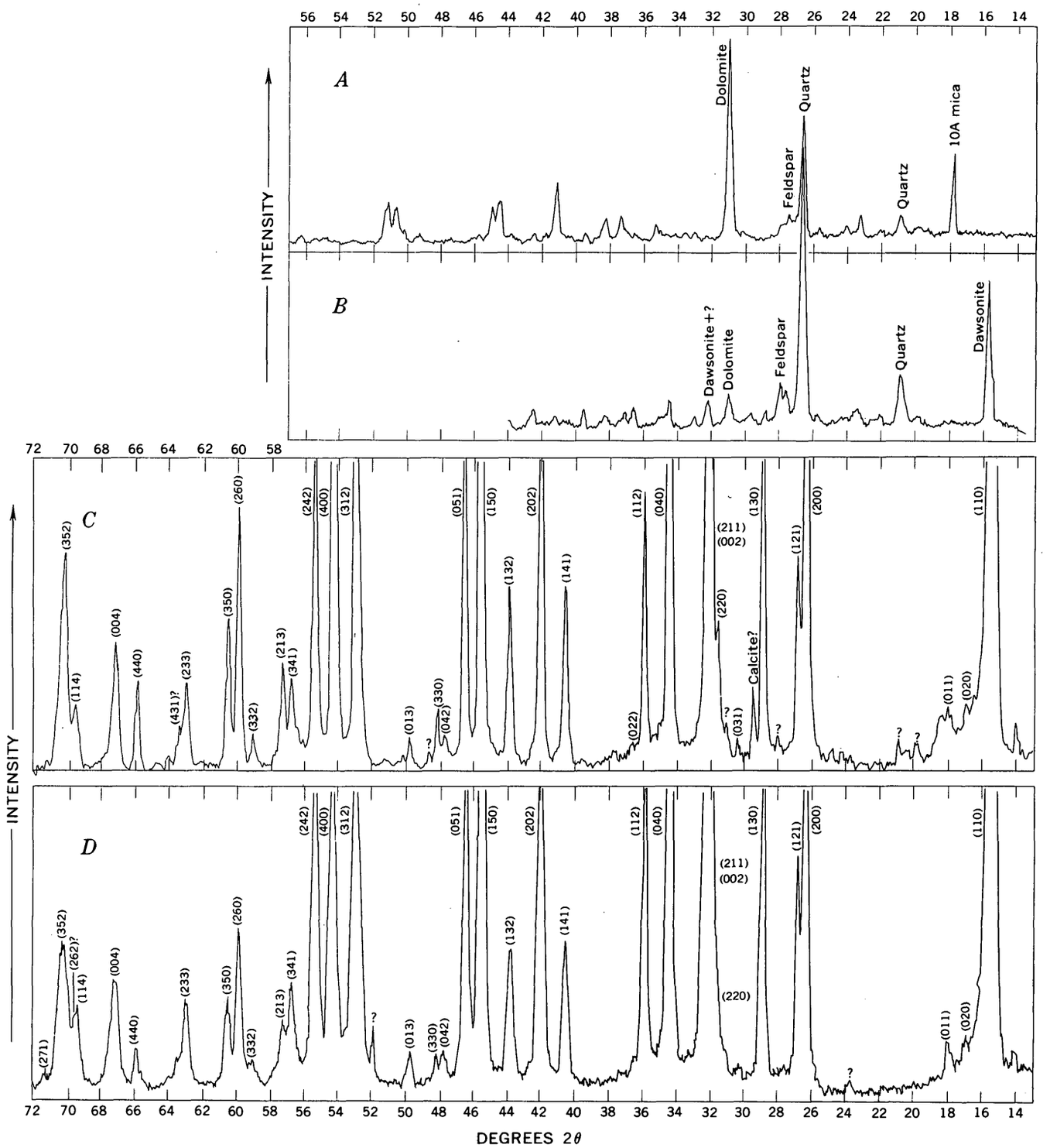

FIGURE 2.—X-ray diffraction patterns of dawsonite and Green River shale used in the experiments. *A*, Dawsonite-free and analcime-free Green River oil shale from Wyoming. *B*, Dawsonite-bearing Green River oil shale from Colorado. *C*, Separate of dawsonite from Kanaskat Junction, King County, Wash. *D*, Dawsonite from Olduvai Gorge, Tanzania (Hay, 1966, p. 42). Notice the better peak quality of trace *C* as compared with *D*. All traces were run on Norelco units, 1° 2θ per minute and ½-in./min chart speed; pressed mount in aluminum holder. Traces *A* and *B*, Geiger counter combined with an AMR monochromator. Time constant, 4 s. Traces *C* and *D*, solid-state detector, full range 200 counts/s. (Use of trade names is for descriptive purposes only and does not constitute an endorsement of the product by the U.S. Geological Survey.)

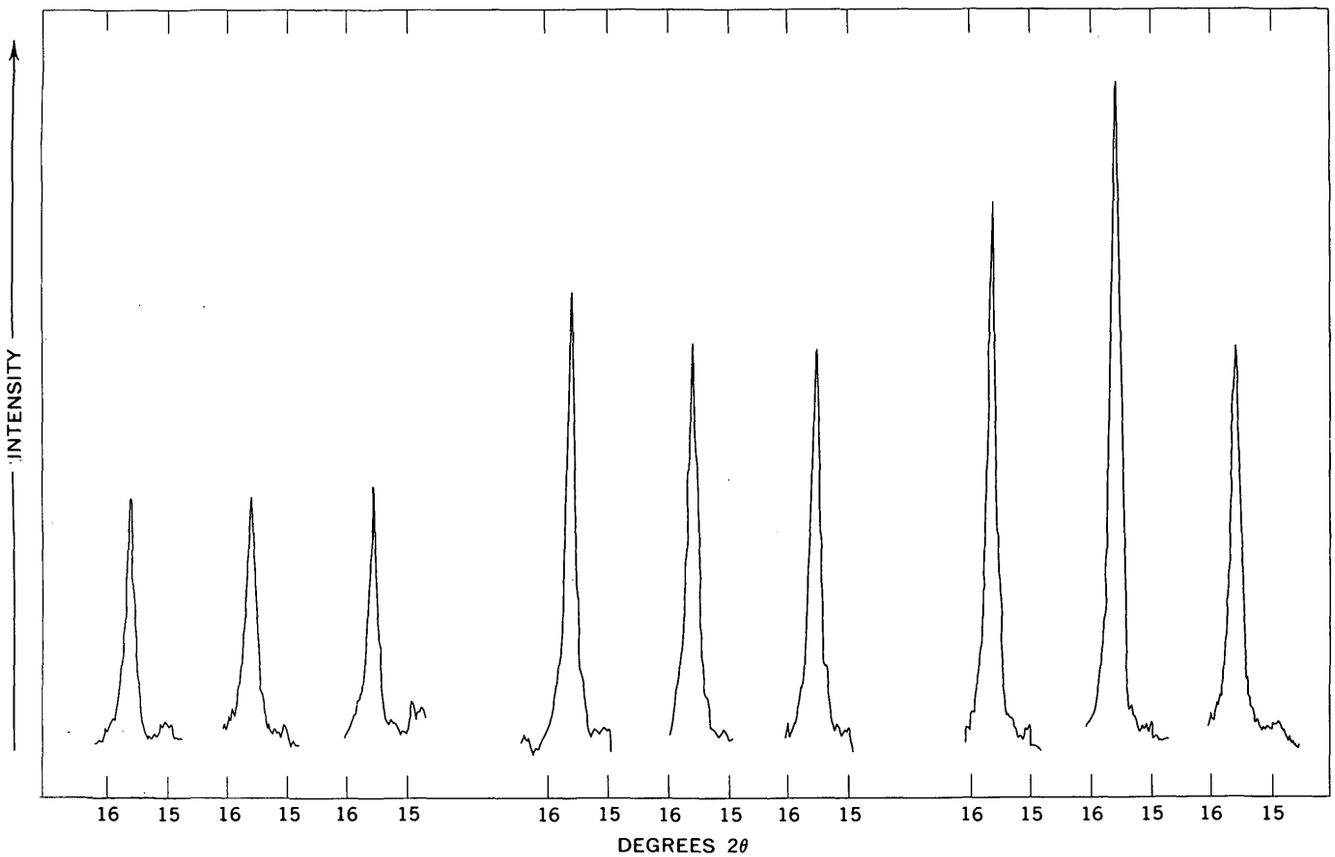

FIGURE 3.—Effect of grain size and grinding on dawsonite peak intensity and reproducibility of peak intensity with different positions of the sample on the goniometer. Dawsonite-bearing Green River shale. Time constant, 4 s; chart speed, ½ in./min. Each triplet shows the sample holder in three different positions in the goniometer; the three triplets were run consecutively on the same sample and the diffractometer unit was idling at untouched instrumental settings while the sample was being treated between triplets of runs. Right-hand triplet, sample reground to pass 150-mesh sieve. Middle triplet, sample reground to pass 270-mesh sieve. Left-hand triplet, sample reground another 5 min. Grinding under acetone.

Individual measurements were averaged, normalized to the same binary-stage instrumental setting, and computed as ratios of peak intensities. These data were then plotted as functions of grinding time.

TABLE 1.—*Sample calculations to show the procedure of peak-intensity measurement and measurement precision on an actual run*

[Quartz and dawsonite; 30 min grinding time]

	Dawsonite								Quartz							
Trace	15.6°				*32.1°				*20.9°				26.6°			
Sample	1	2	3	Avg	1	2	3	Avg	1	2	3	Avg	1	2	3	Avg
Peak height	30	34	29	$31_{.0}$	56	55	53	$54_{.7}$	67	57	65	$63_{.0}$	62	77	68	69
Peak area																
Planimeter measurement No.:																
1	86	98	73		173	173	160		149	159	156		169	206	188	
2	80	100	75		172	166	173		149	153	153		164	209	180	
3	87	101	83	88	169	169	160	169	152	155	153	153	171	205	185	187
4	85	99	83		169	169	167		144	157	150		175	207	180	
5	84	98	83		174	168	172		153	153	152		169	207	187	

*Because of a different setting of the binary stages on the recording panel, these intensity values must be divided by 4 for comparison with the other values.

RESULTS

The data of our study are summarized in figures 4–7. Figure 4 plots various combinations of peak-intensity ratios against increment grinding times. The curves labeled "run 1" refer to a mixture whose starting particle size is no more than 50 μm (−325 mesh); the curves labeled "run 2" refer to a mixture whose starting particle size is in the 75–150 μm range. Equal weights of dawsonite and quartz were used for both series of runs.

The symbols $D_{15.6}$ and $D_{32.1}$ will be used throughout for the intensities of the two dawsonite peaks having 2θ values shown by the subscript; similarly, the symbols $Q_{20.9}$ and $Q_{26.6}$ denote the intensities of the two quartz peaks.

Each point in figures 4–7 is associated with an error bar, which measures the reproducibility of each peak intensity. (See the next section on errors.) For each set of runs the median values of bars are used to derive least-squares regression lines shown; the solid lines are for straight-line regression; the dashed lines, for quadratic regression. The latter led to a much better fit of the data, even though the degrees of freedom remaining are only two or three.

The averaged measurements for $D_{15.6}$ drop sharply (by about 30 percent) between 10- and 20-min grinding and then continue to diminish at a less drastic rate. After 50-min grinding, the peak intensities, measured either way, become practically identical and are independent of the starting grain size, presumably reflecting the fact that after the long grinding the grains have attained a uniform, stationary, though unknown fine state. The value of $D_{32.1}$ is practically unaffected by grinding and is also nearly independent of the initial grain size.

The value of $Q_{26.6}$ (101) is increased by grinding; this result agrees with the conclusions of Brindley and Udagawa (1959). The value of $Q_{20.9}$ (100) is less subject to the effect of grinding, but the effect is still noticeable and is apparently sensitive to initial grain size. These facts of course are reflected in the intensity ratios.

Although ratio plots tend to smooth out the data somewhat, the rapid initial loss of dawsonite intensity

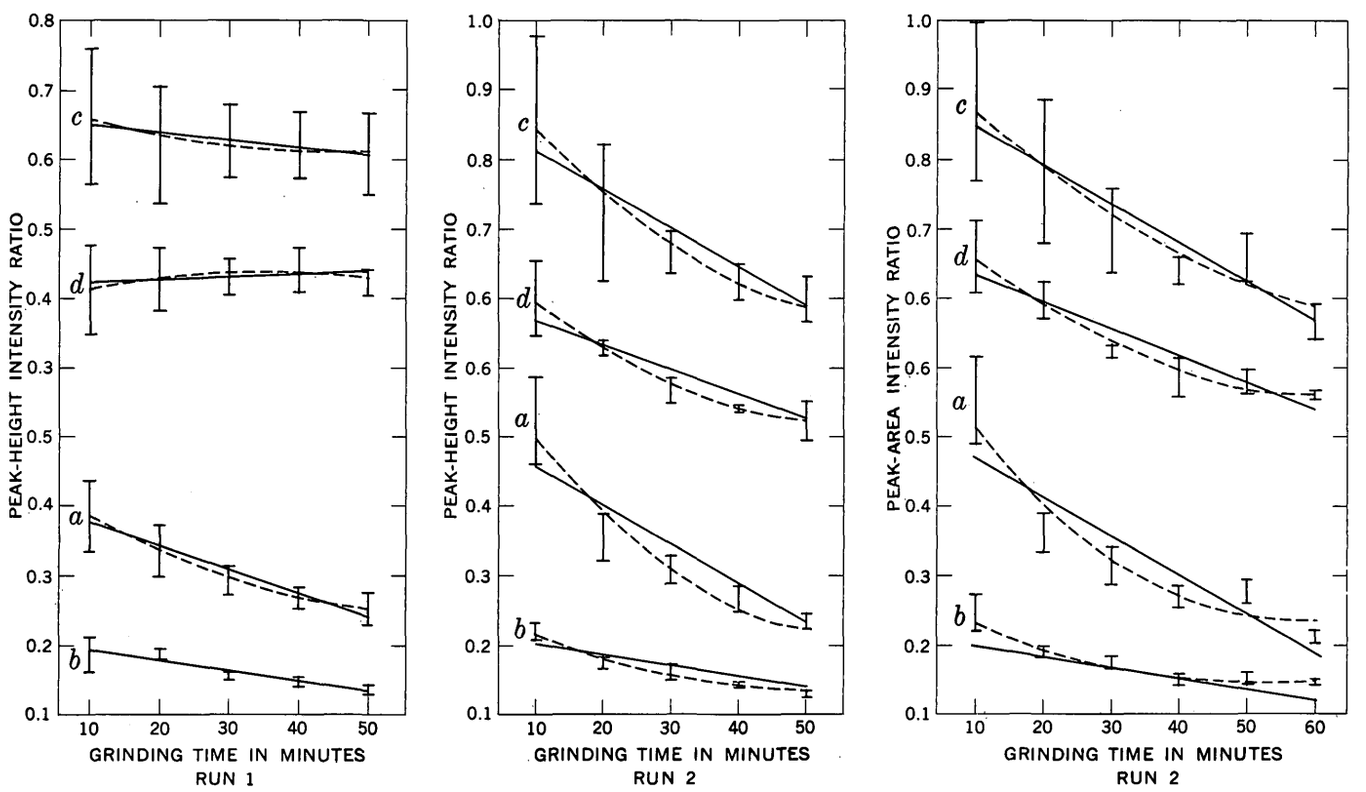

FIGURE 4.—Peak-intensity ratios plotted as functions of grinding time for two mixtures, each containing equal amounts of dawsonite and quartz. Run 1, materials passed through a 325-mesh sieve (50 μm); run 2, starting materials had particle sizes in the 75- to 150-μm range. Data for run 2 are given both as integrated areas and as peak heights to demonstrate the similarity in results obtained by the two methods of measurement. The solid lines represent a linear least-squares regression fit of the averaged data; the dashed lines represent a quadratic fit of the same data. $a = D_{15.6}/(D_{15.6} + Q_{26.6})$; $b = D_{32.1}/(D_{32.1} + Q_{26.6})$; $c = D_{15.6}/(D_{15.6} + Q_{20.9})$; $d = D_{32.1}/(D_{32.1} + Q_{20.9})$.

is obvious. The finer starting material (run 1) diminishes the intensity ratios; it does not, however, eliminate the steady decrease in ratio intensities as grinding time increases.

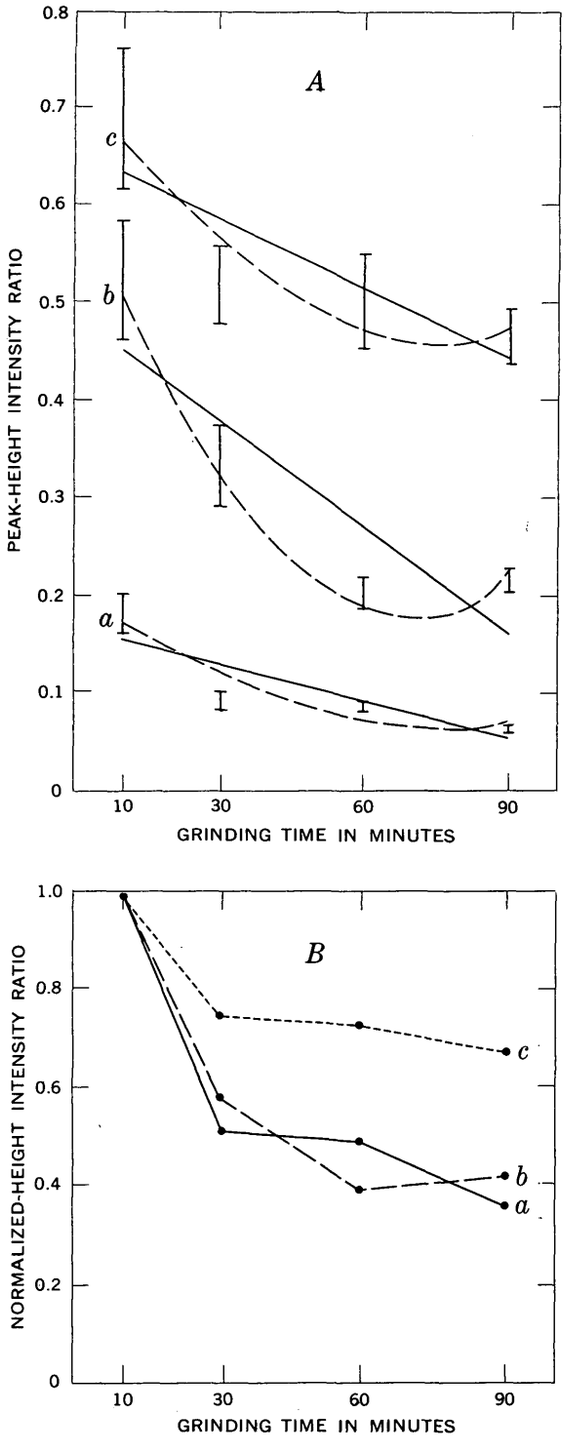

FIGURE 5.—Trend of peak-height intensity ratio, $D_{15.6}/(D_{15.6} + Q_{26.6})$, with increased grinding for three mixtures of dawsonite and quartz are given in *A*. The same data normalized to results of 10-min grinding time are given in *B*. *a*, 25-weight-percent dawsonite; *b*, 50-weight-percent dawsonite; and *c*, 75-weight-percent dawsonite.

The consistent diminution in error bars indicates that increased grinding time improves homogeneity of the sample. Both peak-area and peak-height data are given for run 2 to demonstrate the close agreement between the two methods of measurement.

Figure 5*A* shows the effect of the relative amount of dawsonite on the $D_{15.6}/(Q_{26.6} + D_{15.6})$ ratio, in simple binary quartz-dawsonite mixtures. Three mixtures, respectively containing 25, 50, and 75 percent by weight of dawsonite, were prepared. These mixtures have initial grain size in the 75–150 μm range and were X-rayed after 10, 30, 60, and 90 min of grinding. The rapid decrease in the ratio of intensities after a short period of grinding is again apparent. The impression given that lesser amounts of dawsonite result in less decrease in intensity with time, however, is not real. Figure 5*B* plots the same data, normalized to the intensity values of 10-min grinding. The curves for 25- and 50-percent dawsonite mixtures are indistinguishable. The 75-percent mixture shows the least amount of relative decrease in intensity, presumably because this mixture contains the least amount of the hard mineral quartz.

Figure 6 shows the result of using dawsonite-free Green River shale as matrix. The intensity ratios of peak heights for two mixtures, runs 3 and 4, are plotted against grinding time. Run 3 contained 15-weight-percent dawsonite, and run 4 contained 30-weight-percent dawsonite. The runs contained half again as much quartz as dawsonite in the initial material; the balance of the mixture was made up of shale, which, as previously stated, contained some quartz. The three starting materials had all been ground to pass a 325-mesh sieve before mixing. Again, it is clear that the dawsonite 32.1° peak is least affected by grinding.

A batch sample of dawsonite-bearing Green River oil shale sample was ground to a maximum particle size of about 100 μm. This starting material was ground under acetone at 10-min intervals and was X-rayed by the usual procedure. Figure 7 plots the results of intensity ratios of peak heights. The dawsonite 32.1° peak in this sample was very broad and ill defined; its intensity, however, does not appear to be affected by grinding. This peak in the shale may not be a single peak but may result from superposition of peaks from several phases.

ERRORS

Two kinds of errors contribute to the uncertainties of our data: errors in statistics and errors in technique.

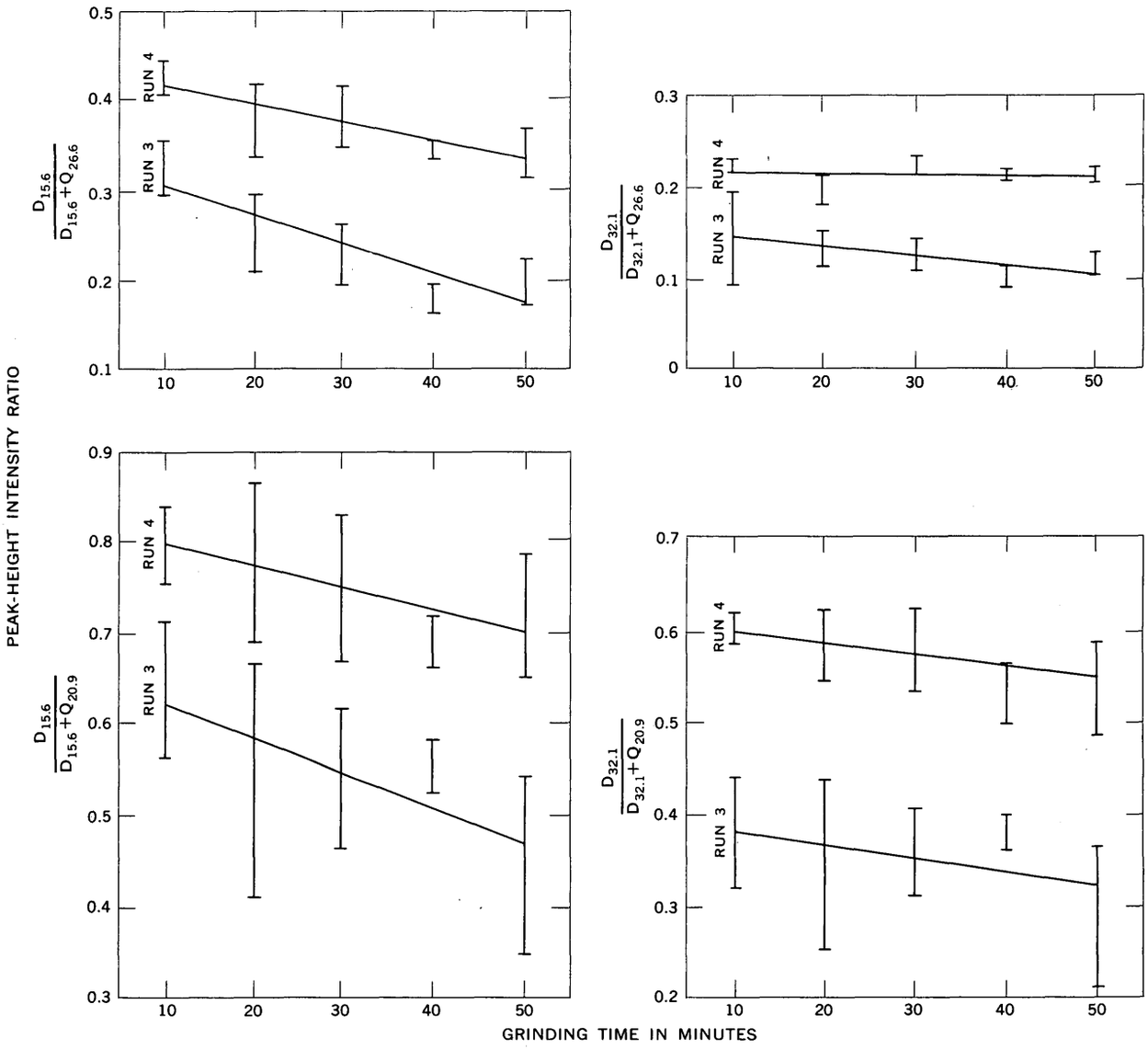

FIGURE 6.—Peak-height intensity ratios versus grinding time for mixtures of Washington dawsonite + quartz + Wyoming Green River oil shale. Run 3 contains 15-weight-percent dawsonite; run 4 contains 30-weight-percent dawsonite. All starting materials were finer than 50 μm in diameter.

Statistical errors are estimated by calculating the probable error of the data points through multiple measurements. Error bars are used in the figures to represent the probable errors about a given intensity ratio, R_{DQ}, where $R_{DQ}=D/(D+Q)$. D and Q, as before, stand for the intensities of chosen dawsonite and quartz peaks.

The probable error on the measurements for one peak, pD (for dawsonite) and pQ (for quartz), is

$$p=\pm 0.6745\ [\Sigma(\Delta)^2/(n-1)]^{0.5} \qquad (1)$$

where Δ is the difference between individual measurements and the average and n is the number of measurements of a given peak.

The probable error on the sum of two values, each having a probable error of pD or pQ (eq 1), is

$$pS=\pm(p\mathrm{D}^2+p\mathrm{Q}^2)^{0.5} \qquad (2)$$

The probable error (pR) on the ratio R_{DQ} is

$$pR_{DQ}=\pm\left[(p\mathrm{D})^2+\frac{\mathrm{D}^2(pS)^2}{(\mathrm{D}+\mathrm{Q})^2}\right]^{0.5}/(\mathrm{D}+\mathrm{Q})$$

The equations for error calculation are based on the discussion in Daniels and others (1949).

Quantitative determination of mineral mixtures by use of the X-ray diffractometer is subject to many sources of error in technique. Figure 3 illustrates the effect of initial particle size and grinding on homogenizing a mineral mixture; it also demonstrates

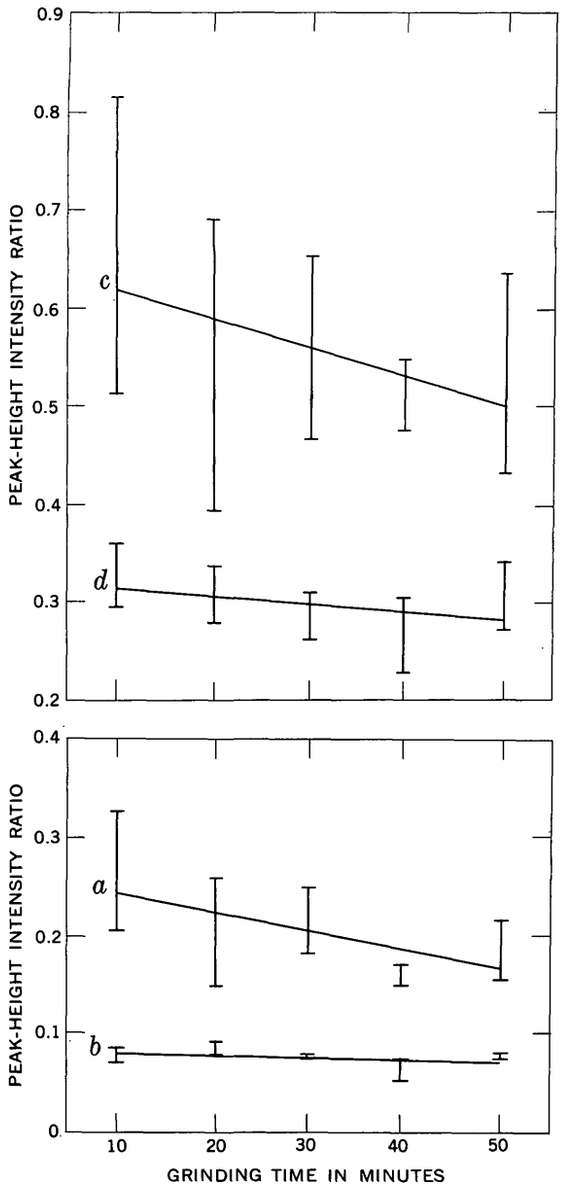

FIGURE 7.—Peak-height intensity ratios versus grinding time for an actual dawsonite-bearing sample of Green River oil shale; *a–d* explained in figure 4.

the reduction of $D_{15.6}$ with grinding. Here, then, are two immediate sources of error due to technique.

Grinding of the mineral mixtures was done in a liquid medium in order to reduce the chance of thermal decomposition of dawsonite and to improve mixing of the materials. Dawsonite is water soluble and also decomposes in most of the common organic solvents. We chose acetone as a wetting agent for grinding because it evaporates quickly without leaving a residue, is less toxic than many other solvents, and within the limits of our experiments shows no evidence of affecting the stability of dawsonite.

In preliminary experiments, we found that dawsonite tends to mat and smear during grinding, thus not to mix evenly with quartz or shale. Powered mortar and pestle are unsuitable even for short grinding times because the dawsonite sticks to the face of the pestle, resulting in a stick-and-slip motion and percussion of the grinding surfaces and lack of homogenization, even when a liquid is used in grinding.

All starting materials were at least finer than 150 μm in diameter (passed through a 100-mesh screen), and weighed mixtures were hand ground for 10 min before X-ray measurements were started. We feel that all materials were fine enough to eliminate the bulk of extinction effects, yet coarse enough to reduce the effects of microabsorption as a principal cause of intensity loss (Klug and Alexander, 1954; Schmalz, 1958). Schmalz (1958) demonstrated that the pressure applied to the handpress in the preparation of sample mounts does not significantly affect the diffracted intensity ratios, if the applied pressure exceeds about 6 bars (100 pounds per square inch).

Lack of homogenization of a sample is a major source of scatter of data. By checking the mount at various positions in the goniometer head, this problem can be somewhat controlled (fig. 3). This problem of achieving a homogeneous sample exists even for the dawsonite-bearing Green River shale (fig. 7) because this mineral tends to be concentrated in thin bands so that an X-ray homogeneous sample still must be artificially achieved.

EVALUATION

The results of our study suggest that use of the X-ray diffraction method for quantitative determination of dawsonite in shales from the Green River Formation must be undertaken with great care.

Klug and Alexander (1954), Bragg (1967), and Braun and Ramspot (1970) discussed various effects that must be taken into account in quantitative mineralogical work by X-ray diffraction methods. Their discussion was complemented, for example, by discussions by Schultz (1964) in a specific application to fine-grained shales.

In addition to the various general factors discussed in the papers cited above, and many others, the following conditions, mainly of mineralogical nature, must be fulfilled:

1. There must be no serious interference between the peaks chosen for measurement and peaks from other minerals.
2. The mineral must be present above a certain mini-

mum amount, so that the method of X-ray diffraction can detect its presence quantitatively. Smith and Milton (1966) reported that the detection threshold for dawsonite in the Green River shale is 3 percent.

3. The mineral must be "resistant" to grinding, or at least its reduction in intensity relative to some reference mineral (such as quartz) must be a reproducible function of time, independent of the amount of the mineral present or the nature of the matrix material.

With these conditions in mind, let us examine the results of our experiments and evaluate the X-ray method for quantitative determination of dawsonite in Green River shale.

In the quartz-dawsonite mixtures, there is no major interference between X-ray peaks. At slow scanning speeds and short grinding times, the dawsonite (200) peak shows up as a slight hump on the flank of the much stronger quartz 26.6° peak, but constitutes no real problem. In the quartz-dawsonite-Green River shale mixtures, the dawsonite 32.1° peak cannot be demonstrated to be free of interference from peaks of other minerals in the shale; therefore the constancy of the peak intensity (fig. 6) may not be real. Many samples of the Green River shale contain significant amounts of analcime (Brobst and Tucker, 1973). The second most intense diffraction peak of analcime, (211), is at 15.8° 2θ. This analcime peak can be resolved from the dawsonite (110) peak at 15.6° 2θ for identification purposes; however, we could not completely separate these two peaks even at slow scanning speeds. Therefore, if analcime is present in appreciable amounts, the intensity of the dawsonite 15.6° peak may not be relied upon even for semiquantitative work because the traces of the two peaks will be partly superimposed and cannot be easily disentangled quantitatively. (See also Brobst and Tucker, 1973, p. 25.) Because the precise cell parameters of analcime formed in sedimentary conditions depend on its chemistry (Coombs and Whetten, 1967), the separation between the dawsonite and analcime peaks in the 15.6°–15.8° region is not a wholly controllable factor.

Though the dawsonite 32.1° peak is the combined effect of the (211) and (002) diffraction maxima, in a truly random powder sample the intensity of this combined peak should be, and is assumed to be, a reproducible quantity.

The effect of organic material—notably kerogen—in the Green River shale on the X-ray diffraction characteristics of minerals has not been studied. J. R. Dyni (written commun., 1970) noted that "organic matter in oil shale rocks has an inhibiting effect in X-ray diffraction analysis, and is not 'transparent' as is commonly thought." Dyni suggested that the organic matter might act as X-ray energy absorbers. Our own X-ray studies on sedimentary and low-grade metamorphic rocks containing high proportions of carbonaceous matter also indicate that carbonaceous matter seriously affects peak intensities. This effect may or may not act on all minerals to the same extent, presumably in part depending on the surface properties of the minerals. Thus, organic matter, abundant in the Green River oil shale, could be another impediment to the use of X-ray diffraction for estimating the relative amounts of minerals.

One of the more striking effects of our data is that apparently erratic results are noted even for fairly well controlled experimental conditions. These are shown by the large error bars associated with most of the ratio plots. These large scatters in results suggest that reliable quantitative data are not easily obtained by this method.

Figures 4–7 show the importance of grinding time on dawsonite peak intensity. Without exception, these peak intensities decrease as grinding time increases, as was already noted by J. R. Dyni (written commun., 1970), Brobst and Tucker (1973), and Huggins, Green, and Turner (1973). Our results (figs. 4–7) show that the initial period of grinding, as long as about 20 min, causes the most severe reduction in $D_{15.6}$, and this part of the curve should be avoided in quantitative work.

By comparing equivalent curves in figures 5–7, rough estimates of the amount of dawsonite in the Green River shale from Colorado can provide a crude test of the method. Comparison of the result with that derived from artificial mixtures of dawsonite and quartz yields estimates of 25 to 50 percent dawsonite in the shale, all seemingly high. The lowest estimate corresponds to the comparisons at short grinding time. Comparison with shale + dawsonite + quartz mixtures yields more realistic estimates of 15 percent or less. However, we do not believe that these numbers are quantitatively significant.

In order to get reproducible results by the X-ray method, longer grinding times are more desirable because the intensities of the peaks are then less sensitive to the vagaries of grinding, as evidenced by the general trend for error bars to shorten as grinding times increases. Short grinding times, although most desirable to attain maximum dawsonite peak intensities, are to be avoided. These points, combined with the fact that much Green River oil shale contains significant amounts of analcime, suggest that X-ray methods are not suited to rapid reliable determination of dawsonite in Green River shale. Other methods,

such as direct chemical assaying (as developed, for instance, by Smith and Young, 1969), and Young and Smith, (1970) or the infrared method (Estep and Karr, 1968) or the statistical method from oil-yield assay (Smith and others, 1972) may be more promising. Huggins, Green, and Turner (1973) suggested that the best method is to combine quantitative X-ray diffraction with the direct chemical method of Smith and Young (1969); however, use of the chemical method would seem to make the X-ray technique redundant.

Where present in appreciable amounts and free of other interfering phases, dawsonite can be estimated by X-ray diffraction to 30 percent of the amount present with relative ease; however, more refined determination requires a disproportionate amount of labor and is not feasible for production-line work.

REFERENCES CITED

Bragg, R. H., 1967, Quantitative analysis by powder diffraction, *in* Kaelble, E. F., ed., Handbook of X-rays for diffraction, emission, absorption, and microscopy: New York, McGraw-Hill Book Co., p. 12–1—12–12.

Braun, R. L., and Ramspot, L. D., 1970, Quantitative phase analysis of rocks by X-ray diffractometry: Livermore, California Univ., Lawrence Radiation Lab. [Rept.] UCLR–50921, 19 p.

Brindley, G. W., and Udagawa, S., 1959, Sources of error in the X-ray determination of quartz: Am. Ceramic Soc. Jour., v. 42, no. 12, p. 643–644.

Brobst, D. A., and Tucker, J. D., 1973, X-ray mineralogy of the Parachute Creek Member, Green River Formation, in the northern Piceance Creek basin, Colorado: U.S. Geol. Survey Prof. Paper 803, 53 p.

Coombs, D. S., and Whetten, J. T., 1967, Composition of analcime from sedimentary and burial metamorphic rocks: Geol. Soc. America Bull., v. 78, no. 2, p. 269–282.

Daniels, Farrington, and others, 1949, Experimental physical chemistry: New York, McGraw-Hill Book Co., 568 p.

Dyni, J. R., and Hite, R. J., 1968, Potential resources of dawsonite and nahcolite in the oil-shale deposits of the Green River Formation, northwest Colorado, U.S.A., *in* United Nations symposium, Development and utilization of oil shale resources, Aug. 26–Sept. 9, 1968, Tallinn, U.S.S.R.: 26 p.

Estep, P. A., and Karr, Clarence, Jr., 1968, The infrared spectra of dawsonite: Am. Mineralogist, v. 53, nos. 1–2, p. 305–309.

Hay, R. L., 1966, Zeolites and zeolitic reactions in sedimentary rocks: Geol. Soc. America Spec. Paper 85, 130 p.

Hite, R. J., and Dyni, J. R., 1967, Potential resources of dawsonite and nahcolite in the Piceance Creek basin, northwest Colorado: Colorado School Mines Quart., v. 62, no. 3, p. 25–38.

Huggins, C. W., Green, T. E., and Turner, T. L., 1973, Evaluation of methods for determining nahcolite and dawsonite in oil shales: U.S. Bur. Mines Rept. Inv. 7781, 21 p.

Klug, H. P., and Alexander, L. E., 1954, X-ray diffraction procedures—for polycrystalline and amorphous materials: New York, John Wiley and Sons, 716 p.

Schmalz, R. F., 1958, A technique for quantitative modal analysis by X-ray diffraction and its application to modern sediments of the Peru-Chile Trench: Cambridge, Mass., Harvard Univ., Ph. D. thesis, 150 p.

Schultz, L. G., 1964, Quantitative interpretation of mineralogical composition from X-ray and chemical data for the Pierre Shale: U.S. Geol. Survey Prof. Paper 391–C, 31 p.

Smith, J. W., Beard, T. N., and Wade, P. M., 1972, Estimating nahcolite and dawsonite contents of Colorado oil shale from oil-yield assay data: U.S. Bur. Mines Rept. Inv. 7689, 24 p.

Smith, J. W., and Milton, Charles, 1966, Dawsonite in the Green River Formation of Colorado: Econ. Geology, v. 61, no. 6, p. 1029–1042.

Smith, J. W., and Young, N. B., 1969, Determination of dawsonite and nahcolite in Green River Formation oil shales: U.S. Bur. Mines Rept. Inv. 7286, 20 p.

Trudell, L. G., Beard, T. N., Smith, J. W., 1970, Green River Formation lithology and oil shale correlations in the Piceance Creek basin, Colorado: U.S. Bur. Mines Rept. Inv. 7357, 212 p.

Vine, J. D., 1969, Geology and coal resources of the Cumberland, Hobart, and Maple Valley quadrangles, King County, Washington: U.S. Geol. Survey Prof. Paper 624, 67 p.

Young, N. B., and Smith, J. W., 1970, Dawsonite and nahcolite analyses of Green River Formation oil-shale sections, Piceance Creek basin, Colorado: U.S. Bur. Mines Rept. Inv. 7445, 22 p.

Jour. Research U.S. Geol. Survey
Vol. 3, No. 1, Jan.–Feb. 1975, p. 31–38

NOTES ON THE ORIGIN OF COLLUMA CRATER, BOLIVIA

By SAM ROSENBLUM, REED J. ANDERSON; ISMAEL MONTES DE OCA,[1]
and EDGAR DELGADILLO;[1] Denver, Colo.; La Paz, Bolivia

Work done in cooperation with the Servicio Geológico de Bolivia

Abstract.—Colluma Crater, on the semiarid Altiplano (high plain) of western Bolivia, is an oval structure having overall dimensions of 6.7 km by 6.0 km. The structure has two almost concentric cuestaform rims (the inner rim is 3.6 km by 3.1 km) composed of poorly consolidated clastic sediments that dip outward. The center of the crater is about 80 m below the maximum height of the rims and about at the altitude of the surrounding plain. Because of the double rim, the centripetal drainage, and the absence of volcanic rocks, this structure is considered a collapsed dome. We believe it was probably formed by the doming of lower Quaternary(?) sediments by a subjacent igneous intrusion, partial retreat of the magma, collapse of the central part of the dome, erosional etching of the two rims, and partial filling of the center by detritus from the walls. Evidence for origin by impact (nickel-iron materials, shock structures, ejecta, and so forth) is lacking or was unrecognized, but this mode of origin is not rejected at this time. Geophysical surveys are recommended to determine whether the structure continues in depth and if an igneous plug is below the crater.

In 1964, geologists of the Geological Survey of Bolivia (Geobol) mapped Colluma Crater as an explosion crater (Paz and Alverez, 1965), probably because of the proximity of volcanoes of the Western Cordillera along the Chilean border, 30–100 km to the west. However, examination of aerial photographs suggests that the structure may have had any one of several origins. Meteorite impact is a likely possibility because of the existence of impact craters and strewn fields in northern Argentina and Chile (Henderson, 1941; Cassidy and others, 1956; Sanchez and Cassidy, 1966).

We visited the crater on May 3–5, 1966, to collect data that might indicate the mode of origin. Our visit was part of a cooperative project of the U.S. Geological Survey and Servicio Geológico de Bolivia; the project was sponsored by the Government of Bolivia and the Agency for International Development, U.S. Department of State. Three geophysical traverses were made; 10 soil samples were taken for analysis; the structure in the northeast half of the crater was mapped; samples of shiny black pebbles and white clayey strata believed to contain microfossils were collected, and nearby Tertiary strata were examined and compared with lithology in the crater. A preliminary report on Colluma Crater was published by Rosenblum, Anderson, Montes de Oca, and Delgadillo (1968). The present report provides additional information about the geology and modes of origin.

Acknowledgments.—We thank J. E. Hazel and T. G. Gibson of the U.S. Geological Survey for work done on the microfossils, and the laboratory staff at Geobol for differential thermal, X-ray, and spectrographic analyses on the samples collected.

REGIONAL SETTING

Colluma Crater, on a large alluvial plain of the Altiplano of western Bolivia at 18°35′ S., 68°05′ W., is about 120 km west-southwest of Oruro, 100 km east of the border with Chile, and 225 km south of La Paz (fig. 1). The plain slopes gently southward to the Salar de Coipasa, a large salt flat. From 12 to 25 km northeast of the crater, the plain is interrupted by partly buried low ridges of folded sedimentary rocks of Tertiary age. The ridges extend discontinuously many kilometres northwest and southeast; several small stocks are concentrated in these Tertiary rocks, 50–60 km southeast of the crater. Similar strata cut by stocks 10–17 km north and 35 km to the west-northwest represent high points of buried mature topography. About 35 km southwest, near Huachacalla, two conical volcanoes stand about 1,000 m higher than the plains, and 100 km to the northwest is the volcano Nevado Sajama, 6,520 m in altitude.

The region is a windswept, semiarid, treeless desert that receives 300 mm or less precipitation per year. Only a sagebrush-type shrub, thola, and grass clumps, paja brava, grow on this high plain; they provide grazing for small herds of llamas. Large expenses of the plain are covered by sand which in places forms

[1] Servicio Geológico de Bolivia.

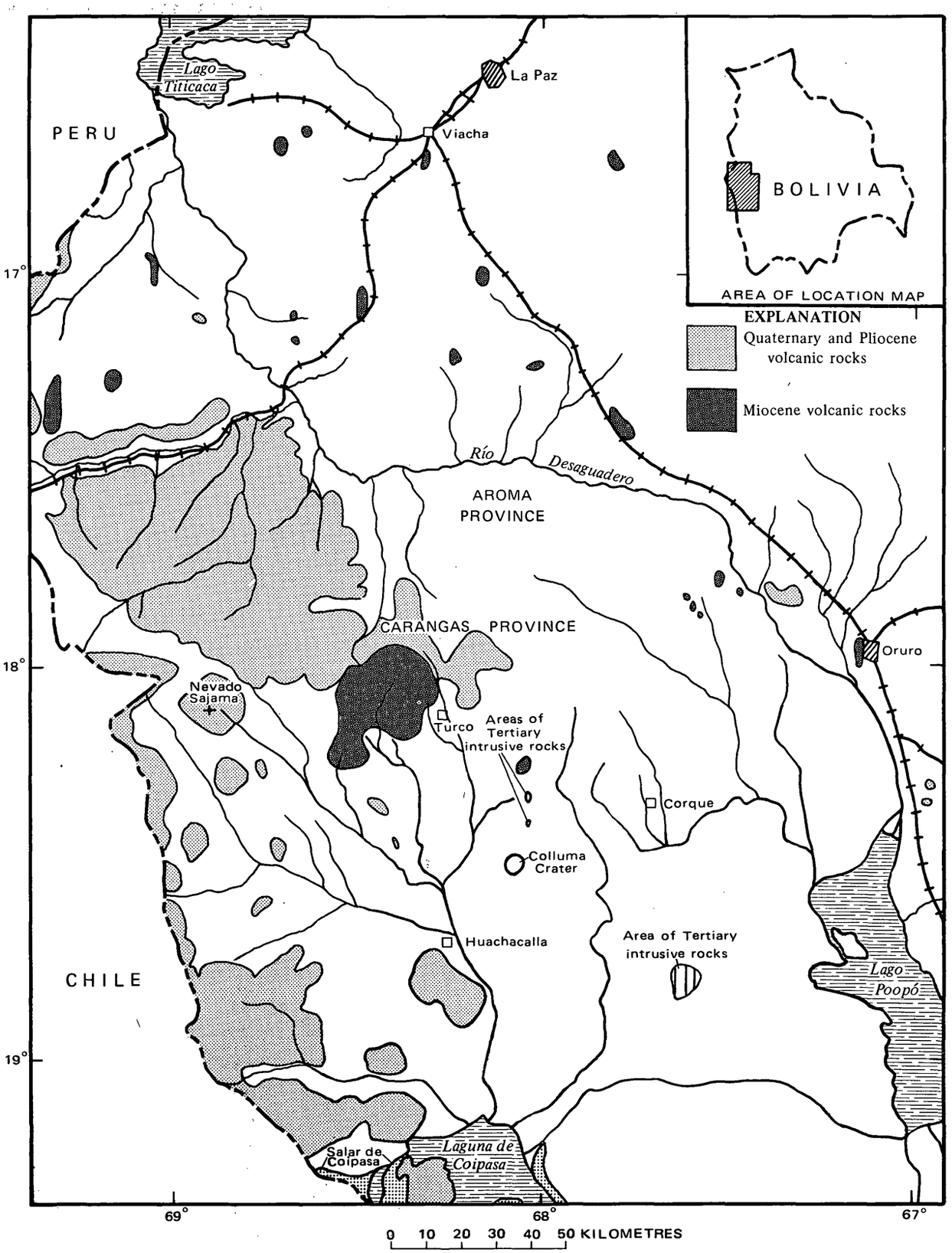

FIGURE 1.—Map showing location of Colluma Crater, Department of Oruro, Bolivia. Geology from Ahlfield and Braniša (1960) and Paz and Alvarez (1965).

dunes as much as 3 m high. Water may be found in temporary shallow lakes only during the rainy season, November to February.

The average altitude of the plain around the crater is about 3,830 m. Rim crests of the crater average 3,900 m and are as much as 3,920 m in altitude on the northwest part of the inner rim; the rims appear, on aerial photographs (fig. 2), to be breached on the west side. However, examination in the field showed a divide about 6 m high between an interior dried lake area (playa) and the external drainage west of the inner rim. All drainage within the inner rim is toward the small playa; drainage between the rims is annular and joins the radial drainage on the outside slope of the structure. The large external intermittent stream courses, east and west of the crater, are entirely in Holocene alluvium and were apparently unaffected by the process that formed the crater.

GEOLOGY OF THE CRATER

Colluma Crater is an eroded dome-shaped structure that consists of two subparallel cuestalike rims; it is oval in plan, the long axis trending about N. 15° E. (see figs. 2 and 3). The overall dimensions are 6.7 km by 6.0 km; the outer rim crest diameters are 5.2 km and 4.1 km, and the inner ridge diameters are 3.6 km and 3.1 km.

The double rim of the crater consists mostly of soft, poorly consolidated, bedded clastic sediments. They are mainly reddish-brown to buff silt, medium to coarse sand, and conglomeratic sand in the inner cuesta; and fine sand, silt, and clay in the outer rim. The fine drainage texture on the northeast half of the outer rim (fig. 2) indicates a very fine grained facies that wedges out to the southwest. Dips of the bedded sediments in the entire structure are generally quaquaversal, but, locally, strikes diverge as much as 75° from the trend of the rim (fig. 3). Because of the short time allotted to the survey, attitudes were measured only in the northeast half of the structure; those shown in parentheses in the southwest half of the inner cuesta on figure 3 were estimated from aerial photographs.

The spacing of the inner and outer rim crests is wider on the west side than on the east, indicating either that the axis of the dome (if the structure is a dome) plunges to the west, or (more likely) that the layers on the west side are thicker than those on the east side of the crater.

Among the sandy layers of the inner cuesta are several lenses of white clayey material, as much as a metre thick, that were thought to be altered volcanic tuff. A sample collected in the northern wall effervesced with dilute acid, and the surface showed minute rodlike and globular forms. A sample of this material was sent to the U.S. Geological Survey in Washington, D.C., for determination of the microfossil content, but microfossil experts were unable to determine whether these forms were of organic origin. A similar sample that was treated with dilute acid gave an insoluble residue (40 percent by weight) of montmorillonite, as identified in Geobol laboratories by differential thermal analysis and X-ray powder diffraction.

The surfaces of the eastern rims are sparsely strewn with shiny limonite nodules that apparently weathered out of the poorly cemented sandy layers. No glass, volcanic or impact, was found.

Most of the floor of the crater is covered with sand, silt, and clay washed from the walls of the inner ridge and carried toward the small playa on the west side of the crater floor. Outcrops of undifferentiated, poorly consolidated sandy strata are partly buried by this material. It is noteworthy that the playa representing the low area of the crater floor is west of the center of the structure. Moreover, erosion is in a youthful to mature stage; thus, considering the incompetence of the strata, we infer that the crater was formed in Holocene time.

We made a brief visit to a low ridge about 15 km northeast of the crater, a ridge where Paz and Alvarez (1965) had mapped Tertiary strata; our objective was to compare these strata with those in the crater. The Tertiary strata were found to be well-indurated moderately dipping conglomeratic sandstone beds that are vastly different from the poorly consolidated sediments of the crater. The many large Tertiary clasts are mainly granitic in composition; the relatively small clasts in the crater sediments are volcanic. The sediments of the crater are decidely younger than these Tertiary rocks.

In the Carangas and Aroma provinces, 60–120 km north of Colluma Crater, soft sediments of the Miocene-Pliocene Totora Formation (described by Meyer and Murillo, 1961, p. 48) resemble the sediments of the crater. The middle part of this formation consists of 920 m of friable, very fine sand and clay that overlie 350 m of medium-hard, medium sand in layers 2–3 m thick.

According to Jenks (1956, p. 184), "The present-day lakes and salt flats of the Altiplano (Poopó, Coipasa, and Uyuni) are relicts of Lake Minchin." Ahlfeld and Branisa (1960, p. 158–164) described Lake Minchin in some detail, and their map (p. 159) indicated that a large area of the Altiplano, including Colluma Crater, was covered by the lake during the last glaciation. They indicated that the lake deposits

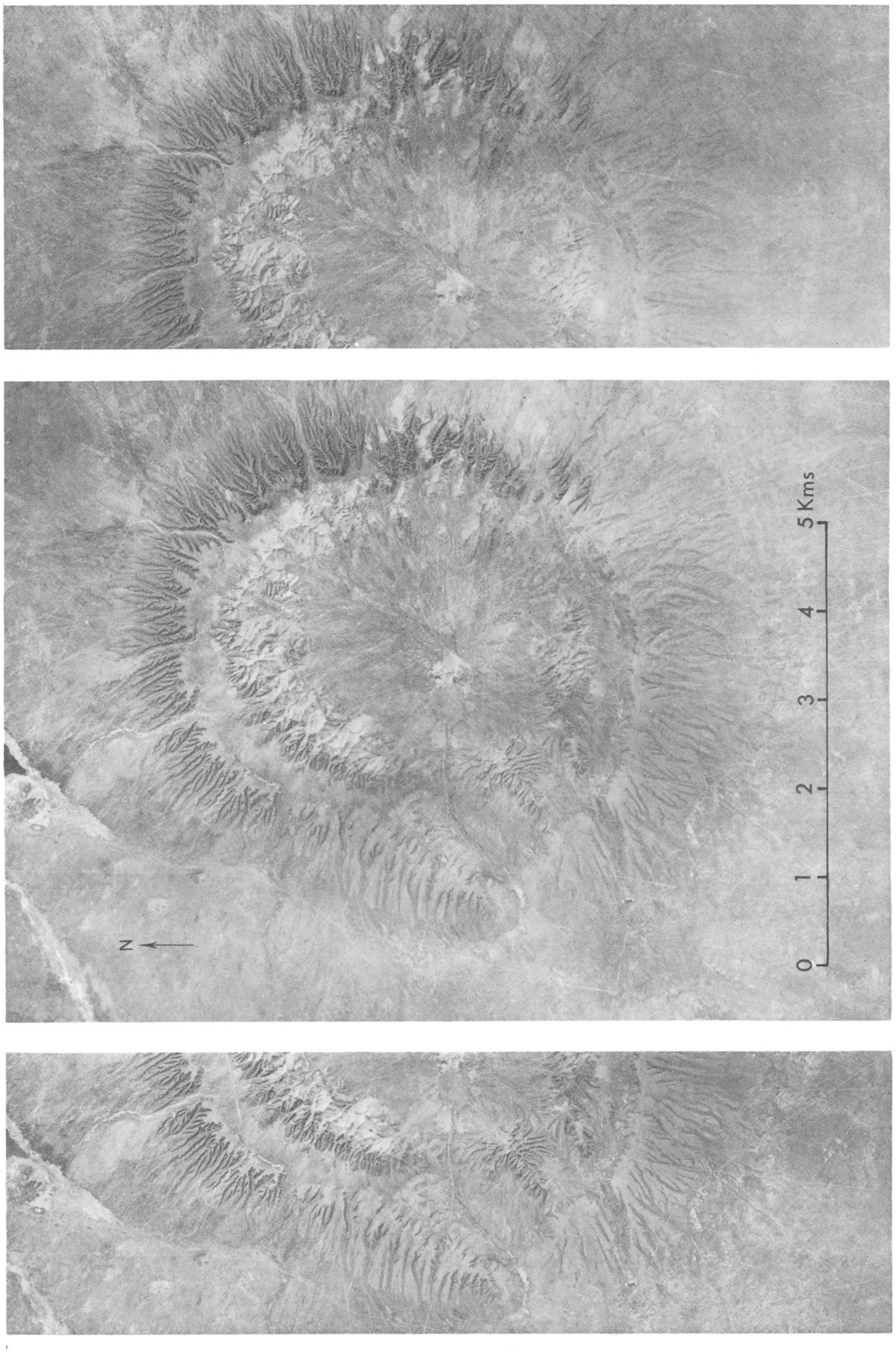

FIGURE 2.—Stereogram of Colluma Crater, for use with pocket stereoscope. Fine white lines are remarkably straight trails about 3 m wide made by Altiplano inhabitants.

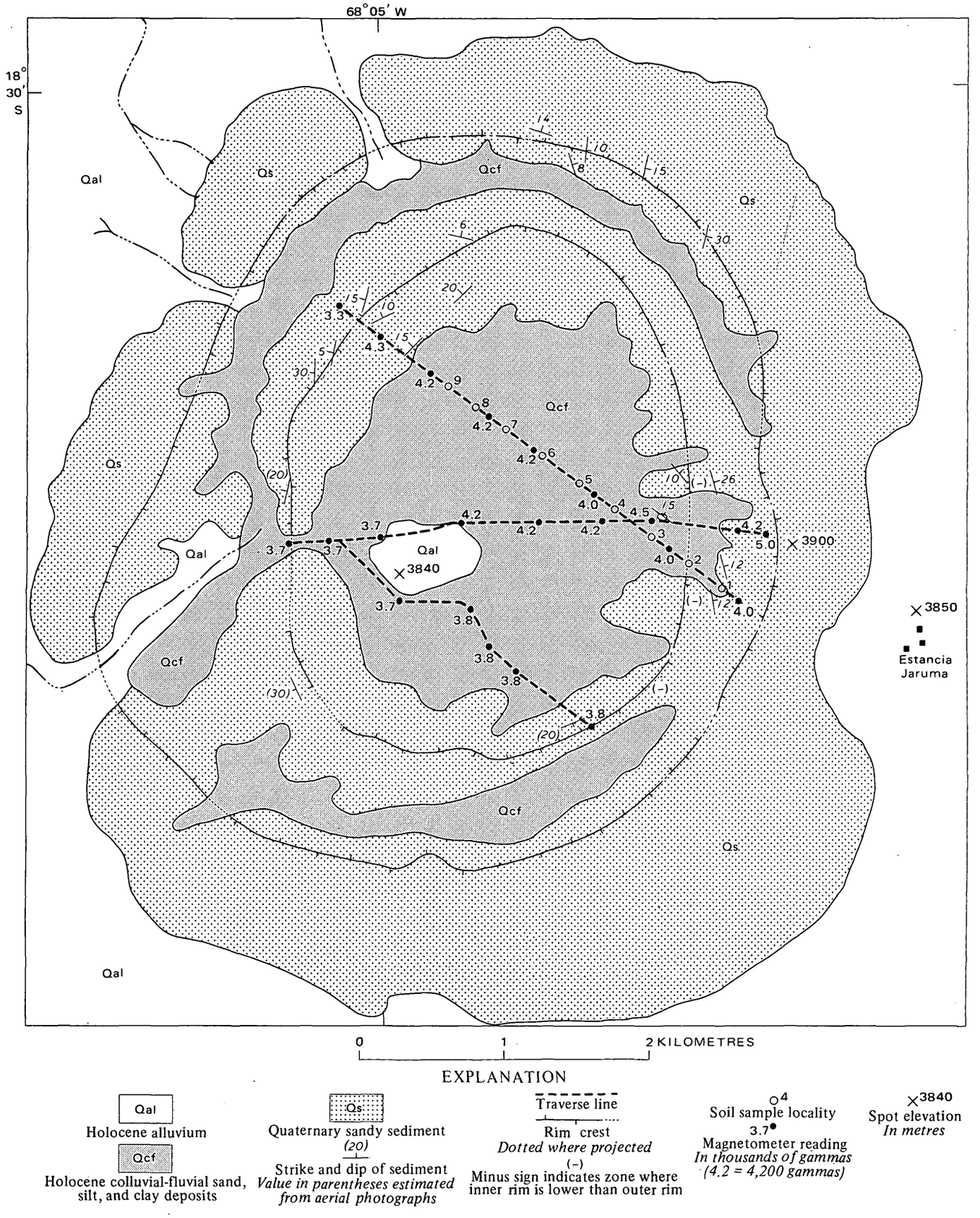

Figure 3.—Geologic sketch map of Colluma Crater. Geology mapped by F. Paz and J. Alvarez, Servicio Geológico de Bolivia, 1965.

include fine sand, clay, calcareous tuff, marl, organic travertine, and calcareous algae.

GEOCHEMICAL AND GEOPHYSICAL DATA

Nine soil samples were collected 250–300 m apart along a trial from southeast to northwest across the crater floor (fig. 3), and, for comparison, another sample was taken from the plain about 12 km east of the structure. Semiquantitative spectrochemical analysis by the Geobol staff indicated that all samples were essentially the same. In view of the hexahedrite-type meteorite occurrences in northern Argentina and Chile (Cassidy and others, 1965; Henderson, 1941), the nickel and iron contents were of great interest, but only traces of nickel and small amounts of iron were found in all samples (table 1).

TABLE 1.—*Spectrographic analyses, in weight percent, of 10 soil samples fom Colluma Crater, Bolivia*

[Analyses by the Servicio Geológico de Bolivia laboratory. M, major constituent; +, detected; tr., trace]

	1	2	3	4	5	6	7	8	9	[1]10
Si	M	M	M	M	M	M	M	M	M	M
Al	M	M	M	M	M	M	M	M	M	M
Fe	+	+	+	+	+	+	+	+	+	+
Mg	M	M	M	M	M	M	M	M	M	M
Ca	+	+	+	+	+	+	+	+	+	+
Na	+	+	+	+	+	+	+	+	+	+
Ti	>1	1	1	1	1	1	1	1	1	1
Mn	+	+	+	+	+	+	+	+	+	+
Ag	Tr.	Tr.	Tr.	Tr.	Tr.	Tr.	Tr.	Tr.	Tr.	Tr.
Ba	.06	.06	Tr.	.06	.06	.06	Tr.	.06	06	.06
Co	Tr.	Tr.	Tr.	0	0	Tr	Tr.	Tr.	0	0
Cu	.001	.0004	.001	.001	.001	.001	.001	.002	.002	.002
Ni	.002	.001	.001	.001	.001	001	.001	.001	.001	.002
Pb	Tr.	Tr.	Tr.	Tr.	Tr.	Tr	Tr.	Tr.	Tr.	Tr.
Su	Tr.	Tr.	Tr.	Tr.	Tr.	.004	.004	.004	.01	.01
Sr	.1	.02	.02	.01	.01	.01	.01	.01	.01	.004
Ga	.01	.01	.01	.01	.01	.01	.01	.01	.01	.01
V	01	.01	.02	.02	.02	02	.02	.02	.01	.02
Zr	.01	.006	.01	.003	.01	.01	.03	.01	.003	.006

[1] Soil sample collected about 12 km east of Colluma Crater.

Geophysical surveys were made with a pocket-type magnetometer and a small electromagnetic unit along a southeast-northwest trail, along an east-west trail, and in a traverse from the west side of the dry lakebed to a point on the southeast inner rim. The signal on the electromagnetic unit was fairly constant except over the dry lake area where it was somewhat higher, probably because of underground water. The magnetometer reading at the base camp, Estancia Jaruma, was −4,200 gammas. Across the crater floor on all three traverses, readings were between −3,700 and −4,500 gammas. The only anomalies noted were on the east inner rim where the reading was −5,000 gammas and on the northwest inner rim where the instrument read −3,300 gammas (fig. 3). Thus, within the limitations of the two instruments, no subjacent nickel-iron masses were detected that might indicate a metallic meteorite origin for the structure.

MODE OF ORIGIN

Six possible modes of origin for Colluma Crater were postulated before the visit to the site:

1. Volcanic caldera formation.
2. Explosion crater formation.
3. Normal dome formation due to compressive forces.
4. Salt dome.
5. Meteorite impact.
6. Collapsed dome.

Considering the above data and the lack of volcanic layers and ejecta, the first two modes of origin can be rejected. Much more disturbance of the layers and widespread debris would be expected if a volcanic explosion had caused this structure.

Colluma Crater has all the features of a normal dome formed by compression, except for the singular feature of interior drainage. A dome that had formed as a result of compressive forces and was eroded to its present ground level during and after deformation could only have been carved by a through-flowing or an out-flowing stream. By projecting the 15° average dip of the layers over the structure it can be estimated that at least 2.5×10^9 m^3 of material would have had to be removed to produce the crater as it is today. As there is no out-flowing drainage—indeed the floor of the crater is aggrading owing to infilling—formation by compression must be rejected.

Doming by a salt plug (about 3 km in diameter) is unlikely for similar reasons; moreover, salt domes are unknown in this part of the Andes. Local diapiric structures of gypsum occur in the nearby Tertiary strata, but these are at most tens of metres wide. Doming by a salt plug and collapse following solution of large amounts of salt is unlikely, for such a process would require cavern formation on an immense scale, and such caverns are not known in this region. Moreover, extensive solution of subjacent soluble material would necessitate upward flow of water to the base level of this region, the Salar de Coipasa.

The absence of impact glass, recognizable meteorite fragments, and impact-shocked structures makes a meteorite-impact origin doubtful. A mass large enough to have formed this crater would surely have vaporized completely on impact and perhaps thrown debris several kilometres in all directions. Presumably, the soil within and around the structure would contain anomalous amounts of nickel and iron, if the meteorite were like the hexahedrite meteorites of northern Argentina (Cassidy and others, 1965) and northern Chile (Sanchez and Cassidy, 1966; Henderson, 1941). Cassidy, Villar, Burch, Kohman, and Milton (1965, p. 1062) postulated that the Chilean meteorites represent a second fall from the same swarm of me-

teorites that in part fell at Campo del Cielo in northern Argentina after the Earth had turned 22° (fig. 4). On projecting the N. 60° E. line of flight beyond the Chilean strewn field into Bolivia, Colluma Crater is

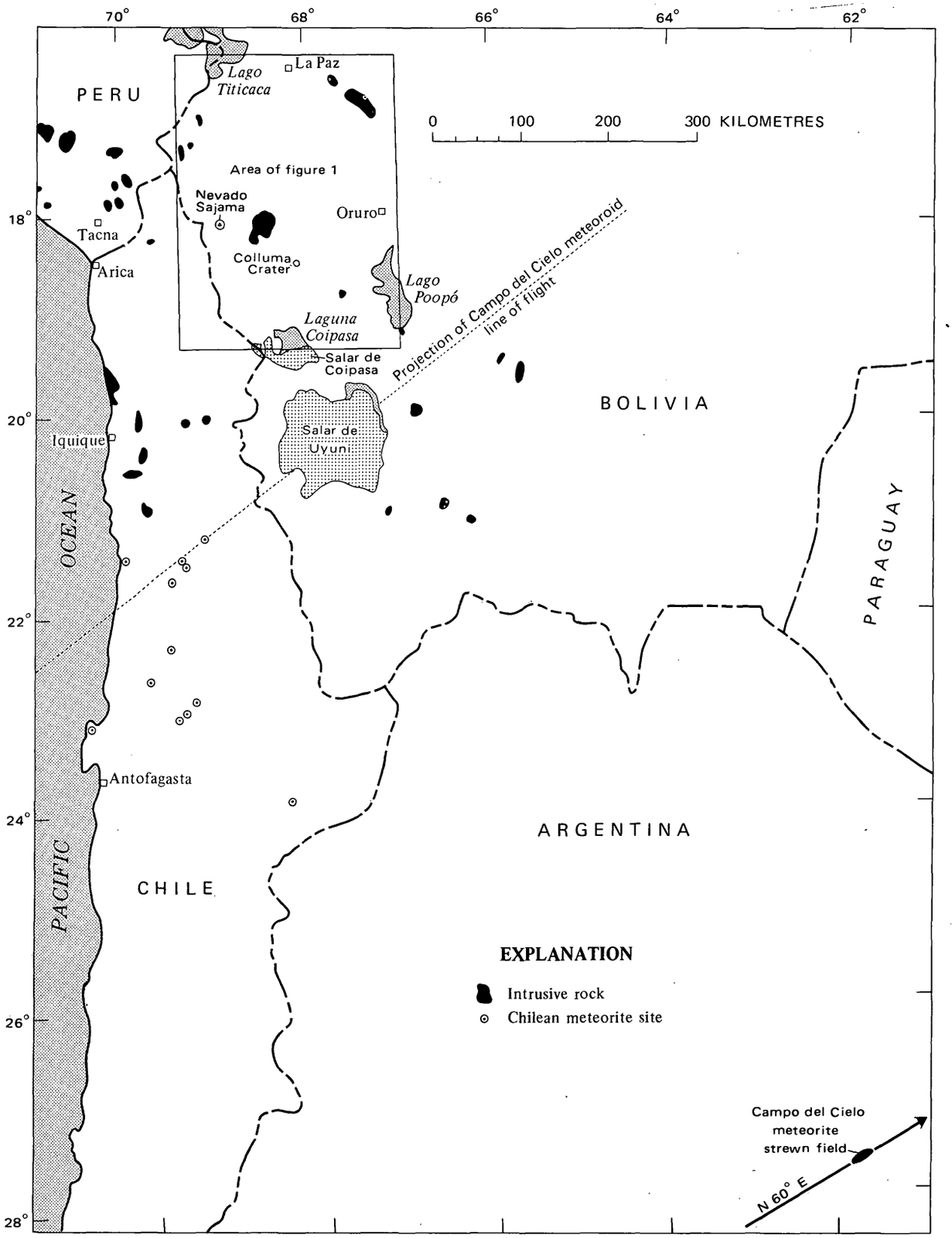

Figure 4.—Relation of Colluma Crater to meteorite sites in Argentina and Chile.

seen to lie about 175 km northwest of this line. A path starting about 23°30′ west of Campo del Cielo would intersect Colluma Crater, but not the Chilean meteorite sites as well. It must be concluded that if Colluma Crater was formed by impact, then the event was unrelated to the events in northern Argentina and Chile.

Four groups of presumed impact craters noted by Thomas (1969) lie along the same projected line of flight, but the material found in the craters is glassy to fine grained and resembles amygdaloidal lava. Thomas (1969, p. 908) interpreted this material to be from a metorite swarm or a large meteorite which must have subdivided high in the Earth's atmosphere. On projecting the N. 42° E. trend of these groups of craters northeastward, we note that this line also fails to come close to Colluma Crater.

One hypothesis suggests a satisfactory mode of origin: the collapse of a sedimentary dome over a partly retreated igneous plug. Origin of this structure would have required the unique condition whereby an igneous mass rose close enough to the surface to form a "blister" about 6½ km in diameter. As indicated in figure 5, a subjacent intrusion probably domed the soft sediments, then retracted to form an empty space into which the center of the dome collapsed of its own weight. Considering the outcrop pattern of the sandy layers of the inner rim, the ring fault or zone of fault planes along which the collapse occurred must have been about 3–3½ km in diameter. The center of the dome had to drop at least 900 m, and possibly as much as 1,300 m.

Evidence for the ring faults was difficult to find on our brief visit. Exposures of the poorly consolidated sandy layers of the inner rim did not yield any evidence of faulting or shearing, and infilling has covered most of the inside slopes of this rim. However, the diverse dip directions of outcrops within the crater are considered to be evidence in favor of collapse. These partly buried segments of the roof of the dome would have been rotated enough to show attitudes that differed from those of the less disturbed parts of the rim. The singular feature of interior drainage (noted above) provides strong evidence for origin by collapse.

Finally, the possibility of a subjacent intrusive is strongly supported by the existence in the region of a number of Quaternary(?) stocks that are of the same order of magnitude that is required of the postulated igneous piston below Colluma Crater. We recommend geophysical surveys of Colluma Crater that would determine whether the domal structure continues in depth and whether a subjacent igneous body exists that caused the doming.

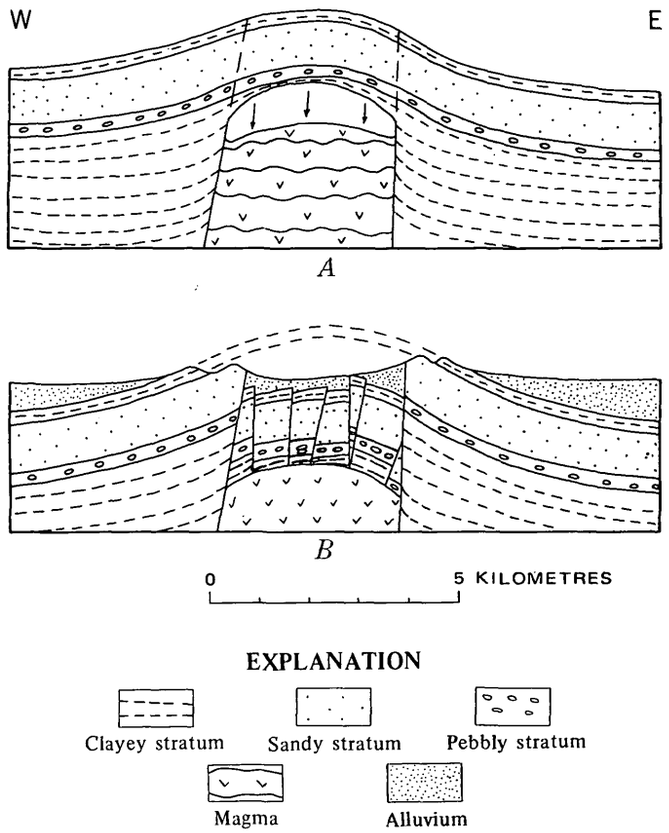

FIGURE 5.—Diagrammatic mode of formation of a collapsed dome. *A*, Molten or mushy magma has retreated after doming soft sediments. *B*, Center of dome collapsed into empty space above plug.

REFERENCES CITED

Ahlfeld, Federico, and Braniša, Leonardo, 1960, Geología de Bolivia: Inst. Boliviano Petróleo, 245 p.

Cassidy, W. A., Villar, L. M., Bunch, T. E., Kohman, T. P., and Milton, D. J., 1965, Meteorites and craters of Campo del Cielo, Argentina: Science, v. 149, no. 3688, p. 1055–1064.

Henderson, E. P., 1941, Chilean hexahedrites and the composition of all hexahedrites: Am. Mineralogist, v. 26, no. 9, p. 546–550.

Jenks, W. F., ed., 1956, Handbook of South American geology —An explanation of the geologic map of South America: Geol. Soc. America Mem. 65, 378 p.

Meyer, H. C., and Murillo, J. E., 1961 Investigaciones geológicas en le Faja cuprífera altiplánica; sobre la geología en las provincias Aroma, Pacajes y Carangas: Bolivia, Dept. Nac. Geol. Bol. 1, p. 1–49.

Paz, F., and Alvarez, J., 1965, Titiri: Servicio Geol. de Bolivia geologic map sheet 5938, scale 1:100,000.

Rosenblum, S., Anderson, R., Montes de Oca, I., and Delgadillo, E., 1968, Crater Colluma—impacto de meteorito o estructura de colapso: Soc. Geol. Boliviana, Bol. 7, p. 1–10.

Sanchez, Joaquin, and Cassidy, William, 1966, A previously undescribed meteorite crater in Chile: Jour. Geophys. Research, v. 71, no. 20, p. 4891–4895.

Thomas N., Arturo, 1969, Vorläufige Mitteilung über einen Meteoritenregen an der Quillagua-Oase, Provinz Antofagasta, Chile: Geol. Rundschau, v. 58, no. 3, p. 903–908.

Jour. Research U.S. Geol. Survey
Vol. 3, No. 1, Jan.–Feb. 1975, p. 39–43

K-Ar AGE OF THE SIMILKAMEEN BATHOLITH AND KRUGER ALKALIC COMPLEX, WASHINGTON AND BRITISH COLUMBIA

By K. F. FOX, Jr., C. D. RINEHART, and J. C. ENGELS, Menlo Park, Calif.

Abstract.—Twelve K-Ar age determinations from the Similkameen batholith and the contiguous Kruger Alkalic Complex, including seven newly reported here, range from 69.9 m.y. to 177.2 m.y. Ages of coexisting hornblende and biotite show discordancies ranging from about 72 m.y. to 106 m.y., with hornblende consistently showing the greater analytical age. The hornblendes, with one exception, show increasing analytical age with increasing potassium content and approximately fit a 191.0-m.y. ^{40}Ar (radiogenic)/K isochron. The isochron shows a negative intersection with the ^{40}Ar (radiogenic) axis, indicating partial argon loss. The large negative deviation from the isochron of one low-potassium sample suggests that the isochron is biased to older ages. If so, the Similkameen and Kruger rocks probably crystallized between roughly 177 m.y. and 191 m.y. ago. The discordancies between hornblende and coexisting biotite are attributed to argon loss during one or possibly more episodes of thermal metamorphism, the most recent of which was probably between about 50 and 70 m.y. ago. This bracket is based on the age of apparently unmetamorphosed sedimentary deposits containing detritus from the Similkameen and Kruger bodies and the analytical age of the youngest biotite.

The Similkameen batholith (Daly, 1906, 1912) is composed of quartz monzonite, granodiorite, and monzonite totaling about 315 km^2 (122 mi^2) in area. It is partly girdled by shonkinite, malignite, pyroxenite, and nepheline syenite of the Kruger Alkalic Complex, totaling about 45 km^2 (17 mi^2) in area. The complex, here named for Mount Kruger, located 2 km (1.2 mi) to the northeast (fig. 1), has previously been described by Daly (1906, 1912) and by Campbell (1939). The batholith is zoned, with quartz monzonite and granodiorite in the interior grading outward to monzonite at the contact with the bordering alkalic rocks (Rinehart and Fox, 53–56, 1972). The alkalic rocks intrude the enclosing metamorphic rocks of the Kobau Formation (fig. 1) and grade inward to the monzonitic outer shell of the batholith. The alkalic complex is also cut by dikes resembling rocks of the batholith. These relations suggest that, although the exterior phases were emplaced first, the batholith and Kruger Alkalic Complex are the coeval elements of a composite pluton (Rinehart and Fox, 1972).

The Kobau Formation unconformably overlies the Upper(?) Permian Anarchist Group and is cut by the Loomis pluton (fig. 1), from which hornblende and biotite yielded K-Ar ages of 194±6 m.y. and 179±5 m.y., respectively (Rinehart and Fox, 1972, p. 46, 52). Judging from the K-Ar data, the Loomis pluton is probably Late Triassic, or perhaps older. Therefore the Kobau is probably Late Permian or Triassic in age. The Kobau consists of an unfossiliferous sequence of greenstone, greenschist, and metachert, lithologically similar to the Upper Triassic Nicola Group northwest of the area of figure 1, in Canada. The Kobau has been regionally metamorphosed within the greenschist facies in the eastern part of the study area and within the amphibolite facies in the western part.

Arkose and interlayered conglomerate composed of coarse, bouldery detritus, including cobbles of granodiorite, monzonite, and shonkinite eroded from the Similkameen batholith and Kruger Alkalic Complex, contain a fossil flora of probable Eocene age (J. A. Wolfe, in Rinehart and Fox, 1972, p. 61). These epielastic deposits are cut by several dacite plugs, two of which yielded hornblende K-Ar ages of 51.4 and 52.1 m.y., respectively (Rinehart and Fox, 1972, p. 62).

The foregoing field relations indicate that the Similkameen batholith and the Kruger Alkalic Complex are definitely Permian or younger and—considering the likely correlation of the Kobau with the Nicola—are probably Late Triassic or younger. They are not younger than Eocene.

Cannon (1966) measured a hornblende-augite K-Ar age of 152±9 m.y. on a sample (W–65–1, table 1) described as "Kruger syenite" from a locality near the north edge of the composite pluton (fig. 1). In addition, Engels (1971) reported K-Ar ages of two samples collected from the composite pluton (L–301, L–618, table 1).

A Pb-alpha age of 114 m.y. was reported by Larsen, Gottfried, Jaffe, and Waring (p. 57, 1958) for a sample (G–122) of tonalite collected from an outcrop

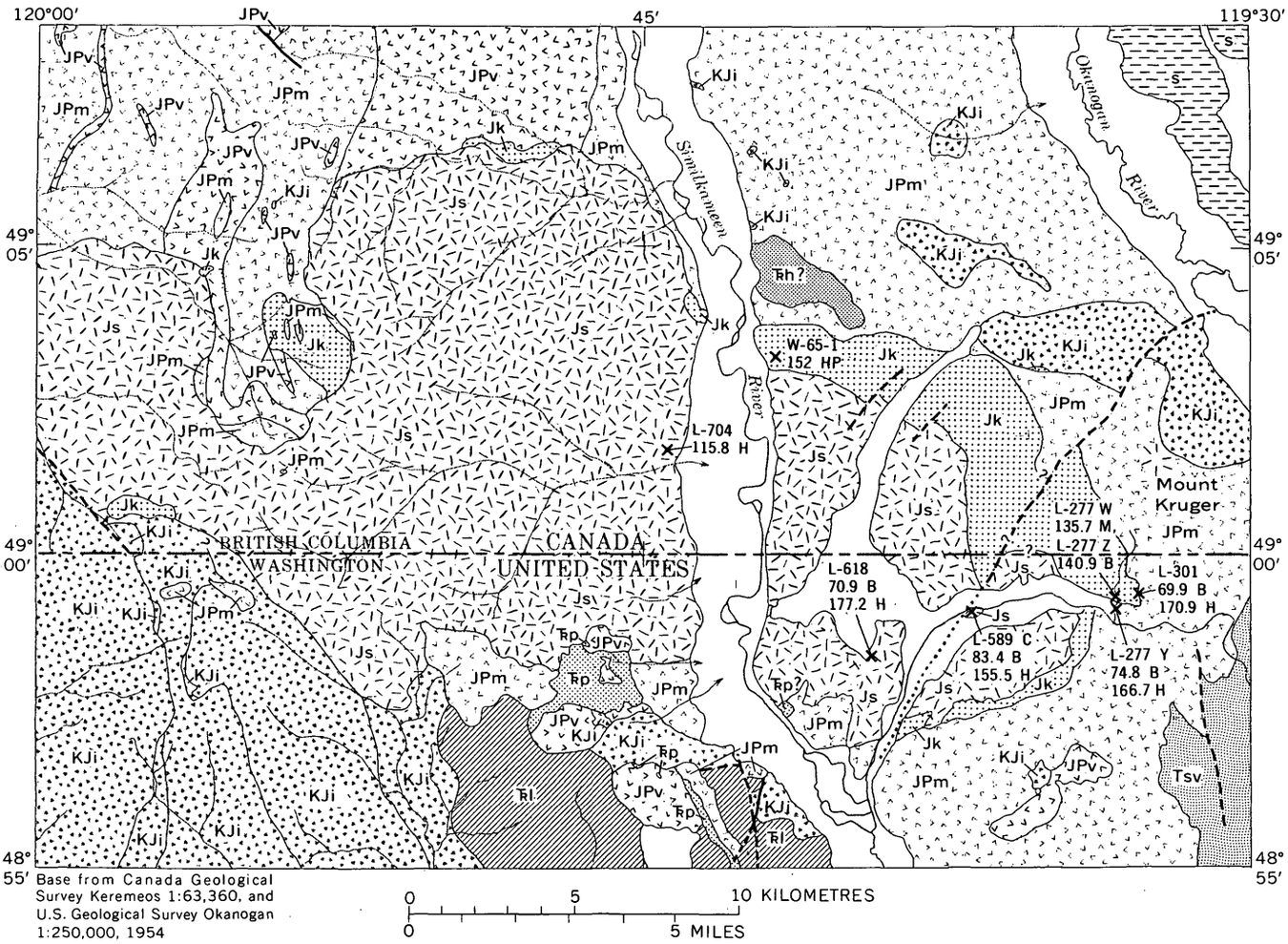

FIGURE 1.—Geologic map of the Similkameen batholith and Kruger Alkalic Complex, showing sample localities and age determinations.

within the northeastern part of the Similkameen batholith. Reported lead content was low (averaging 7.3 ppm), and in view of the fact that the lead determinations were made before later improvements in analytical techniques (Stern and Rose, p. 607–608, 1961), the reported lead value is suspect; hence this Pb-alpha age is disregarded here.

Both the batholith and the Kruger Alkalic Complex show evidence suggestive of postconsolidation cataclasis. For example, intergrain contacts in both Similkameen monzonite and Kruger shonkinite and malignite commonly are markedly to slightly mortared. Daly (p. 455, 1912) hypothesized that the cataclasis of the Kruger resulted from forceful intrusion of the nearby Similkameen batholith. Since similar textures are also widely distributed through at least the southeast fifth of the batholith itself, we infer that the mortar texture is probably due to tectonic forces applied to the Kruger and the Similkameen simultaneously at some time after their consolidation.

In addition, primary mafic minerals in the composite pluton, including hornblende (hastingsite in the alkalic rocks), augite, and biotite are extensively replaced by epidote and chlorite. Also, primary plagioclase, typically andesine in the batholith and oligoclase in the alkalic rocks, is weakly to strongly saussuritized. The alteration implied by the presence of these secondary minerals is consistent with the interpretation of thermal metamorphism of the composite pluton, although it is possible that the alteration is deuteric.

ANALYTICAL METHODS AND RESULTS

Argon determinations were made using standard techniques of isotope dilution on a Nier-type 6-in. 60° mass spectrometer. Potassium determinations were made by Lois Schlocker on an Instrumentation Lab-

EXPLANATION

	Surficial deposits—Alluvium and glacial drift	QUATERNARY
Tsv	Sedimentary rocks, andesitic to dacitic lava flows, and hypabyssal intrusive rocks	TERTIARY
KJi	Quartz monzonite and granodiorite—Contacts between contiguous plutons shown where known	CRETACEOUS AND JURASSIC
Js	Similkameen batholith—Quartz monzonite, granodiorite, and monzonite	JURASSIC
Jk	Kruger Alkalic Complex—Malignite, shonkinite, nepheline syenite, and pyroxenite	JURASSIC
Ŧl	Loomis pluton—Quartz diorite and granodiorite	TRIASSIC
Ŧp, Ŧh	Ultramafic rocks Ŧp, peridotite, serpentinized peridotite, and serpentinite Ŧh, hornblendite	TRIASSIC
JPm, JPv	Eugeosynclinal stratified volcanogenic rocks and related hypabyssal intrusive rocks JPm, Kobau, Ellemeham, and Shoemaker Formations, and Anarchist Group—Mainly greenstone, metachert, phyllite, metaconglomerate, slate, marble, and schist JPv, Old Tom and Palmer Mountain Formations—Mainly greenstone, amphibolite, and metagabbro	JURASSIC(?) TO PERMIAN
s	Shuswap Series—Mainly layered gneiss, orthogneiss, and pegmatite. Includes Vaseaux Formation	AGE UNKNOWN
× L-618 70.9 B 177.2 H	Sample locality showing sample number and age in million years—Suffix denotes mineral as follows: B, biotite; M, muscovite; H, hornblende; HP, hornblende-pyroxene mixture	
———	Contact—Approximately located, queried where doubtful	
———	Fault—Dashed where approximately located, dotted where concealed, and queried where doubtful	

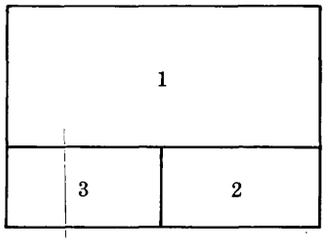

Data for geologic map modified from indicated sources
1. Bostock (1940)
2. Rinehart and Fox (1972)
3. Hibbard (1971)

FIGURE 1.—Continued.

TABLE 1.—K-Ar *mineral ages, in million years, of the Similkameen batholith and Kruger Alkalic Complex*

[J. C. Engels, analyst, this paper. Sample locations in fig. 1]

Sample	Lithology	Mineral	K (percent)	^{40}Ar (radiogenic) (mol/g)	Atmospheric Ar (percent)	Age	Sources of data
Similkameen batholith							
L-589C	Granodiorite	Biotite	6.71 6.72	1.020×10^{-9}	7.4	83.4±2.5	This paper.
		Hornblende	.98 .99	2.843×10^{-10}	11.2	155.5±4.7	Do.
L-618	Granodiorite	Biotite	-----	----------	---	[1] 70.9±2.1	Engels, 1971.
		Hornblende	-----	----------	---	[1] 177.2±5.3	Do.
L-704	Granodiorite	Hornblende	.799 .804	1.692×10^{-10} 1.717×10^{-10}	9.5 7.4	115.8±3.6	This paper.
Kruger Alkalic Complex							
L-277W	Pegmatite-alaskite dike, cuts pyroxenite.	Muscovite	8.47 8.55	2.132×10^{-9} 2.130×10^{-9}	3.1 6.2	135.7±4.1	This paper.
L-277Y	Hornfelsed Kobau Formation, at contact with alkalic complex.	Biotite	7.63 7.65	1.038×10^{-9}	8.0	74.8±2.2	Do.
		Hornblende	1.28 1.29	3.988×10^{-10}	6.2	166.7±5.0	Do.
L-277Z	Biotite pyroxenite	Biotite	7.87 7.87	2.050×10^{-9}	10.7	140.9±4.2	Do.
L-301	Shonkinite	Biotite	-----	----------	---	69.9±2.1	Engels, 1971.
		Hornblende [Hastingsite].	-----	----------	---	170.9±5.1	Do.
W-65-1	"Kruger syenite"	Hornblende augite mixture.	-----	----------	---	152±9	Cannon, 1966.

[1] Corrected for cross-contamination of mineral separates. (See Engels, 1971.)

oratories flame photometer with lithium internal standard.

The following constants were employed in calculation of the K-Ar ages:

^{40}K atomic percent = 0.0119

$\lambda_\epsilon = 0.585 \times 10^{-10}\ yr^{-1}$

$\lambda_\beta = 4.72 \times 10^{-10}\ yr^{-1}$

Results of argon and potassium determinations, including those by Engels (1971) and Cannon (1966), are listed in table 1.

DISCUSSION

K-Ar ages of samples from the composite pluton—including one sample (L–277Y) of hornfelsed Kobau collected a few metres (yards) away from the contact with Kruger pyroxenite—range from 69.9 m.y. to 177.2 m.y. (table 1). Mineral pairs show discordancies ranging from about 72 to 106 m.y., with hornblende consistently showing greater analytical age than coexisting biotite.

Biotite coexisting with hornblende in one sample (L–704) was almost completely chloritized and for that reason was not dated. It is significant that hornblende from this sample shown the lowest analytical age (avg 115.8 m.y.) of the group. For the hornblendes it is apparent (fig. 2 and table 1) that except for sample L–618, the analytical age increases with increasing potassium content, a relationship that would not be expected if the discordance between the biotite and hornblende ages were due to incorporation of excess argon by the hornblende at the time of its initial crystallization. These circumstances, coupled with the petrographic evidence of cataclasis and thermal metamorphism or alteration, suggest to us that the discordance reflects argon loss owing to metamorphism after initial solidification of the composite pluton.

The ratio of ^{40}Ar (radiogenic) to K in hornblendes shows a roughly linear distribution (fig. 2) along a 191.0-m.y. isochron and a slightly negative intersection with the ^{40}Ar (radiogenic) axis. The negative intersection of this type of isochron has been interpreted as an indication of argon loss (Shafiqullah and Damon, 1971, p. 929). The isochron could be valid only if all samples had lost approximately the same amount of radiogenic argon, but this condition probably does not hold. Sample L–704, for example, gave the lowest analytical age and showed a higher degree of chloritization than the other samples; thus it might be expected to have lost proportionately more radiogenic argon. This sample does show a relatively large negative deviation from the isochron, and because of its relatively low potassium content, its inclusion biases the isochron toward steeper slopes (older ages). Were

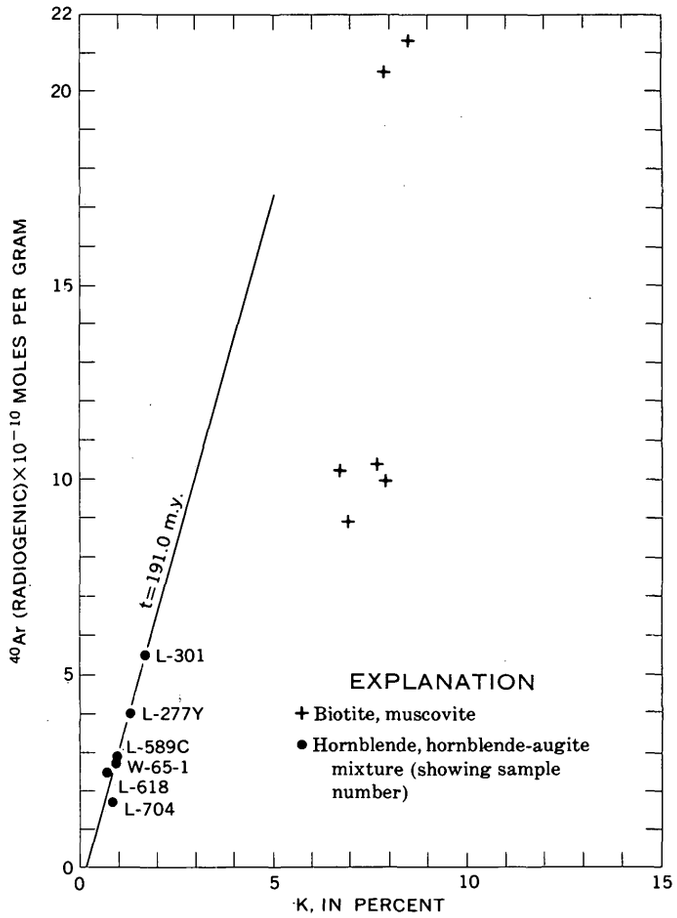

FIGURE 2.—Plot of argon (radiogenic) versus potassium for hornblende, biotite, and muscovite from the Similkameen batholith and Kruger Alkalic Complex (samples listed in table 1). Isochron fit by regression analysis to hornblende data: $^{40}Ar(radiogenic) = (-6.93 \cdot 10^{-11}) + (3.58 \cdot 10^{-10})(K)$.

sample L–704 omitted from the analysis the resulting isochron, $^{40}Ar(radiogenic) = (-2.71 \times 10^{-11}) + (3.3 \times 10^{-10})(K)$, would be 176.8 m.y. As before, the isochron would intersect the ^{40}Ar (radiogenic) axis at a slightly negative value. We conclude, therefore, that the actual age of the composite pluton is less than that given by the 191.0-m.y. isochron but probably somewhat more than the age of the oldest hornblende. Thus the age of the composite pluton is probably between about 177 m.y. and 191 m.y. (Early Jurassic).

The biotite and muscovite ages do not form a linear group when plotted on the ^{40}Ar (radiogenic)/K diagram (fig. 2). If the real age of the composite pluton is between about 177 m.y. and 191 m.y., as suggested by the hornblende data, the biotite and muscovite ages probably reflect varying partial degassing during one or possibly more metamorphic episodes. The most recent of these must necessarily be 70 m.y. old or less—

the analytical age of the youngest biotite. However, the metamorphic episode responsible must be about 50 m.y. old or more, judging from the presence nearby of apparently unmetamorphosed Eocene deposits containing detritus from the composite pluton. Thus we conclude that the Similkameen batholith and Kruger Alkalic Complex were thermally metamorphosed between 50 m.y. and 70 m.y. ago.

It is puzzling that the age of biotite from Kruger pyroxenite (141 m.y., L–277Z) and of muscovite from an alaskite-pegmatite dike (136 m.y., L–277W) cutting the pyroxenite substantially exceeds that of all other related biotites; namely, from hornfels (75 m.y., L–277Y) at the pyroxenite-Kobau Formation contact, from shonkinite (70 m.y., L–301), and from granodiorite (83 m.y., L–589C, and 71 m.y., L–618). The sample localities of the pyroxenite and the alaskite-pegmatite dike (L–277Z and L–277W, respectively) lie about 0.25 km (0.15 mi) northeast of the hornfels locality (L–277Y), 0.58 km (0.36 mi) west of the shonkinite locality (L–301), and 4.4 km (2.7 mi) and 7.6 km (4.7 mi) east of the granodiorite localities (L–589C and L–618, respectively) (fig. 1), which seems to rule out an increase in indicated age due simply to a progressive increase in distance from a source of heat.

Muscovite commonly shows greater argon retentivity than biotite (Hanson and Gast, 1967), perhaps accounting for its greater age relative to most of the biotites. The apparent higher argon retentivity of biotite in the pyroxenite suggests, perhaps, that the composition of this biotite is different from that of the biotite in the other rocks.

The youngest hornblende age is at the westernmost sample locality (L–704) while the youngest biotite age is at the easternmost sample locality (L–301). Thus the orientation of the thermal gradient during metamorphism is not independently demonstrable from the Similkameen and Kruger K-Ar data.

REFERENCES CITED

Bostock, H. S., 1940, Keremeos, Similkameen district, British Columbia: Canada Geol. Survey Map 341A, scale 1:63,360.

Campbell, C. D., 1939, The Kruger alkaline syenites of southern British Columbia: Am. Jour. Sci., v. 237, no. 8, p. 527–549.

Cannon, R. W., 1966, Geochronology and petrographic studies of the intrusive rocks of the Oliver area, Oliver, B. C.: Vancouver, British Columbia Univ., B.S. thesis, 23 p.

Daly, R. A., 1906, The Okanogan composite batholith of the Cascade Mountain system: Geol. Soc. America Bull., v. 17, p. 329–376.

——— 1912, Geology of the North American Cordillera at the forty-ninth parallel: Canada Geol. Survey Mem. 38, pts. 1–3, 857 p.

Engels, J. C., 1971, Effects of sample purity on discordant mineral ages found in K-Ar dating: Jour. Geology, v. 79, p. 609–616.

Hanson, G. N., and Gast, P. W., 1967, Kinetic studies in contact metamorphic zones: Geochim. et Cosmochim. Acta, v. 31, p. 1119–1153.

Hibbard, M. J., 1971, Evolution of a plutonic complex, Okanogan Range, Washington: Geol. Soc. America Bull., v. 82, p. 3013–3047.

Larsen, E. S., Jr., Gottfried, David, Jaffe, H. W., and Waring, C. L., 1958, Lead-alpha ages of the Mesozoic batholiths of western North America: U.S. Geol. Survey Prof. Paper 1070–B, p. III–IV, 35–62.

Rinehart, C. D., and Fox, K. F., Jr., 1972, Geology of the Loomis quadrangle, Okanogan County, Washington: Washington Div. Mines and Geology Bull. 64, 124 p.

Shafiqullah, M., and Damon, P. E., 1971, Evaluation of K-Ar isochron methods [abs.]: EOS (Am. Geophys. Union Trans.), v. 52, p. 929.

Stern, T. W., and Rose, H. J., Jr., 1961, New results from lead-alpha age measurements: Am. Mineralogist, v. 46, p. 606–612.

Jour. Research U.S. Geol. Survey
Vol. 3, No. 1, Jan.–Feb. 1975, p. 45–46

RADIOCARBON DATES INDICATE RATES OF GRABEN DOWNFAULTING, SAN JACINTO VALLEY, CALIFORNIA

By BEN E. LOFGREN and MEYER RUBIN, Sacramento, Calif., Reston, Va.

Abstract.—Recent radiocarbon dates for wood samples collected from three depths in San Jacinto Valley graben indicate active tectonic downfaulting during the past 42,000 yr. The flood plain of graded San Jacinto River, entering the valley from the southeast and leaving toward the west, serves as a reference datum across the graben. Depositional rates suggest that downfaulting averaged about 0.007 ft (2.1 mm)/yr from 42,000 to 15,270 yr B.P. and since 15,270 yr B.P. has increased to about 0.019 ft (5.8 mm)/yr.

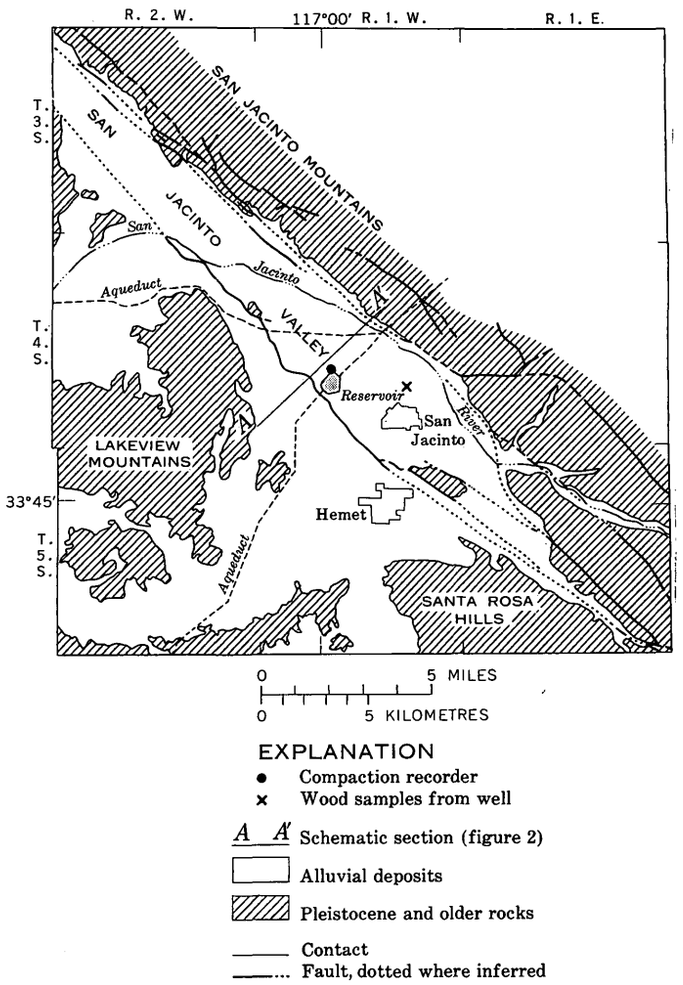

FIGURE 1.—Geologic features of San Jacinto Valley, Calif., and location of collected wood samples and compaction recorder. (Modified from California Division of Mines and Geology, 1966.)

San Jacinto Valley is an alluviated structural valley (fig. 1) about 80 mi (130 km) east of downtown Los Angeles, Calif. It is a relatively flat-lying depositional surface surrounded by hills and mountains and consists of a graben trough on the east and a broad alluvial mesa on the west. The northwest-trending graben is bounded on the east by the Claremont fault, which forms the east margin of the valley, and on the west by the Casa Loma fault (fig. 2). These principal

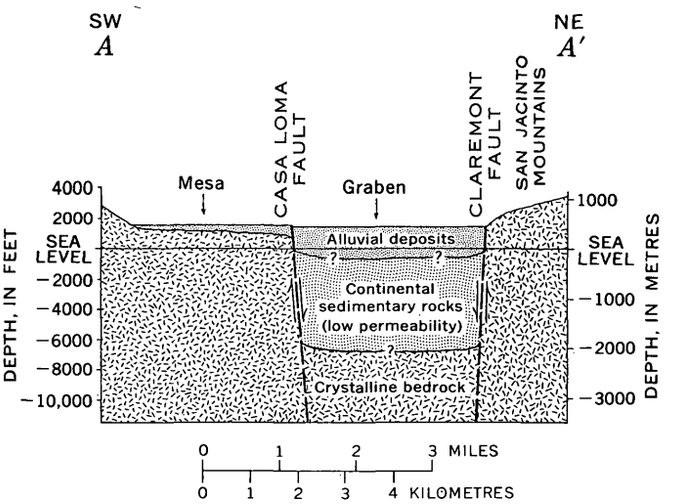

FIGURE 2.—Schematic geologic section across San Jacinto Valley, one-half mile north of San Jacinto Reservoir. (Modified from J. D. Fett and Associates, written commun., 1967.)

faults, with numerous associated minor faults, compose the complex San Jacinto fault zone which merges with the San Andreas fault system about 30 mi (50 km) to the northwest.

The San Jacinto fault zone is one of the most seismically active systems in southern California. Although physiographic evidence indicates large tectonic displacements in the vicinity of San Jacinto Valley, little direct information is available for estimating rates of movement during the past 50,000 yr. Distinct scarps, sag ponds, and springs clearly define the traces of major faults in the valley. Recent mapping (Sharp, 1967, p. 711, and Sharp, 1972) suggests that, although

right-lateral offsets have dominated within the San Jacinto fault zone in Quaternary time, recent movement along the Casa Loma fault has been largely dip slip. Neither the current rate of vertical downfaulting of the graben nor the amount of tectonic displacement in historic time have been defined heretofore.

RADIOCARBON DATES

Radiocarbon dates by the U.S. Geological Survey on wood samples recently collected from three depths give an approximation of the rate of graben downfaulting in the past 42,000 yr. The samples were collected in June 1971 by geologists of the Eastern Municipal Water District and Metropolitan Water District from rotary drilled water well 4S/1W-23P11, 1 mi (1.6 km) due north of the city of San Jacinto. Specific details on the three samples are as follows:

Laboratory number	*Depth of sample*		*Age determination (years B.P.)*
	Feet	*Metres*	
W-2729 --------	292	89	15,270±450
W-2827 --------	322	98	21,260±650
W-2828 --------	480	146	42,000±1,500

The San Jacinto River, entering the valley from the southeast and leaving toward the west (fig. 1), has apparently maintained a uniform graded flood plain through much of Quaternary time. This flood plain serves as a reference datum for measuring rates of graben downfaulting. Figure 3 shows radiocarbon age of the three wood samples, and the apparent rate of downfaulting implied by these data. The actual depth of the collected sample is shown as well as the corrected depth to eliminate the effects of compaction of deeper fluvial deposits due to increased overburden, using compressibility data from a nearby compaction recorder. Apparent average rates of tectonic downfaulting of about 0.007 ft(2.1 mm)/yr from 42,000 yr to 15,270 yr B.P. and about 0.019 ft(5.8 mm)/yr since 15,270 yr B.P. are indicated. Since no data younger than 15,270 yr B.P. are available, tectonic downfaulting during Holocene time may have proceeded at a uniform rate or may have had one or more episodes of abrupt subsidence.

Estimated rates of graben faulting are of more than just academic interest in this part of the San Jacinto fault zone. Excessive pumping of ground water in the graben trough is producing significant subsidence of the land surface. Subsidence resulting from the compaction of the producing aquifer system has averaged about 0.076 ft(23 mm)/yr since 1959 in the central part of the graben. To differentiate the effects of ground-water pumping from those of tectonic downfaulting is one aspect of the Geological Survey's continuing research interest in the area.

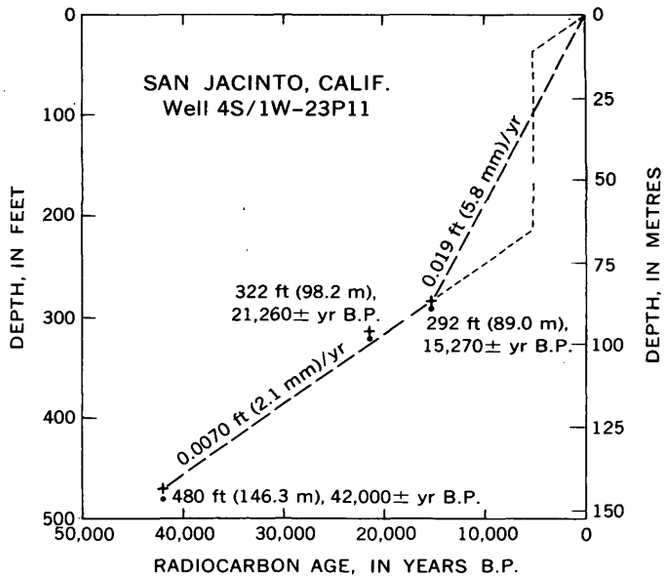

FIGURE 3.—Radiocarbon age of three wood samples from the San Jacinto graben, and the implied rate of tectonic downfaulting. •, actual depth of collected sample. +, corrected depth to eliminate the effects of compaction of deeper fluvial deposits due to increased overburden, using compressibility data from a nearby compaction recorder. Dashed lines indicate apparent average rates of tectonic downfaulting.

REFERENCES CITED

Sharp, R. V., 1967, San Jacinto fault zone in the Peninsular Ranges of southern California: Geol. Soc. America Bull., v. 78, no. 6, p. 705–730.

——— 1972, Map showing recently active breaks along the San Jacinto fault zone between the San Bernardino area and Borego Valley, Calif.: U.S. Geol. Survey Misc. Geol. Inv. Map I-675, sheet 2 of 3, scale 1:24,000.

Jour. Research U.S. Geol. Survey
Vol. 3, No. 1, Jan.–Feb. 1975, p. 47–51

STRATIGRAPHIC RELATIONSHIPS WITHIN THE BARAGA GROUP OF PRECAMBRIAN AGE, CENTRAL UPPER PENINSULA, MICHIGAN

By W. F. CANNON and JOHN S. KLASNER, Reston, Va., Macomb, Illinois

Work done in cooperation with Geological Survey Division,

Michigan Department of Natural Resources

Abstract.—Details of the stratigraphic section in parts of northern Michigan have been known for many years, but correlation of units between geographically separated areas has been partly speculative. Mapping in the Witch Lake quadrangle has filled the gap between well-studied areas of the Marquette trough and parts of Iron and Dickinson Counties and has helped to correlate units in the Baraga Group (Precambrian X). Iron-formations are important marker beds; because of their magnetic properties they can be traced with certainty through poorly exposed areas. The magnetic Fence River Formation is now known to be stratigraphically beneath the Bijiki Iron-formation Member of the Michigamme Formation but may be equivalent to the Greenwood Iron-formation Member which crops out in parts of the Marquette trough to the east. The Hemlock Formation (volcanic) underlies the Fence River and has been traced from near its type locality in Iron County to the south flank of the Marquette trough. These relationships provide the key to understanding the lateral facies changes responsible for the stratigraphic complexities of the Baraga Group.

The Baraga Group is a greatly varied sequence of metasedimentary and metavolcanic rocks. It was defined by James (1958) as consisting of five formations (Goodrich Quartzite, Hemlock Formation, Fence River Formation, Michigamme Slate,[1] and Badwater Greenstone) and was named for Baraga County where it is widely exposed. It is the most extensive of four groups composing the Marquette Range Supergroup (Precambrian X) (Cannon and Gair, 1970). Detailed mapping by many workers (Gair and Wier, 1956; Bayley, 1959; James and others, 1961, 1968; Wier 1967; Cannon, 1975a,b) reveals many changes in detail within the stratigraphic column from area to area as well as differences from James' (1958) generalized column.

In the Marquette trough (table 1), the column has

[1] The Michigamme Slate is here renamed Michigamme Formation because most of the rocks, including those near the type locality, are not slate.

TABLE 1.—*Generalized descriptions of stratigraphic units in the Baraga Group in the central part of the Upper Peninsula of Michigan*

[Rocks are metamorphosed to degrees ranging from chlorite to sillimanite grade]

Iron and Dickinson Counties (James and others, 1961, 1968; Gair and Wier, 1956; Bayley, 1959)	Witch Lake quadrangle	Marquette trough (Van Hise and Bayley, 1897; Cannon, 1975a, b)
Badwater Greenstone: mafic submarine volcanic rocks, commonly ellipsoidal greenstone.	Michigamme Formation: Upper slate member: interbedded graywacke and schist much like Michigamme Formation of Iron and Dickinson counties.	Michigamme Formation: Upper slate member (see col. 2).
Michigamme Formation: interbedded graywacke and slate or schist.	Bijiki Iron-formation Member: not exposed; traced by magnetic anomaly from outcrop areas in Marquette trough.	Bijiki Iron-formation Member: banded iron silicate–magnetite iron-formation.
Fence River Formation: banded iron silicate—magnetite iron-formation, commonly containing pelitic beds.	Strata near Fence Lake: poorly exposed sequence of amphibolitic schist, graywacke, iron-formation, conglomerate, and pyroclastic rocks.	Lower slate member: graphitic and pyritic slate and lesser siltstone and rare graywacke and conglomerate beds.
Hemlock Formation: largely basaltic rocks and less common felsic units and sedimentary beds. Contains flow and pyroclastic rocks.	Fence River Formation (see col. 1).	Clarksburg Volcanics Member: mostly mafic pyroclastic rocks and beds of pelitic and iron-rich sedimentary rocks.
Goodrich Quartzite: quartzite and ferruginous quartzite or conglomerate.	Hemlock Formation (see col. 1); the few outcrops on east side of Smith Creek uplift are felsic tuff or rhyolite.	Greenwood Iron-formation Member: banded iron silicate–magnetite iron-formation.
	Goodrich Quartzite (see col. 1).	Goodrich Quartzite: feldspathic quartzite and discontinuous basal conglomerate rich in iron-formation detritus.

long been known to consist of the Goodrich Quartzite and the Michigamme Formation. The latter can be divided into lower slate, Bijiki Iron-formation, and upper slate members; the Clarksburg Volcanics and Greenwood Iron-formation locally are members between the Goodrich and lower slate member of the Michigamme (Leith and others, 1935). About 40 km to the south, near the Amasa uplift, the group was shown by Gair and Wier (1956) and by James and others (1968) to consist of the Goodrich Quartzite (which is only locally present), the Hemlock Formation, the Fence River Formation, the Michigamme Formation, and the Badwater Greenstone. Elsewhere, as in parts of central Dickinson County, the section consists entirely of the Michigamme Formation and the Badwater Greenstone (James and others, 1961).

Clearly, lateral facies changes occur within distances of a few kilometres to a few tens of kilometres, resulting in many units of only local extent. The correlation of many of these units between well-studied areas in the Marquette trough to the north and Iron and Dickinson Counties to the south has been conjectural, largely because detailed maps linking these areas were lacking. Our recent mapping in western Marquette County and adjacent parts of Baraga and Iron Counties has filled this gap; this paper presents our interpretation of the facies relationships between many of the local units in the Baraga Group.

Figure 1 shows the proposed physical relationship between rock units. We do not intend to imply an exact time equivalence of any parts of the section except locally where interfingering obviously indicates contemporaneity. The bases of volcanic units, however, probably approximate time lines.

The data on which the relationships in the central part of the figure 1 are based were derived from, in, and near the Witch Lake 15-minute quadrangle (fig. 2). There, although outcrops are few, aeromagnetic data (U.S. Geol. Survey, 1967) and diamond drilling support the proposed relationships.

Iron-rich units are especially useful as magnetic marker beds and can be traced with certainty for many kilometres. The Fence River Formation (Gair and Wier, 1956) is a magnetic iron-formation known on the east side of the Amasa uplift (fig. 2) from a few outcrops and test pits and several diamond-drill holes. The magnetic pattern suggests that simple synclines separate the Amasa uplift from the Smith Creek uplift and Wilson Creek uplift and that the Fence River Formation causes the magnetic anomaly encircling these latter uplifts where, although the unit does not crop out, drill-hole samples show it to be lithologically similar to the Fence River Formation of the Amasa uplift. This interpretation is supported by the presence of volcanic rocks, much like the Hemlock Formation of the Amasa uplift, which crop out stratigraphically beneath the magnetic unit on the south and east flanks of the Smith Creek uplift and are inferred from their distinctive magnetic pattern also to underlie the Fence River Formation on the west and north flanks of the Smith Creek uplift and also in the Wilson Creek uplift. Thus the Hemlock and Fence River Formations appear to extend from their type areas in Iron and Dickinson Counties northward to the south flank of the Marquette trough.

The Fence River Formation in the Sagola basin is overlain by graywacke and slate of the Michigamme Formation, the youngest unit preserved there. The

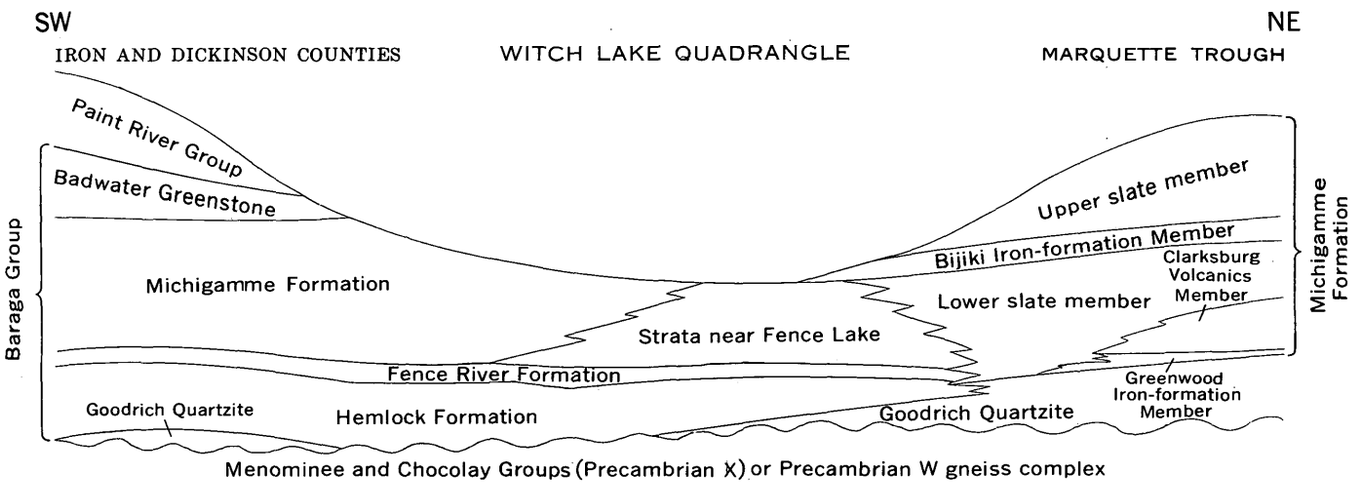

FIGURE 1.—Generalized section showing physical relationships between stratigraphic units of the Baraga Group (no vertical scale implied). Base of group unconformably overlies older Precambrian X or W rocks. Upper profile of diagram is an approximation of the youngest stratigraphic unit preserved on the present peneplane as a result of erosion of major structures formed during late Precambrian X deformation. Width of section is about 50 km.

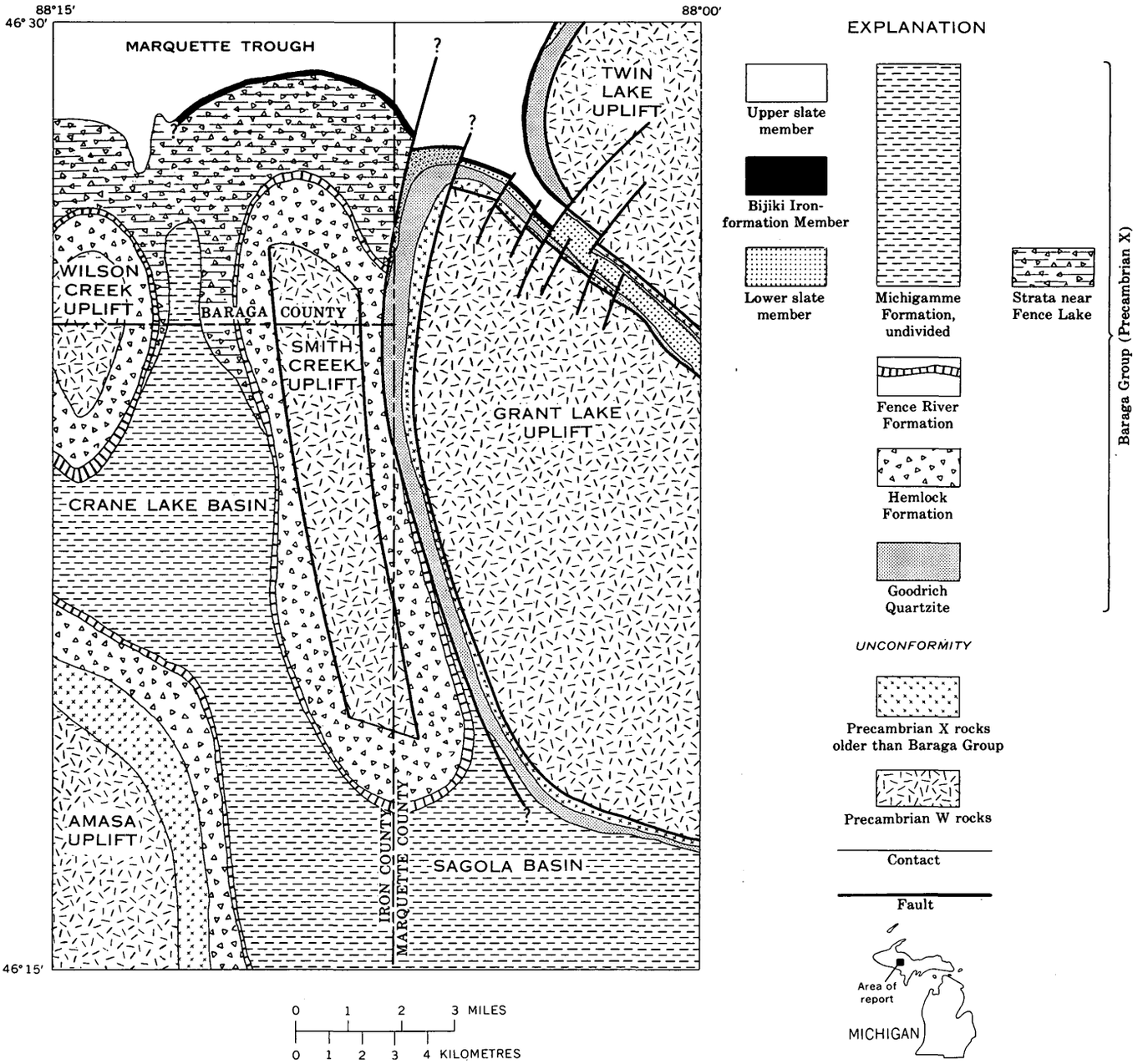

FIGURE 2.—Generalized geologic map of the Witch Lake quadrangle, showing the distribution of stratigraphic units within the Baraga Group. Metadiabase sills, not shown on the map, locally constitute a major part of the section.

Michigamme is characterized on magnetic maps by low values and uniform gradients, and on this basis it is projected north into the Crane Lake basin, which is devoid of outcrops. West of the Amasa uplift, the Michigamme is overlain with presumed conformity by submarine volcanic rocks of the Badwater Greenstone (James, 1958).

In the Marquette trough, the Bijiki Iron-formation Member is an intermediate unit of the Michigamme Formation and lies between the upper and lower slate members (Van Hise and Bayley, 1897). It has been traced in outcrop along the north and west flanks of the Twin Lake uplift to about the north edge of the Witch Lake quadrangle (Klasner, 1972), and from there it can be traced by its magnetic anomaly through the Republic trough and onto the north flank of the Smith Creek uplift, where it is only 3 km from the Fence River Formation. There the Bijiki is clearly stratigraphically above the Fence River and is apparently separated from it by approximately ½ km of

stratigraphic section. The rocks in this interval are poorly exposed but evidently are largely a sequence of volcanic and sedimentary rocks containing intercalated metadiabase sills. The few existing outcrops are mostly metadiabase and lesser amounts of ferruginous schist, amphibolitic schist (metavolcanic? rocks), and graywacke and conglomerate, which are at least in part volcanogenic. Large glacial boulders of mafic pyroclastic rocks, which are common in parts of this area, are probably locally derived. The stratigraphic interval between the Fence River and Bijiki on the north flank of the Smith Creek and Wilson Creek uplifts is characterized by a very irregular magnetic pattern, and the underlying rock units can thus be projected from areas where they crop out on the Smith Creek uplift onto the north flank of the Wilson Creek uplift. On the basis of the magnetic pattern, the sequence of volcanic and sedimentary rocks seems restricted to the north flanks of these two uplifts. The unit is here informally named "strata near Fence Lake" and is considered part of the Michigamme Formation. On the north flank of the Marquette trough, north of the Witch Lake quadrangle, the part of the Baraga Group beneath the Bijiki Iron-formation Member consists of graphitic slate of the lower slate member of the Michigamme Formation and the Goodrich Quartzite (Van Hise and Bayley, 1897). The Hemlock Formation, Fence River Formation, and strata near Fence Lake, which compose this part of the section to the south, are absent and may pass by lateral facies change within distances of a few kilometres into the quartzite and slate.

The stratigraphic section changes abruptly across a fault along the center of the Mitchigan River trough trending north-northwest parallel to the trough margins (fig. 2). The Hemlock Formation, Fence River Formation, and strata near Fence Lake are west of the fault, but the equivalent stratigraphic position east of the fault is occupied by the Goodrich Quartzite. This abrupt change is difficult to explain solely by facies changes, even when allowing for substantial later offset along the fault. However, if the fault was active during sedimentation, a west-facing scarp may have prevented eastward spreading of volcanic rocks.

A few kilometres east of the Witch Lake quadrangle, on the south limb of the Marquette trough, the Clarksburg Volcanics (Van Hise and Bayley, 1897) and Greenwood Iron-formation (Leith and others, 1935), now considered members of the Michigamme Formation (James, 1958), lie between the Goodrich Quartzite and the lower slate member of the Michigamme Formation. They have stratigraphic position and lithologies analagous to the Fence River Formation and the strata near Fence Lake but are not continuous with these latter units at the surface; the lower slate member lies directly on the Goodrich Quartzite along the west flank of the Twin Lake uplift (Klasner, 1972) and throughout most of the Republic trough.

If the bases of volcanic units are approximate time lines, a generalized sedimentary history of the Baraga Group can be reconstructed. At the base of the section is the Goodrich Quartzite, which unconformably overlies older rocks but is not continuous throughout the area. It is not known to be present in the west half of the Witch Lake quadrangle where the Hemlock Formation apparently lies directly on pre-Baraga Group rocks. A few kilometres south of the quadrangle, Gair and Wier (1956) have shown that the Goodrich underlies the Hemlock and is there clearly older than the volcanic rocks, but to the north, in the Marquette trough where the volcanic rocks pinch out, they could be at least in part contemporaneous with the Goodrich or the lower slate member of the Michigamme. The Hemlock was deposited as both flows and pyroclastic ejecta which spread over most of the area now occupied by the Amasa, Smith Creek, and Wilson Creek uplifts, while synchronous deposition of the Goodrich Quartzite or lower slate member of the Michigamme took place to the north and northeast. The Hemlock in the Witch Lake quadrangle apparently forms a broad apron, as much as a kilometre thick peripheral to a central volcanic area, which, judging from thickening of the volcanic pile (Gair and Wier, 1956; Wier, 1967), centered west or south of the Amasa uplift. As volcanism ceased, iron-rich chemical precipitates accumulated and formed the Fence River Formation which blankets the Hemlock volcanic rocks and appears to be approximately coextensive with them. Volcanism resumed abruptly, and the Clarksburg Volcanics Member was deposited in parts of the Marquette trough; the strata near Fence Lake are possibly, at least in part, correlative with the Clarksburg, for they can be traced to within less than 10 km of the Clarksburg at a similar stratigraphic horizon. This, in turn, suggests that the Greenwood Iron-formation Member underlying the Clarksburg and the Fence River Formation underlying the strata near Fence Lake are approximately correlative. Further deposition of iron-rich precipitates (Bijiki Iron-formation Member) directly succeeded deposition of the strata near Fence Lake but was separated from Clarksburg deposition by a period in which, in places, a kilometre or more of carbonaceous shale was deposited. A great but undetermined thickness of graywacke and shale was deposited next, largely as turbidites, over the Bijiki in the Marquette trough and formed the upper slate mem-

ber of the Michigamme. Elsewhere turbidite deposition may have been partly synchronous with or earlier than deposition of the Bijiki. Turbidite deposition was succeeded by mafic submarine flows of the Badwater Greenstone, which are now preserved only west and south of the Amasa uplift but were perhaps originally more extensive.

REFERENCES CITED

Bayley, R. W., 1959, Geology of the Lake Mary quadrangle, Iron County, Michigan: U.S. Geol. Survey Bull. 1077, 112 p.

Cannon, W. F., 1975a, Bedrock geologic map of the Greenwood quadrangle, Marquette County, Michigan: U.S. Geol. Survey Geol. Quad. Map GQ–1168, (In press.)

———1975b, Bedrock geologic map of the Republic quadrangle, Marquette County, Michigan: U.S. Geol. Survey Misc. Geol. Inv. Map I–862. (In press.)

Cannon, W. F., and Gair, J. E., 1970, A revision of stratigraphic nomenclature for middle Precambrian rocks in northern Michigan: Geol. Soc. America Bull., v. 81, no. 9, p. 2843–2846.

Gair, J. E., and Wier, K. L., 1956, Geology of the Kiernan quadrangle, Iron County, Michigan: U.S. Geol. Survey Bull. 1044, 88 p.

James, H. L., 1958, Stratigraphy of pre-Keweenawan rocks in parts of northern Michigan: U.S. Geol. Survey Prof. Paper 314–C, p. 27–44.

James, H. L., Clark, L. D., Lamey, C. A., and Pettijohn, F. J., 1961, Geology of central Dickinson County, Michigan: U.S. Geol. Survey Prof. Paper 310, 176 p.

James, H. L., Dutton, C. E., Pettijohn, F. J., and Wier, K. L., 1968, Geology and ore deposits of the Iron River-Crystal Falls district, Iron County, Michigan: U.S. Geol. Survey Prof. Paper 570, 134 p.

Klasner, J. S., 1972, Style and sequence of deformation and associated metamorphism due to the Penokean orogeny in the western Marquette Range, northern Michigan: Houghton, Mich., Michigan Technological Univ., unpub. Ph. D. thesis, 132 p.

Leith, C. K., Lund, R. J., and Leith, Andrew, 1935, Pre-Cambrian rocks of the Lake Superior region: U.S. Geol. Survey Prof. Paper 184, 34 p.

U.S. Geological Survey, 1967, Aeromagnetic map of the Ned Lake quadrangle and part of the Witch Lake quadrangle, Iron, Baraga, and Marquette Counties, Michigan: U.S. Geol. Survey Geophys. Inv. Map GP–609.

Van Hise, C. R., and Bayley, W. S., 1897, The Marquette iron-bearing district of Michigan: U.S. Geol. Survey Mon. 28, 608 p., atlas.

Wier, K. L., 1967, Geology of the Kelso Junction quadrangle, Iron County, Michigan: U.S. Geol. Survey Bull. 1226, 47 p.

Jour. Research U.S. Geol. Survey
Vol. 3, No. 1, Jan.–Feb. 1975, p. 53–58

THE NECTARIAN SYSTEM, A NEW LUNAR TIME-STRATIGRAPHIC UNIT

By DESIREE E. STUART-ALEXANDER and DON E. WILHELMS,
Menlo Park, Calif.

Abstract.—Geologic mapping of the limbs and far side of the Moon has demonstrated the desirability of subdividing the pre-Imbrian rocks. A convenient datum is the Janssen Formation, the ejecta blanket of the Nectaris basin. A new system, herein named the Nectarian System, extends from the base of the Janssen Formation up to, but not including, the Fra Mauro Formation, which is the ejecta blanket of the Imbrium basin and the basal unit of the Imbrian System. As all rocks older than the Janssen Formation are informally called pre-Nectarian, the name "pre-Imbrian" is superseded by Nectarian and pre-Nectarian where rocks of these ages can be recognized.

Systematic geologic mapping of the Moon has led to the development of a lunar stratigraphic column that is continually tested and refined. Telescopic observations of the near side first provided the basis for dividing lunar rocks into time-stratigraphic units (latest summary by Wilhelms, 1970). Spacecraft data have permitted extending the geologic mapping to the poles, limbs, and far side. (Five maps—North Pole region, South Pole region, east side, west side, and central far side are being compiled.) This mapping entails assignment of many new rock units to time-stratigraphic units. Detailed mapping of the new areas has confirmed the validity and usefulness of the three systems established for the youngest lunar rocks: Imbrian, Eratosthenian, and Copernican. The mapping has demonstrated the desirability of formally subdividing the next older rocks, heretofore informally included within the pre-Imbrian, because of their abundance, wide areal extent, and stratigraphic importance—most basins and large craters are pre-Imbrian. Materials of pre-Imbrian craters had been ranked into three age groups on the basis of their morphologic degradation, assuming like initial form (Pohn and Offield, 1970; Wilhelms and McCauley, 1971), but this classification was informal. It is the intent of this paper to define a new lunar time-stratigraphic unit for the upper pre-Imbrian and to name it the Nectarian System.

A convenient stratigraphic datum for subdivision within the pre-Imbrian units is the base of the Janssen Formation, the probable ejecta blanket of the Nectaris basin (Stuart-Alexander, 1971). The Janssen Formation is relatively extensive (fig. 1); it both overlies and underlies a significant variety of craters (figs. 2, 3) that can be correlated by morphology with craters elsewhere. Areas covered by terra features that are older and younger than the Janssen are about equal.

Acknowledgments.—This work was done under NASA contract W13–1310.

NAME

The Nectarian System is here named for Mare Nectaris, which fills the innermost ring (fig. 1) of the Nectaris basin, centered at lat 15° S. and long 35° W. (The mare material is younger than the Nectarian System and has no clear genetic relation to the basin.) The impact that formed the Nectaris basin marks the beginning of the Nectarian Period, and the base of the Nectaris basin ejecta blanket marks the base of the Nectarian System. The preceding time and the rocks older than Nectarian are called pre-Nectarian, a term with the same informal status as pre-Imbrian. The term "pre-Imbrian" is replaced by the terms "Nectarian" and "pre-Nectarian" where rocks of these ages can be recognized.

STRATIGRAPHIC BOUNDARIES

The base of the Nectarian System is defined as the base of the Janssen Formation, whose type area (figs. 2, 3) is in the crater Janssen between lat 43° and 45° S., long 37½° and 39° E. (Stuart-Alexander, 1971). A reference area where the Janssen Formation is well developed extends from lat 40° to 42° S., long 50° to 52° E. The type and reference areas are included in the type area for the system, which we designate as extending from lat 40° to 48° S. and long 37½° to 65° E., even though not all rocks of the system are present in this area. The top of the Nectarian System is defined as the base of the Fra Mauro Formation, the

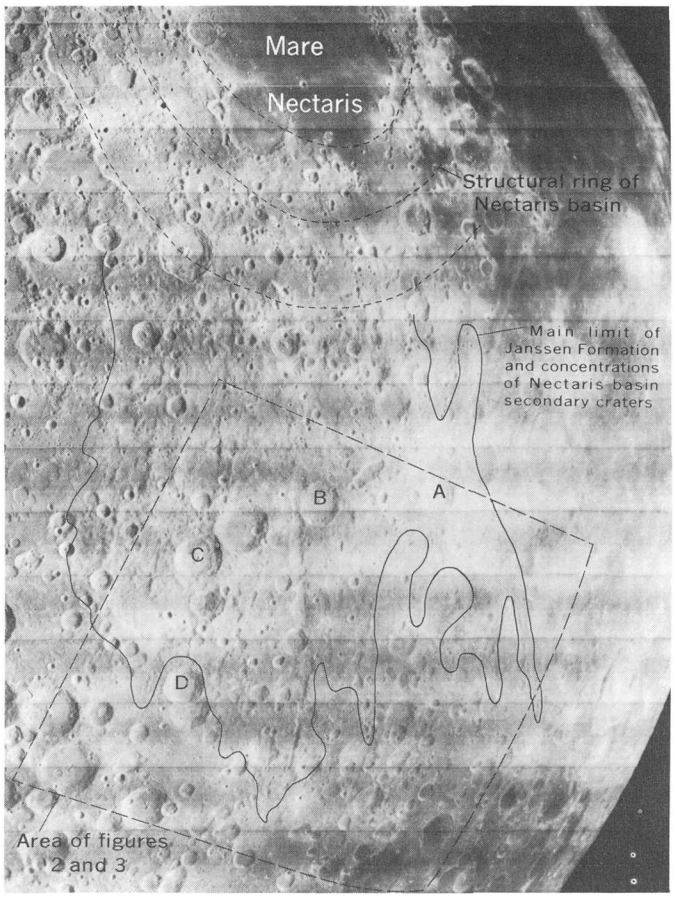

FIGURE 1.—Southeast limb of the Moon showing three main structural rings of the Nectaris basin and main limit of both the Janssen Formation and concentrations of Nectaris basin secondary craters. Lettered craters correspond to those of figures 2 and 3. Part of Lunar Orbiter IV photograph 83M.

basal rock-stratigraphic unit of the Imbrian System, in the type area of the Fra Mauro Formation north of the crater Fra Mauro between lat 0° and 2°S., long 16° and 17½° W. (Wilhelms, 1970, p. F25).

CHARACTERISTICS

The Nectarian System consists of the Janssen Formation, materials of clustered craters believed to be contemporaneous with the Janssen, and materials of other craters as well as plains and terra-mantling deposits younger than the Janssen but older than the Fra Mauro. The Janssen Formation, like most terrestrial rock-stratigraphic units, consists of laterally extensive and continuous beds, whereas many of the other materials, like most lunar material units, occur as numerous isolated patches.

Physical characteristics of the Janssen Formation are reasonably easy to identify. Linear textures in a rolling terra that extends southeastward from the outermost ring of the Nectaris basin (figs. 1, 2) include ridges, escarpments, and minor grooves, all approximately radial to the basin. Confident interpretations of origin as an ejecta blanket can be made by comparison with the younger, and therefore better preserved, Orientale basin and its ejecta blanket (McCauley, 1968; Mutch, 1970, p. 143–156; Wilhelms and McCauley, 1971) and the Imbrian basin and its ejecta blanket, the Fra Mauro Formation (Eggleton, 1964; Wilhelms, 1970, p. F23–F27; Wilhelms and McCauley, 1971). The Janssen Formation, like the two younger blankets, seems to be thickest next to the basin and to thin progressively outward; pre-Nectarian craters are progressively less buried and become more clearly visible toward the outer edges of the blanket.

A dominant crater-trough valley, Vallis Rheita (fig. 2), lies within the Janssen Formation; numerous craters occur in chains and clusters in and beyond the outer fringes of the Janssen Formation. These craters resemble satellitic craters of the Orientale and Imbrium basins, though more subdued, and are almost certainly secondary impact craters of the Nectaris basin. The origin of Vallis Rheita and its analogs at other basins is less certain, but we believe it to have been formed by low-angle secondary impacts contemporaneous with the Janssen Formation, as first suggested by Baldwin (1963, p. 317–318).

The Nectarian System includes materials not directly related to the formation of the Nectaris basin, such as abundant complexly structured crater materials as seen in figure 2 and mapped in figure 3. In general, the crater materials are morphologically sharper than any overlain by Nectaris basin materials but less sharp than any that overlie Imbrium basin materials. Nectarian-age plains and terra-mantling deposits appear to have crater densities equal to or lower than those on the Janssen Formation but greater than those on the Fra Mauro Formation.

CORRELATIONS

Relative-age correlations of Nectarian rocks are determined from superposition relations in the immediate vicinity of the Janssen Formation, secondary impact craters of the Nectaris basin, and the Fra Mauro Formation. The numerous patches of craters, plains, and terra-mantling deposits superposed on the Janssen Formation and the Nectaris secondary craters (figs. 2, 3) are Nectarian or younger. The upper limit of the Nectarian System in the area of the Janssen Formation is best recognized by superposition relations with secondary craters of the Imbrium basin. An extensive field of craters lies west of the main Janssen blanket and overlaps the Janssen Formation (Scott, 1972).

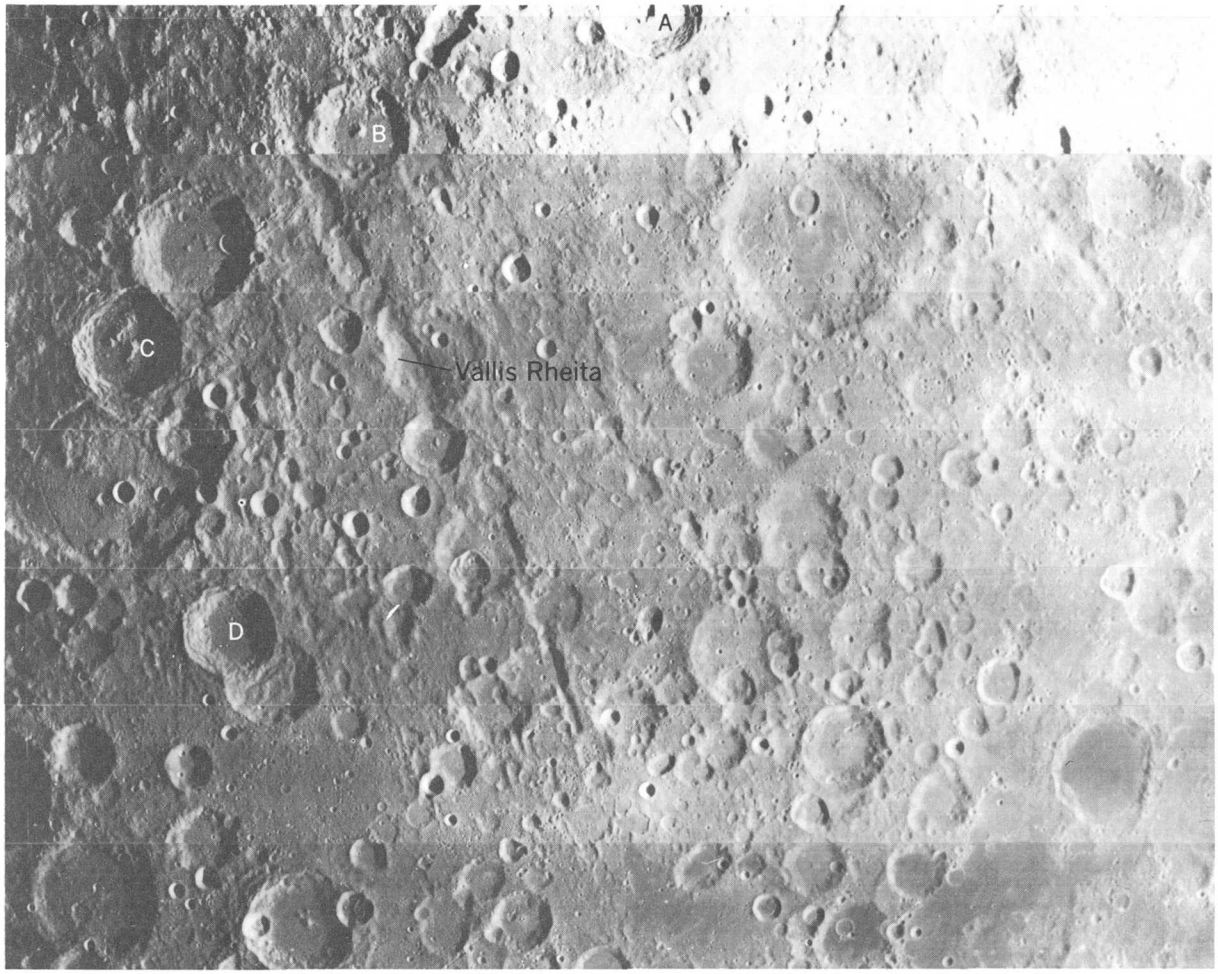

FIGURE 2.—Southern two-thirds of the Nectaris basin ejecta blanket (Janssen Formation) and adjacent units (see fig. 3 for geologic map). Topographic lineations running diagonally from upper left toward lower right in top half to two-thirds of area of photograph are approximately radial to the basin. Vallis Rheita (Rheita Valley) is the largest of these lineations. Craters lettered as in figures 1 and 3. Central part of Lunar Orbiter IV photograph 52M.

Less abundant Imbrium secondary craters are scattered over the rest of the Janssen Formation (Stuart-Alexander, 1971) and on materials southeast of it (D. E. Wilhelms and Farouk El-Baz, unpub. data, 1974).

Morphologic characteristics and frequency distribution of craters in contact with materials of the two basins are used for age correlations where there are no direct overlap relations. Secondary craters of Nectaris basin are especially useful in identifying and correlating pre-Nectarian crater materials because they commonly nick the pre-Nectarian craters but do not obliterate their distinguishing characteristics. Correlations based on crater morphologies can be made with reasonable certainty by assuming like initial form for analogous crater features, then judging degree of degradation (Pohn and Offield, 1970; Wilhelms and McCauley, 1971). By the same method, basins are assigned relative ages through morphologic comparisons with the Imbrium and Nectaris basins (Stuart-Alexander and Howard, 1970). Crater-frequency counts have been used primarily to assist in the correlations of plains (Soderblom and Boyce, 1972; Soderblom and Lebofsky, 1972) and basins (Hartmann and Wood, 1971).

AGE

The Nectarian Period represents a time of extensive cratering over the entire Moon, although the period may have been short. Age limits (fig. 4) can be set for the base of the Nectarian by estimates of the early lunar cratering flux and for the top by extrapolating from the radiometric ages of Imbrian rocks collected by the Apollo astronauts; no dated rocks have been identified as material of the Nectarian System. The

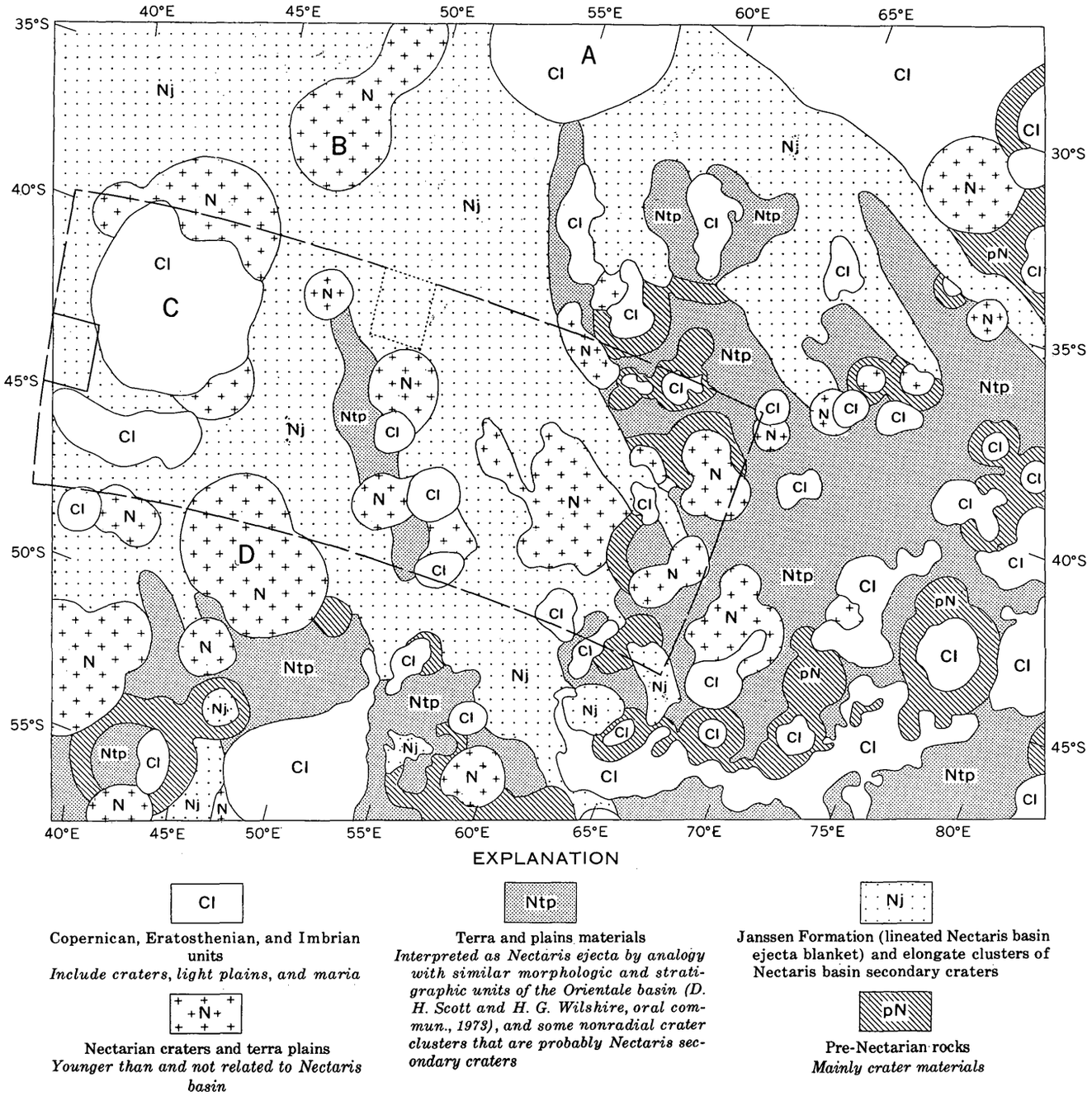

FIGURE 3.—Geologic map of area of figure 2 showing Nectarian System and relation to older and younger rocks. Type area of Janssen Formation is indicated by heavy line; reference area of Janssen Formation is indicated by dotted line; type area of Nectarian System is indicated by dashed line. Craters are lettered as in figures 1 and 2. Latitude and longitude lines are approximate and adjusted from LAC 114, 1st ed., 1966; Lunar Polar Chart (LMP–3), 2d ed., 1970; and Lunar Earthside Chart (LMP–1), 2 ed., 1970.

age of the base of the Imbrian depends upon the interpretation of the dated Fra Mauro Formation breccias collected by Apollo 14. Many workers believe that the date of the youngest basaltic clast (determined as 3.87 b.y. by Tera and others, 1973, but more than 3.90 b.y. by other workers) is older than the time it was incorporated into the Fra Mauro breccia. This means that the base of the Imbrian System is younger than 3.90 b.y. It must be older than 3.77 b.y., the oldest dated mare basalt (Tera and others, 1973; 3.82 b.y., Evans and others, 1973). Other workers (Compston and others, 1971; Tera and others, 1973) suggest that the

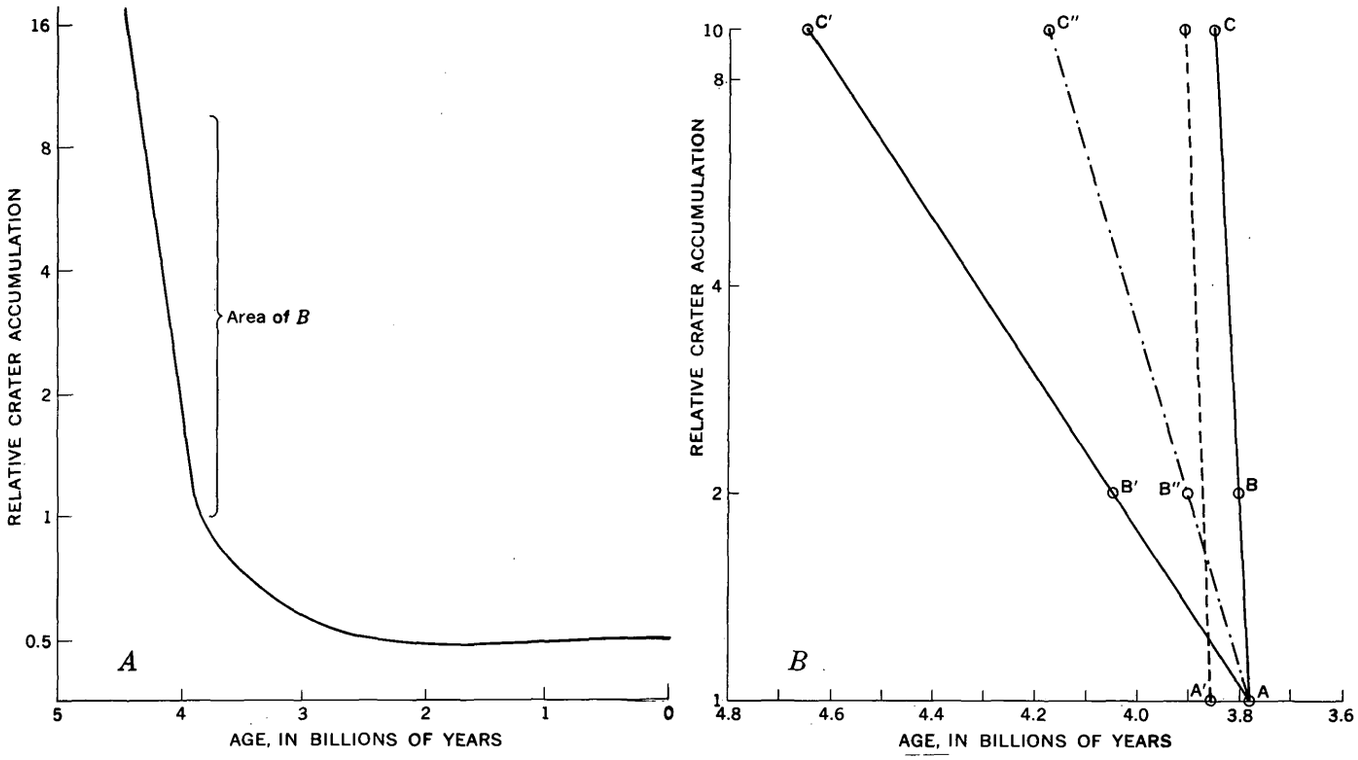

FIGURE 4.—Possible lunar cratering histories. Ordinates are normalized to crater accumulation of post-mare Imbrium and an exponential half-life decay. *A*, Generalized flux curve (adapted from Hartmann, 1970, fig. 2). *B*, Examples of cratering flux within the Nectarian and early Imbrian Periods. A–C and A–C′, maximum range of Nectarian ages; A–C″, more reasonable upper limit of 4.18 b.y. to Nectarian age using 3.90 b.y. (point B″) as base of Imbrian; dashed line, example of possible intermediate Nectarian ages based on maximum age of flux break and a minimum flux half-life. Letters represent possible ages of key events: A's, break in flux decay; B's, boundary between base of Imbrian and top of Nectarian; C's, base of Nectarian.

Apollo-14 breccias actually date the Fra Mauro, implying that the base of the Imbrian may be as old as the oldest dated Fra Mauro breccia, variably reported as 3.96 b.y. (Tera and others, 1973) to a maximum of 4.05 b.y. (Mark and others, 1973). From this, the most reasonable limits to the top of the Nectarian are 3.80 to 3.90 b.y. (fig. 4*B*, B and B″) but may be as great as 4.05 b.y. (fig. 4*B*, B′).

Cratering-flux estimates control dating of the beginning of the Nectarian Period; such estimates rely largely on the assumption that the heavy early lunar flux declined exponentially with a short half-life. This contrasts with the much lighter and relatively constant post-mare flux as determined from radiometric dates correlated with crater counts (Hartmann, 1970, 1972; Soderblom and Boyce, 1972). Crater studies on the central far side (D. E. Stuart-Alexander, unpub data, 1974) combined with Baldwin's statistics (1969) show that the proportion of craters larger than 20 km in diameter increased with increasing age of the system yet formed in a progressively shorter time. The Nectarian System contains about five times as many basins and craters larger than 160 km as does the Imbrian System (0.5 to 0.7 b.y.), which in turn contains more 20-km and larger craters than do the Copernican and Eratosthenian Systems combined (≈ 3.2 b.y. long); the Copernican and Eratosthenian contain no basins. There are more than twice as many pre-Nectarian basins as Nectarian basins, but pre-Nectarian craters are less numerous than Nectarian craters, presumably because of obliteration by widespread younger materials. These data are generalized in figure 4*A* and combined with the radiometric age dates in figure 4*B*. The maximum age curve (A–C′), derived from the unlikely basal Imbrian age of 4.05 b.y., is improbable because it projects the base of the Nectarian to 4.65 b.y., the probable age of the Moon (Nunes and others, 1973), which leaves no time for deposition of the pre-Nectarian. Using the more reasonable limits of 3.80 to 3.90 b.y. as the base of the Imbrian, the base of the Nectarian probably lies between 3.85 and 4.20 b.y., and the length of the period is not more than 300 m.y. and may be less than 50 m.y. Regardless of its exact age, the Nectarian is a useful time-stratigraphic unit because of the wide extent of its deposits.

REFERENCES CITED

Baldwin, R. B., 1963 The measure of the Moon: Chicago, Ill., Univ. Chicago Press, 488 p.

——— 1969, Absolute ages of the lunar maria and large craters: Icarus, v, 11, no. 3, p. 320–331.

Compston, W., Vernon, M. J., Berry, H., and Rudowski, R., 1971, The age of the Fra Mauro Formation—a radiometric older limit: Earth and Planetary Sci. Letters, v. 12, p 55–58.

Eggleton, R. E., 1964, Preliminary geology of the Riphaeus quadrangle of the Moon and definition of the Fra Mauro Formation, *in* Astrogeologic studies annual progress report, August 1962 to July 1963, pt. A: U.S. Geol. Survey open-file rept., p. 46–63.

Evans, N. M., Murthy, V. R., and Coscio, M. R., Jr., 1973, Taurus-Littrow—age of mare volcanism; chemical and Rb-Sr isotope systematics of the dark mantle soil: EOS (Am. Geophys. Union Trans.) v. 54; no. 6, p. 587–588.

Hartmann, W. K., 1970, Lunar cratering chronology: Icarus, v. 13, no. 2, p. 299–301.

——— 1972, Moons and planets: Tarrytown-on-Hudson, N.Y., Bogden and Quiglen, 404 p.

Hartmann, W. K. and Wood, C. A., 1971, Moon—origin and evolution of multiring basins: The Moon [Dordrecht, Holland], v. 3, p. 3–78.

Mark, R. K., Cliff, R. A., Lee-Hu C., and Wetherill, G. W., 1973, Rb-Sr studies of lunar breccias and soils, *in* Proceedings of Fourth Lunar Science Conference, Houston, Tex: Geochim. et Cosmochim. Acta, supp. 4, v. 2, p. 1785–1795.

McCauley, J. F., 1968, Geologic results from the lunar precursor probe: AIAA Jour., v. 6, p. 1991–1996.

Mutch, T. A., 1970, Geology of the Moon, a stratigraphic view: Princeton, N.J., Princeton Univ. Press, 324 p.

Nunes, P. D., Tatsumoto, Mitsunobu, Knight, R. J., Unruh, D. M., and Doe, B. R., 1973, U-Th-Pb systematics and some Apollo 16 lunar samples, *in* Proceedings of Fourth Lunar Science Conference, Houston, Tex.: Geochim, et Cosmochim. Acta, supp. 4, v. 2, p. 1797–1822.

Pohn, H. A., and Offield, T. W., 1970, Lunar crater morphology and relative age determinations of lunar geologic units, Part 1, Classification, *in* Geological Survey research 1970: U.S. Geol. Survey Prof. Paper 700–C, p. C153–C162.

Scott, D. H., 1972, Geologic map of the Maurolycus quadrangle of the Moon: U.S. Geol. Survey Misc. Geol. Inv. Map I–695, scale 1:1,000,000.

Soderblom, L. A., and Boyce, J. M., 1972, Relative ages of some near-side terra plains based on Apollo 16 metric photography: Apollo 16 Prelim. Sci. Rept. NASA SP–315, p. 29–3—29–6.

Soderblom, L. A. and Lebofsky, L. A., 1972, Technique for rapid determination of relative ages of lunar areas from orbital photography: Jour. Geophys. Research, v. 77, no. 2, p. 279–296.

Stuart-Alexander, D. E., 1971, Geologic map of the Rheita quadrangle of the Moon: U.S. Geol. Survey Misc. Geol. Inv. Map I–694, scale 1:1,000,000.

Stuart-Alexander, D. E., and Howard, K. A., 1970, Lunar maria and circular basins—a review: Icarus, v. 12, no. 3, p. 440–456.

Tera, Fouad, Papanastassiou, D. S., and Wasserburg, G. J., 1973, A lunar cataclysm at 3.95 AE and the structure of the lunar crust, *in* Lunar Science IV [abs.]: Houston, Tex., Lunar Sci. Inst., p. 723–724.

Wilhelms, D. E., 1970 Summary of lunar stratigraphy—telescopic observations: U.S. Geol. Survey Prof. Paper 599–F, 47 p.

Wilhelms, D. E. and McCauley, J. F., 1971, Geologic map of the near side of the Moon: U.S. Geol. Survey Misc. Geol. Inv. Map I–703, scale 1:5,000,000.

Jour. Research U.S. Geol. Survey
Vol. 3, No. 1, Jan.–Feb. 1975, p. 59–66

GEOMETRY AND GROWTH OF THE WHITE SANDS DUNE FIELD, NEW MEXICO

By EDWIN D. McKEE and RICHARD J. MOIOLA,[1] Denver, Colo., Dallas, Tex.

Abstract.—Recent studies of the cores from four drill holes at the White Sands dune field in New Mexico demonstrated that the eolian sand body below the present active dunes ranges in thickness from 23 to 34 ft in the area tested. It consists of one to two older generations of dune and associated interdune deposits, which rest on playa and fluvial deposits. Relatively thick sheets of clean, well-sorted dune sand are separated from one another by thin zones of darker colored interdune deposits. In vertical sections of test trenches and in cores, these interdune deposits appear as thin zones of tan or buff, poorly sorted, subparallel strata between relatively thick units of white cross-stratified sand. The interdune deposits are buried by the advancing foresets of the encroaching dunes and their thickness is limited by the time of exposure. The subsurface dune deposits are relatively thin as compared to the active surface dunes. This difference in thickness apparently results from the beveling or truncation of dunes by the migration of interdune areas.

This investigation was designed to determine the overall shape of the gypsum-sand dune field in the Tularosa Valley west of Alamogordo, N. Mex., and to ascertain its mode of genesis. The study is the third of a series undertaken to obtain a better understanding of the origin of this spectacular body of sand and of eolian sand seas in general.

The initial White Sands study, undertaken in 1963 and 1964, involved primarily the plotting, recording, and analysis of internal structures in each of four principal types of dunes (dome-shaped, transverse, barchan, parabolic) represented in the White Sands field (McKee, 1966). The second study, which was carried on during 1964–66, was concerned principally with the growth and movement of dunes at White Sands National Monument (McKee and Douglass, 1971). Thus, the present investigation should complete a general analysis, proposed and sponsored by the National Park Service, of the nature and development of the dune field.

Acknowledgments.—The National Park Service arranged for the drilling of four test holes in selected areas of the White Sands dune field, and cores from this drilling provided data critical to conclusions reached in this study. Support rendered by J. F. Turney, superintendent, and Hugh Bozarth, chief ranger, both of White Sands National Monument, is appreciated. Grateful thanks are given George Morrison, interpretive specialist, for his assistance throughout the project—in arranging logistics, furnishing materials, and helping with the fieldwork. We also gratefully acknowledge the assistance of A. B. Spencer and B. J. Phillips of Mobil Research and Development Corp. in studies and analyses of the sediments.

METHODS OF STUDY

In order to determine the geometry or overall shape of the sand sea at White Sands a method of direct approach has been used. Core drilling was done at four selected localities (fig. 1) in the dune field in order to obtain a rough approximation of dune thickness. The entire sand body occupies an area of about 278 mi^2; it extends approximately 12 mi from east to west and more than 30 mi from north to south. The portion of the sand body within the National Monument is about 8 by 12 mi.

While drilling was underway and soon afterward, numerous test trenches, 2–3 ft deep and 6–8 ft long, were hand dug with shovels in interdune areas, mostly at their junctions with advancing dune fronts or in places from which covering dunes had recently migrated. The trenches were designed to expose structure sections at places critical in the relations between superimposed dune sets and in overall dune growth.

SOURCE AND DIRECTION OF SAND MIGRATION

The principal source of gypsum sand that forms the White Sands dune field is a playa known as Lake Lucero and an alkali flat to the north of it that lie to the southwest and west, respectively, of the sand mass and at the eastern base of the San Andres Mountains. Prevailing winds are largely from the southwest but for a short period each year relatively strong winds also come from the north as described in phase one of this study (McKee, 1966, p. 11).

Downwind, an evolution from dome-shaped dunes to transverse, to barchan, to parabolic seems to be the

[1] Mobil Research and Development Corp.

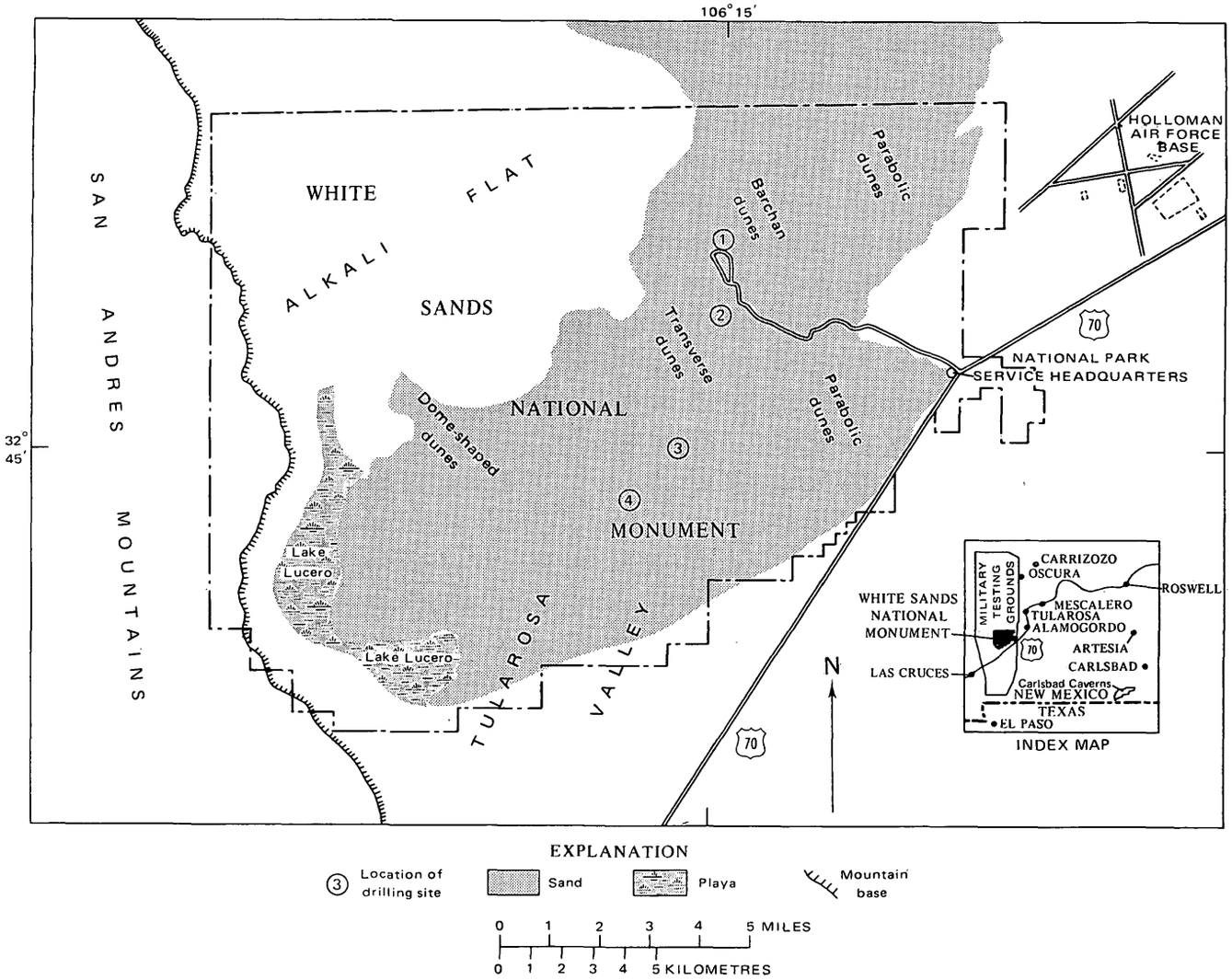

FIGURE 1.—Map showing four drilling localities, White Sands National Monument.

result of a decrease and dissipation of energy from southwest to northeast. Measurements of forward movement in embryonic or dome-shaped dunes near the sand source are recorded as about 30–40 ft/yr and those of the parabolic type downwind are mostly less than 10 ft/yr (McKee and Douglass, 1971, p. D113).

INTERDUNE AREAS

Critical to an understanding of the sand body at the White Sands dune field is an appreciation of the nature and extent of the interdune areas and of the deposits which they contain. The size and shape of these areas are apparent on a mosaic of the dune field (fig. 2). In the downwind or eastern part of the field the interdune areas occupy an amount of space that is equal to or greater than that covered by dunes of the present generation (fig. 3). Upwind, however, the interdune areas are progressively narrower and occupy proportionately less surface space than do adjacent active dunes (fig. 4).

Downwind, where the dunes are mostly barchanoid and form a complex pattern of crescents facing eastward, the interdune spaces appear in aerial view as very irregular blotches or patches that commonly have lengths as great as widths. In contrast, upwind the interdune spaces are delineated by the margins of transverse-type dunes and tend to be linear. These interdune spaces form long narrow bands, wavy and irregular, but continuous for great distances between dunes that are also linear, but several times as wide.

Composition, texture, and structure of deposits in interdune areas are distinctly different from those of contiguous dunes. Because interdune areas form scattered pockets, largely isolated within a sand sea, they commonly form traps for sediment introduced from the atmosphere, and they become havens for vegeta-

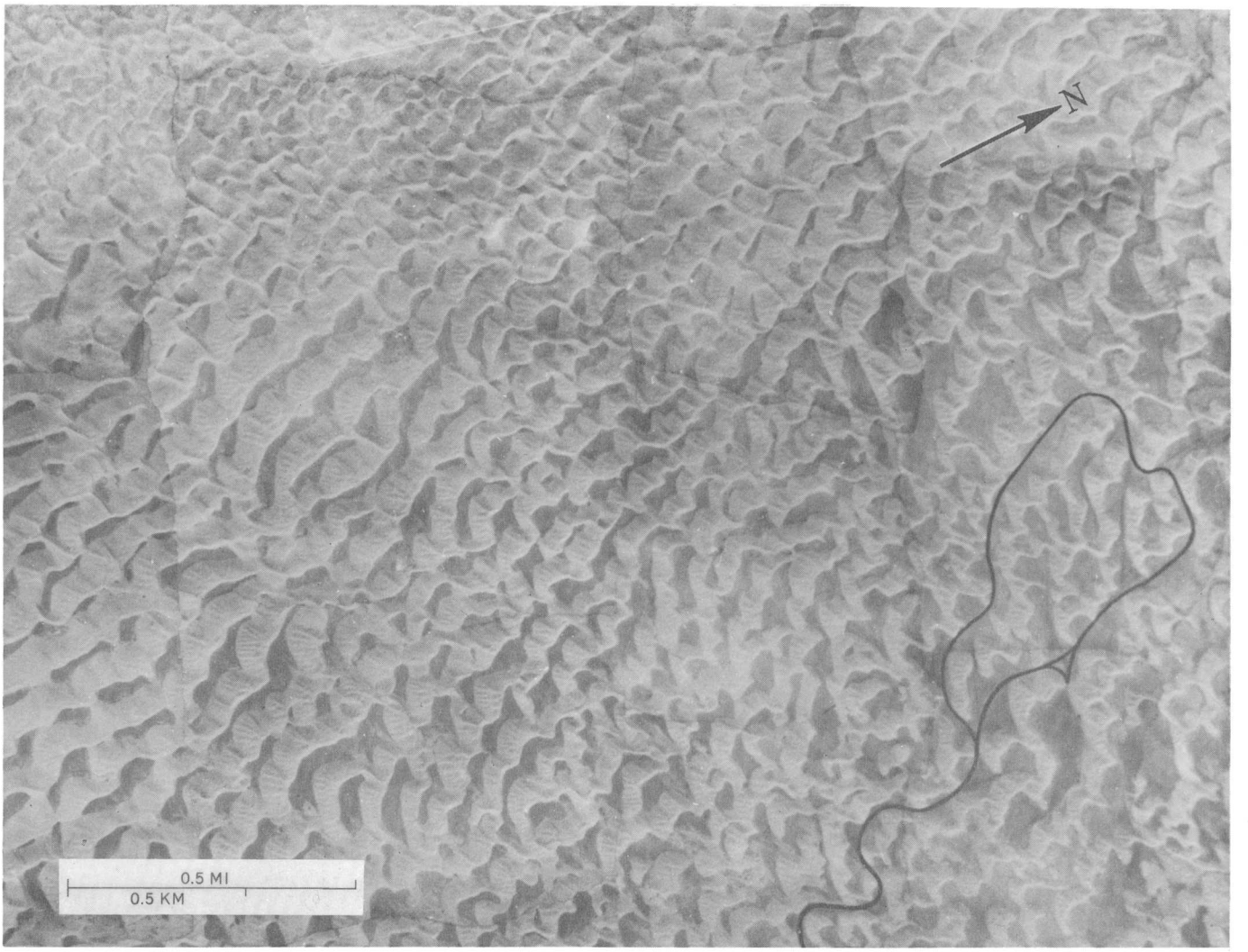

FIGURE 2.—Mosaic of aerial photographs illustrating size and shape of principal dunes and interdune spaces in White Sands dune field. Black line is principal road (paved) used by visitors to White Sands National Monument. Photograph courtesy of Holloman Air Force Base, 1973.

tion, especially xerophytic plants that locally contribute appreciable amounts of organic matter to the accumulating sediment. Only along margins of the dune field do stream-transported sediments find access to the interdune areas, and these occurrences are very uncommon.

Except where derived from vegetable matter, most of the sediment introduced into the interdune areas is dropped from suspension and is not deposited from saltation or avalanching as is the dune sand. For this reason the interdune sands are poorly sorted and contain a relatively high percentage of silt and clay. A conspicuous difference between dune and interdune sediments is shown in the color of each. The pure white of gypsum sand in the dune deposits contrasts with the usual tan or buff of the interdune deposits.

Textural analyses of sediment from the interdune area at locality 2 and from adjacent dunes (fig. 5) demonstrate the great contrast in grain size represented in these two types of deposit. Most of the interdune particles are less than one-fourth millimetre in diameter (fine sand, very fine sand, and silt), whereas the dune sands are well sorted and grains are predominantly medium sand, ¼ to ½ mm in diameter. Similar contrasts are shown in analyses of other paired samples from the White Sands dune field.

In addition to compositional, color, and textural differences, interdune deposits also have distinctive internal structures. They contain subparallel layers that are structureless, flat bedded, or irregularly bedded (figs. 6*C*, 7) in contrast to the dunes which are conspicuously cross-stratified.

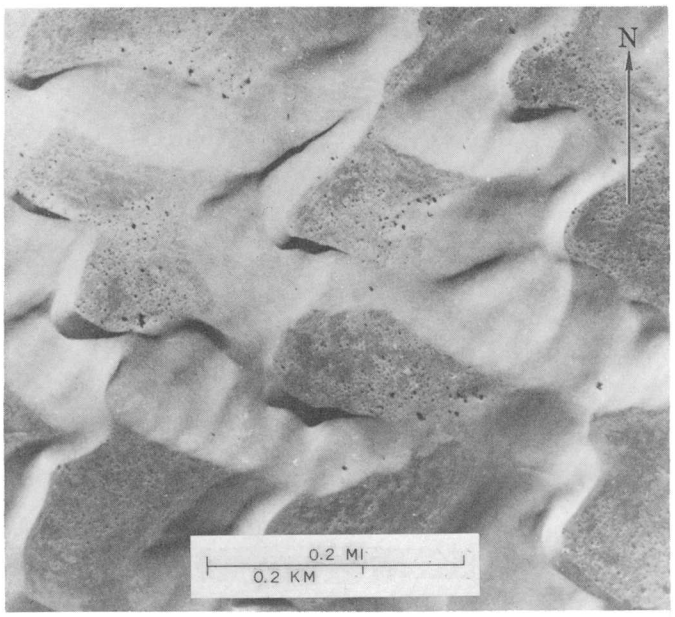

FIGURE 3.—Aerial photograph of compound barchan dunes in downwind area of White Sands field showing dunes and interdune spaces of approximately equal extent. Photograph courtesy of National Park Service, 1973.

MECHANISM OF SAND SEA GROWTH

An understanding of the growth mechanism of the sand sea may be obtained from observations of the present surface of the dune field. This surface consists of alternating dunes and interdune areas.

Interdune areas clearly are very ephemeral. Because all dunes are continuously migrating across the Tularosa Valley under the influence of a prevailing wind, the upwind side of each interdune area is progressively being buried beneath avalanching sand, whereas the opposite, downwind side of each interdune area is increasing in extent. This advance northeastward is a result of erosion and deflation along the margin of the next dune downwind (figs. 6–8). Thus, the lifespan of an interdune area in any particular place is determined by the time required for an approaching dune front to advance across the surface of the interdune area and to bury it.

With the migration of successive thick, cross-stratified dune deposits and thin, flat, or irregularly bedded interdune deposits across a dune field, a series of thick and massive light-colored sand layers and thin darker colored, finer grained units develops. For each generation of dune sand, consisting of one or more sets of cross-strata, the thickness has been shown by Shotton (1937, p. 543) to depend on the amount of sand available and on the strength and constancy of the wind. How thick the interdune units become between each generation of dunes is a function of the amount of time that an interdune area is exposed to the atmosphere before burial and the amount of fine sediment that is introduced during that time.

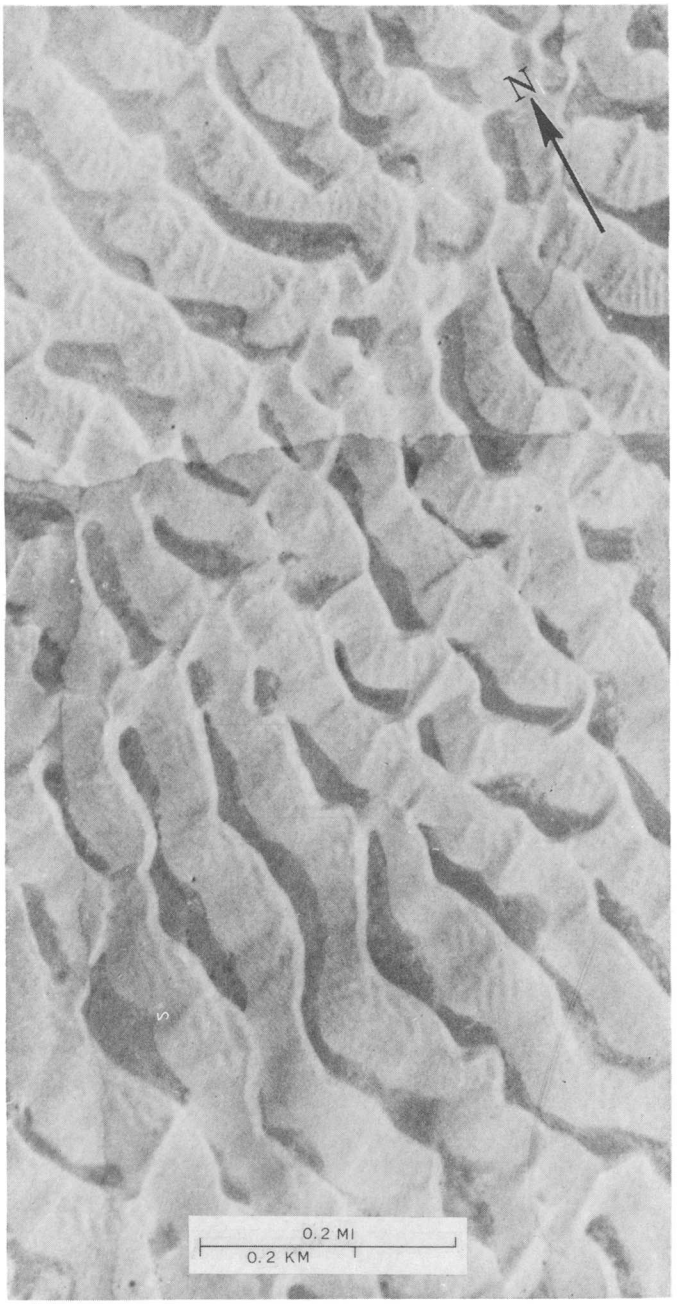

FIGURE 4.—Aerial photograph of transverse dunes in upwind area of White Sands field showing dunes that occupy several times more space than do the interdunes of that area. Photograph courtesy of Holloman Air Force Base, 1973.

Planes formed by the migration of interdune surfaces and marked by accumulation of dust, vegetable matter, and other debris are not precise time planes,

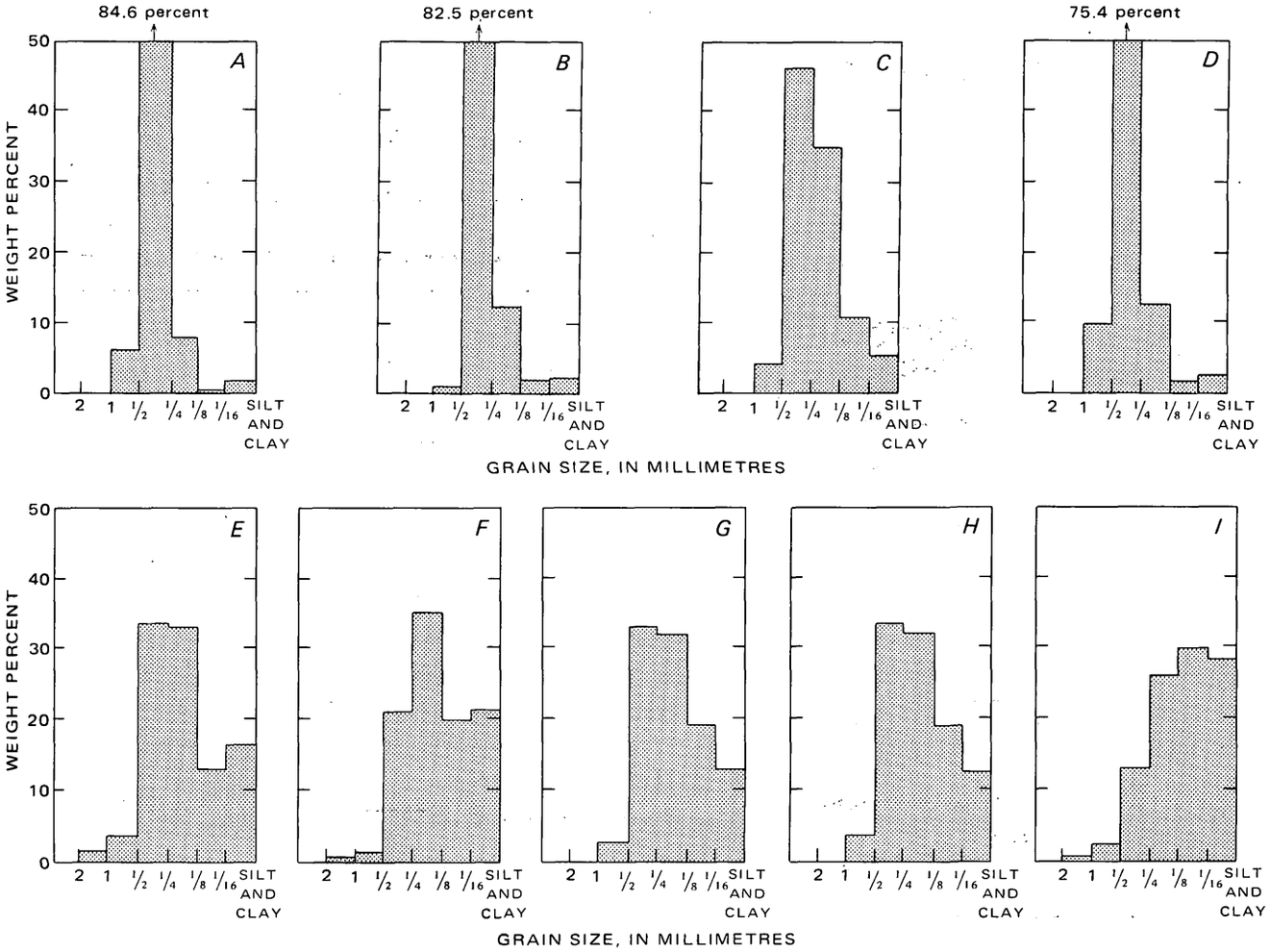

FIGURE 5.—Comparison of texture in some dune and interdune deposits at White Sands dune field. *A–D*, dune sand; *E–I* interdune sand. *A*, Dune sand, surface of transverse dune, slip face near bottom, at drill locality 2. *B*, Dune sand, windward side of crest, surface of transverse dune, at drill locality 2. *C*, Dune sand, from directly under brown flat-bedded sandy zone, in bottom of test trench 1, locality 1. *D*, Dune sand, white crossbedded sand directly above brown, flat-bedded sandy zone, at top of test trench 1. *E*, Interdune sand, from surface at margin of interdune, at drill locality 2. *F*, Interdune sand, from surface at center part of interdune, near drill locality 2. *G*, Interdune sand, flat beds of brown, impure sand from lower part, test trench 1. *H*, Interdune sand, flat beds of brown, impure sand from upper part, test trench 1. *I*, Interdune sand, surface impure sand, one-half mile southwest of drill locality 1.

but on a geologic scale probably approximate them. These subparallel bounding planes, which extend for considerable distances between sets or cosets of cross-stratified dune sands, have been explained (Stokes, 1968) as resulting from the removal by wind of the dry sand above water tables that are nearly horizontal. This explanation does not seem to be tenable, however, because water tables within dune fields are known to be far from horizontal and in laboratory experiments are seen to rise beneath each individual mound or dune. Thus, the explanation of migrating dunes and interdunes, illustrated by the nearly parallel surface A–A′ and B–B′ in figure 8, seems to better account for the parallel bedding planes common to many dune deposits.

THICKNESS OF SAND BODY

The thickness of sediment in a sand sea apparently is determined by the amount of sand and silt preserved beneath successive erosion surfaces that underlie advancing interdune deposits. Each successive layer of sand, with or without a silty parting plane, represents a generation of dune deposition and partial erosion and consists of sets or cosets of stratified dune sand and thin underlying silty interdune deposits. This record, therefore, is a function of the amount

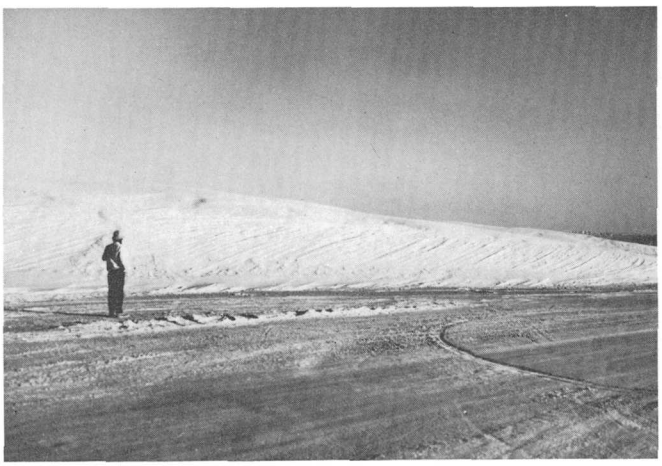

A

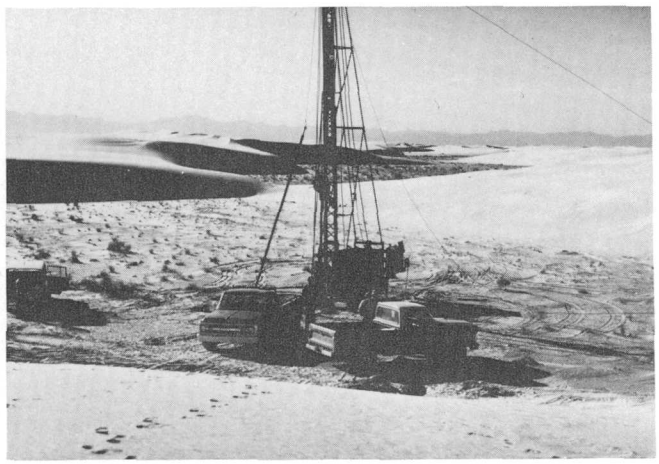

D

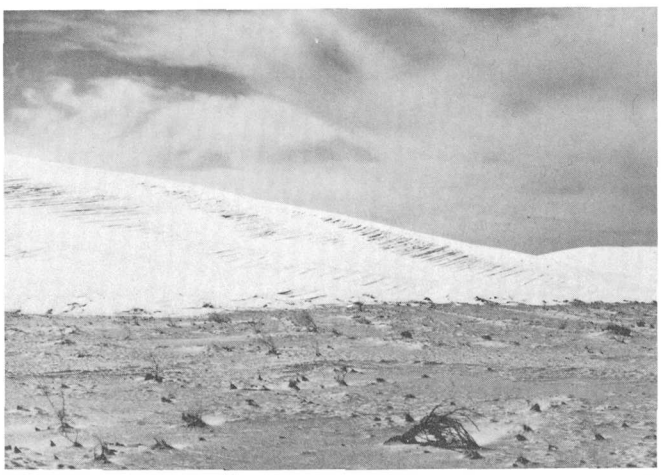

B

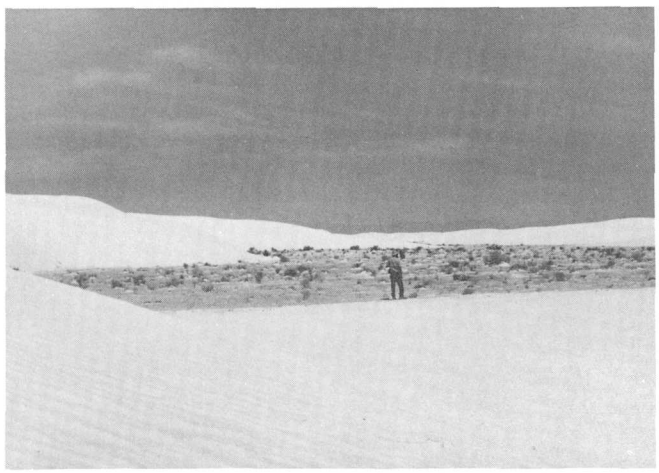

E

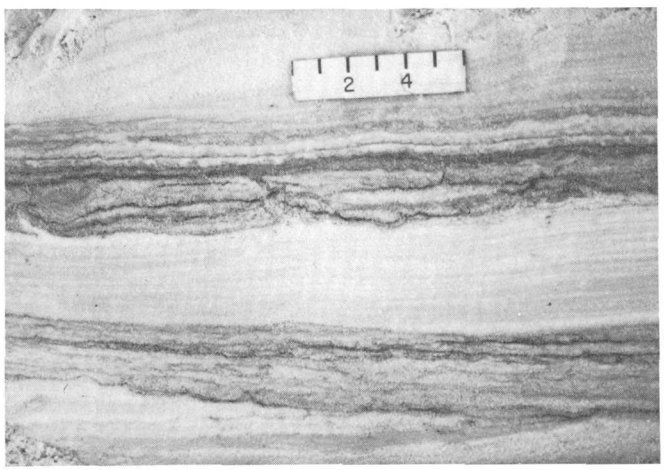

C

F

FIGURE 6.—Sedimentary structures and morphology of interdune areas. *A* and *B*, Beveled surface of dune foresets on upwind side of dune bordering interdune area (drill locality 1) in foreground. *C*, Section in test trench showing three layers of flat and irregularly bedded interdune deposits between dipping dune foresets; scale in inches. *D*, Drilling in interdune area at locality 1; lee side of complex dunes in shadow to left. *E*, Interdune area near locality 1. *F*, Vegetation and trapped sand on surface of interdune area near locality 1.

FIGURE 7.—Test trench in interdune area at lee base of transverse dune, drill locality 3, White Sands dune field. Dipping dune sands at top and bottom; wavy and horizontal interdune deposits between. Photograph by George Morrison.

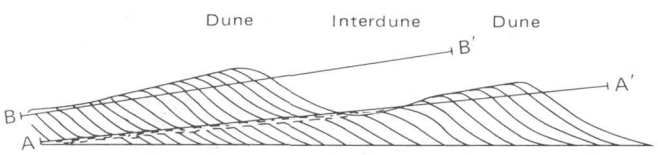

FIGURE 8.—Process of alternate development and burial of interdune surfaces with migration of dunes. Planes *A–A'* and *B–B'* are low-angle truncation planes formed during progression of interdune surfaces. Vertical scale greatly exaggerated.

of sand available at the source, the strength and constancy of the wind, and the time of accumulation with associated truncation.

At the White Sands dune field the thickness of the sand body has been determined at four localities (fig. 1) selected to give a random sampling in areas where dunes are currently well developed and where a better than average sand accumulation may be expected.

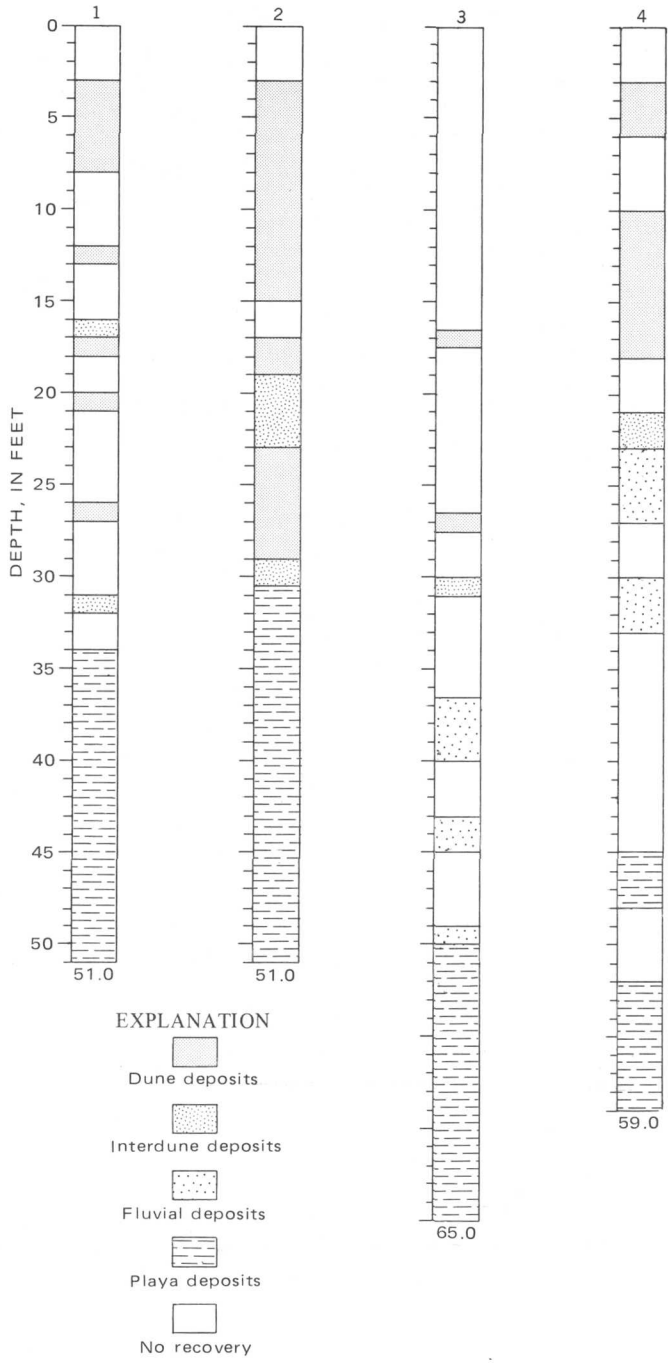

FIGURE 9.—Logs of cores from localities 1–4. Scale on left side of log 1 indicates depth in feet, the total being given at bottom of each log.

At each of the four localities a bore hole was drilled (fig. 6*D*) and cores were obtained for examination (fig. 9). The depth of the sand body as recorded in the cores ranges from 34 ft (at locality 1) to 23 ft (at locality 4). Thus, a thickness averaging about 20–30 ft of eolian sand seems to underlie much of the field. This

sand rests upon a surface of earlier fluvial and playa deposits.

The cores indicate that the sand body contains thin (1–4 ft) zones of tan, silty sand, interpreted as interdune deposits, at various levels within white dune sand. These horizontal to irregularly bedded zones of silty sand subdivide the sand mass into units that represent dune sheets of earlier generations. These sheets, which average approximately 15 ft in thickness, are much thinner than present dune deposits, which range generally from about 20 to 30 ft in thickness. Probably this large difference in thickness between modern dunes and the buried relicts of earlier generations can be explained by a normal truncation or beveling of the upper parts of all dunes before being covered by interdune surface deposits and being buried by new sets of advancing dunes (fig. 8).

Two generations of dunes separated by thin interdune deposits can be recognized in the subsurface at localities 1 and 2. Farther west and south at localities 3 and 4 only one older unit of dune sand appears below the level of the present active dunes (fig. 9).

REFERENCES CITED

McKee, E. D., 1966, Structures of dunes at White Sands National Monument, New Mexico (and a comparison with structures of dunes from other selected areas): Sedimentology, v. 7, no. 1, spec. issue, 69 p.

McKee, E. D., and Douglass, J. R., 1971, Growth and movement of dunes at White Sands National Monument, New Mexico, *in* Geological Survey research 1971: U.S. Geol. Survey Prof. Paper 750–D, p. D108–D114.

Shotton, F. W., 1937. The lower Bunter sandstones of north Worcestershire and east Shropshire: Geol. Mag., v. 74, no. 882, p. 534–553.

Stokes, W. L., 1968, Multiple parallel-truncation bedding planes—A feature of wind-deposited sandstone formations: Jour. Sed. Petrology, v. 38, no. 2, 510–515.

Jour. Research U.S. Geol. Survey
Vol. 3, No. 1, Jan.–Feb. 1975, p. 67–76

A PROPOSED GLACIAL HISTORY OF THE HENRYS LAKE BASIN, IDAHO

By IRVING J. WITKIND, Denver, Colo.

Abstract.—Deposits of several glaciations—from oldest to youngest, pre-Bull Lake, Bull Lake, and Pinedale—are in and near the Henrys Lake basin, a northwest-trending hourglass-shaped trough in southeastern Idaho. Glacial deposits of pre-Bull Lake age are represented by till remnants confined mostly to the higher levels of the surrounding mountains. The extent of Bull Lake ice into the basin is uncertain. Glacial deposits and ice-marginal features suggest that a lobe of Bull Lake ice —the Henrys Lake ice lobe—moved into the basin and advanced as far north as the north edge of Henrys Lake. After this lobe melted back far enough to expose the north end of the basin, melt waters, chiefly from alpine glaciers in Targhee Creek and its tributaries, formed the broad low Howard Creek fan at the mouth of the valley of Howard Creek. Shortly thereafter, a complex of channels was cut into the fan by periodic melt-water floods which flowed westward through Targhee Pass during the waste of another Bull Lake ice lobe which lay in the West Yellowstone Basin. Melt waters from various sources ponded to form a shallow lake in front of the wasting Henrys Lake ice lobe. Waters from this lake drained southwestward around the southwest flank of the lobe via an ice-marginal channel. Upon total melt of the ice lobe, the lake was drained, the ice-marginal channel was abandoned, and the waters resumed their pre-ice course to the southeast. During the interglaciation, prior to the onset of the Pinedale Glaciation, northward-flowing streams deposited a veneer of obsidian sand and gravel along the south edge of the basin. In Pinedale time, alpine glaciers formed in the high mountain valleys near the basin, but none advanced into the basin.

Henrys Lake is a broad shallow body of water that occupies the north end of an hourglass-shaped northwest-trending basin. This basin, known as Henrys Lake Flat or Henrys Lake basin, is wholly within southeastern Idaho, but the surrounding mountains extend into southwestern Montana (fig. 1). The basin, about 26 km (16 mi) long and 3–8 km (2–5 mi) wide, covers about 145 km^2 (90 mi^2).

On the west, north, and east the basin is bounded by the Henrys Lake Mountains, on the southwest by Sawtell Peak which forms the eastern tip of the east-trending Centennial Mountains, and on the south and southeast by a broad forest-covered plain underlain by volcanics that flowed westward from Yellowstone National Park and northward from the Island Park caldera.

KNOWN GLACIAL HISTORY

Deposits of several glaciations are in the area; from oldest to youngest these are pre-Bull Lake, Bull Lake, and Pinedale (Richmond, 1964). The evidence for the pre-Bull Lake glaciations and the Pinedale Glaciation in the Henrys Lake area is clear and abundant, but it is less certain for the Bull Lake Glaciation.

Pre-Bull Lake glaciations

This part of southwestern Montana and southeastern Idaho was overridden by one or more ice sheets during pre-Bull Lake time, but how many ice advances occurred is unknown. Recent geologic investigations in Yellowstone National Park suggest that at least three major ice advances took place during the pre-Bull Lake glaciations (G. M. Richmond, oral commun., 1972). In any event it seems likely that extensive deposits of pre-Bull Lake till were spread across this area. Only remnants of these once-widespread deposits are still preserved; in the Henrys Lake area they are confined to high-altitude benches in the mountains east of the lake (fig. 2).

Bull Lake Glaciation

Conclusive evidence in Yellowstone National Park demonstrates that two widespread ice advances occurred during the Bull Lake Glaciation (Richmond, 1970; 1972, p. 319–321; H. A. Waldrop and K. L. Pierce, unpub. data, 1974). The first took place during early Bull Lake time, and its leading edge extended westward beyond the park boundary. The second occurred during late Bull Lake time, but its leading edge did not extend into the Henrys Lake–West Yellowstone area (H. A. Waldrop and K. L. Pierce, unpub. data, 1974).

The early Bull Lake ice advanced westward as a broad sheet from central Yellowstone National Park into the Henrys Lake–West Yellowstone area (Waldrop, 1974). When the leading edge of the ice reached the southern end of the Henrys Lake Mountains (represented by Mount Two Top), it split into two lobes. The northern lobe, deflected northward, spread across the floor of the West Yellowstone Basin. This lobe, called the Horse Butte lobe (Witkind, 1969, p. 55, 83), reached as far north as Horse Butte, and its western edge rode up onto the east flank of Mount Two Top

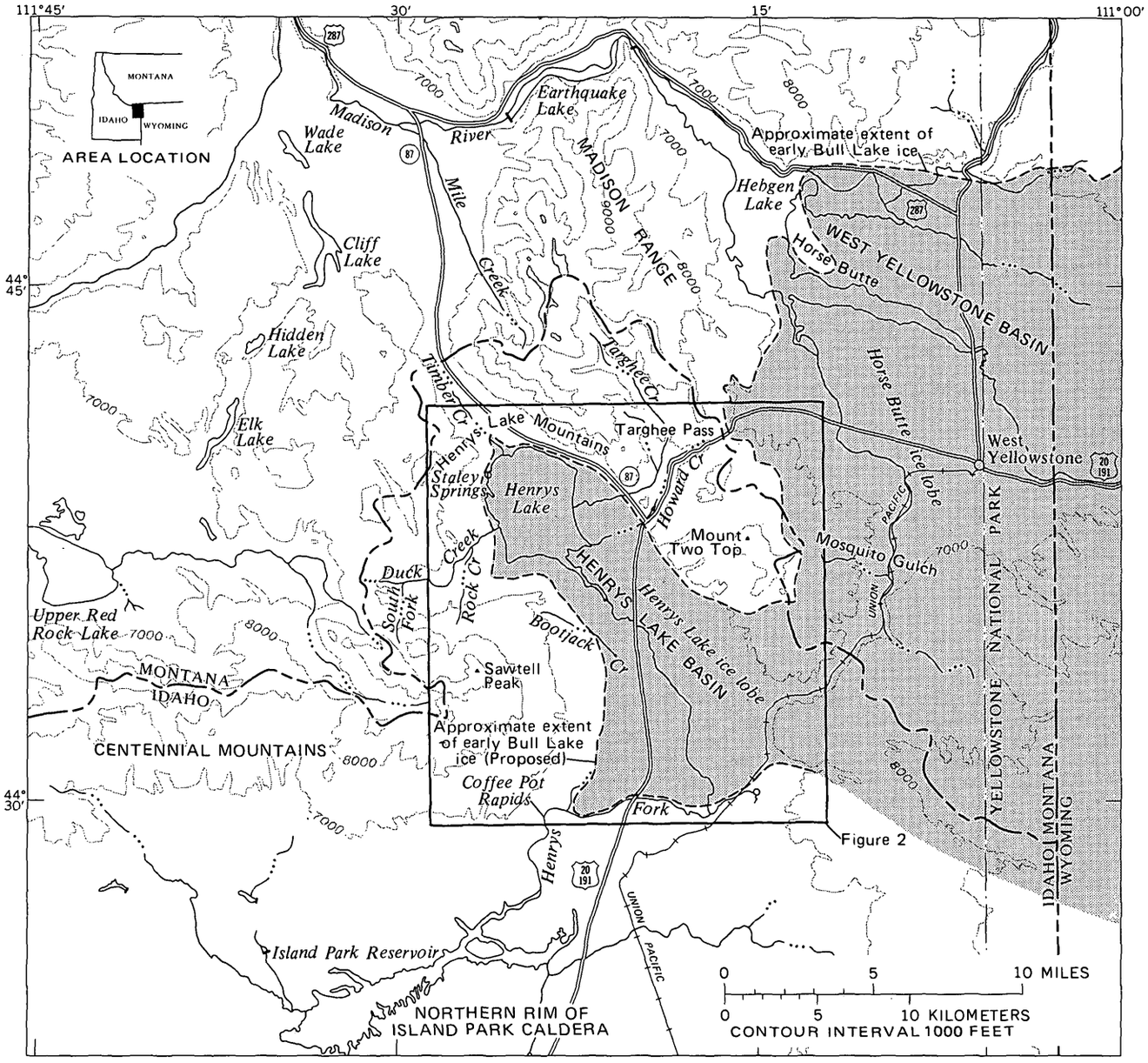

FIGURE 1.—Index map of area near Henrys Lake.

(fig. 1). Its limit, marked by both basalt and obsidian boulders in the till, has been mapped by Waldrop (1974). On the basis of these erratics it appears that the western margin of the Horse Butte lobe may have been just high enough to contribute melt water through Targhee Pass to the Howard Creek drainage. The highest altitude reached by the ice near Targhee Pass cannot be determined unequivocally but at the maximum thickness of the ice it seems likely that its western margin reached an altitude of about 7,150 ft, some 80 ft above the floor of the pass which is at an altitude of 7,072 ft.

Obsidian erratics, marking the early Bull Lake ice limit, can be traced southward from Targhee Pass along the east flank of Mount Two Top until they pass around its south end at an altitude of about 7,760 ft (Waldrop, 1974). It would appear that the southern lobe of Bull Lake ice, here called the Henrys Lake lobe, passed south of the low south end of Mount Two Top and moved westward into the Henrys Lake basin (fig. 1). Likely it followed a broad flat now concealed beneath the toe of the West Yellowstone flow (fig. 2).

How far this ice advanced into the Henrys Lake basin is not clear. I believe that this southern ice lobe

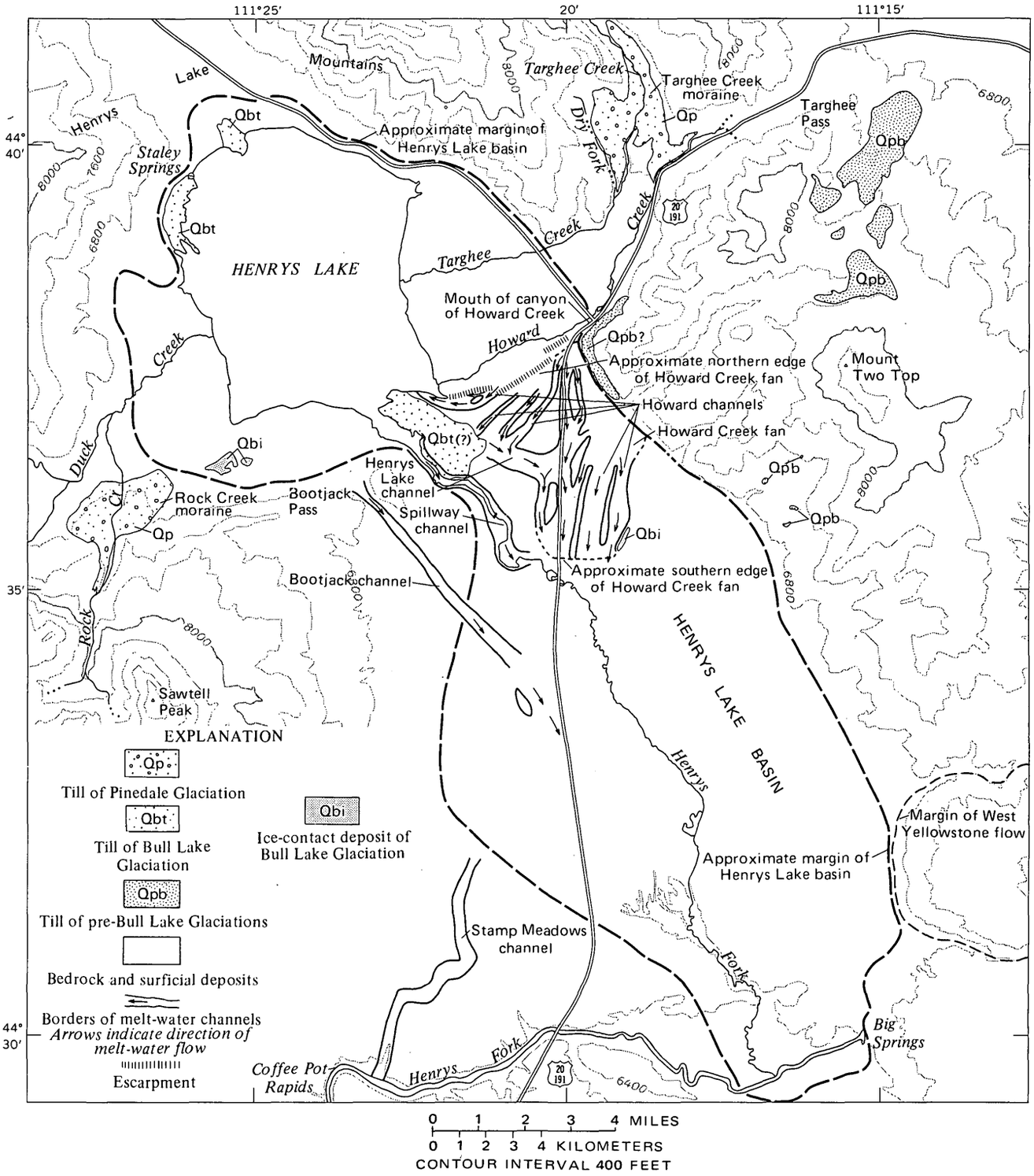

FIGURE 2.— The Henrys Lake basin showing distribution of glacial deposits of various ages, and the pattern of melt-water channels.

advanced to the north edge of the basin and that the glacial features and deposits within and near the basin are the result of its waste. I suggest that during the maximum advance of early Bull Lake ice into this area the southern end of the Henrys Lake Mountains was flanked by two ice lobes—an eastern one (Horse Butte lobe) filling much of the West Yellowstone Basin and a western one (Henrys Lake lobe) occupy-

ing all of the Henrys Lake basin (fig. 1). The thickness of ice probably ranged from a few metres at the northernmost edge of the lobes to possibly 600 m (2,000 ft) near their centers.

Pinedale Glaciation

Pinedale Glaciation in the Henrys Lake area was marked by the development of local alpine glaciers in the high mountains. These glaciers flowed down nearby canyons and several spread out onto the broad alluviated flats of Duck Creek. One, in Targhee Creek, never extended beyond the mountain front. (See "Pinedale Till of mountain glaciers.")

GLACIAL DEPOSITS OF THE HENRYS LAKE AREA

Pre-Bull Lake nonstratified drift: high-altitude till deposits

Patches of bouldery till, marked by a well-integrated drainage pattern, and small clusters of glacial erratics mantle the wide benches directly below the crest of Mount Two Top. These deposits are at altitudes which range from 7,200 to 8,300 ft with most confined to a 400-ft zone between 7,600 and 8,000 ft (fig. 2). In addition, individual glacial erratics, randomly distributed, are found practically everywhere on the uplands except on top of the narrowest ridges. Some are as small as fine gravel; others are boulders as much as 5 m (15 ft) across.

Rock types in the till and in the boulder clusters, irrespective of location, are similar. Precambrian crystalline rocks predominate, with a light-gray coarse-grained metagranodiorite most common. Other abundant lithologies are a pink pegmatite, a dark-gray foliate amphibolite, a brown mica schist, a light-gray to greenish-gray micaceous quartzite, and a light-brown dolomite. There are also small amounts of both mafic and felsic volcanic rocks. Sedimentary rocks are either sparse or absent.

The thickness of the soil that formed on the till is unknown, for in most places whatever soil was formed appears to have been destroyed by erosion.

Till or pitted outwash of Bull Lake age near Henrys Lake

Deposits of what may be till, or possibly pitted outwash, are on the southeast, west, and north sides of Henrys Lake (figs. 2 and 3). All three deposits are similar in appearance and composition. The largest, southeast of the lake, forms part of the northeast flank of the Henrys Lake arm. This deposit covers about 1 km^2 (0.5 mi^2), and its surface—in sharp contrast to the surrounding terrain—is characterized by modified knob-and-kettle topography. Some of the kettles have been breached by northeastward-reaching tributaries of the Henrys Lake arm, but most are still whole and appear little modified. A few kettles near the lakeshore contain water. As the water level in these kettles rises and falls more or less in concert with Henrys Lake, the till or pitted outwash must be somewhat permeable.

The till or pitted outwash is nowhere well exposed, but, judging by the detritus in roadcuts and near small animal burrows, it consists of a mixture of silt and fine to coarse sand and gravel with little to no clay. No cobbles or boulders were noted. Rock types include Precambrian crystalline as well as sedimentary and volcanic rocks.

The two other till or pitted outwash deposits near Henrys Lake are also characterized by good knob-and-kettle topography and many of the kettles are filled with water. The kettles in the deposits along the north shore of the lake show a distinct northeast alinement; a similar alinement, but not as marked, characterizes the deposit along the lake's west shore near Staley Springs. This northeasterly trend, however, may reflect the prevailing wind direction—from the southwest—rather than any preferred orientation of relict ice blocks. The till or outwash is so loose and unconsolidated that the original kettles, of whatever form, may have been modified and shaped by the southwesterly winds.

These deposits are provisionally assigned to the Bull Lake Glaciation on the basis of both their morphology and their geologic setting. Elsewhere in this region the pre-Bull Lake till deposits are marked by a mature well-integrated drainage pattern free of knob-and-kettle topography; obviously they have been exposed to erosion for a long time. And conversely the much younger Pinedale moraines consist of little more than a repetitive sequence of irregularly distributed knobs and kettles; they seem to have been deposited yesterday. Further, the pre-Bull Lake till deposits appear to be confined to the higher reaches of the mountains, whereas those of Pinedale age are confined almost wholly to the mountain valleys. Most of the Pinedale moraines extend but a short distance beyond the canyon mouths. By elimination, then, these till-like deposits on the floor of the Henrys Lake basin are assigned to the intervening Bull Lake Glaciation, for their somewhat modified knob-and-kettle topography suggests that they are younger than the pre-Bull Lake till deposits but older than the Pinedale ones. This age assignment is supported by their position in the middle of the basin beyond the margins of the Pinedale moraines.

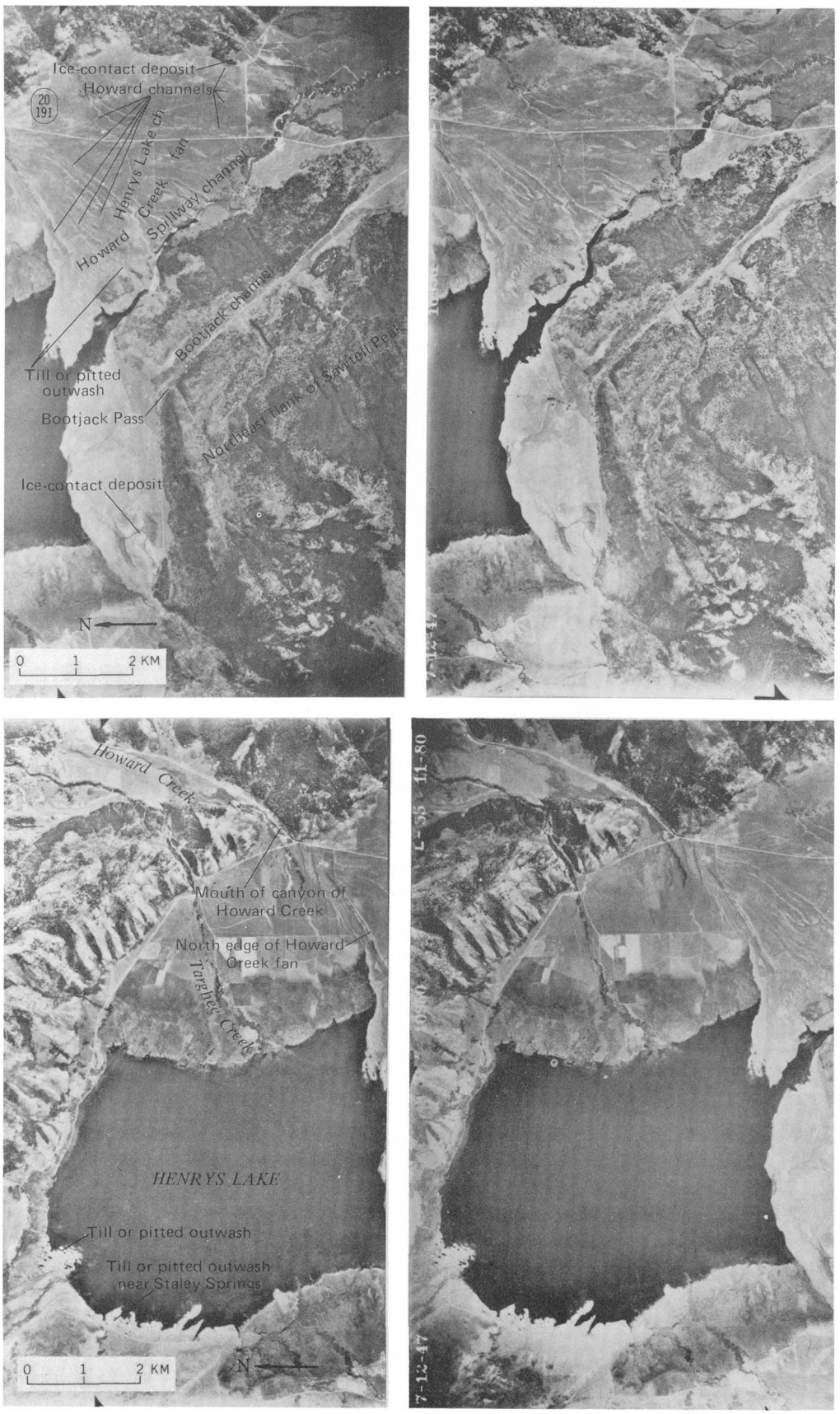

FIGURE 3.—Stereopairs of the north end of the Henrys Lake basin showing most of the geologic features described in text. Aerial photographs taken in 1947.

These till-like deposits may represent debris deposited by alpine glaciers of Bull Lake age but, if so, I am unable to relate them to any specific local moraine formed during that glaciation.

Pinedale Till of mountain glaciers

Although till deposited by mountain glaciers is common in this general area, no such deposits are in the Henrys Lake basin. Three broad, lobate terminal moraines which stem from mountain glaciers are near the basin's margins. Two moraines, at the mouths respectively of Rock Creek and South Fork Duck Creek (along the north face of the Centennial Mountains), have spread onto the wide flood plain of Duck Creek where the flood plain merges with the floor of the Henrys Lake basin. A third moraine fills part of the broad valley of Targhee Creek. A lobe of this moraine extends southeastward across the valley of Howard Creek and confines Howard Creek and U.S. Highway 20–191 to a narrow valley about 60 m (200 ft) wide. North of this constriction the unobstructed valley is about half a kilometre (a third of a mile) wide (fig. 2); south of it the valley merges with the valley of Targhee Creek to form a broad flood plain about three-fourths of a kilometre (half a mile) wide.

In general, all three terminal moraines are about equal in size; each covers an area of about 2.5 km^2 (1.5 mi^2). The two moraines along the north face of the Centennial Mountains are similar; their outer limits consist of several almost parallel curved ridges, some 25–30 m (80–100 ft) high, behind which is a hummocky terrain marked by unmodified knob-and-kettle topography. The Targhee Creek moraine, by contrast, appears to have been modified somewhat by Targhee Creek which has cut it in two. The knob-and-kettle topography which is so marked in the other alpine moraines is not as well defined in this one, either as a result of dissection by the creek or because the moraine is of Bull Lake age, as suggested by F. L. Nials of Eastern New Mexico University (oral commun., 1970), and hence more mature.

Rock types in the moraines reflect the bedrock exposed at the heads and along the flanks of the canyons. Generally Precambrian rocks predominate, but there are also many sedimentary rocks, mainly limestone, dolomite, and sandstone. In size, the debris ranges from rock flour to boulders as much as 3 m (10 ft) on a side. The till is completely unsorted.

The morphology and setting of the Centennial Mountains moraines clearly stamp them as being of Pinedale age; the age of the one in Targhee Creek is uncertain. I believe that it too is Pinedale in age, but others (for example, F. L. Nials, oral commun., 1970) think that it may consist of moraines of both Pinedale and Bull Lake age.

Stratified drift of early Bull Lake age: ice-contact deposits

Two deposits of unconsolidated silt, sand, and gravel are believed to have formed against ice.

One deposit, near the southwest corner of the lake, consists of several low irregular-shaped hills separated by broad shallow kettles (figs. 2 and 3). These hills rise about 8 m (25 ft) above the adjacent terrain. At the few available exposures the hills consist of cross-bedded fine silt and sand with a few interspersed pebbles. The irregular bedding and the intervening kettles imply deposition in close contact with ice.

The other deposit is a narrow, linear, steep-sided ridge of sand and gravel near the east side of the Henrys Lake basin (figs. 2 and 3). The ridge is about half a kilometre (a third of a mile) long and 60 m (200 ft) wide; its uneven crest rises some 8 m (25 ft) above the adjacent surficial deposits. The steep sides and the hummocky irregular crest suggest an ice-contact origin.

The fact that these deposits are beyond the Pinedale moraines suggests that they are older than the Pinedale Glaciation, and the presence of unbreached kettles implies that they are younger than the pre-Bull Lake ones. Hence, I consider that they were formed during the early stade of the Bull Lake Glaciation.

Proglacial deposits of early Bull Lake age: Howard Creek fan

Extending to the southwest from the mouth of the canyon of Howard Creek is the southern half of what once must have been a large low conical alluvial fan, here named the Howard Creek fan (figs. 2 and 3). The northern half of the fan has been removed either by faulting or by erosion (see "Howard channels"), and its place is now occupied by a younger even-floored alluvial fan crossed by Targhee and Howard Creeks.

The fan is composed of unconsolidated sand and gravel. These deposits commonly are light gray, locally crossbedded, and poorly to moderately well sorted. They range in size from silt to small cobbles and in shape from subround to round. The rock types are mainly sedimentary limestones and dolomites, Precambrian crystallines, and some volcanics. Lithologic types consist of: sedimentary rocks—76 percent; metamorphic rocks—13 percent; felsic volcanic rocks—9 percent; and mafic volcanic rocks—2 percent.

Interlayered in the sand and gravel are lenses and beds as much as 2 m (7 ft) thick of a light-gray volcanic ash consisting chiefly of pumice shards. Several beds of clay of unknown thickness and extent are also present.

Alden (1953, p. 178) suggested that this fan was formed by a combination of wash down Targhee Creek and of melt water, discharged through Targhee Pass, from an ice mass which lay in the West Yellowstone Basin. The preponderance of sedimentary and Precambrian crystalline rock types in the fan, however, suggests to me that the fan is dominantly a product of melt waters of glaciers which once occupied the valleys of Targhee Creek and its tributaries, for the rock types in the fan are similar to those rocks which crop out in these stream valleys. By contrast, debris derived from the ice lobe in West Yellowstone Basin—the Horse Butte lobe—would likely be volcanic, for that ice sheet overrode mainly volcanic rocks in its westward movement across the park.

I agree with Alden's suggestion that melt waters flowed through Targhee Pass, but I believe that this flowage occurred after the fan was formed and that these waters are responsible for a complex of channels cut in the fan.

Waldrop's work (1974) has suggested that the Horse Butte lobe, which occupied the West Yellowstone Basin, was of early Bull Lake age. (See "Known Glacial History.")

Presumably it was during the melt of this ice that melt waters cut the channels; the fan then, must have been formed prior to that time. Although the fan possibly was built during one of the pre-Bull Lake glaciations, more likely it was formed as a result of the melt of early Bull Lake alpine glaciers. If so, the Henrys Lake ice lobe by that time must have melted back far enough to expose the northern end of the Henrys Lake basin.

MELT-WATER CHANNELS OF EARLY BULL LAKE AGE

Howard channels

Incised into the preserved part of the fan are 12 channels that trend south and southwestward and fan out from the mouth of the canyon of Howard Creek; hence, I refer to them as the Howard channels (fig. 2 and 3). They are much alike. Each maintains an even width throughout its length. Generally the channels are 0.75–1.50 km (0.5–1.0 mi) long, and 150–500 m (500–1,650 ft) wide; they are cut some 3–6 m (10–20 ft) into the unconsolidated deposits that form the fan.

For much of their length the channels are well delineated with clearly defined walls. But their heads —at the mouth of the canyon of Howard Creek— seem to merge. The walls become less distinct and appear to blend into the general configuration of this part of the fan. Just northwestward beyond this point, the heads and flanks of several of these channels are abruptly truncated by steep northeast-trending escarpments which form the north edge of the preserved part of the Howard Creek fan. To the south the mouths of most of the channels merge with the basin floor. In places, the floors of these channels are mantled by a reddish-brown deeply weathered clayey soil 30–40 cm (12–16 in.) thick.

How these channels formed is uncertain. Of several explanations, only two will be mentioned here. First is the possibility that the channels were formed immediately following the development of the Howard Creek fan. Alden's proposal (1953, p. 178) that the Howard Creek fan was formed in part by sediment-laden melt waters flowing through Targhee Pass leads to the further assumption that after the fan was formed a change in regimen occurred and relatively clear water started flowing through the pass. This water not only scoured away whatever sediments had been deposited in the valley of Howard Creek, but, once beyond the valley mouth, it spread across the fan and cut the channels.

Another alternative, which I favor, is that periodic floods—a result of either seasonal melt or of the seasonal breakage of ice dams—cut the channels. The concept of seasonal melt of the Horse Butte ice lobe is self-explanatory. The concept of the periodic breakage of ice dams is based on the seasonal breakout of Lake George in the Chugach Mountains of Alaska (Stone, 1963). There, during the winter months, the Knik glacier expands and presses against the flank of Mount Palmer, effectively closing off the valley of Lake George. As a result a temporary ice-dammed lake—Lake George—is formed, fed by melt waters from several glaciers. During the summer the ice melts and the impounded waters of Lake George break through the weakened dam in a torrential flood. The lake empties rapidly, generally in a matter of weeks.

One place in the Henrys Lake area where such an ice dam could have formed is suggested by the lobe of the Targhee Creek moraine which extends across the valley of Howard Creek. (See fig. 2 and "Pinedale Till of mountain glaciers.") Presumably each winter the glacier that lay in Targhee Creek expanded across the valley of Howard Creek and pressed against the creek's east valley wall to form an effective ice

dam. If this concept is correct, the lobe of the Targhee Creek moraine must have been deposited during the Bull Lake rather than during the Pinedale glaciation. (See "Pinedale Till of mountain glaciers.") Another possible site for this ice dam is Targhee Pass which may have been periodically sealed by expansion of the Horse Butte ice lobe. In this situation, the melt waters would have been confined between the west edge of the ice lobe and the east wall of the Henrys Lake Mountains.

In whatever way these melt water floods were formed —whether by seasonal melt of the Horse Butte ice lobe, or by periodic breakage of ice dams—I suggest that each spring these floods poured through Targhee Pass and surged down the valley of Howard Creek to spill onto the fan. This sudden torrent of water was probably a very rapid affair, begun and ended quickly, possibly in a matter of days. As the torrential discharge slackened, outwash was deposited at the heads of these channels, effectively blocking their use during subsequent breakouts. When the next breakout occurred, presumably during the following spring thaw, the new flood waters were deflected laterally and, following the configuration of the fan, cut new channels in its surface.

It is unknown how the north half of the fan was removed. W. B. Myers and Warren Hamilton of the U.S. Geological Survey (oral commun., 1959) have suggested that the escarpments which mark the north edge of the preserved part of the fan are fault scarps formed during reactivation of the eastward-trending Centennial fault. Thus, one possible explanation is that this north half of the fan was downthrown along a north-dipping normal fault. I believe, however, that the escarpment reflects the extensive erosion that occurred when melt waters, produced during the late stages in the melting of the Horse Butte ice lobe, flowed through Targhee Pass and the valley of Howard Creek and destroyed the north half of the fan.

Ice-marginal channels at waist of basin

Of the four channels likely formed in close contact with ice, three—Bootjack, Spillway, and Henrys Lake channels—are near the waist of the Henrys Lake basin; the fourth—Stamp Meadows—is about 10 km (6 mi) to the south at the southwestern end of the basin.

Two of the three channels at the basin's waist—Bootjack and Spillway—are incised into the northeast-sloping flank of Sawtell Peak, and thus are almost at right angles to the local slope of the land (figs. 2 and 3). They are classed as ice-marginal channels. The third, at the break in slope between the northeast flank of Sawtell Peak and the toe of the Howard Creek fan, probably acted as a collector channel for melt waters flowing through several of the Howard channels.

Bootjack channel—This channel is the farther southwest of the two and also the higher, at an altitude of 6,720 ft. It is on the flank of Sawtell Peak. The channel is straight, trends about S. 40° E., and is about 5 km (3 mi) long and about 122 m (400 ft) wide. For part of its length it is cut in rhyolitic tuff. Its northwest end forms a small windgap known as Bootjack Pass, some 76 m (250 ft) above Henrys Lake. Its southeast end merges with the broad alluvium-covered floor of the south end of the Henrys Lake basin. The channel floor slopes about 75 ft per mile.

Spillway channel.—This channel, at an altitude of about 6,520 ft, still serves as the outlet for waters of modern Henrys Lake. It trends about S. 50° E., and is about 5 km (3 mi) long and 110 m (360 ft) wide. It also is incised into rhyolitic tuff. The channel floor slopes about 50 ft per mile.

The position of the channels athwart and incised into the northeast-sloping flank of Sawtell Peak implies that those channels are ice-marginal features. If so, they reflect the southwest margin of a former ice mass that lay northeast of Sawtell Peak. Their parallelism suggests that they were formed as this ice wasted and its margin withdrew downslope (northeastward).

Collector channel: Henrys Lake channel. —This channel is a broad shallow trough that follows the break in slope between the northeast flank of Sawtell Peak and the toe of the Howard Creek fan. It heads in the mass of till or pitted outwash along the southeast corner of Henrys Lake and cuts obliquely southeastward to end at one of the larger Howard channels (figs. 2 and 3). The floor of the channel is at an altitude of about 6,500 ft. The north flank of the channel is an abrupt escarpment broken only by the mouths of three of the westernmost Howard channels; its south wall, however, is less abrupt and slopes gently up to the edge of the incised Spillway channel. It trends about S. 70° E., and is about 1.5 km (1 mi) long and 500 m (1,650 ft) wide. Its north wall is cut about 10 m (30 ft) into the unconsolidated sand and gravel that makes up the Howard Creek fan. It appears to have been occupied by melt waters that flowed into it from the three Howard channels.

Ice-marginal channel at southwestern end of basin

Stamp Meadows channel.—This channel, some 10 km (6 mi) south of the channels previously discussed, is astride the southeast flank of Sawtell Peak, in contrast to the others that are incised into the northeast flank.

The channel trends southwest almost at right angles to the local slope of the land (fig. 2); it is sinuous and about 5 km (3 mi) long and is cut in rhyolitic tuff. Its northern end merges with the floor of the Henrys Lake basin, and its southern end—now much dissected by a modern stream—opens into the valley of Henrys Fork. The channel floor is 15–20 m (50–65 ft) below the adjacent upland benches, and it maintains an even width of about 120 m (400 ft) throughout its length. Commonly the floor is smooth and unbroken, but in a few places it is marked by elongate shallow depressions—possibly blowouts. Silt and fine sand, presumably blown and washed in from the adjacent benches, mantle the channel floor.

The position of the channel athwart and incised into the southeast flank of Sawtell Peak must mean that the southeast-trending drainageway of upper Henrys Fork was blocked, presumably by ice (fig. 2). Waters from the north found an escape route to the south around the southwest flank of this ice and in so doing cut the Stamp Meadows channel. Yet neither glacial erratics nor glacial deposits were found on the broad bench of volcanic rock, southeast of this channel, that must have been overlain by this ice. I interpret this absence of glacial deposits to mean either that the ice was clean or that it contained only rhyolitic tuff which cannot be distinguished from similar debris derived locally.

This ice dam may have caused a temporary ponding of the melt waters to form a short-lived shallow lake. This possibility is suggested both by the broad even floor of the basin south of the Howard fan and by the fact that the floors of the Howard channels as well as those of the Bootjack and Spillway channels merge with the basin floor. Further, the head of the Stamp Meadows channel also blends with the basin floor. If, indeed, such a lake was formed, it probably never exceeded 15 m (50 ft) in depth. Its outlet—the head of the Stamp Meadows ice-marginal channel—at an altitude of 6,435 ft, regulated its extent. Its western limit was probably about 1.5 km (1 mi) west of U.S. Highway 20–191; its northern edge is now delineated by the mouths of the Howard outwash channels, and its eastern edge was probably along the west flank of Mount Two Top. Thus as outlined, it probably covered an area of about 26 km^2 (16 mi^2).

As soon as the ice dam melted, the Stamp Meadows channel was abandoned, the lake was drained, and the waters resumed their former southeastward course via the Henrys Fork drainage.

PROPOSED GLACIAL HISTORY

Pre-Bull Lake glaciations

At least three major ice sheets overrode this part of southwestern Montana and southeastern Idaho during pre-Bull Lake time. (See "Known Glacial History.") Till was spread widely across the Henrys Lake area, but only remnants of these once-extensive deposits are now preserved, chiefly in the mountains east of Henrys Lake.

Bull Lake Glaciation

During early Bull Lake time an ice sheet, advancing westward from Yellowstone National Park, overrode the southern end of the Madison Range (Mount Two Top) and split into two lobes. The northern lobe—the Horse Butte lobe—moved northwestward across the West Yellowstone Basin to reach as far north as Horse Butte (Alden, 1953; Richmond, 1964). The southern lobe—the Henrys Lake lobe—flowed into the Henrys Lake basin and advanced as far northwest as the north shore of Henrys Lake (fig. 4*A*).

Glacial deposits formed during the waste of the Henry Lake lobe include the till or pitted outwash along the southeast, west, and north shores of Henrys Lake, and the various ice-contact deposits both southwest and southeast of the lake. The ice-marginal Bootjack, Spillway, and Stamp Meadows channels were cut by melt waters of this ice lobe which found an escape route to the south around the southwest flank of the lobe (fig. 4*B*). As this lobe wasted, it gradually withdrew southeastward. At some time after the north half of the basin was free of ice, the broad low Howard Creek fan was formed at the mouth of the valley of Howard Creek, probably by melt waters from the waste of alpine glaciers that lay in the valleys of Targhee Creek and its tributaries (fig. 4*B*). Shortly after the fan was formed, periodic floods of melt water from the waste of the Horse Butte ice lobe (in the West Yellowstone Basin) flowed through Targhee Pass, down the valley of Howard Creek, and onto the fan. These floods cut the Howard channels and emptied into an ice-dammed lake that occupied much of the southern end of the Henrys Lake basin. This lake drained southwestward via the Stamp Meadows channel (fig. 4*C*). As soon as the icedam melted, the lake was drained, the Stamp Meadows channel was abandoned, and the waters resumed their former southeastward course (fig. 4*D*).

Interglaciation

With the disappearance of Bull Lake ice from the Henrys Lake basin, north-flowing streams deposited a thin veneer of obsidian sand and gravel along the southeast edge of the basin.

Pinedale Glaciation

During the Pinedale Glaciation, alpine glaciers were formed in the high mountain valleys. These flowed

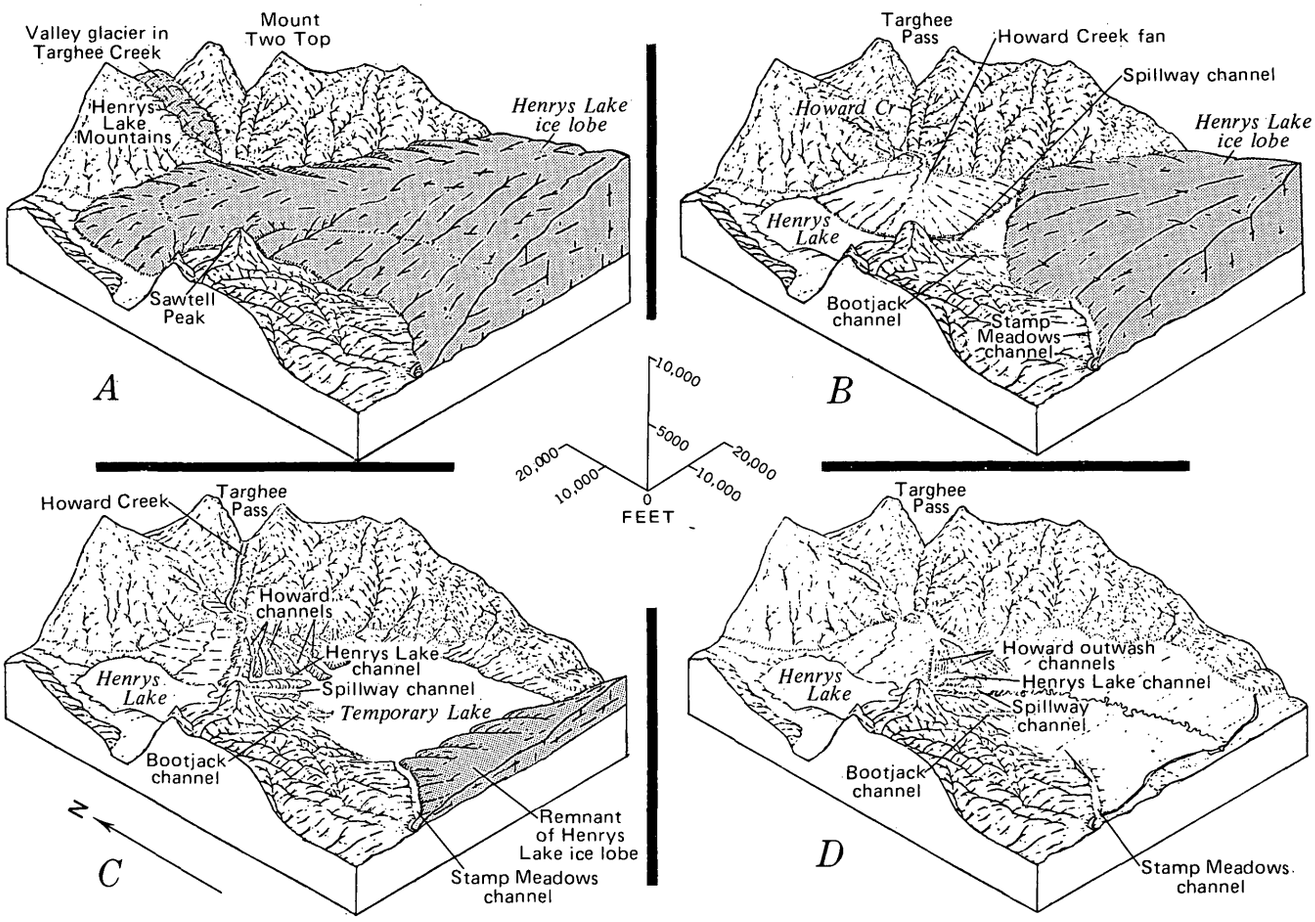

FIGURE 4.—Four sketches suggesting how the glacial features and deposits in the Henrys lake basin were formed. Vertical exaggeration is three times.

A. The Henrys Lake ice lobe advances northwestward to the north shore of Henrys Lake.

B. During the gradual waste of the ice lobe, a series of ice marginal channels are formed (Bootjack, Spillway, and Stamp Meadows). Other melt waters, flowing through Targhee and Howard Creeks, form a broad low alluvial fan—the Howward Creek fan—at the mouth of the valley of Howard Creek.

C. Subsequently, periodic floods flow through Howard Creek onto the Howard Creek fan and cut a series of radiating channels—the Howard channels—in the fan. These waters, temporarily ponded in front of the wasting ice lobe, form a small lake which drains southwestward through the Stamp Meadows channel (around the margin of the ice) to empty into Henrys Fork. Still later, other melt waters, flowing through Targhee and Howard Creeks, destroy the north half of the Howard Creek fan.

D. With the complete disappearance of the ice, the Stamp Meadows channel is abandoned, the temporary lake is drained, and the waters resume their pre-ice course to the southeast.

down the canyons, and some of them extended a short distance beyond the canyon mouths. No morainic deposits of Pinedale age are on the floor of the Henrys Lake basin; the nearest such deposits partially choke the valleys of Targhee and Howard Creeks.

REFERENCES CITED

Alden, W. C., 1953, Physiography and glacial geology of western Montana and adjacent areas: U.S. Geol. Survey Prof. Paper 231, 200 p.

Richmond, G. M., 1964, Glacial geology of the West Yellowstone Basin and adjacent parts of Yellowstone National Park: U.S. Geol. Survey Prof. Paper 435–T, p. 223–236.

——— 1970, Glacial history of the Yellowstone Lake basin: Am. Quaternary Assoc. Mtg., 1st, Yellowstone Park, Wyo., and Bozeman, Mont., 1970, Abs., p. 112–113.

——— 1972, Appraisal of the future climate of the Holocene in the Rocky Mountains: Quaternary Research, v. 2, no. 3, p. 315–322.

Stone, K. H., 1963, Alaskan ice-dammed lakes: Assoc. Am. Geographers Annals, v. 53, no. 3, p. 332–349.

Waldrop, H. A., 1974, Surficial geologic map of the West Yellowstone quadrangle, Yellowstone National Park and adjoining area, Montana, Wyoming, and Idaho: U.S. Geol. Survey Misc. Geol. Inv. Map I–648. (In press.)

Witkind, I. J., 1969, Geology of the Tepee Creek quadrangle, Montana—Wyoming: U.S. Geol. Survey Prof. Paper 609, 101 p.

Jour. Research U.S. Geol. Survey
Vol. 3, No. 1, Jan.–Feb. 1975, p. 77–87

RECURRENT GEOTHERMALLY INDUCED DEBRIS AVALANCHES ON BOULDER GLACIER, MOUNT BAKER, WASHINGTON

By DAVID FRANK, AUSTIN POST; and JULES D. FRIEDMAN;
Tacoma Wash.; Denver, Colo.

Work done in cooperation with the U.S. Forest Service and the National Aeronautics and Space Administration

Abstract.—Avalanches of snow, firn and hydrothermally altered rock and mud have been released six times since 1958 from Sherman Peak, part of the crater rim south of the main summit of Mount Baker, Wash. The avalanches traveled nearly identical paths 2.0–2.6 km down Boulder Glacier on the east slope of the volcano. Debris from at least one past avalanche can be seen as a thin bed of acidic mud in the glacier terminus. Fumaroles, thermal springs, and areas of warm ground, some of which are subglacial, are concentrated in the crater and were mapped by aerial infrared thermography. The outgoing radiant flux per unit area from a cluster of infrared anomalies within 50–150 m of the avalanche source was estimated to be 319 W m^{-2} (7,620 μcal $cm^{-2}s^{-1}$) in November 1972, which is sufficient to account for observed ice perforations. In addition vapor emission, not apparent in thermography, was observed along the source margin after the avalanche of August 1973. The principal conditions that produce the avalanches are considered to be the large accumulation of snow and firn on top of hydrothermally altered clay-rich ground at Sherman Peak and the saturation near the ground-firn interface by melt water produced both by summer snow ablation and by geothermal emission. The periodic avalanches have a potential for impounding water in the crater in addition to ponded water already known to occur. Sudden release of impounded water could present a danger to the Boulder Creek valley below.

A large debris avalanche descended the Boulder Glacier from the crater rim of Mount Baker, Wash., between 0700 P.d.t., August 20, and 1000 P.d.t. August 21, 1973. Debris from past avalanches has been photographed on Boulder Glacier every few years during recent decades (fig. 1). Because both large avalanches on glaciers and noneruptive volcanic heat may initiate destructive lahars (Crandell, 1971), this preliminary study was undertaken to determine the nature, causes, and dangers of the Boulder Glacier avalanches.

Acknowledgments.—Special appreciation is extended to Peter Shreve for participation in the 1972 field investigations at Mount Baker. This study is a cooperative effort of the U.S. Geological Survey Glaciology Project Office and ERTS experiment SR 251, thermal surveillance of the Cascade Range volcanoes. It was funded in part by the National Aeronautics and Space Administration and supported by the NP3–A survey aircraft from the Johnson Spacecraft Center in 1972. Additional aerial infrared scanner missions were flown yearly from 1970 to 1973 by U.S. Forest Service Fire Depot aircraft from Missoula, Mont., and Boise, Idaho, expressly for the thermal surveillance project.

BACKGROUND

Mount Baker (48°47′N., 121°49′W.) is the northernmost of the Quaternary stratovolcanoes of the Cascade Range of northern California, Oregon, and Washington (fig. 2). Andesitic lava flows and breccias form a cone which rises 2 km above a basement complex of metasedimentary rocks (Coombs, 1939). The summit is 3,285 m above sea level and about 3,200 m above the Skagit River valley 26 km to the south. Owing to high precipitation and northern latitude the volcano is almost completely covered by glaciers which flow radially from the central summit. All the higher lava flows on the cone appear to have originated from an area now covered by a summit ice dome. In this area a crater rim is partly visible on aerial photographs taken during a time of particularly low snow accumulation—1940 (*a* in fig. 3). A second more prominent crater (*b* in fig. 3), referred to informally as Sherman crater,[1] is centered 760 m south of and 350 m lower than the ice dome. Ice which descends from the mountain's summit to the north partly fills Sherman crater.

[1] Shown incorrectly as Summit Crater on some maps; the true summit crater is hidden under the central summit ice dome.

FIGURE 1.—East slope of Mount Baker. The debris avalanche path extends 2.6 km down Boulder Glacier from Sherman Peak, the southeast remnant of a crater rim. Aerial photograph 69R1–21, August 22, 1969.

DEBRIS AVALANCHES

Since the last eruptive sequence, which occurred in the mid-1800's (Davidson, 1885, p. 262; Gibbs, 1874, p. 357–358; Pioneer Democrat [newspaper], 1859), there have been reports of several large mass movements of undetermined cause. Charles F. Easton[2] described mass movement phenomena in almost every valley heading at a Mount Baker glacier. These include a debris avalanche which traveled 11 km beyond the Rainbow Glacier terminus about 1860 and a number of either debris avalanches, debris flows, or jökulhlaups which swept 5 km below the Easton Glacier in 1911, 9 km from the Deming Glacier in 1927, and repeatedly to unspecified distances downvalley from the Mazama, Roosevelt, and Thunder Glaciers.

The first known description of an avalanche deposit similar to that which was formed in 1973 is by Easton; in 1906 "* * * he observed that the crater had been filled with rock and lava which had tumbled down from Sherman Peak" (Adams, 1919, p. 341). Later, two photographs were published which show an avalanche scar identical to that of 1973. (McNeil, 1930,

[2] Pages 158, 215, and 216 of "Mt. Baker, Its Trails and Legends:" an unpublished 262-page compilation of photographs, newspaper articles, and manuscript commissioned in 1911 by the Mount Baker Club and archived at the Whatcom County Museum of Natural History, Bellingham, Wash.

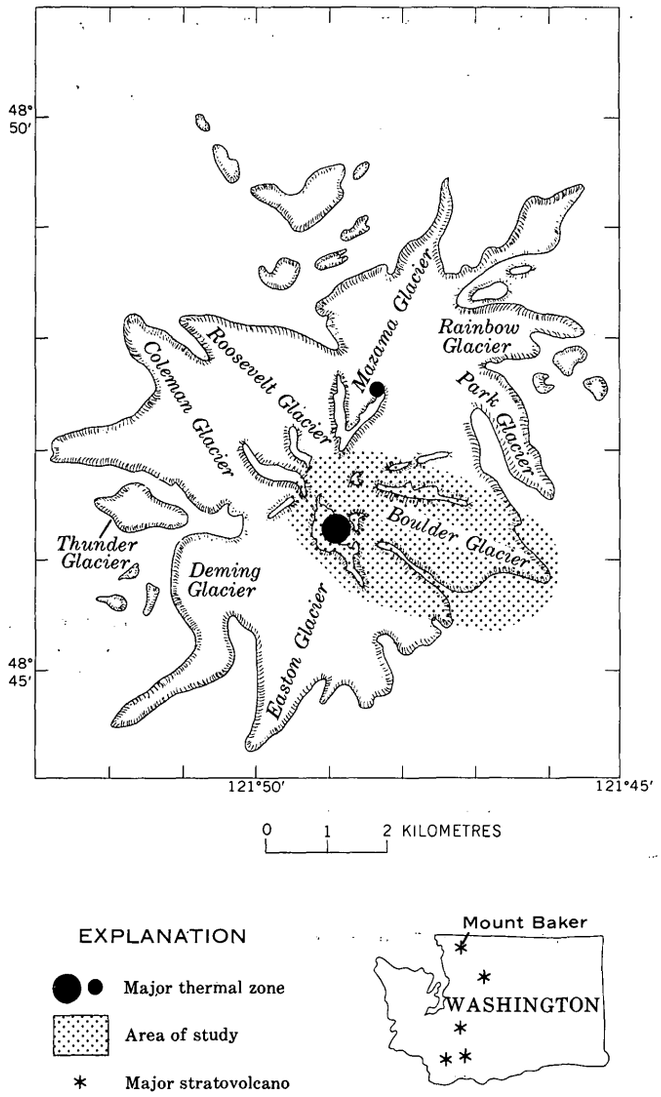

FIGURE 2.—Regional setting of Boulder Glacier, Mount Baker, Wash.

p. 15–16). Aerial photographs acquired annually since 1958 record six such avalanches in 1958, 1960, 1962, 1966, 1969, and 1973.

Observations were conducted shortly after the 1973 avalanche to determine its extent and character. When aerial photographs obtained August 22, 1973, are compared with photographs of previous years, striking similarities to past debris avalanches on Boulder Glacier can be seen (fig. 4). Each time the debris source was a steep, northeast-facing slope of Sherman Peak. a remnant of the Sherman crater rim (*c* in fig. 3, 5). Here snow can accumulate rapidly through the winter season and be maintained year round. In 1973 snow, firn, rock, and mud slid from this area and traveled 2.6 km down Boulder Glacier ending about 1.4 km short of the glacier terminus. A graphic reconstruction of material missing from the wedge-shaped scar on Sherman Peak gave an estimate of 35,000 m^3 of snow, ice, and rock involved in the avalanche, not including snow and ice added downslope.

The steep (>30°) slope of Sherman Peak was stripped bare of snow and firn over an area of 7,400 m^2. An ice escarpment overhung the bare slope and appeared decidely unstable, making close examination of the scar area hazardous. However, on September 3, 1973, a field reconnaissance was made of marginal portions of the source area as well as the remaining avalanche path. Hydrothermally altered rocks and light-brown to dark-gray soil were freshly exposed in the source area. Near the margin of the bare slope vapor slowly emanated from a few small vents, while snow and ice melt water coursed down the exposure. Just below the source area an outcrop of altered breccia was sheathed by intact sulphur stalactites as much as 1 m long indicating past emission of volcanic gases or fluids. Huge avalanche firn blocks and normal snow accumulation had filled the east breach of the crater rim to an estimated depth of 10 m. The nature of this deposit is of considerable importance as will be shown later.

On the upper half of Boulder Glacier, avalanche debris consisted largely of firn and snow blocks as much as several meters across. Firn (snow which was at least 1 year old) composed most of the debris. Thin patches of rock and mud covered much of the slide path. Samples from the path midpoint contained gray, angular, slightly to highly hydrothermally altered rock fragments generally less than 5 mm in diameter. These fragments were embedded in a matrix of extremely sticky dense gray mud. Although the avalanche terminus was not examined, aerial photographs indicate that debris in that area included much larger rock fragments. Snow and firn cored levees, 1 to at least 5 m thick and visible in photographs as dark stripes, extended along the avalanche path. The levees appeared to have been produced by both scouring and debris deposition on the snow-covered glacier surface.

Although none of the avalanches since 1958 reached the glacier margin at the time of their occurrence, there is now a considerable accumulation of mud at the terminus. The glacier front is active and about 10 m high, so that several upper ablation horizons may be recognized easily. In the upper part of the ice face a thin horizontal layer of medium-gray sticky mud was exposed. Debris from this source completely covered the lower two-thirds surface of the north part of the terminal face. Field inspection showed no distinctive difference between mud from the August avalanche

FIGURE 3.—Vertical view of the upper cone of Mount Baker. The southwest rim of a crater (*a*) partly protrudes from a broad summit ice dome. Sherman crater (*b*), a partly ice-filled crater to the south, is the site of numerous ice perforations caused by heat emission (*d* and *e* are ice perforations mentioned in text). Sherman Peak (*c*) is the southeast rim of Sherman crater. At the time of the photograph, snow had slumped on the northeast slope of Sherman Peak, although a full-scale avalanche had not occurred. Debris visible on Boulder Glacier is due to nearly continuous rockfall from an outcrop unrelated to Sherman Peak. Vertical aerial photograph W–1232–236, September 1940.

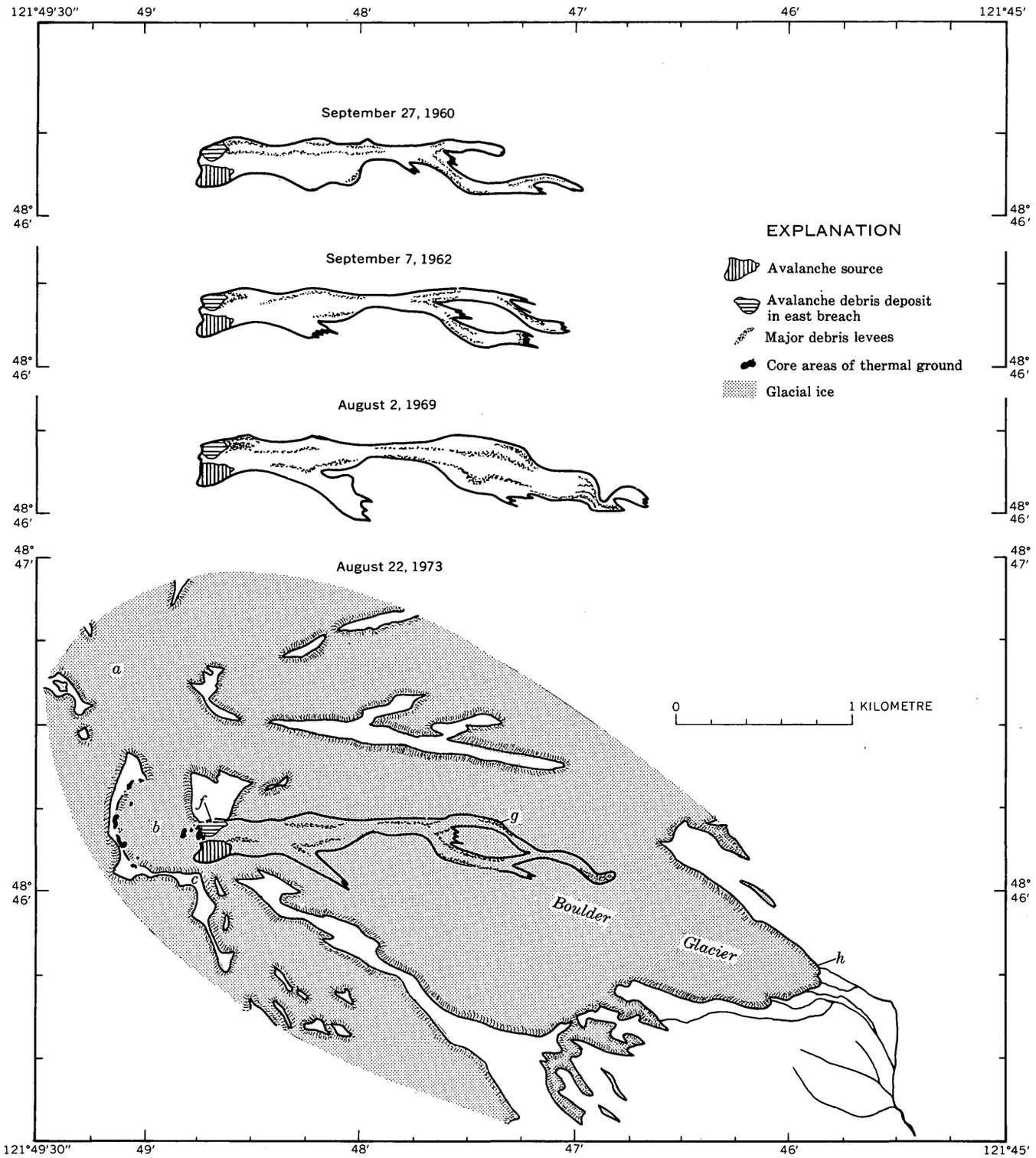

FIGURE 4.—Avalanche paths on Boulder Glacier and relationship to thermal features in adjacent crater. Dates refer to time of photography used to map avalanche paths. Exact time of avalanche release is unknown. *a*, crater buried beneath summit ice dome; *b*, Sherman crater; *c*, Sherman Peak; *f*, *g*, *h*, debris sample sites.

FIGURE 5.—Avalanche source on Sherman Peak (*c*). Each avalanche has deposited firn in the east breach of the crater rim (foreground). Ice perforations are evident along the inner rim of the crater (pointers; *d* and *e* referred to in text). Aerial photograph K692–5, August 2, 1969.

and mud incorporated in the glacier ice. Subsequent acidity analyses (table 1) of mud debris from the terminus, the 1973 avalanche, and the crater rim also were similar. All samples had a high acidity (pH <2.3) consistent with pH determinations of hydrothermally altered rock in the crater walls (Bockheim and Ballard, 1973).

Acidic material at the Boulder Glacier terminus

TABLE 1.—*Acidity values for debris samples at Mount Baker*

Sample site	pH
East breach debris cone (site *f*)	2.0
Middle avalanche surface (site *g*)	1.9
Boulder Glacier terminus (site *h*)	2.3
Crater soil (Bockheim and Ballard, 1973)	1.2–3.7

Note.—Measurements were made of mixtures of 50 ml of distilled water (pH≈6.7) and 50 g of air-dried debris. Sample sites are shown in figure 4.

probably came from the crater rim and represents a stratigraphic record of a past avalanche. The August 1973 avalanche thus is not an isolated incident but rather the latest episode of mass wastage of the crater rim. It is suggested here that these recurrent events are related to heat emission and solfataric alteration in the crater area.

CRATER HEAT EMISSION

Aerial thermal infrared images acquired for the U.S. Geological Survey's volcanic thermal monitoring project show the extent of surface infrared anomalies in the Sherman crater (Friedman and Frank, 1974). Figure 6 is a predawn thermographic image of the crater obtained by the U.S. Forest Service on April 29, 1973, using an aircraft-mounted RS–7 line scanner sensitive to radiant emission in the 8–14 μm spectral band. For geographic reference it is approximately the same scale as the vertical photograph (fig. 3). This springtime thermographic image shows clusters of infrared anomalies which cover 7,500 m^2, about 6 percent of the crater area. These anomalies occupy 90 percent of the maximum anomalous area recorded 6 mo earlier during a period of relatively lower snowpack and are coincident with areas of warm ground, fumaroles, and boiling pools. Typical warmer temperatures in the crater as measured by bimetallic thermometer during the summers of 1972 and 1973 are 90°C for vapor, 60°C at <1 cm ground depth, and 90°C at 50 cm ground depth. Since these were isolated measurements, they do not indicate the full thermal range but do suggest that the boiling point of water (90°C at 3,000 m alt) limits the maximum fumarole temperatures. Coincident solfataric activity has effectively transformed crater rock to kaolinitic and opalitic alteration products (Coombs, 1939, p. 1500).

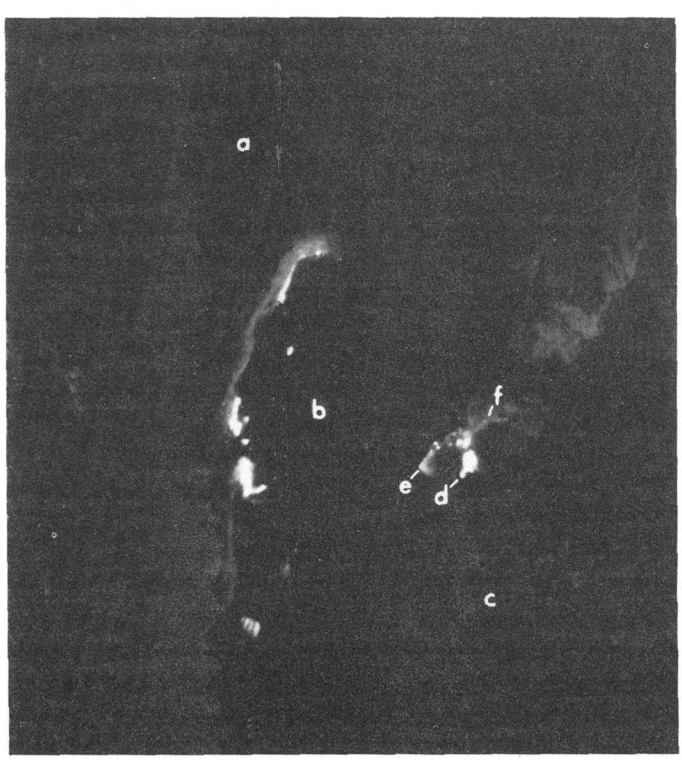

FIGURE 6.—Aerial infrared thermograph of Sherman crater, 0438 P.d.t., April 29, 1973. Image was produced by an RS–7 line scanner operated by personnel of the U.S. Forest Service Aerial Fire Depot, Missoula, Mont. Letters refer to those in figures 3, 4, and text. North is to the top of the image.

The most active part of the crater fumarole field (*d*, *e* in fig. 6) is located within ice perforations which occur just inside the east breach of the Sherman crater rim and 50–150 m downslope from the avalanche source. Solfataric ground is flanked on the west by the crater glacier and on the east by a wedge of avalanche debris and snow which has accumulated in the east breach. A stream fed by snow and ice melt water and thermal springs issues from the crater glacier, flows across the fumarole area, and disappears beneath the avalanche deposit in the east breach. The most impressive feature here is a roaring fumarole on the streambank which forcefully ejects vapor and water 1–10 m from sulfur-encrusted crevices a few centimeters in diameter in a rock outcrop. Warm ground, boiling pools, and numerous smaller fumaroles cover the remaining area. Small fumaroles also perforate the margins of the avalanche deposit in the east breach and extend up the slope of Sherman Peak to the south and around the base of the rock exposure to the north. These thermal features to the north appear as two dim point anomalies in the thermographic image (*f* in fig. 6). The warmest areas which extend up Sherman Peak are also portrayed on the thermographic image (*d* in fig. 6). However, no anomalies in the image correspond to vapor vents observed in September 1973 on the upper avalanche scar area. This may be due to the thick snowpack on Sherman Peak at the time of the aerial infrared survey.

HEAT FLOW REQUIRED TO MELT SNOW AND ICE IN THE EAST BREACH AREA

An earlier thermographic overflight was made November 20, 1972, by the NASA NP3–A earth resources aircraft using an internally calibrated RS–14 line scanner sensitive to radiation in the 8–14 μm band. Line-scan thermographic images were film recorded on board the aircraft with a 10-step gray scale calibration strip which gave black-body radiation temperatures ranging from 293 to 373 K (20°–100°C). In addition, uncalibrated images encompassing the total temperature range of the scanner were reproduced from videotape. The total area, on video-processed images, of the infrared anomalies in Sherman crater was measured by planimeter to be 8,800 m^2. Of this area, 3,600 m^2 is included in the east breach sector. On the calibrated images 230 m^2 registered more intense than the first gray step or higher than 293 K (20° C). Background radiation temperature for nearby nonanomalous ice areas averaged 255 K (−18°C) as measured along a Barnes PRT–5 infrared-radiometer traverse carried out simultaneously from the NP3–A aircraft along the axis of the infrared-scanner ground swath.

Table 2 is based on the calibrated thermographic images and gives the estimated radiant flux from the east breach anomalies. The following expression for the Stefan-Boltzmann equation is used here:

TABLE 2.—*Estimating outgoing radiant flux from the east breach anomalies, Mount Baker*

Apparent black-body radiation temperature, T (K)	Area, A (m^2)	Radiant flux per unit area, M (W m^{-2})	Radiant flux, $M\ A$ (W)
[1] 273	3,370	315	1.06×10^6
293	200	419	0.08×10^6
301	30	466	0.01×10^6
Total	3,600	---	[2] 1.15×10^6

[1] The base radiation temperature isotherm of 273 K is below the first calibrated gray step of the NP3–A survey of November 20, 1972. It is defined as equivalent to the isoline separating anomalously warm bare ground and adjacent snow-covered ground after a fresh snowfall a few days before the November 20th survey.
[2] Equal to 0.275×10^6 cal s^{-1}.

$$M=\sigma\epsilon(T^4)$$

where σ is 5.679×10^{-8} W m^{-2} K^{-4} (Reynolds, and others, 1963),
ϵ is 1 (for black body),
T is given in K in the table, and
M is the outgoing radiant flux per unit area.

The average outgoing radiant flux per unit area based on data in table 2 is 319 W m^{-2} (7,620 μcal cm^{-2}s^{-1}), equivalent to a total radiant flux for the east breach area of 1.15×10^6 W (275,000 cal s^{-1}). Although no data exist for snow accumulation in the crater, a minimum estimate can be made of snow melted by the thermal zones. Various snow course data for lower altitudes are available. The Marten Lake snow survey site 7 km from the crater and 1,100 m in altitude was selected for the following estimates. On April 28, 1973, 1.5 m water equivalent of snow was measured at Marten Lake (Davis, 1973) and is assumed to approximate the minimum snow accumulation in the east breach. Actual accumulation was probably much greater because of wind-deposited snow. On April 29, 1973, thermographic images showed about 3,000 m^2 of anomalous snow-free ground (fig. 6) from which a volume of 4,500 m^3 water equivalent of snow would have been melted if accumulation was 1.5 m. This would have required an energy input of 0.5×10^9 J m^{-2} (12,000 cal cm^{-2}) over the principal accumulation period of 4 mo (January–April, fig. 7). The east breach radiation anomalies, however, yielded 3.3×10^9 J m^{-2} (79,000 cal cm^{-2}) over a 4-mo period, clearly enough to melt assumed snow accumulation in the east breach area, not taking into account additional melting caused by advective heat transfer from subglacial melt-water streams. Moreover, at no time during the year has the east breach area been seen to be completely snow covered, which indicates snow probably melts as fast as it falls in the core area of the anomalies. White (1969, p. 5198) has suggested that in such areas total heat-flow rates are at least 419 W m^{-2} (10,000 μcal cm^{-2}s^{-1}). If this estimate is correct, table 2 shows that radiant flux alone is sufficient to keep at least 230 m^2 of ground in the east breach free of snow the year round.

AVALANCHE CONDITIONS

Although there is insufficient evidence to determine the ultimate trigger for the avalanches, the probable contributing conditions may be examined. Factors that have been considered are storms, large annual accumulations of snow, seasonal production of melt water, and geothermal heat emission.

A close estimate of the time of release has been obtained for only one avalanche; that is, August 20–21, 1973. Observations from various local weather stations indicate that a previous storm had ended August 16 and that weather patterns for the following 6 d were generally partly cloudy with no sharp air temperature fluctuations. Thus the most recent avalanche evidently was not caused by rapidly changing weather. If it is assumed that the similarity of past avalanches indicates a common cause, short-term weather effects may be neglected as an important factor.

Long-term weather patterns also do not seem very important. If the local 16-yr record of snow accumulation at Marten Lake (fig. 7) is taken as an index

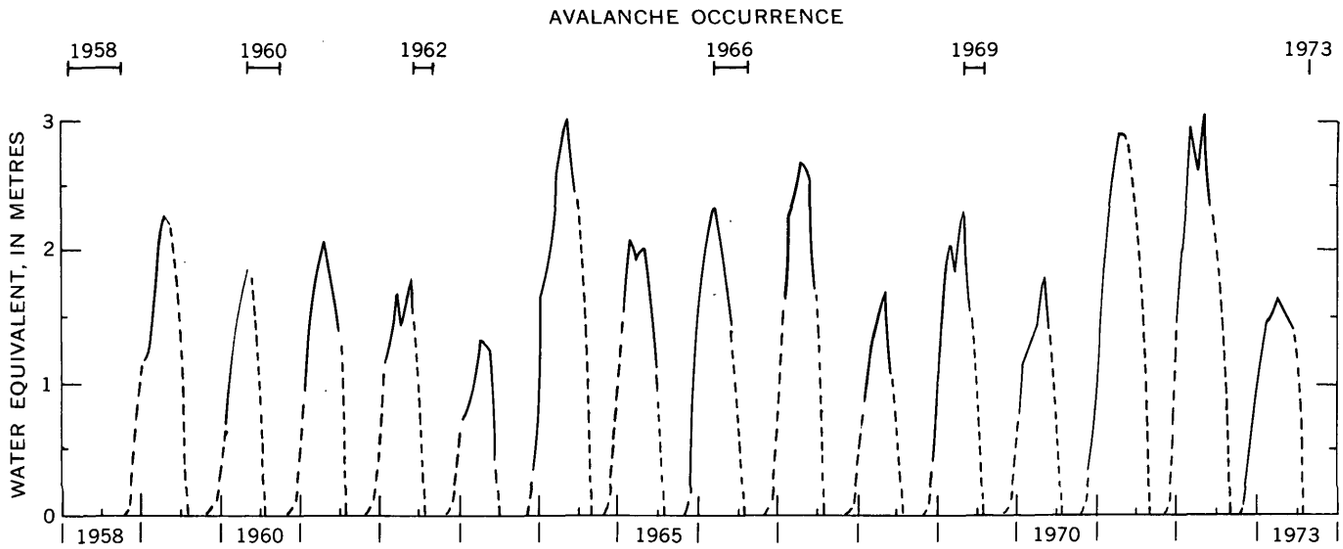

FIGURE 7.—Water equivalent of snow depth 1959–73 at Marten Lake snow course, 1,100 m altitude and 6.9 km east of avalanche source. Marten Lake is the closest snow course to the avalanche source; the data show annual variations similar to other snow courses in the region. Solid lines integrate data from Davis (1970–73) and U.S. Soil Conservation Service (1971). Dashed lines extend the inferred snow accumulation into summer. Brackets indicate estimated period during which each avalanche occurred. There is no apparent relationship between snow accumulation and avalanche occurrence.

of the yearly winter precipitation pattern at Mount Baker, there is no apparent relationship between avalanche release and snowpack peaks. Snow, judged to be due largely to wind drift, readily covers the avalanche source area in 1 yr. This is enough to build up the snowpack on Sherman Peak to the volume present at the time of avalanche release. For example, photographs show that the amount of snow covering the avalanche source in late summer 1963, 1 yr after an avalanche, is not appreciably different from the amount in late summer 1965, 1 yr preceding the next avalanche, even though there was an intervening season of extremely heavy snowfall. It appears that wind conditions quickly produce a stable shape for the snowpack and that excess snow is blown off and deposited elsewhere. The snowpack at the avalanche source area thus soon attains a nearly constant volume which provides the major load on the slope, but which is insufficient by itself to cause avalanche release.

Photographs show that all but one observed avalanche path lie on top of snow accumulated during the previous winter. Therefore, most avalanches must have occurred during the ablation season, after the time of maximum snowpack. A late spring or summer occurrence indicates that seasonal melting is probably an important factor. Moreover conditions at or near the ground-firn interface are also important, as avalanche release appears to have taken place either at the interface or in the ground itself. Because much of the ground on Sherman Peak contains clay-rich material which results from hydrothermal alteration, major causes of instability probably are water saturation of this clay-rich material as well as water lubrication at the ground-firn interface. The main source of water is from the melting of snow and firn as a result of both summer ablation from above and ground heat emission from below. Heat emission at the avalanche source likely occurs at a low level—enough to produce the localized vapor emission observed along the source margin after the 1973 avalanche but not enough to prevent rapid thick snow accumulation. Thus the important conditions are that (1) a large quantity of snow accumulates on Sherman Peak, (2) rock is hydrothermally altered to clay-rich material, and (3) melt water, which is produced by summer snow ablation and by geothermal heat emission, saturates the ground and firn. Every 2 to 4 yr a combination of these conditions leads to the release of snow, firn, and a surface layer of rock and mud from Sherman Peak.

AVALANCHE SIGNIFICANCE AND POTENTIAL FOR CRATER LAKE FORMATION

Since the major component of debris from known avalanches has been snow and firn and only a limited quantity of snow accumulates prior to release, the amount of debris has been insufficient to flow beyond the Boulder Glacier terminus and into the lower Boulder Creek valley. The rate of solfataric alteration of the crater area may be significant in this con-

nection since, if the rate is increasing, greater amounts of rock would become susceptible to structural failure. Furthermore, as the avalanches erode into the middle part of Sherman Peak (fig. 5), the upper part will be undercut so that conceivably a large volume of Sherman Peak above the avalanche source could eventually break loose. The inclusion of this rock mass, estimated at 5×10^6 m^3, in a single future avalanche would increase the amount of debris by at least 100 times compared with the last avalanche and would likely extend well into the lower Boulder Creek valley in a manner similar to large rock avalanches which fell from Little Tahoma Peak, Mount Rainier, in 1963 (Crandell and Fahnestock, 1965). At present the most obvious hazard posed by debris avalanches is to mountain climbers traveling on Boulder Glacier or following the established Boulder Creek route to the summit of Mount Baker (American Alpine Club committee, 1961, p. 241–242). The avalanches probably are released during the most popular climbing season.

Avalanches have occurred at fairly regular intervals since 1958. This suggests that a debris avalanche of comparable magnitude could occur on Boulder Glacier sometime between 1975 and 1977 and every 2 to 4 yr thereafter, as long as current thermal activity is maintained. Greater potential danger would exist if avalanche debris should dam the crater outlet in the east rim and form a lake. This, like many glacier-dammed lakes, would be subject to sudden release from dam failure (Post and Mayo, 1971). Some ponding is known to occur in the crater even when avalanche debris does not form a dam. A schematic profile of Sherman crater, based on field observations, is presented in figure 8. In September 1973, in the larger ice perforation (*e*), a small alcove was melted into the edge of the glacier wall where ponded water extended beneath the ice for an unknown distance. During an aerial photographic overflight in September 1963, a lake emitting vapor was observed in this same ice perforation. Assuming a normal funnel-shaped crater floor, the existence of a sizable body of water under the ice is implied. Furthermore a surficial depression in the ice in the center of the crater, similar to that found above the lake in the west crater of Mount Rainier (Kiver and Steele, 1972), suggests the presence of either a central source of heat emission or a subglacial lake.

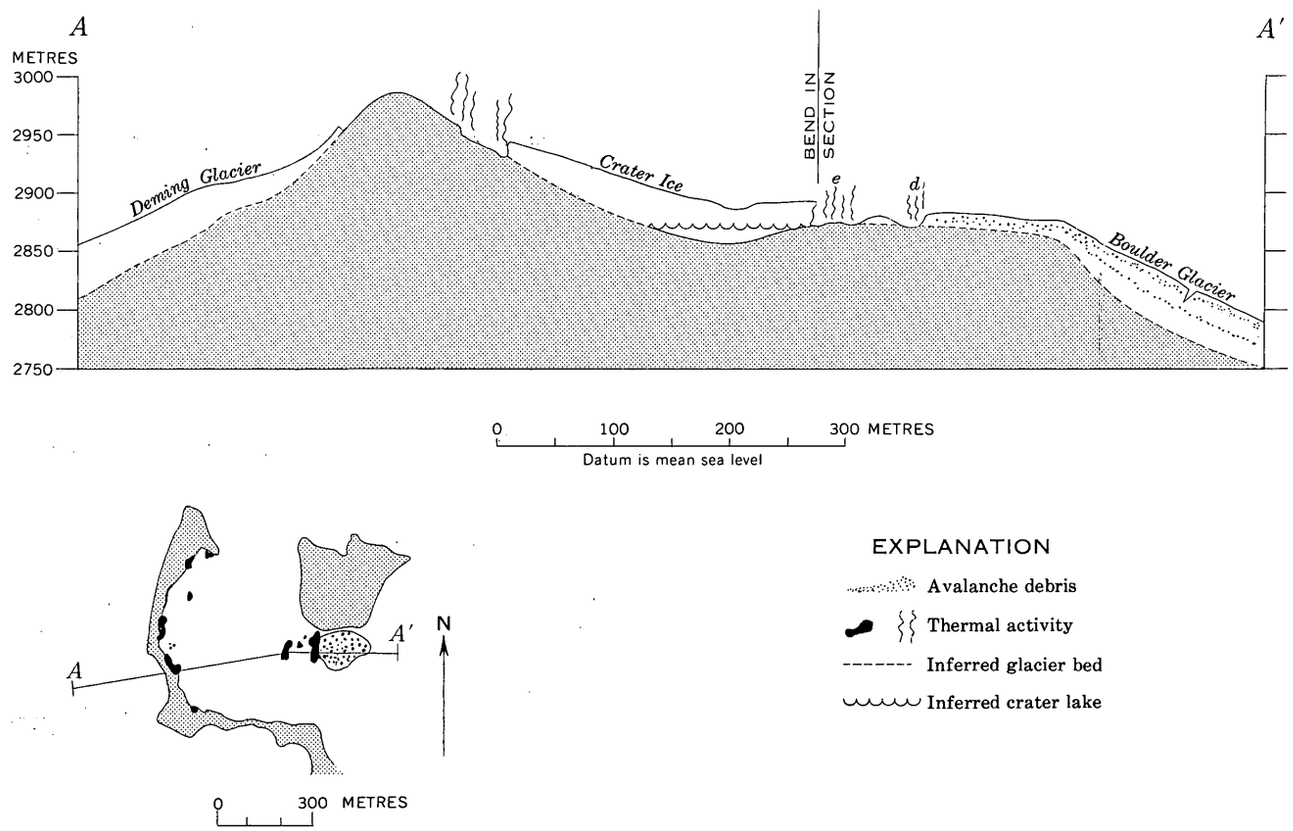

FIGURE 8.—Schematic section of Sherman crater. A stream fed by melting snow and ice and by thermal springs was observed in ice perforation *d*, and ponding was observed in perforation *e*.

The drainage from such a lake, whatever its size, combines with other crater runoff and flows through a narrow gorge in the east breach of the crater rim. Debris from the avalanches plus normal snow accumulation maintain a wedge-shaped deposit of snow and ice at least 10 m thick in this gorge. In August 1972 and September 1973 surface streamflow discharged from the crater at an estimated 10 $l \cdot s^{-1}$ and continued into an ice tunnel beneath the avalanche debris deposit. In September 1973 there was no blockage of water by the avalanche deposit as demonstrated by an injection of tracer dye which flowed subglacially from the crater to the Boulder Glacier terminus within 3 h.

Should a future avalanche cause collapse of the ice tunnel in the east breach, water will be impounded in addition to that ordinarily contained in the crater. At least 36,000 m^3 of water could be contained in the perforations if the water level reaches the top of the 1973 avalanche deposit. The volume of ice missing from the perforations is estimated to be of the same order of magnitude as the deposit in the east breach. Thus, if the present vertically directed heat flow were diverted horizontally toward the avalanche deposit, as by a warm lake, rapid melting and water percolation through the deposit would result in a lake outburst. Destructive potential in the Boulder Creek valley from failure of an ice dam would depend on such factors as (1) rapidity of release of floodwaters, (2) availability of additional stored water within the crater ice and within Boulder Glacier, (3) availability of loose debris as water moves downvalley, (4) temporary storage and diversion capability of debris, and (5) possibility of release during seasons when flood conditions already prevail.

REFERENCES CITED

Adams, W. C., 1919, Reminiscences of Mt. Baker: Mazama, v. 5, no. 4, p. 338–342.

American Alpine Club committee, Sainsbury, G. R., chm., 1961, Climber's guide to the Cascade and Olympic Mountains of Washington: American Alpine Club, 387 p.

Bockheim, J. G., and Ballard, T. M., 1973, Hydrothermal soils of the crater of Mt. Baker, Washington [abs.]: Northwest Science, 46th Ann. Mtg., Mar. 29–31, 1973, p. 4.

Coombs, H. A., 1939, Mt. Baker, a Cascade volcano: Geol. Soc. America Bull., v. 50, p. 1493–1510.

Crandell, D. R., 1971, Postglacial lahars from Mount Rainier volcano, Washington: U.S. Geol. Survey Prof. Paper 677, 75 p.

Crandell, D. R., and Fahnestock, R. K., 1965, Rockfalls and avalanches from Little Tahoma Peak on Mount Rainier, Washington: U.S. Geol. Survey Bull. 1221–A, 30 p.

Davidson, George, 1885, Recent volcanic activity in the United States: Eruption of Mount Baker: Science, v. VI, no. 138, p. 362.

Davis, R. I., 1970–1973, Water supply outlook for Washington: U.S. Soil Conserv. Service (published monthly during winter and spring).

Friedman, J. D., and Frank, D. G., 1974, Thermal activity at Mount Baker volcano, Washington [abs.]: Am. Geophys. Union Trans. (EOS), v. 55, no. 4, p. 488.

Gibbs, George, 1874, Physical geography of the northwestern boundary of the United States: Am. Geog. Soc. of New York Jour., v. 4, p. 298–392.

Kiver, E. P., and Steele, W. K., 1972, Summit firn cave research, August 1971, Mount Rainier National Park, Washington [abs.]: Geol. Soc. America Abs. with Programs, v. 4, no. 6, p. 385.

McNeil, F. H., 1930, Backtracking old trails: Mazama, v. 12, no. 12, p. 6–16.

Pioneer Democrat [newspaper], 1859, Olympia, Washington Territory: Pioneer Democrat, Nov. 25, 1859, v. 8, no. 1, p. 2.

Post, Austin, and Mayo, L. R., 1971, Glacier dammed lakes and outbrust floods in Alaska: U.S. Geol. Survey Hydrol. Inv. Atlas HA–455.

Reynolds, M. M., Corraccini, R .J., Fulk, M. M., and Burley, R. M., 1963, Radiometry, Chap 6–K *in* Gray, D. T., ed., American Institute of Physics Handbook [2d ed.]: Natl. Bur. Standards Misc. Pub. 253, p. 6–153—6–156.

U.S. Soil Conservation Service, 1971, Summary of snow survey measurements for Washington (1915–1969): U.S. Soil Conserv. Service and Washington Dept. Ecology, 263 p.

White, D. E., 1969, Rapid heat-flow surveying of geothermal areas utilizing individual snowfalls as calorimeters: Jour. Geophys. Research, v. 74, no. 22, p. 5191–5201.

Jour. Research U.S. Geol. Survey
Vol. 3, No. 1, Jan.–Feb. 1975, p. 89–92

CHANGES IN CONCENTRATION OF CERTAIN CONSTITUENTS OF TREATED WASTE WATER DURING MOVEMENT THROUGH THE MAGOTHY AQUIFER, BAY PARK, NEW YORK

By HENRY F. H. KU, JOHN VECCHIOLI, and STEPHEN E. RAGONE, Mineola, N.Y.

Prepared in cooperation with the Nassau County Department of Public Works

Abstract.—Approximately 7 million gallons (27 million litres) of tertiary-treated sewage (reclaimed water) was injected by well into the Magothy aquifer and was subsequently pumped out. As the reclaimed water moved through the aquifer, concentrations of certain dissolved constituents decreased as follows: Total nitrogen, 7 percent; methylene blue active substances, 49 percent; chemical oxygen demand, 50 percent; and phosphate, more than 93 percent.

As part of an experimental deep-weli recharge program at Bay Park, N.Y. (Cohen and Durfor, 1967), the U.S. Geological Survey, in cooperation with the Nassau County Department of Public Works, has been studying the geochemical interactions of recharged water, tertiary-treated sewage (reclaimed water), with the Magothy aquifer. The Magothy aquifer is the major source of potable water in Nassau County. Results of some of the experiments have been reported by Vecchioli and Ku (1972), Vecchioli (1970), Faust and Vecchioli (1974), and Ragone, Vecchioli, and Ku (1973).

Concentrations of most of the chemical constituents in the reclaimed water are many times greater than they are in the native water. Of particular concern are some of the constituents of sewage origin: nitrogen, phosphate, COD, and MBAS. Over the long run, increased concentrations of these constituents could render Magothy water impotable without extensive treatment. The fate of these constituents during injection and repumping phases of a recharge experiment, test number 10, is evaluated in this report.

The water reclamation and recharge facilities are on the grounds of the Bay Park Water Pollution Control Plant in southwest Nassau County. The facilities have been described extensively by Peters and Rose (1968), Cohen and Durfor (1966 and 1967), and Koch, Giaimo, and Sulam (1973). Briefly, about 400 gal/min (26 l/s) of secondary-treated sewage from the Bay Park plant is diverted to a pilot plant, where it is further purified. The reclaimed water is piped about half a mile (0.8 km) to the recharge site, where it is recharged into the Magothy aquifer through a well screened at a depth of 418 to 480 ft (127–146 m) below land surface. The aquifer at the screened interval consists of slightly silty, fine to medium sand and thin beds of coarse sand. The sand units are micaceous, lignitic, and slightly pyritic (Vecchioli and others, 1974).

TEST PROCEDURES

Injection test 10 involved two periods of recharge, RW10 and RW10A. In the first period, 5 Mgal (20 Ml) of reclaimed water not filtered through activated carbon was recharged at a rate of 350 gal/min (22 l/s) for 10 d. COD and MBAS concentrations of this water were about two and eight times, respectively, the concentrations usually observed in reclaimed water filtered through activated carbon. Nitrogen and phosphate concentrations were unaffected.

After the first recharge period (RW10), the recharge well was pumped briefly five times; 130,000 gal (490,000 l) of water was removed. After the well had remained idle for about 2 mo, a second period of recharge (RW10A) was made in which an additional 2 Mgal (8 Ml) of reclaimed water filtered through activated carbon was recharged at a rate of 350 gal/min (22 l/s) for 4 d. The MBAS and COD concentrations of this carbon-filtered water were substantially less than those of the unfiltered water in the first period of recharge (table 1). The second recharge period was followed by a lengthy pumping period in which virtually all the water injected during the two recharge periods was withdrawn from the aquifer. Repumping was stopped once the quality of the water withdrawn was similar to that of pretest conditions.

TABLE 1.—*Concentrations of selected constituents in the reclaimed water recharged in test 10*

[All data reported in milligrams per litre except specific conductance, which is reported in micromhos per centimetre at 25°C]

	RW10		RW10A	
	Mean	Standard deviation	Mean	Standard deviation
Total nitrogen	27	2	27	1
Total phosphate	.69	.46	.13	.03
COD (0.025 *N* $K_2Cr_2O_7$)	22	1	9	3
MBAS	.55	.10	.07	.01
Chloride	85	9	63	1
Specific conductance	760	31	708	13

The injectant was sampled four times each day, and these four samples were combined to form one composite sample. At appropriate intervals during recharge, samples were pumped from an observation well 20 ft (6.1 m) from the recharge well. This well is screened at the same depth interval as the recharge well. Samples of the repumped water were collected periodically from a tap on the discharge line of the deep-well turbine pump installed in the recharge well. Samples were analyzed at the Geological Survey laboratory in Albany, N. Y.

RESULTS AND DISCUSSION

Changes in the concentration of total nitrogen, total phosphate, MBAS, COD, and chloride at the observation well during the two periods of recharge are shown in figure 1. Chloride concentration of the reclaimed water remains virtually constant as the water moves through the Magothy aquifer (Faust and Vecchioli, 1974); therefore, chloride concentration is used as an indicator of both the arrival of the reclaimed water at the observation well and the extent to which the reclaimed and native waters mix during travel through the aquifer.

The chloride curve (fig. 1) indicates that the injected water displaced virtually all the native water within 20 ft (6.1 m) of the recharge well after 1 Mgal (4 Ml) had been recharged. The concentration of

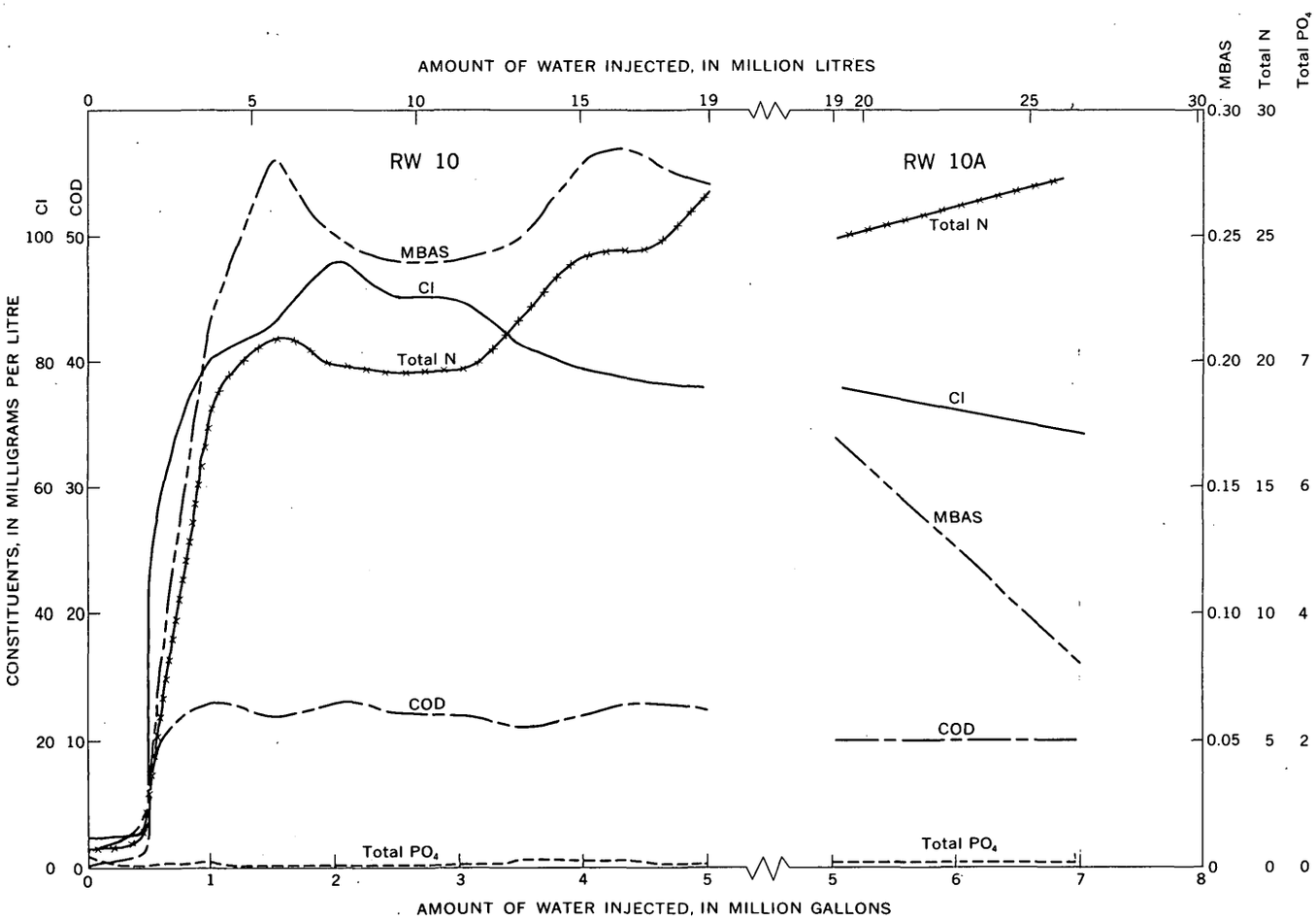

FIGURE 1.—Changes in the concentration of total nitrogen, total phosphate, MBAS, COD, and chloride at the observation well during recharge.

nitrogen at the observation well approached that of nitrogen in the reclaimed water, although at a slightly slower rate than chloride. The concentrations of MBAS and COD stabilized at about 50 percent of the respective concentrations in the reclaimed water. The concentration of phosphate increased slightly but remained more than an order of magnitude below the concentration of that in reclaimed water.

Changes in concentration depicted by the segments of the curves for the second period of recharge in figure 1 reflect the difference in the quality of the reclaimed water during the different recharge periods (table 1).

The volume of water withdrawn from the recharge well in order to restore the quality of the ground water to pretest conditions was about 1½ times the volume recharged. Changes in concentration of the constituents of interest in the repumped water are shown in figure 2. Except for COD and phosphate, the curves are roughly the reverse of the curves observed during recharge (fig. 1). The gradual decline of the curves after 5 Mgal (20 Ml) had been pumped out is due to dispersion phenomena at the injected-water front. The very high concentrations of COD and phosphate at the start of the redevelopment indicate an accumulation of these constituents in the immediate vicinity of the recharge well. Virtually all the phosphate that was recovered was withdrawn during the initial repumping surges, which consisted of five separate pump startups.

TABLE 2.—*Mass balance data for chloride, total nitrogen, MBAS, COD, and total phosphate during injection and redevelopment*

	Cl	Total N	MBAS	COD	Total PO_4
Injected ----------kilograms --	2,110	755	11.2	494	14.3
Repumped ----------do----	1,780	588	4.85	207	.85
Recovered, actually --percent--	84	78	43	42	6
Recovered, assuming 100 percent recovery of chloride-percent--	100	93	51	50	7

Mass balance calculations for each constituent were made using the mean concentrations for the reclaimed water shown in table 1 and the integration of the area below the curves in figure 2. These data are presented in table 2. All but 16 percent of the chloride added to the aquifer during part one (RW10) and part two (RW10A) of recharge was recovered during the short and long repumping phases (table 2). As chloride is considered to be an unreactive constituent, the difference between the amount added during recharge and recovered during redevelopment can be attributed to one or a combination of the following: (1) Sampling error, (2) dispersion, or (3) a somewhat different flow regime in the aquifer during pumping as compared with that during recharge. Percentage recovery of each of the other constituents was less than that of chloride. Factors controlling the recovery of chloride probably affected the other constituents similarly. Accordingly, the amounts recovered were adjusted in proportion to an adjustment of chloride to 100 percent.

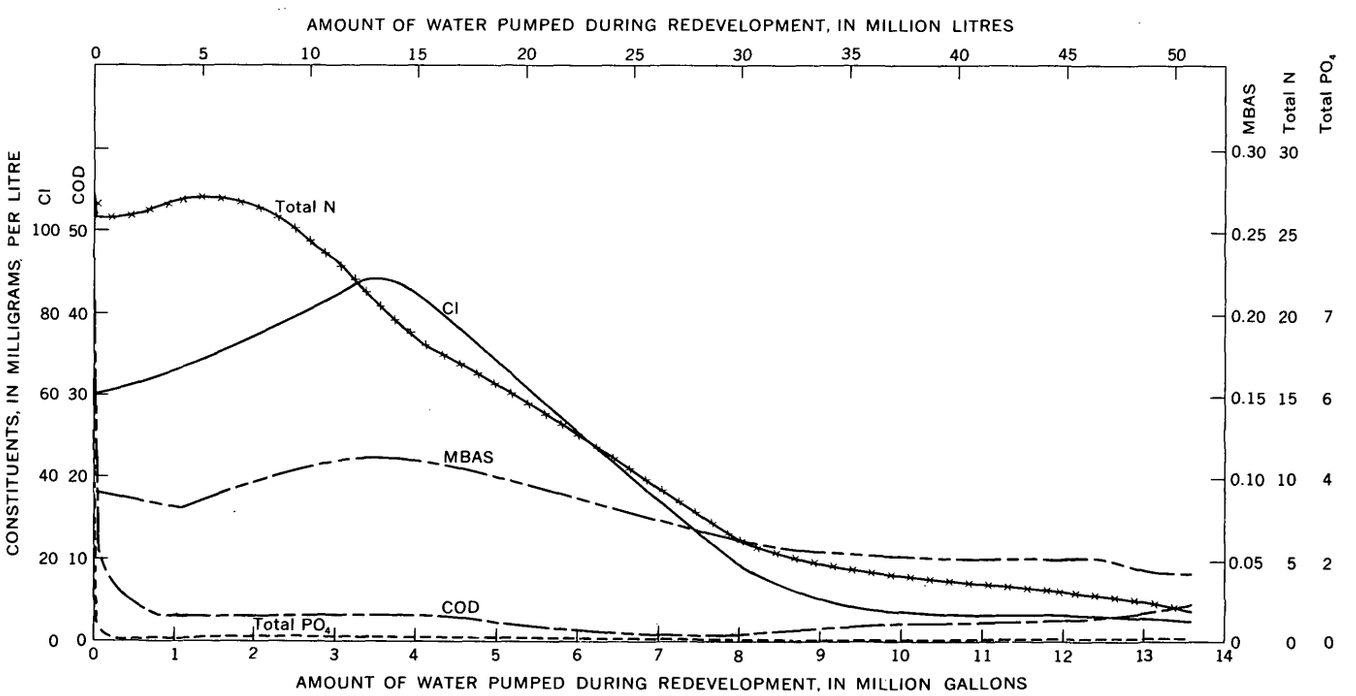

FIGURE 2.—Distribution of total nitrogen, total phosphate, MBAS, COD, and chloride in relation to the amount of water pumped out of recharge well.

The nearly total recovery of total nitrogen agrees with the observation that the concentration of nitrogen in water from the observation well during recharge approached that of the recharged water. The slight loss and the retardation of the total nitrogen concentration shown in figure 1, as compared with chloride, may result from cation-exchange reactions reported by Faust and Vecchioli (1974); or it may be due to membrane filtration by clay reported by Kharaka (1973).

Approximately 50 percent of the COD and MBAS constituents that were recharged were recovered during pumping. Similarly, the concentrations of these constituents at the observation well during recharge were about half those in the recharged water. Loss of these constituents is probably due to adsorption on clay and lignite in the Magothy aquifer. High concentrations of COD constituents in the water repumped initially indicate that some of the COD constituents, particularly those in the particulate or colloidal state, accumulate in the immediate vicinity of the recharge well.

Only 7 percent of the injected phosphate was recovered during pumping, and most of this was withdrawn during the initial pumping surges. A small part of the phosphate in the reclaimed water was probably in the particulate or colloidal state and was accumulated at the well-aquifer interface. The dissolved phosphate in the reclaimed water was immobilized either by precipitation as aluminum, iron, and (or) calcium salts, or was removed through reaction with clay in the Magothy aquifer. Little increase in phosphate was observed at the observation well during recharge, which indicates that virtually all phosphate from solution is removed within short distances from the injection well. This was supported in an earlier test in which acid treatment of the recharge well, after a major effort of redevelopment by pumping and surging, dislodged substantial amounts of phosphate and resulted in nearly a 50 percent improvement in the specific capacity of the well (Vecchioli, 1972, p. 94). This suggests that most of the phosphate was removed from solution at or near the aquifer-well interface.

A report by Baier and Wesner (1971), on the injection of trickling filter effluent into a fine to coarse sand aquifer in Orange County, Calif., shows results similar to those of this study. In the California study, the nitrogen concentration of water in an observation well 100 ft (30.5 m) from the recharge well was virtually unchanged from that of the injection water. The COD concentration was reduced 50 percent. MBAS and orthophosphate were removed completely by the aquifer. Because the aquifer material and the distance between the injection well and the observation well are different in these two studies, the results are not directly comparable. However, in general, the results are in good agreement.

Of the five constituents studied at Bay Park during test 10 excluding chloride, only nitrogen content remains relatively unchanged by passage of reclaimed water through the Magothy aquifer. Half of the MBAS and COD are lost to the aquifer, and almost all phosphate is lost to the aquifer or accumulated at the interface between the well and the formation face.

REFERENCES CITED

Baier, D. C., and Wesner, G. M., 1971, Reclaimed waste water for ground water recharge: Am. Water Resources Assoc. Jour., v. 7, no. 5, p. 991–1001.

Cohen, Philip, and Durfor, C. N., 1966, Design and construction of a unique injection well on Long Island, New York, *in* Geological Survey research 1966: U.S. Geol. Survey Prof. Paper 550–D, p. D253–D257.

——— 1967, Artificial-recharge experiments utilizing renovated sewage-plant effluent—a feasibility study at Bay Park, New York, U.S.A., *in* Symposium of Haifa, Artificial recharge and management of aquifers: Internat. Assoc. Sci. Hydrology Pub., no. 72, p. 193–199.

Faust, S. D., and Vecchioli, John, 1974, Injecting highly treated sewage into a deep-sand aquifer: Am. Water Works Assoc. Jour., v. 66, no. 6, p. 371–377.

Kharaka, Y. K., 1973, Retention of dissolved constituents of waste by geologic membranes, *in* Preprints of second international symposium on underground waste management and artificial recharge, New Orleans, La., Sept. 26–30, 1973: Am. Assoc. Petroleum Geologists, v. 1, p. 420–435.

Koch, Ellis, Giaimo, A. A., and Sulam, D. J., 1973, Design and operation of the Bay Park artificial-recharge plant, Bay Park, New York: U.S. Geol. Survey Prof. Paper 751–B, 14 p.

Peters, J. H., and Rose, J. L., 1968, Water conservation by reclamation and recharge: Am. Soc. Civil Engineers, Sanitary Eng. Div. Jour., v. 94, no. SA4, p. 625–639.

Ragone, S. E., Vecchioli, John, and Ku, H. F. H., 1973, Short-term effect of injection of tertiary-treated sewage on the concentration of iron in water in the Magothy aquifer, Bay Park, New York, *in* Preprints of second international symposium on underground waste management and artificial recharge, New Orleans, La, Sept. 26–30, 1973: Am. Assoc. Petroleum Geologists, v. 1, p. 273–290.

Vecchioli, John, 1970, A note on bacterial growth around a recharge well at Bay Park, Long Island, New York: Water Resources Research, v. 6, no. 5, p. 1415–1419.

——— 1972, Experimental injection of tertiary-treated sewage in a deep well at Bay Park, Long Island, New York—A summary of early results: New England Water Works Assoc. Jour., v. 86, no. 2, p. 87–103.

Vecchioli, John, Bennett, G. D., Pearson, F. J., Jr., and Cerrillo, L. A., 1974, Geohydrology of the artificial-recharge site at Bay Park, Long Island, New York: U.S. Geol. Survey Prof. Paper 751–C, 29 p.

Vecchioli, John, and Ku, H. F. H., 1972, Preliminary results of injecting highly treated sewage-plant effluent into a deep sand aquifer at Bay Park, New York: U.S. Geol. Survey Prof. Paper 751–A, 14 p.

Jour. Research U.S. Geol. Survey
Vol. 3, No. 1, Jan.–Feb. 1975, p. 93–98

MOBILIZATION OF IRON IN WATER IN THE MAGOTHY AQUIFER DURING LONG-TERM RECHARGE WITH TERTIARY-TREATED SEWAGE, BAY PARK, NEW YORK

By STEPHEN E. RAGONE, HENRY F. H. KU, and JOHN VECCHIOLI,
Mineola, N.Y.

Prepared in cooperation with the Nassau County Department of Public Works

Abstract.—Tertiary-treated sewage (reclaimed water) has been recharged by well into the Magothy aquifer at Bay Park, N. Y., intermittently since 1968. The longest of 13 recharge tests, the subject of this report, lasted 84.5 days. This was sufficient time for the reclaimed water to reach an observation well 200 ft (61 m) from the recharge well. Although the iron concentrations of the reclaimed water and the native water were less than 0.4 mg/l, the iron concentrations of samples from observation wells 20, 100, and 200 ft (6, 30, and 61 m) from the recharge well at times approached 3 mg/l. Source of the iron is pyrite that is native to the aquifer.

As part of an experimental deep-well recharge program at Bay Park, N.Y., the U.S. Geological Survey, in cooperation with the Nassau County Department of Public Works, has been studying the geochemical effects of recharging tertiary-treated sewage (reclaimed water) into the Magothy aquifer, Nassau County's primary source of potable water.

Of particular interest are the changes in the concentration of iron observed during recharge. An earlier report on the short-term (10-d) changes in iron concentration indicated that, although the iron concentrations in both the reclaimed and the native waters were less than 0.4 mg/l, the iron concentration in the mixed- (reclaimed- and native-)water front reaching an observation well 20 ft (6 m) away exceeded 3 mg/l and then decreased to 0.7 mg/l at the end of the test (Ragone and others, 1973). The authors attributed this iron peak to the oxidation of native pyrite in the Magothy aquifer by the dissolved oxygen in the reclaimed water and subsequent precipitation of ferric hydroxide. In a recent recharge experiment, RW13,[1] continuing intermittently for 84.5 d in a 199-d period, the changes in iron concentration and other pertinent water-quality parameters were measured at additional observation wells 100 and 200 ft (30 and 61 m) from the recharge well. Changes in the concentration of iron observed with time and distance from the recharge well are summarized in this report.

Acknowledgments.—The authors gratefully acknowledge the work of J. H. Peters, Commissioner, Nassau County Department of Public Works, in supporting the project. Thanks are given also to Ms. L. B. Maclin, U.S. Geological Survey, for her continued diligent efforts in making the numerous onsite chemical analyses on which this report is based.

PROCEDURE

Water reclamation and recharge

A small part of the effluent from the Bay Park activated-sludge type sewage-treatment plant in Nassau County, N.Y., is diverted to a 400 gal/min (25 l/s) pilot plant using physical-chemical, tertiary-treatment processes. Virtually potable water is obtained by the tertiary-treatment process, which consists of coagulation by use of aluminum sulfate, $Al_2(SO_4)_3$, filtration by mixed-bed sand filters, and adsorption on activated-carbon filters (Peters and Rose, 1968). The water is chlorinated before it is pumped about 0.5 mi (0.8 km) to a 50,000-gal (189,000-l) storage tank at the recharge site.

Details of the operation of the recharge well are reported elsewhere (Koch and others, 1973; Perlmutter and others, 1968; Cohen and Durfor, 1966, 1967). Briefly, in addition to the storage tank, the recharge plant has an 18-in(46-cm)-diam fiberglass-cased well finished with a 16-in(41-cm)-diam by 62ft(19-m)-long stainless-steel screen at a depth of 418 to 480 ft (127–146 m) below land surface; various equipment for further treating the reclaimed water (dechlorination, degasification, and pH and Eh adjustments); and 18 observation wells at distances ranging from a few

[1] RW13 means reclaimed water test 13, the thirteenth in a series of tests in which reclaimed water was recharged.

inches to 200 ft (61 m) from the recharge well and screened at various depths.

The Magothy aquifer is 490 ft (149 m) thick at Bay Park and consists of very fine to medium quartzose sand containing some clay, lignite, muscovite, and pyrite-marcasite (Vecchioli and others, 1974). Pumping tests before the beginning of the recharge experiments indicated that response of the recharge zone to pumping or recharge is similar to that of a semiconfined aquifer (Vecchioli and others, 1974).

The long-term recharge experiment, RW13, was started October 24, 1972, and was completed May 11, 1973 (table 1). Recharge was intermittent for 84.5 d of a 199-d period. Recharge segments of time ranged from 0.33 to 11.5 d, whereas shutdowns ranged from 1 to 27 d. Consequently, the reclaimed water moved through the formation in a series of pulses rather than as continuous flow. The pumping rate was 355 gal/min (22 l/s), and the volume of reclaimed water recharged during RW13 was 4.2×10^7 gal (1.6×10^8 l).

TABLE 1.—*Recharge data for test RW13 for 84.5 days*

Segment	Date Started	Date Ended	Number of days	Q (gallons)	ΣQ (gallons)
1	10–24–72	10–27–72	3	1,598,400	1,598,400
2	11– 7–72	11–17–72	10.5	5,192,400	6,790,800
3	11–20–72	11–22–72	2.5	1,213,600	8,004,400
4	11–27–72	12– 8–72	11.5	5,657,300	13,661,700
5	12–13–72	12–15–72	2.5	1,246,800	14,908,500
6	12–19–72	12–21–72	2.5	1,255,400	16,163,900
7	1– 3–73	1–12–73	9.5	4,706,700	20,870,600
8	1–15–73	1–19–73	4.5	2,246,600	23,117,200
9	1–29–73	2– 4–73	6.5	3,206,300	26,323,500
10	2– 6–73	2– 9–73	3	1,470,600	27,794,100
11	2–10–73	2–10–73	.33	149,400	27,943,500
12	2–12–73	2–13–73	.67	324,700	28,268,200
13	3–12–73	3–16–73	4.5	2,207,700	30,475,900
14	3–19–73	3–30–73	11.5	5,678,200	36,154,100
15	4– 2–73	4– 6–73	4	1,963,000	38,117,100
16	4– 9–73	4– 9–73	.5	233,500	38,350,600
17	5– 2–73	5– 4–73	2.5	1,177,400	39,528,000
18	5– 7–73	5–11–73	4.5	2,166,700	41,694,700

Redevelopment of the recharge well

During recharge, suspended material in the reclaimed water collected at or near the well screen-aquifer interface and caused the specific capacity of the well to decrease and the head to increase. Whenever head buildup reached 50 to 60 ft (15–18 m), the well was redeveloped by pumping. The recharge well was redeveloped several times during the recharge experiment.

Sampling and analytical methods

Samples from three observation wells screened in the recharge zone were collected at appropriate times by submersible and suction pumps and, on occasion, by a Foerst sampler. Two of the wells are 20 and 200 ft (6 and 61) m) away from and are screened at the same depth interval as the recharge well, 420 to 480 ft (128–146 m) below land surface. The third well is 100 ft (30 m) away from the recharge well and is screened 452 to 462 ft (138–141 m) below land surface. The 20-ft (6-m) and 100-ft (30-m) wells are southwest of the recharge well and the 200-ft (61-m) well is northwest of the recharge site.

Total iron, Fe^{+2}, HCO_3^-, dissolved oxygen, temperature, specific conductance, pH, turbidity, and chlorine residual were determined in the field by procedures outlined in Brown, Skougstad, and Fishman (1970). Additional analyses were done at the Geological Survey laboratory in Albany, N.Y.

RESULTS AND DISCUSSION

Comparison of chemical and physical qualities of native water and reclaimed water

Selected chemical and physical qualities of native and reclaimed water are compared in table 2. Native water from the different observation wells is characterized by its relatively low dissolved-solids concentration of 22 to 25 mg/l and, consequently, low specific conductance of 28 to 32 μmho/cm. The water has a slightly acidic pH of 5.22 to 5.72. Concentration of Fe^{+2} ranges from 0.14 to 0.30 mg/l. Dissolved oxygen and COD (chemical oxygen demand) concentrations are 0 mg/l.

TABLE 2.—*Pertinent chemical and physical qualities of native water at the 20-, 100-, 200-ft observation wells and of reclaimed water*

[All data in milligrams per litre, except pH and specific conductance]

	Native water[1] range	Reclaimed water[2] Mean	Deviation Standard	Deviation Relative (percent)
Dissolved solids	22–25	463	48	10
pH[3]	5.22– 5.72	6.1	.2	3
Specific conductance (μmho/cm at 25°C)	28–32	786	81	10
Iron:				
Total	0.14– 0.30	.41	.26	63
Dissolved	0.14– 0.30	.23	.18	78
Dissolved oxygen	0	4.5	1.6	36
Chemical oxygen demand (0.025 N $K_2Cr_2O_7$)	0	9	5	56

[1] Range of average values for water at the 20-, 100-, and 200-ft observation wells (Vecchioli and others, 1974).
[2] Based on a weighted average of at least 35 daily and weekly composite samples collected during the RW13 test.
[3] Calculated after converting pH values from logarithmic form to exponential form.

Reclaimed water has an average dissolved-solids concentration of 463 mg/l, which is more than an order of magnitude greater than that of native water, and an average specific conductance of 786 μmho/cm

(table 2). The pH averages 6.1. Iron occurs in both the filtrable (>0.45 μm) and unfiltrable (<0.45 μm) fractions, whose concentrations average 0.41 mg/l and 0.23 mg/l respectively. Reclaimed water has an average DO concentration of 4.5 mg/l and a COD concentration of 9 mg/l.

The relative deviation from the mean values for reclaimed water varies widely (table 2) The variation in COD concentrations is probably the result of poor analytical precision at the low concentrations measured. Variations in dissolved oxygen and iron reflect real changes in the quality of the reclaimed water. Specific conductance is relatively constant over most of the recharge experiment, as is indicated by its low relative deviation (10 percent); but some large, short-time increases, to almost 1,000 μmho/cm, were observed in specific conductance at the end of the recharge test.

Changes in concentration of iron at the 20-foot observation well

Changes in the concentration of total iron, pH, and specific conductance of samples from the 20-ft observation well during recharge are plotted in figure 1. The changes in the curves up to about 5.2×10^6 gal (20×10^6 l) of recharge have been reported previously (Ragone and others, 1973) and is given only a brief description here. Samples taken from the first 0.35×10^6 gal (1.3×10^6 l), from the 20-ft well reflect native-water conditions. As recharge continues, the reclaimed water front reaches the 20-ft observation well. Arrival of the front is indicated by the increase in specific conductance, for the specific conductance of reclaimed water is more than 25 times that of native water (table 2). Specific conductance increases sharply until about 0.6×10^6 gal (2.3×10^6 l) has been recharged. At 1.1×10^6 gal (4.2×10^6 l) the specific conductance becomes fairly constant at about 710 μmho/cm. This suggests that the native water has been displaced by the reclaimed water throughout the screened section of the observation well.

Simultaneously with the arrival of the reclaimed water at the 20-ft well, total iron increases and pH decreases. Iron concentration reaches 2.8 mg/l after 0.5×10^6 gal (1.9×10^6 l) has been recharged, then de-

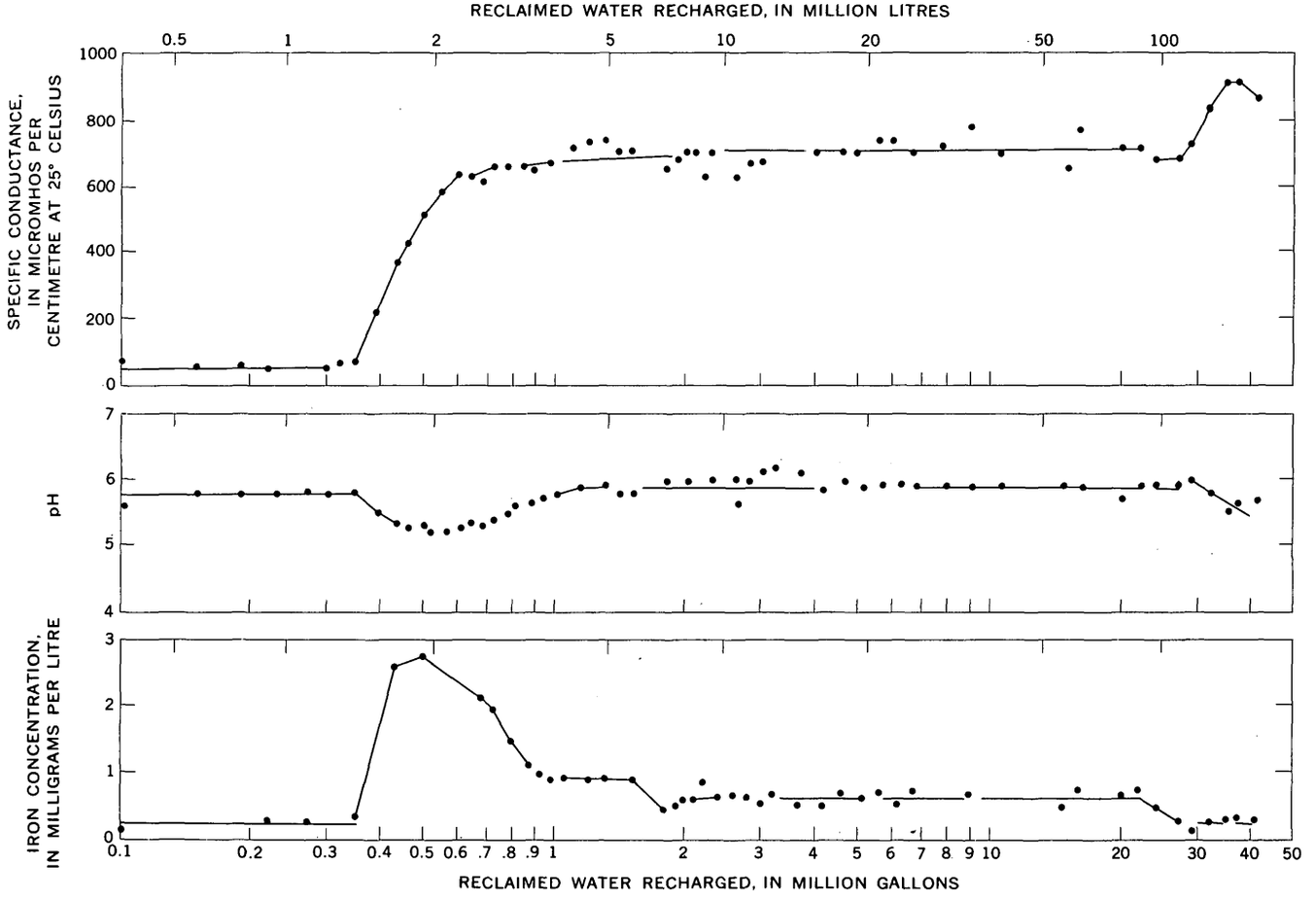

FIGURE 1.—Change in iron concentration, pH, and specific conductance of water from observation well N7886, 20 ft from the recharge well.

creases to 0.6 mg/l at 5.2×10^6 gal (20×10^6 l). The pH drops to a minimum of 5.29 after 0.5×10^6 gal (1.9×10^6 l) of recharge, but increases to 5.90 after 5.2×10^6 gal (20×10^6 l) of recharge. These changes in iron concentration and pH occur in the mixed-water front, as indicated by the specific conductance curve during a time interval of about 4 d. The authors attributed these changes to the oxidation of pyrite, which is native to the Magothy aquifer, by the dissolved oxygen in the reclaimed water (eq 1). If oxygen is in excess, this could be followed by the precipitation of ferric hydroxide (eq 3).

$$FeS_2+\tfrac{7}{2}O_2+H_2O=Fe^{+2}+2SO_4^{-2}+2H^+ \quad (1)$$

$$Fe^{+2}+\tfrac{1}{4}O_2+H^+=Fe^{+3}+\tfrac{1}{2}H_2O \quad (2)$$

$$Fe^{+3}+3H_2O=Fe(OH)_3(s)+3H^+ \quad (3)$$

With continued recharge beyond 5.2×10^6 gal (20×10^6 l), iron concentration and pH eventually decrease. Iron concentration remains at 0.6 mg/l until 20×10^6 gal (76×10^6 l) has been recharged; then it decreases to 0.2 mg/l for native-water after 27×10^6 gal (100×10^6 l) has been recharged and remains at this level until the end of the test.

The pH remains at 5.95 until 30×10^6 gal (110×10^6 l) has been recharged. It then decreases to values for native water after 35×10^6 gal (130×10^6 l) has been recharged.

Changes in concentration of iron at the 100- and 200-foot observation wells

The changes in iron concentration at the 100- and 200-ft observation wells follow a pattern similar to that described for the 20-ft well. The reclaimed water reaches the 100-ft well after about 3.4×10^6 gal (13×10^6 l) has been recharged, as indicated by the increase in specific conductance (fig. 2).

At the time specific conductance starts to increase, iron concentration begins to increase. The data for iron concentration and pH for samples collected at the 100-ft well were more scattered than those for samples collected at the 20- and 200-ft observation wells. Apparently, slight head changes caused by ocean tides are sufficient to affect the rate of movement of the reclaimed water in the aquifer and cause the data to scatter. After 6.2×10^6 gal (23×10^6 l) has been recharged, the iron concentration reaches 3 mg/l and then levels off at 1.85 mg/l. After 20×10^6 gal (76×10^6 l) has been recharged, Fe^{+2} concentration decreases to 1.1 mg/l at the end of the test. The pH data also seem to be scattered, presumably owing to the tidal effect, but the overall trend indicates that pH decreases with the arrival of the reclaimed water.

The reclaimed-water front reaches the 200-ft well after 10×10^6 gal (38×10^6 l) has been recharged (fig. 2). Iron concentration increases to 3 mg/l at the end of recharge. With the arrival of the reclaimed-water front, the pH decreases from 5.4, representative of native conditions, to 4.4 at the end of the test.

Iron content increase with movement away from recharge well

The quantities of Fe^{+2} that are estimated to have passed the 20-, 100-, and 200-ft observation wells during recharge are given in table 3. These values represent the areas under those parts of the iron concentration curves in figures 1 and 2 for which the concentration is greater than that of native water. The quantity of iron passing the 20-ft well, for example, is based on the part of the curve extending from 0.35×10^6 gal (1.3×10^6 l) to 29×10^6 gal (110×10^6 l).

TABLE 3.—*Iron content, in milligrams, of water at the 20-, 100-, and 200-ft observation wells*

20-ft well N7886	100-ft well N7890	200-ft well N8022
6.4×10^7	20.1×10^7	18.5×10^7

A simplified aquifer-flow model was used in calculating the iron load passing each observation well even though it was not entirely correct. With the model, injected water is assumed to move radially from the recharge well as an expanding cylinder having a height equal to that of the 418- to 480-ft (127- to 146-m)-depth interval of the recharge-well screen. Analysis of pumping-test data (Vecchioli and others, 1974) shows that within a radius of 200 ft (61 m) of the recharge well, flow is in a nearly horizontal-radial pattern. A flow net based on a steady-state, radially symmetric, electric-analog simulation of the well-aquifer system indicates that at 200 ft (61 m) 70 percent of the flow is within the screened interval (Vecchioli and others, 1974). Thus, the flow in the screened interval at a radius of 200 ft (61 m) should be no less than 70 percent of the flow at a radius of 20 ft (6 m).

The flow system depicted by the hydraulic data is not supported by the water-quality observations. Analysis of the breakthrough curve of specific conductance at the 20-ft well suggests that only 50 percent of the water flows through the 418- to 480-ft (127- to 146-m) interval at that radius. However, at the 200-ft well, a similar analysis suggests that nearly 100 percent of the reclaimed water remains in the recharge zone. Reasons for this anomalous depiction of the flow pattern are not clear, and speculation thereon is beyond the scope of this paper.

Regardless of the exact nature of the flow pattern, the percentage of flow passing the screen of the 200-ft

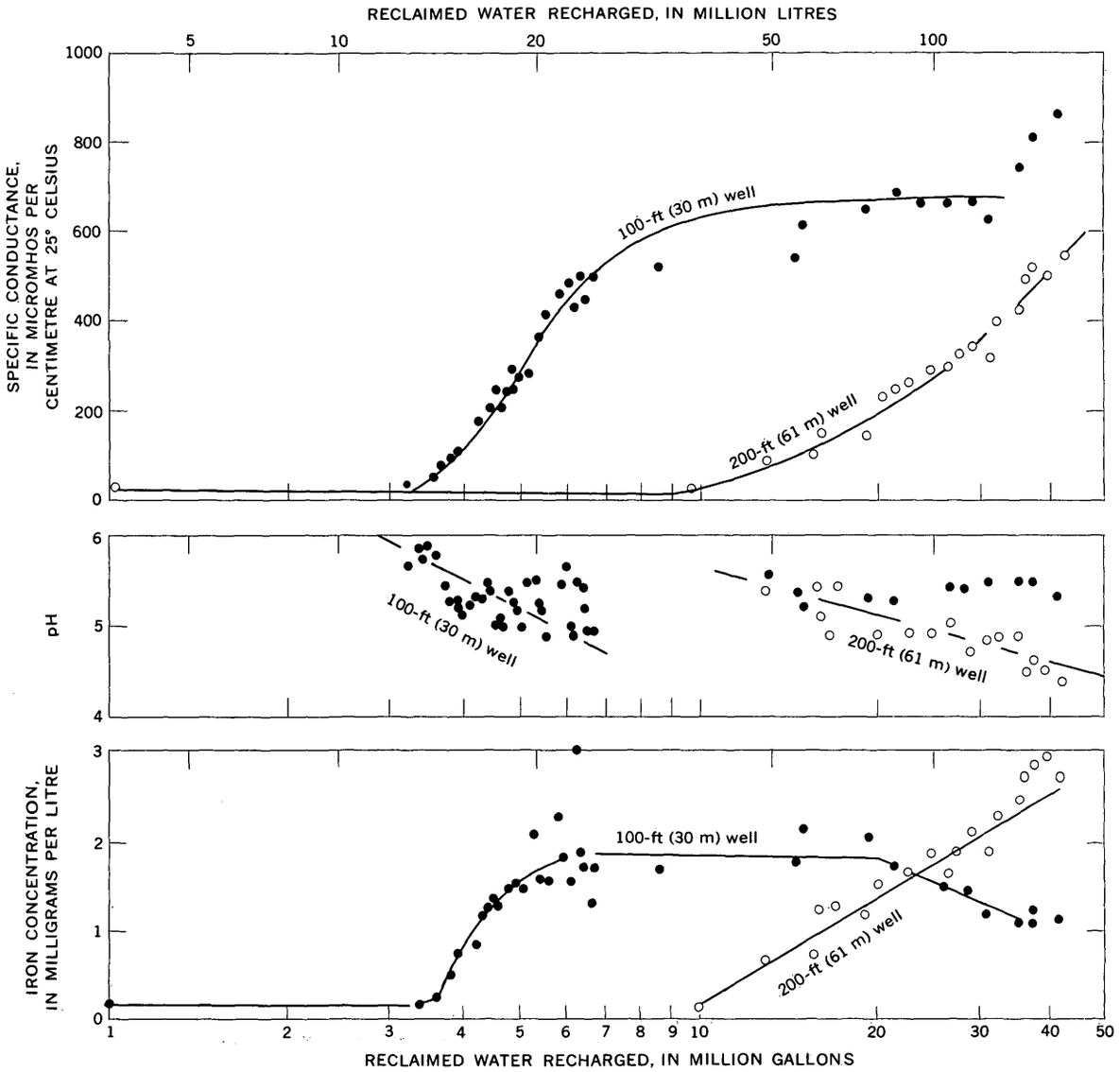

FIGURE 2.—Change in iron concentration, pH, and specific conductance of water from observation wells N7890 and N8022, 100 and 200 ft from the recharge well.

well is unlikely to be much different from that passing the screen of the 20-ft well; both wells are screened in the same interval as the recharge well, and this zone behaves virtually as a confined zone in the vicinity of the recharge well. Therefore, calculations based on a simplified flow model are useful in showing relative changes in the amount of iron in the water passing the observation wells. The emphasis here is on the trends rather than the actual values of iron.

The quantity of iron in water passing the 20-ft observation well is 6.4×10^7 mg (table 3). The quantity of iron in water passing the 100-ft well is 20.1×10^7 mg, which indicates a threefold gain between these two wells. However, the restricted 10-ft (3-m) screened zone of the 100-ft well may not give a representative sample of the entire recharge zone.

Because the recharge test ended before all the reclaimed water displaced native water at the 200-ft well, it is not possible to calculate the quantity of iron that would ultimately pass this point. A minimum value of 18.5×10^7 mg seems realistic; the value would be substantially greater if the increase in iron followed the same sequence as that observed at the 20- and 100-ft wells. Because the 200-ft well is screened at the same depth interval as the 20-ft well and the recharge well, the increase in iron should be representative of the entire recharge zone.

The data indicate that the amount of iron passing

the observation wells screened in the recharge zone increases with distance from the recharge well. This suggests that pyrite is reacting not only within 20 ft (6 m) of the recharge well (Ragone and others, 1973) but also at distances beyond the 20- and 100-ft observation wells. As dissolved oxygen concentration in water passing the 20-ft well is too low to be detected, the chemical mechanism by which the iron is picked up is not fully understood and is the subject of continued study.

SUMMARY

Recharging the Magothy aquifer with reclaimed water causes iron to be taken into solution. During recharge, the natural reducing condition around the recharge well is displaced by a more oxidizing one. This results, initially, in the dissolution of pyrite and the release of Fe^{+2}, H^{+}, and SO_4^{-2} to solution as the reclaimed water advances through the aquifer. Oxidation of Fe^{+2} to Fe^{+3} and precipitation of $Fe(OH)_3$ occurs in the more oxidizing water that follows. As recharge continues, the concentration of Fe^{+2} in water at the 20-ft well decreases to that of native water. Thus, initially, a slug of iron-rich water passes the 20-ft observation well.

Iron content of reclaimed water continues to increase with movement beyond the 20-ft well. The chemical mechanism of the increase in iron at the 100- and 200-ft observation wells is not fully understood, however, and is under study.

REFERENCES CITED

Brown, Eugene, Skougstad, M. W., and Fishman, M. J., 1970, Methods for collection and analysis of water samples for dissolved minerals and gases: U.S. Geol. Survey Techniques Water-Resources Inv., book 5, chap. A1, 160 p.

Cohen, Philip, and Durfor, C. N., 1966, Design and construction of a unique injection well on Long Island, N.Y., *in* Geological Survey research 1966: U.S. Geol. Survey Prof. Paper 550–D, p. D253–257.

——— 1967, Artificial-recharge experiments utilizing renovated sewage-plant effluent—A feasibility study at Bay Park, New York, U.S.A., *in* Artificial recharge and management of aquifers—Symposium of Haifa, 1967: Internat. Assoc. Sci. Hydrology Pub. 72, p. 193–199.

Koch, Ellis, Giaimo, A. A., and Sulam, D. J., 1973, Design and operation of the artificial-recharge plant at Bay Park, New York, U.S. Geol. Survey Prof. Paper 751–B, 14 p.

Perlmutter, N. M., Pearson, F. J., and Bennett, G. D., 1968, Deep-well injection of treated waste water—An experiment in re-use of ground water in western Long Island, N.Y., *in* New York State Geol. Assoc. Guidebook, 40th Ann. Mtg., 1968: p. 221–231.

Peters, J. H., and Rose, J. L., 1968, Water conservation by reclamation and recharge: Am. Soc. Civil Engineers, Sanitary Eng. Div. Jour., v. 94, no. SA4, p. 625–639.

Ragone, S. E., Vecchioli, John, and Ku, H. F. H., 1973, Short-term effect of injection of tertiary-treated sewage on the concentration of iron in water in the Magothy aquifer, Bay Park, New York, *in* Preprints of second international symposium on underground waste management and artificial recharge, New Orleans, La., Sept. 26–30, 1973: Am. Assoc. Petroleum Geologists, v. 1, p. 273–290.

Vecchioli, John, Bennett, G. D., Pearson, F. J., Jr., and Cerrillo, L. A., 1974, Geohydrology of the artificial-recharge site at Bay Park, Long Island, New York: U.S. Geol. Survey Prof. Paper 751–C, 29 p.

Jour. Research U.S. Geol. Survey
Vol. 3, No. 1, Jan.–Feb. 1975, p. 99–102

NORMAN CREEK, A SOURCE OF RECHARGE TO MARAMEC SPRING, PHELPS COUNTY, MISSOURI

By E. E. GANN and E. J. HARVEY, Rolla, Mo.

Work done in cooperation with the Missouri Geological Survey and Water Resources

Abstract.—Rhodamine WT dye was used to trace the subsurface movement of water from Norman Creek, a losing Ozark stream, to Maramec Spring, a straight-line distance of 8.7 mi (14.0 km). Grab samples and activated charcoal packets were used to check possible emergent points of the dye. The leading edge of the dye reached Maramec Spring 68–75 days after the dye injection, and the peak concentration reached the spring 82–93 d after injection. Small quantities of dye were still being recovered at the spring 114 d after injection and 39–46 d after the dye first arrived at the spring. Computed average velocities, assuming straight-line travel, are 0.47–0.42 ft(0.14–0.13 m)/min for the leading edge and 0.39–0.34 ft(0.12–0.10 m)/min for the peak. This apparent rate of travel compares favorably with other recent subsurface tracing studies in southern Missouri which generally range from 0.4 to 25 ft(0.12 to 7.6 m)/min.

The hydrology of a limestone and dolomite terrane is often complicated because of subsurface movement of water to other nearby basins. The diverted water generally emerges in the receiving basin at a large spring or a series of springs. As water from many such springs is used for public and domestic supplies, fish hatcheries, recreational areas, and growing aquatic plants, it is desirable to define the recharge areas of springs so that possible contamination from surface sources may be prevented.

The purpose of this article is to describe a successful field experiment to trace the subsurface movement of water from a losing Ozark stream, Norman Creek, to Maramec Spring. Documentation of such tracing experiments will aid the karst hydrologist in quantifying subsurface water movement in a karst terrane.

Variations of the tracing methodology described herein have also been used in recent years by personnel of the Missouri Geological Survey and Water Resources and the U.S. Forest Service as an aid in defining recharge areas of other springs in the Ozarks of southern Missouri.

Acknowledgments.—The authors express their gratitude to the James Foundation, owners of Maramec Spring Park, for their cooperation in allowing access to Maramec Spring. The assistance of Mr. Phil Reppert and Mr. Dave Moeslein of the park staff in collecting grab samples from Maramec Spring is also greatly appreciated.

NORMAN CREEK BASIN

Norman Creek, a tributary to Dry Fork, is located about 10 mi (16 km) southeast of Rolla, Mo. (fig. 1). The ephemeral stream drains an area of about 57 mi^2 (148 km^2) and flows across the Roubidoux Formation and the upper part of the Gasconade Dolomite of Early Ordovician age. Bedrock is exposed at numerous places along the stream, but for long reaches it is overlain by sand and gravel. In places, the rocks have minor tilts in various directions which are believed to be due to slumping caused by solution accompanied by subsidence or collapse of underlying beds. In general, the bedrock formations have a gentle northwesterly dip of about 15 ft/mi (2.8 m/km).

The valley of Norman Creek and much of the adjacent uplands are in pasture or hayfields. The stream receives no municipal or industrial wastes, only runoff from agricultural lands. Willow bushes and other phreatic vegetation are abundant in the upper reach of the stream and at the confluence with Dry Fork, signifying a shallow water table, but are virtually absent in the middle and lower reaches. In the upstream reach where ground-water levels stand at about the same altitude as the streambed, Norman Creek generally flows except during dry weather when the flow gives way to pooled conditions. Ground-water levels stand as much as 100 ft (30.5 m) below the level of the streambed in the middle reach (Maxwell and others, 1967). Flow occurs throughout the length of Norman Creek only after intense rainfalls of about 2–4 in (51–102 mm) when the accumulated runoff in the main channel exceeds the infiltration capacity of the sand and gravel streambed.

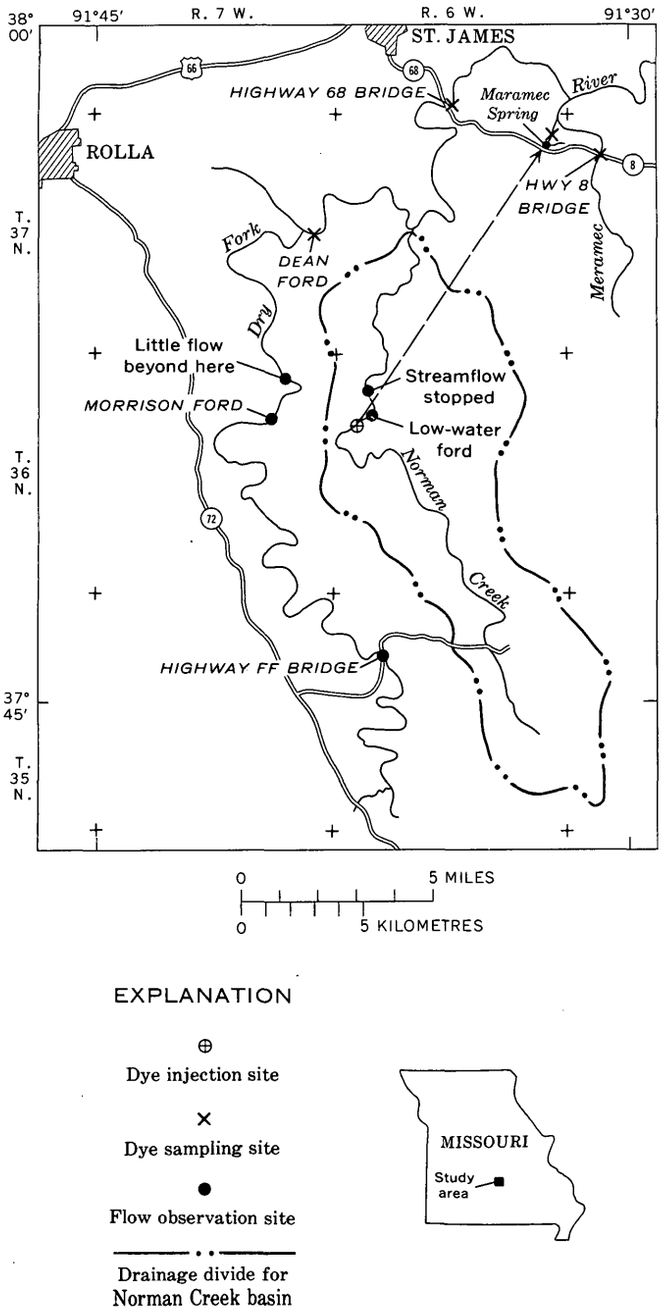

FIGURE 1.—Map of Norman Creek basin and parts of Dry Fork and Meramec River basins showing location of dye injection site, sampling sites, and flow observation sites.

MARAMEC SPRING

Maramec Spring,[1] the seventh largest spring in Missouri (Vineyard and Feder, 1974), is located about 4 mi (6.4 km) northeast of the mouth of Norman Creek (fig. 1). The spring rises in a circular basin at the base of a high bluff of Gasconade Dolomite and flows, at a distance of several hundred feet, into the Meramec River. The maximum, minimum, and mean flows of Maramec Spring for a 16-yr period of record are 650, 56, and 144 ft^3/s (18.4, 1.6, and 4.1 m^3/s), respectively. The privately owned spring and surrounding area are operated as a public park. Trout, reared in special basins supplied by the spring, are released in downstream reaches of the spring branch for sport fishing.

[1] Maramec Spring is the spelling approved in 1970 by the Board on Geographic Names, although all other features in the area, including the river, carry the Meramec spelling.

NORMAN CREEK–MARAMEC SPRING DYE TRACE

After a 2-in (51-mm) rain on the Dry Fork basin on the night of August 22, 1972, 1 gal (3.8 l) of Rhodamine WT (20 percent) dye was poured into the dry streambed of Norman Creek in the NE¼SE¼, sec. 7, T. 36 N., R. 6 W. about 0.25 mi (0.4 km) upstream from the low-water ford (fig. 1). The dye was injected at 1400 h (2:00 p.m.) on August 23, 1972, in front of a slug of water (fig. 2) which was observed

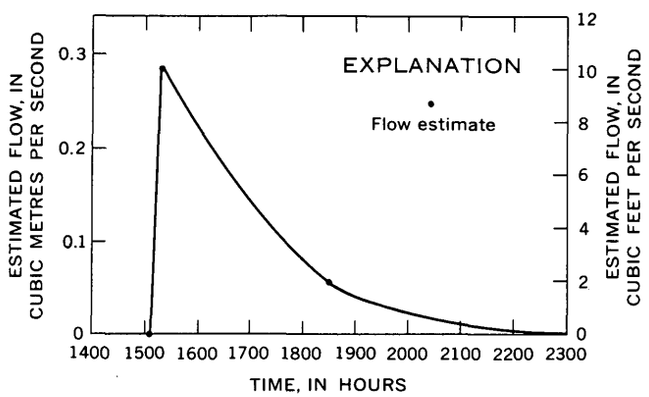

FIGURE 2.—Estimated flow hydrograph for Norman Creek at low-water ford on August 23, 1972.

to be traveling down Norman Creek at a rate of about 0.25–0.5 mi (0.4–0.8 km)/h. The dye was not visible when the flow reached the low-water ford at 1505 h (3:05 p.m.).

At 0915 h (9:15 a.m.) on August 24, 1972, small pools were observed at the low-water ford, but no water was flowing. The dye and approximately 2 acre-ft (2,470 m^3) of water had disappeared into the sand and gravel streambed within about 1 mi (1.6 km) of the point of dye injection. Streamflow had stopped at a point in the SE¼SE¼, sec. 6, T. 36 N., R. 6 W. (fig. 1).

A larger slug of water was observed moving down the dry streambed of Dry Fork after the same rainfall. A flow of 75–100 ft^3/s (2.1–2.8 m^3/s) was estimated at 0905 h (9:05 a.m.) on August 23 at Highway FF bridge (fig. 1) in the SW¼NW¼, sec. 8, T. 35 N., R. 6 W. Flow reached Morrison Ford (fig. 1) in the

NE¼SW¼, sec. 11, T. 36 N., R. 7 W. at 1230 h (12:30 p.m.) on August 24, and at 1250 h (12:50 p.m.) an estimated peak of 60 ft^3/s (1.7 m^3/s) was observed (fig. 3). Most of this flow had disappeared into the

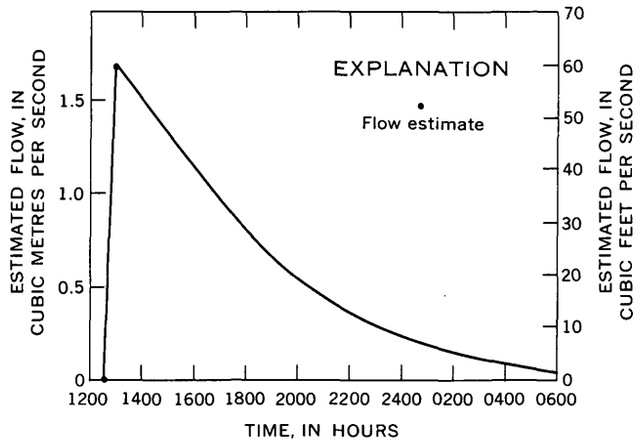

FIGURE 3.—Estimated flow hydrograph for Dry Fork at Morrison Ford on August 24 and 25, 1972.

sand and gravel streambed by the time the water reached a point in the NE¼SW¼, sec. 2, T. 36 N., R. 7 W. (fig. 1) where an inspection of the streambed indicated that a peak of less than about 2 ft^3/s (0.06 m^3/s) had occurred.

After the dye injection in Norman Creek, a variation of a method developed by Dunn (1957) and recommended by Hass (1959) was used to check possible emergent points of the dye. Small packets made from fine-mesh window screening and filled with about 10 g of activated charcoal were placed in the flow of Maramec Spring, 8.7 mi (14 km) northeast of the injection site, and arrangements were made for obtaining periodic grab samples. The packets were placed at two sites in Maramec Spring as a double check for any dye emerging at the spring. Activated charcoal packets were also placed in Dry Fork at Dean Ford and Highway 68 bridge and in Meramec River at Highway 8 bridge (fig. 1) to check other possible emergent points of the dye.

Grab samples were obtained at Maramec Spring twice daily through September 14 and daily grab samples were continued through October 21. All grab samples were tested on a fluorometer and no dye was recovered during this period.

The activated charcoal packets were replaced approximately at weekly intervals. Charcoal from the exposed packets was submerged in a 5-percent solution of ammonium hydroxide in ethyl alcohol (Scanlan, 1968) for 1 h to remove any dye absorbed by the charcoal. The solvent was then filtered and tested on a fluorometer for the presence of dye. Fluorometer dial readings, converted to equivalent readings for the 30× scale, for the various charcoal packets and sampling sites are summarized in table 1.

TABLE 1.—*Fluorometer dial readings, 30× scale, August 23 to December 15, 1972*

[Samples were tested at room temperature (about 24°C) with far ultraviolet lamp, high-sensitivity door kit, 546 primary and 590 secondary filters. Values in parentheses are computed values for 30× scale based on dial readings for less sensitive scales (10×, 3×, or 1×]

Period exposed to flow	Maramec Spring		Dry Fork		Meramec River, Highway 8
	Site A	Site B	Dean Ford	Highway 68	
8-23— 9- 1	17	20	--	--	--
8-29— 9- 1	--	--	43	45	43
9- 1— 9- 8	20	48	56	49	32
9- 8— 9-15	36	27	66	55	47
9-15— 9-22	33	21	88	100	38
9-22— 9-29	29	27	94	64	(1)
9-29—10- 6	(1)	24	(1)	57	34
10- 6—10-13	59	47	(129)	(108)	80
10-13—10-20	49	37	(1)	(117)	68
10-20—10-30	55	46	82	100	(1)
10-30—11- 6	(1)	80	96	(1)	(1)
11- 6—11-13	(166)	(2)	(2)	(2)	(2)
11- 6—11-24	--	(635)	(1)	45	(1)
11-13—11-24	(1220)	--	--	--	--
11-24—12- 5	(593)	(414)	--	41	--
12- 5—12-15	(163)	(129)	--	(1)	--

[1] Packet missing or charcoal missing from packet.

[2] Unable to replace packet because of high water.

Some difficulty was encountered with the charcoal packets because of the necessity of locating the packets in the faster water near the center of the stream for maximum exposure to any dye passing the site. The packets were wired to rocks or other obstructions so that water could pass through freely. Some packets were recovered with little or no charcoal remaining, possibly because the charcoal had been broken into smaller pieces and washed from the fine-mesh container by the current. High water in mid-November and an ice storm in December also complicated the recovery of the charcoal packets.

INTERPRETATION OF RESULTS

Fluorometer dial readings for Maramec Spring and Dry Fork at Highway 68 bridge are plotted in figure 4 on the date of removal of each packet. These plots indicate that the leading edge of the dye reached Maramec Spring sometime between October 30 and November 6 (68–75 d after injection) and that the dye peak arrived during the period November 13–24 (82–93 d after injection). Small quantities of dye were still being absorbed by the charcoal packets on December 15 (114 d after the dye injection and 39–46 d after the dye first arrived at Maramec Spring).

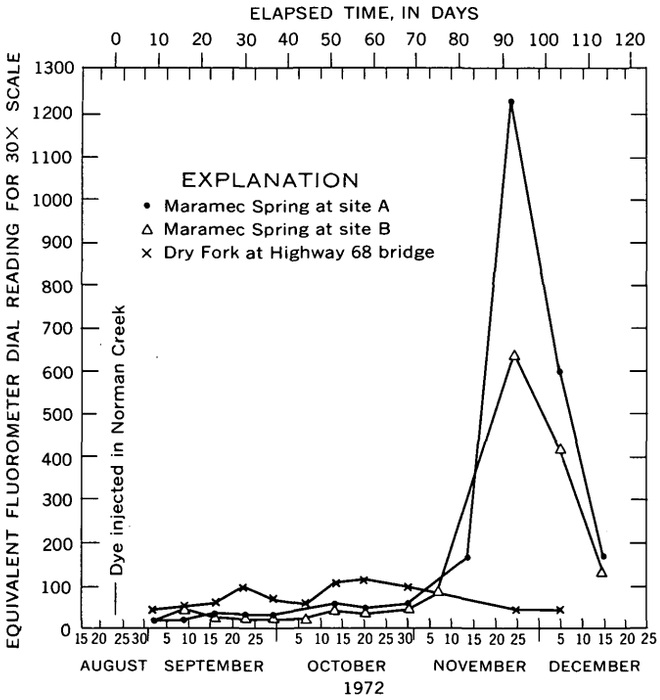

FIGURE 4.—Fluorometer dial readings (30× scale) for Maramec Spring and Dry Fork at Highway 68 bridge.

A 4-in (102-mm) rainfall which occurred over the Norman Creek basin on November 1 was probably instrumental in flushing the dye through the subterranean drainage system. In the absence of this rainfall, an even longer period of time undoubtedly would have elapsed before emergence of the dye at Maramec Spring.

Dye was not recovered at sampling sites on Dry Fork and Meramec River. The data do not prove conclusively that dye did not pass these sites, however. Dye could have passed the Highway 8 site during the period September 22–29 or after October 20. The continuity of data at the two sites on Dry Fork makes it unlikely that any dye passed these points as any dye passing the Dean Ford site would have also passed the Highway 68 site.

Computed average velocities, assuming straight-line travel along the 8.7 mi (14 km) between the injection site and Maramec Spring, are 0.47–0.42 ft(0.14–0.13 m)/min for the leading edge and 0.39–0.34 ft(0.12–0.10 m)/min for the peak. This apparent rate of travel compares favorably with other recent subsurface tracing studies in southern Missouri which generally range from 0.4 to 25 ft(0.12 to 7.6 m)/min.

CONCLUSIONS

This experiment illustrates five facts: (1) Norman Creek is a source of recharge to Maramec Spring, (2) relatively large quantities of flow are lost to subsurface drainage from losing streams in Missouri's Ozarks, (3) a contaminant either discharged or washed into a losing stream may emerge at one of the large springs in the region, (4) several weeks or months may elapse before the contaminant resurges in a spring, and (5) a relatively long period of time may be required to completely flush all the contaminant through the subterranean drainage system.

REFERENCES CITED

Dunn, J. R., 1957, Stream tracing, Mid-Appalachian region: Natl. Speleol. Soc. Bull, v. 2, p. 7.

Hass, J. L., Jr., 1959, Evaluation of ground water tracing methods used in speleology: Natl. Speleol. Soc. Bull., v. 21, pt. 2, p. 67–76.

Maxwell, J. C., Gevecker, V. A. C., and Grigoropoulous, S. G., 1967, Availability, distribution, quantity, and quality of water resources in carbonate karst terrain: Missouri Univ., Water Resources Research Center, Ann. Program Rept., 15 p.

Scanlan, J. W., 1968, Evaluation and application of dye tracing in karst terrain: Rolla, Missouri Univ., M. S. thesis, 87 p.

Vineyard, J. D., and Feder, G. L., 1974, Springs of Missouri: Missouri Geol. Survey and Water Resources, Water Resources Rept. 29, 266 p.

Jour. Research U.S. Geol. Survey
Vol. 3, No. 1, Jan.–Feb. 1975, p. 103–106

WATER-QUALITY CHANGES DURING A SALMON RUN IN AN INTERIOR ALASKAN STREAM

By JON W. NAUMAN and DONALD R. KERNODLE, Anchorage, Alaska

Abstract.—Increased activity at sunset of sockeye (red) salmon (*Oncorhynchus nerka*) in an Alaskan stream resulted in increases in carbon dioxide, turbidity, suspended chlorophyll *a*, and drift invertebrates, and a decrease in pH and dissolved oxygen.

The report presented here is auxiliary to a study to determine the seasonal water-quality characteristics of selected streams along the proposed trans-Alaska pipeline corridor. The purpose of the study was to document the diel changes—events which recur at intervals of 24 h or less (Odum, 1959)—during summer in a small alpine salmon stream in interior Alaska. An unexpected salmon run during the study period provided a unique opportunity to record the effects of migrating salmon on a stream of this type.

On July 28, 1972, at 1100 h (Alaska daylight time), a 24-h study was begun on Fish Creek near Paxson, Alaska, about 100 yd (approximately 100 m) upstream from the Richardson Highway crossing (fig. 1).

Fish Creek has a drainage area of 10.6 mi^2 (27.4 km^2) and originates in a chain of two lakes in the upper Gulkana River drainage of the Alaska Range (fig. 1). From Upper Fish Lake to the confluence with the Gulkana River, the stream drops 150 ft (approximately 50 m) in 4 mi (6.4 km). The area drained is an alpine region; the dominant cover is willows, dwarf birch trees, and cranberry bushes.

In Fish Creek the red salmon (*Oncorhynchus nerka*) run begins in mid-May and extends to mid-August. Salmon congregate in a large quiescent pool in the Gulkana River at the mouth of Fish Creek before moving up Fish Creek to spawn in Upper Fish Lake.

The salmon population, estimated by the Alaska Department of Fish and Game personnel on July 30, 1972, was 2,900 in the Gulkana River pool, 350 in Fish Creek, and 4,500 in Upper Fish Lake. A total population of 6,000–6,500 salmon was counted after spawning on September 2, 1972 (Ken Roberson, Alaska Dept. Fish and Game, oral commun., 1972).

During the daylight hours of the study, salmon either singly or in pairs, were continually moving up the creek at a moderately slow but consistent rate. At 2000 h on July 28 a school of approximately 50 very active salmon moved into the study reach. The school seemed to be in a frenzy, moving back and forth within the study reach. This frenzy lasted approximately 20 min. Subsequently, the normal run of fewer salmon resumed.

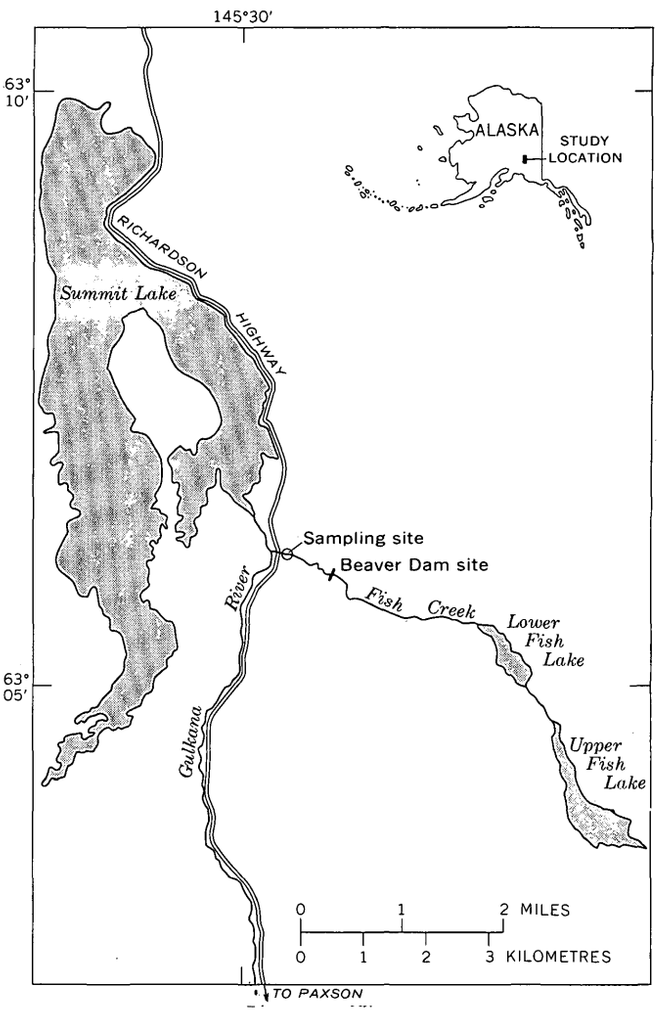

FIGURE 1.—Location of study area, Fish Creek near Paxson, Alaska.

METHODS

Sampling was done hourly or bihourly between 1100 and 2100 h on July 28 and at 0200 h and hourly between 0600 to 1100 h the following day. Water samples were collected at midstream and analyses were performed without delay. Water temperature, specific conductance, total alkalinity, pH, chlorophyll *a*, turbidity, discharge, water stage, barometric pressure, light reflectance, percentage of cloud cover, wind direction and velocity, and air temperature were measured at these times. These data were reported by Nauman and Kernodle (1973).

The data for the parameters which fluctuated during the time interval encompassed in this study are given in figure 2. Carbon dioxide was computed from alkalinity and pH data (Brown and others, 1970). The precision of the pH measurements (±0.02) limited the accuracy of the free carbon dioxide determination to ±0.5 mg/l.

Drifting debris and invertebrates were collected with a modified Surber sampler equipped with a 3-ft (1-m) long net. The netting had 89 meshes to the inch with a mesh opening of 216 μm. The net was positioned in maximum flow for 1 h at bihourly intervals, except for the samples collected at 0200 and 0630 h which were removed after one-half hour. Drifting invertebrates were separated from debris for the samples collected during the 1400–1500 and 2000–2100 h periods only. After identification and counting, the invertebrates and one vertebrate were recombined with the debris in order to obtain total dry and organic weights for the eight drift samples.

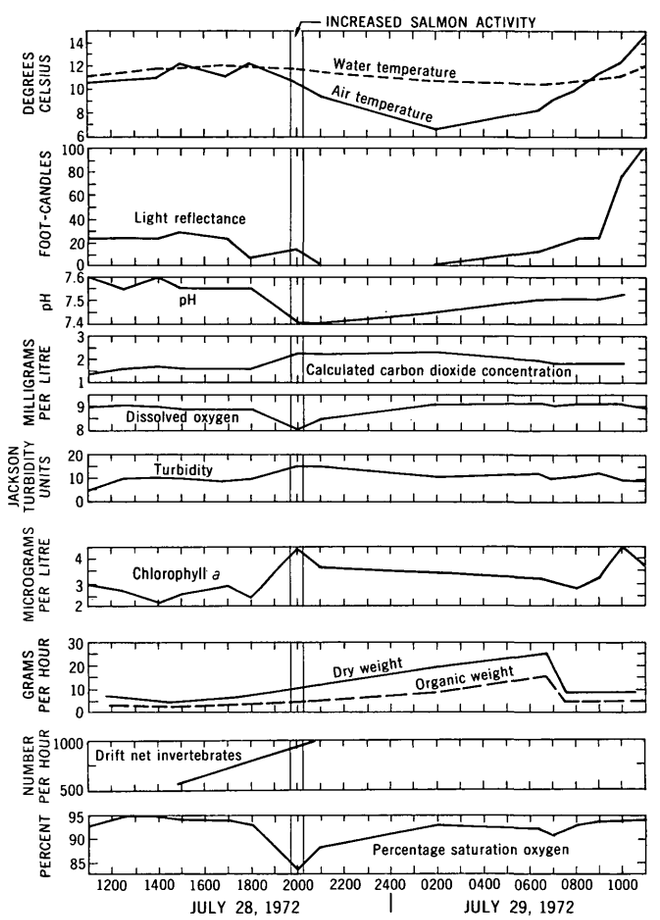

Figure 2.—Meteorological and water-quality changes for Fish Creek, July 28–29, 1972. (1 ft-c = 10.76 lm/m².)

OBSERVATIONS

A light rain fell between July 25 and early morning of July 28; total rainfall was 0.34 in (8.6 mm) at Summit Lake, approximately 4 mi (7.2 km) from the study site. (U.S. Environmental Data Service, 1972, p. 126). At the beginning of the study period, however, the skies began to clear with gradually rising barometric pressure and air temperature. On July 28 sunset occurred at 2100 h with sunrise occurring between 0200 and 0300 h on July 29. Water stage remained fairly constant, varying 0.03 ft (91 mm) during the study (Nauman and Kernodle, 1973). Discharge was 15.3 ft³/s (0.4 m³/s) at 1500 h. The studied stream reach was 16 ft (5 m) wide and 0.6 ft (0.2 m) deep and had an average water velocity of 1.5 ft/s (0.5 m/s). The bottom was covered with cobbles, coarse gravel, and sand, creating a nearly continuous riffle area from the beaver dam site to the Richardson Highway crossing (fig. 1).

Specific conductance and alkalinity remained constant, 58 μmho and 36 mg/l, respectively, during the study. Figure 2 shows a tendency for the following parameters to vary directly: water temperature to air temperature, dissolved oxygen to pH, chlorophyll *a* to relative light intensity, turbidity to chlorophyll *a*; while carbon dioxide to pH, dissolved oxygen to carbon dioxide, drifting debris dry and organic weight to relative light intensity tended to vary inversely.

Drift samples collected for counting and identification of drift invertebrates were selected from the minimum (1400 h) and maximum (2000 h) chlorophyll *a* concentration values (fig. 2). Table 1 shows that the number of invertebrates had doubled in the sample collected at 2000–2100 h compared with the sample collected at 1400–1500 h on July 28; Chironomid larvae, Ostracoda, Acari, and Copepoda increased by at least a factor of 2, whereas Ephemeroptera and Plecoptera nymphs and Simuliidae larvae and Nematoda increased by a minimum factor of 8.

TABLE 1.—*Drift organisms collected from Fish Creek on July 28, 1972*

Taxa	Number collected during indicated sampling time	
	1400—1500 h	2000—2100 h
Salmonid (length 38 mm)	1	0
Chironomid larvae	291	604
Cladocera	101	56
Acari	50	101
Ostracoda	19	37
Copepoda	18	47
Diptera pupae	27	36
Ephemeroptera nymphs	9	78
Syrphidae larvae	2	0
Oligochaeta	3	2
Blephariceridae	2	0
Tabanidae larvae	1	2
Plecoptera nymphs	1	16
Trichoptera nymphs	1	2
Muscidae larvae	1	0
Simuliidae larvae	1	8
Nematoda	1	9
Total	529	998

DISCUSSION

In running water, diel changes in water temperature, stage turbidity, chlorophyll *a* and dissolved oxygen can be related to atmospheric, biologic, and physical conditions. On July 28 at about 2000 h there were changes in dissolved oxygen, pH, carbon dioxide, turbidity, chlorophyll *a*, drift invertebrates, and organic material, with little or no change in conductance, alkalinity, and atmospheric conditions. These changes occurred about the time of the increased salmon activity. The phenomenon of increased salmon activity near sunset has been reported elsewhere (Peterson, 1972).

On the basis of other studies conducted by the authors along the proposed pipeline corridor and those by Wright and Mills (1967), minimum pH values normally occur near sunrise; however, the minimum pH value for this study occurred near sundown and gradually rose to the termination of the study.

Dissolved-oxygen content varies with physical conditions, oxygen production by aquatic plants, oxygen removal by respiration of plants and animals, and oxygen demand of organic detritus. Streams normally exhibit diel changes in dissolved oxygen caused by changes in oxygen saturation, with fast flowing streams usually having oxygen saturation near 100 percent (Ellis, 1937; Hynes, 1970; McConnel and Sigler, 1959).

During this study dissolved oxygen never exceeded 95-percent saturation, dropping to 83 percent at 2000 h on July 28. Oviatt, Gall, and Nixon (1972) reported dissolved-oxygen values lowered by as much as 12 percent as a result of activity of schools of Atlantic menhaden; this corresponds to the decreased dissolved oxygen observed during the increased salmon activity in this study. Hargrave (1972) reported that aquatic sediment and detritus consume more oxygen when stirred in aerated water; this corresponds to the slightly higher turbidities and lower oxygen concentrations noted during the increased salmon activity.

In flowing water dissolved oxygen varies inversely with temperature, but during this study when water temperature dropped at 0200 h (July 29), so did the dissolved-oxygen levels, with an almost immediate increase between 2000–2100 h. The more usual inverse relationship between dissolved oxygen and temperature was not evident until 1000 h on July 29. Dissolved oxygen tended to vary inversely with carbon dioxide which is directly related to pH. During this study and in other studies conducted by the U.S. Geological Survey along the proposed pipeline corridor and by Wright and Mills (1967), it was found that lower values of carbon dioxide normally occurred between 1000 and 16000 h when photosynthetic activity was greatest.

Turbidity may be defined as an unclear condition or cloudiness of water (Brown and others, 1970). Fish Creek turbidity values were low, and to the eye the water appeared to have the clarity of distilled water. However, turbidity as measured in this study showed a diurnal fluctuation, with the lower turbidity values occurring near midday and the highest readings occurring at 2000 h on July 28 (fig. 2).

Much of the free-moving plant material in streams is due to the disturbance of algae cells by water currents which dislodge cells from substrates and transport them downstream. Algae cells respond to light by increasing photosynthesis. Chlorophyll *a* indicates the amount of biomass of photosynethic plants in the water. The peak of chlorophyll *a* concentration at 2000 h on July 28 corresponds to the dislocation of algae cells caused by salmon activity, whereas the rise between 0900 and 1100 h on July 29 corresponds to increased light values.

Drift samples collected both drifting organisms and debris. Higher drift rates during the night such as those observed in this study have been reported elsewhere (Waters, 1962). Waters reported that drifting organisms respond to light by increasing about an hour after sundown and then decreasing at dawn. Drift debris seemed to follow those observations in this study. Waters further reported that physical disturbance caused larval forms to be detached, increasing the drift rate of Simuliidae larvae and Ephemeroptera nymphs. Total numbers of invertebrates increased from 529 to 998 with Ephemeroptera, Simuliidae, Plecoptera, and Nematoda increasing by a minimum factor of 8 in the two samples analyzed.

CONCLUSION

Published data on Fish Creek and other streams along the proposed trans-Alaska pipeline corridor indicate that some of the water-quality changes occurring on Fish Creek near sunset were as great as measured seasonal changes (Nauman and Kernodle, 1973). Water-quality changes in Fish Creek are normally slight except when some physical change occurs, such as high or low air temperatures, high or low rainfall, and man-induced disturbances. During this study pH and dissolved oxygen decreased, whereas suspended chlorophyll *a*, turbidity, drift invertebrates, and carbon dioxide increased; invertebrates normally attached firmly to bottom substrates were dislodged. Within the accuracy and precision of the measurements, this study documented the diel and diurnal water characteristics for Fish Creek during July 28–29, 1972. As shown in figure 2, certain parameters tended to change with increased salmon activity.

REFERENCES CITED

Brown, Eugene, Skougstad, M. W., and Fishman, M. J., 1970, Methods for collection and analysis of water samples for dissolved minerals and gases: U.S. Geol. Survey Techniques Water-Resources Inv., book 5, chap. A1, 160 p.

Ellis, M. M., 1937, Detection and measurement of stream pollution: Bur. Fisheries Bull. 48, p. 365–437.

Hargrave, B. T., 1972, Aerobic decomposition of sediment and detritus as a function of particle surface area and organic content. Limnology and Oceanography, v. 17, no. 4, p. 583–596.

Hynes, H. B. N., 1970, The ecology of running waters. Univ. Toronto Press, 555 p.

McConnell, W. J., and Sigler, W. F., 1959, Chlorophyll and productivity in a mountain river: Limnology and Oceanography, v. 4, no. 3 p. 335–351.

Nauman, J. W., and Kernodle, D. R., 1973, Field water-quality information along the trans-Alaska pipeline corridor, September 1970 through September 1972: U.S. Geol. Survey basic-data rept., 22 p.

Odum, E. P., 1959, Fundamentals of ecology: Philadelphia, Pa., W. B. Saunders Company, 274 p.

Oviatt, C. A., Gall, A. L., and Nixon, S. W., 1972, Environmental effects of Atlantic menhaden on surrounding water: Chesapeake Science, v. 13, no. 14, p. 321–322.

Peterson, D. A., 1972, Barometric pressure and its effect on spawning activities of Rainbow trout: The Progressive Fish-Culturist, v. 34, no. 2, p. 110–112.

U.S. Environmental Data Service, 1972, Climatological data, Alaska: U.S. Environmental Data Service, Tech. Memo., v. 58, no. 7, p. 126.

Waters, T. F., 1962, Diurnal periodicity in drift of stream invertebrates: Ecology, v. 43, no. 2, p. 316–320.

Wright, J. C., and Mills, I. K., 1967, Productivity studies on the Madison River, Yellowstone National Park: Limnology and Oceanography, v. 12, no. 4, p. 568–577.

Jour. Research U.S. Geol. Survey
Vol. 3, No. 1, Jan.–Feb. 1975, p. 107–112

COMBINING ESTIMATES OF LOW-FLOW CHARACTERISTICS OF STREAMS IN MASSACHUSETTS AND RHODE ISLAND

By GARY D. TASKER, Boston, Mass.

Prepared in cooperation with the Massachusetts Water Resources Commission

Abstract.—The number of base-flow measurements needed to meet specified accuracy goals for estimating low-flow characteristics at ungaged sites can be reduced by combining an estimate based on a regression of base-flow measurements on discharges from a nearby continuous long-term gaging station with an estimate based on a regional relationship developed from regressing the low-flow characteristics on basin characteristics. The estimates should be combined by weighting each inversely with its variance from the true value. Empirically estimated values of variance of the estimated 7-day, 10-year low flow from its true value indicate that more than six or eight base-flow measurements add little to the confidence with which such an estimate is made.

Hydrologists often are called upon to furnish low-flow characteristics of streams. In Massachusetts the characteristic most often requested is the annual minimum 7-d mean flow at the 10-yr recurrence interval (7-d, 10-yr low flow), which is a legal index for pollution control. Usually the characteristics are required at sites where no discharge records are available. Therefore, estimates must be based on regional relationships or on discharge data collected during a restricted period.

Johnson (1970) estimated low-flow characteristics from basin characteristics in central New England by multiple-regression analysis. Riggs (1965) suggested that low-flow characteristics may be estimated by regression of logarithms of base-flow measurements on logarithms of base flow recorded at a nearby gaging station. Values of low-flow characteristics estimated by these two methods can be combined to give a better estimate than either individual estimate. If the best estimate is considered to be the one which gives the minimum variance from the true value, then the estimate based on regression of basin characteristics, Q_r, and the estimate based on regression of base flows, Q_b, should be averaged according to the formula

$$q = \frac{q_r + (S_r^2/S_b^2)q_b}{1+(S_r^2/S_b^2)}, \qquad (1)$$

where q is the logarithm of the estimated low-flow characteristic,
q_r is $\log Q_r$,
q_b is $\log Q_b$, and
S_b^2 and S_r^2 are the variances, in square log units, of the estimates from the true value of the low-flow characteristics based on the regressions on base flows and basin characteristics, respectively.

In order to verify that equation 1 minimizes the variance and produces a better estimate of the low-flow characteristic than q_r or q_b, consider the variance, S^2, of a simply weighted average of two values,

$$S^2 = \mathrm{E}\left[\left(\frac{q_r + c\cdot q_b}{1+c}\right) - q_o\right]^2,$$

where c is a weighting constant, E is the mathematical expectation operator, and q_r and q_b are independent, unbiased estimates of q_o. Expanding the expression yields

$$S^2 = \mathrm{E}\left[\frac{(q_r-q_o)^2 + 2c(q_r-q_o)(q_b-q_o) + c^2(q_b-q_o)^2}{(1+c)^2}\right] \qquad (2)$$

Because q_r and q_b are independent, unbiased estimates of q_o, $\mathrm{E}[(q_r-q_o)(q_b-q_o)]=0$, and equation 2 reduces to

$$S^2 = \frac{\mathrm{E}[(q_r-q_o)^2] + c^2\,\mathrm{E}[(q_b-q_o)^2]}{(1+c)^2}$$

If S^2 is a minimum, then

$$\frac{d}{dc}\left[\frac{\mathrm{E}[(q_r-q_o)^2] + c^2\,\mathrm{E}[(q_b-q_o)^2]}{(1+c)^2}\right] = 0. \qquad (3)$$

Solving equation 3 for c, $c = \frac{\mathrm{E}(q_r-q_o)^2}{\mathrm{E}(q_b-q_o)^2}$. Recognizing that the expectation of $(q_r-q_o)^2$ is S_r^2 and the expectation of $(q_b-q_o)^2$ is S_b^2 leads to $c = S_r^2/S_b^2$. Also, if S^2 is a minimum, then the second derivative at $c = S_r^2/S_b^2$ must be positive, as follows:

$$\frac{d^2}{dc^2}\left(\frac{S_r^2+c^2 S_b^2}{(1+c)^2}\right)\Bigg|_{c=\frac{S_r^2}{S_b^2}}=\frac{2S_b^2+2S_r^2}{[1+(S_r^2/S_b^2)]^4}>0$$

Therefore, the minimum S^2 occurs with $c=S_r^2/S_b^2$.

If equation 1 produces a better estimate of the true value than either q_r or q_b, then

$$S^2 \leqq S_r^2 \text{ and } S^2 \leqq S_b^2. \qquad (4)$$

This is shown to be true by the following:

$$S^2=\frac{S_r^2+\left(\frac{S_r^2}{S_b^2}\right)^2 S_b^2}{\left[1+\left(\frac{S_r^2}{S_b^2}\right)\right]^2},$$

which reduces to

$$S^2=\left(\frac{S_b^2}{S_r^2+S_b^2}\right)S_r^2=\left(\frac{S_r^2}{S_r^2+S_b^2}\right)S_b^2. \qquad (4a)$$

Because $\left(\frac{S_b^2}{S_r^2+S_b^2}\right)\leqq 1$ and $\left(\frac{S_r^2}{S_r^2+S_b^2}\right)\leqq 1$, inequality 4 is always true.

It should be noted that only when S_r and S_b are about the same magnitude is q a substantially better estimate than q_b and q_r. This is apparent from equation 4a. As S_r becomes large relative to S_b, the value of S approaches S_b (and vice versa). For example, if $S_b=S_r=0.1$, then $S=0.0707$; but if $S_r=1$ and $S_b=0.1$, then $S=0.0995$, which is less than S_b but not much less.

The above procedures assume that the population values of the variances are known. In fact, estimates of the variances, $\hat{S}_b^2$ and $\hat{S}_r^2$, must be used, and the minimum property is no longer guaranteed (E. J. Gilroy, written commun., 1973). However, using the weighting formula (eq 1) with $\hat{S}_r^2$ and $\hat{S}_b^2$ will be shown to reduce significantly the average variance of prediction of the 7-d, 10-yr low flow for nine sites in Massachusetts and Rhode Island.

ESTIMATING S_r^2

Hardison (1971, p. C229, eq 5) presented an equation for the variance of a prediction made at an ungaged site from a multiple-regression equation. In different notation, this equation becomes

$$\hat{S}_r^2=S_e^2[1+(1/N)+(1/N)\sum_{i=1}^{m}\sum_{j=1}^{m}C_{ij}(X_i-\bar{X}_i)(X_j-\bar{X}_j)]-V_T(1-2\rho) \qquad (5)$$

in which S_e is the standard error of estimate of the regression,

N is the number of stations used in the regression,

C_{ij} is the (i,j)th element of the inverse of the variance-covariance matrix of the independent variables,

$(X_i-\bar{X}_i)$ is the departure of independent variable X_i from its mean,

m is the number of variables in the regression,

V_T is the average time-sampling error at the stations used in the regression, and

ρ is the average interstation correlation coefficient, as defined by Matalas and Gilroy (1968).

For the computation of $\hat{S}_r^2$ and the empirically estimated value of $\hat{S}_b^2$ described in the next section, the low-flow characteristics derived from long-term discharge records are assumed to be the true value; that is, $V_T=0$. This assumption makes the calculations more convenient and may be partly justified because it is the relative value of $\hat{S}_r^2$ and $\hat{S}_b^2$ which is of interest rather than a precise estimate of either parameter. Therefore, the last term on the right side of equation 5 may be neglected in this analysis.

For example, Johnson (1970, p. A-11) estimates the 7-d, 10-yr flow, $M_{7,10}$, by the multiple-regression equation

$$M_{7,10}=0.00103\,A^{1.41}\,P^{1.36}\,T^{-0.47}$$

in which A is the drainage area, in square miles (1 mi^2 =2.59 km^2),

P is the mean annual precipitation reduced by 30, in inches (1 in.=2.54 cm),

T is the mean minimum January temperature plus one, in degrees Fahrenheit (°F—32° ×5/9=°C).

Therefore, the variance of prediction at a site will be

$$S_r=\frac{S_e}{N}(N+1+c_{AA}(X_A-\bar{X}_A)^2+c_{PP}(X_P-\bar{X}_P)^2+c_{TT}(X_T-\bar{X}_T)^2+2c_{AP}(X_A-\bar{X}_A)(X_P-\bar{X}_P)+2c_{AT}(X_A-\bar{X}_A)(X_T-\bar{X}_T)+2c_{PT}(X_P-\bar{X}_P)(X_T-\bar{X}_T), \qquad (6)$$

in square log units (base 10); where X_A, X_P, and X_T are the logs (base 10) of A, P, and T, respectively, at the site. Substituting into equation 6 the values obtained from the regression analysis, S_r^2 for the 7-d, 10-yr low flow at an ungaged site in central New England is given by

$$\hat{S}_r^2=0.1301+0.0098(X_A-1.9763)^2+0.1769(X_P-1.1530)^2+0.0524(X_T-1.0378)^2-0.0134(X_A-1.9763)(X_P-1.1530)+0.0136(X_A-1.9763)(X_T-1.0378)-0.0430(X_P-1.153)(X_T-1.0378),$$ in square log units.

The values $\hat{S}_r^2$ for the 7-d, 10-yr low flow shown in table 1 (col. 8) are derived from this equation.

TABLE 1.—*List of long-term stations used in analysis, estimated 7-d, 10-yr low flows, and variance of estimate based on regression of basin characteristics*

[1 mi² = 2.59 km²; 1 ft³/s = 0 0283 m³/s]

Dependent station	Drainage area, in square miles	Number of years used for computing q_o	7-d, 10-yr low flow, in cubic feet per second: Q_o, computed from long-term record	Q_r, estimated from regression on basin characteristics	Estimated from 21 base-flow measurements using the control-point method	Estimated from 21 base-flow measurements using the least-squares method	S_r^2, variance of estimate based on regression of basin characteristics. Derived from equation 7, in square log units	Average variance of estimate based on three simulated base-flow measurements, in square log units	Index station
1	2	3	4	5	6	7	8	9	10
Parker River at Byfield, Mass	21.6	20	0.15	0.42	0.19	0.21	0.1348	0.0756	Ipswich River near Ipswich, Mass.
Ipswich River at Ipswich, Mass	124	35	1.84	7.0	.91	1.05	.1398	.1251	Parker River at Byfield, Mass.
Charles River at Charles River Village, Mass	184	29	10.8	13.0	17.6	18.9	.1364	.0710	Wading River near Norton, Mass.
Adamsville Brook at Adamsville, R.I.	7.91	25	.07	.09	.11	.10	.1425	.2061	Do.
Wading River near Norton, Mass	42.4	40	2.23	1.7	.91	1.14	.1339	.2604	Charles River at Charles River Village, Mass.
Quinsigamond River at North Grafton, Mass	25.5	27	.60	.74	.92	1.16	.1361	.1831	Do.
Pawcatuck River at Wood River Junction, R.I.	100	25	26.7	6.8	21.3	25.9	.1348	.0314	Adamsville Brook at Adamsville, Mass.
Moss Brook at Wendell Depot, Mass	12.3	49	.57	.39	.38	.50	.1371	.0903	West Branch Westfield River at Huntington, Mass.
West Branch Westfield River at Huntington, Mass.	93.7	30	5.09	9.2	6.10	6.05	.1315	.0468	Moss Brook at Wendell Depot, Mass.

ESTIMATING S_b^2 AND S^2

The value $\hat{S}_b^2$ is a function of the number of base-flow measurements and their correlation with long-term records of nearby gaging stations. Hardison and Moss (1972, p. 37) recommend an equation for computing the variance at an ungaged site, which can be used as an estimate of S_b^2. In this equation variance is a function of the number of base-flow measurements, of several statistical parameters related to regression of base flows, and of the frequency distribution of the low-flow characteristic at the index station. However, statistical parameters related to regression of base flows may be difficult to estimate for a small number (less than six) of independent base-flow measurements.

The value $\hat{S}_b^2$ also may be estimated empirically from data generated at sites where low-flow characteristics can be estimated from long-term discharge records. The values thus computed for several sites in a region can be averaged to form a regional value of $\hat{S}_b^2$ as a function of the number of independent base-flow measurements. Such a regional relation for the 7-d, 10-yr low flow in Massachusetts (fig. 1) is computed in the manner shown in the following sections.

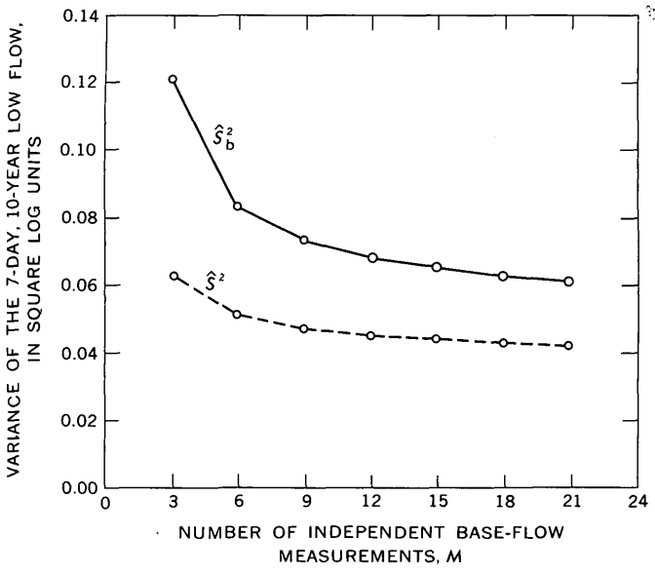

FIGURE 1.—Relation of variance of the estimated 7-d, 10-yr low flow to the number of independent base-flow measurements used to make the estimate.

A. Generation of data

Nine long-term gaging stations were selected to represent the streams in Massachusetts (table 1). At each station and for each year from 1950 to 1968, three observed discharges were selected from the record to simulate three base-flow measurements made by an experienced hydrologist. One simulated discharge measurement was selected randomly from the five lowest mean daily discharges of each of the months July, September, and November. Therefore, the three simulated discharge measurements for each year were equal to the mean daily discharges for days which were at least 30 d apart. As a partial check to ascertain that the discharge occurred during a base-flow period, the discharge on the day previous to the day selected must be greater than, or equal to, that of the selected day.

B. Base-flow regressions

A concurrent daily mean discharge at the index stations (table 1, col. 10) was extracted from the record for each discharge selected at the dependent station (table 1, col. 1) in step A. (The index station for each dependent station was selected from the list of dependent stations based on its proximity to the dependent station.) The logarithm of all discharges was determined and used for the remainder of the calculations. Hydrologists usually draw base-flow regression curves by hand, using the hypothesis that regression of the logarithms will normally plot in an approximately straight line for small discharges and will approach the equal-yield line for large discharges. However, because of the large number of regressions involved in calculating a regional average, regressions were computed by a digital computer using the control-point method.

The control-point method, generally accredited to C. H. Hardison of the U.S. Geological Survey, assumes that the base-flow regression plots on log-log paper as the straight line which best fits the data and which intersects the equal-yield line at a discharge that is 1.5 times the average for the index station. The control-point method is used to simulate the regression line as drawn by an experienced hydrologist and is assumed to introduce an insignificant error in the analysis. As partial justification for this assumption, consider the estimates of 7-d, 10-yr low flows for gaging stations shown in table 1. The estimates, based on 21 simulated base-flow measurements using the control-point method, are shown in column 6. An estimate using the same data points but fitted by the method of least-squares (col. 7) approaches the same value, which is significantly different from the value observed from the long-term record (col. 4). This would indicate that errors eliminated by refining the method for drawing the regression line may be relatively small when compared to the total error of the estimate based on a regression of base flows.

C. Determining S_b^2 and S^2

Knowledge of the 7-d, 10-yr low flow at the index station and the relation defined by the control-point method allow estimates of the 7-d, 10-yr low flow, $q_b(i, j, k)$, for dependent station i (i=1, 2, ... 9) based on k (k=1, 2, ... 7) consecutive years of three base-flow measurements each year beginning with year j (j=1950, 1951, ... 1968). The value of $q_o(i)$ was determined from the long-term record by fitting the annual minimum 7-d mean flow to a log-Pearson type III frequency distribution.

The value of S_b^2 for $3k$ base-flow measurements was estimated by the equation:

$$\hat{S}_b^2(k) = \frac{1}{9(19-k+1)} \sum_{j=1950}^{1968-k+1} \sum_{i=1}^{9} [q_b(i, j, k) - q_o(i)]^2$$

and plotted as the solid line in figure 1.

Let $C(i) = \frac{S_r^2(i)}{S_b^2(k)}$, in which $S_r^2(i)$ is given in table 1, column 8. Thus, the estimate weighted according to equation 1 is:

$$q(i, j, k) = \frac{q_r(i) + C(i)\, q_b(i, j, k)}{1 + C(i)}$$

Hence, the value of S^2 for $3k$ base-flow measurements was estimated by the equation

$$\hat{S}^2(k)=\frac{1}{9(19-k+1)}\sum_{j=1950}^{1968-k+1}\sum_{i=1}^{9}[q(i,j,k)-q_o(i)]^2$$

and plotted as the dotted line in figure 1.

The values of S_b^2 and S^2 were also estimated by averaging with time only by the equations

$$\hat{S}_b^2(i,k)=\frac{1}{19-k+1}\sum_{j=1950}^{1968-k+1}[q_b(i,j,k)-q_o(i)]^2,$$

and $$\hat{S}^2(i,k)=\frac{1}{19-k+1}\sum_{j=1950}^{1968-k+1}[q(i,j,k)-q_o(i)]^2.$$

These values are plotted in figures 2 and 3, respectively. Examination of figures 1, 2, and 3 indicates that, although S^2 may be higher than S_b^2 for a specific site, the regional average S^2 is significantly less than the regional average S_b^2 or S_r^2. Computations in steps A, B, and C were greatly facilitated by computer programs developed by A. W. Burns of the U.S. Geological Survey.

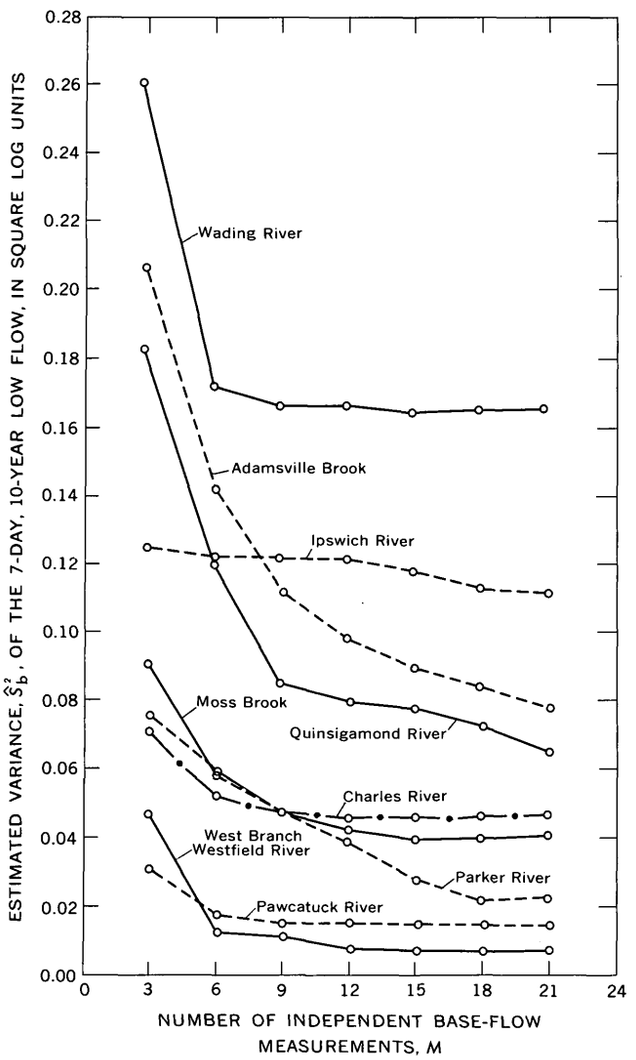

FIGURE 2.—Relation of the variance of an estimate (based on base-flow measurements) of 7-d, 10-yr low flow to the number of independent base-flow measurements used to make the estimate.

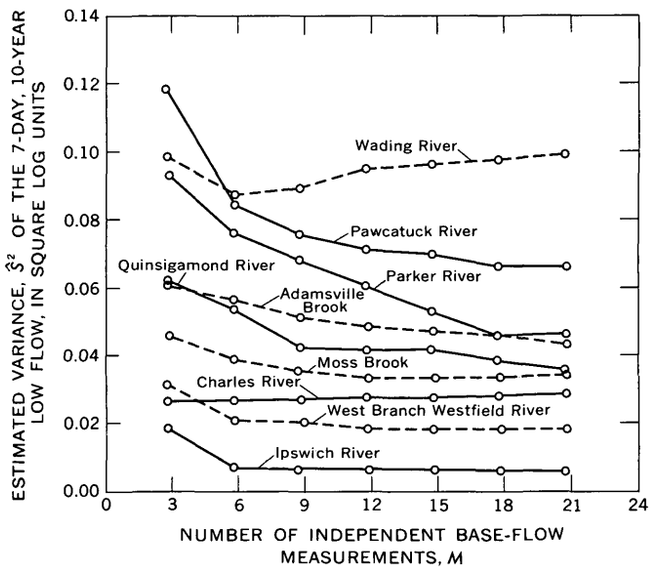

FIGURE 3.—Relation of the variance of an estimate (based on base-flow measurements and basin characteristics) of 7-d, 10-yr low flow to the number of independent base-flow measurements used to make the estimate.

CONCLUSIONS

The number of base-flow measurements needed to meet a specified accuracy for estimating low-flow characteristics can be significantly reduced by considering prior knowledge of the low-flow characteristics quantitatively. For example, suppose an accuracy goal equivalent to an average standard error of 0.25 log units (variance, 0.0625 square log units) is selected for a study area. According to figure 1, the average estimate in the area, based on three base-flow measurements combined with an estimate from the regression of basin characteristics, would be equivalent to the average estimate based on 18 measurements alone. Moreover, the dashed line in figure 1 indicates that, in Massachusetts, more than six or eight independent measurements of base flow at a site adds little to the confidence with which the estimate is made. Because of the small sample size, the methods should be tested further to provide more definitive results.

REFERENCES CITED

Hardison, C. H., 1971, Prediction error of regression estimates of streamflow characteristics at ungaged sites, *in* Geological Survey research 1971: U.S. Geol. Survey Prof. Paper 750–C, p. C228–C236.

Hardison, C. H., and Moss, M. E., 1972, Accuracy of low-flow characteristics estimated by correlation of base-flow measurements, *with a section on* Outline of derivations by E. J. Gilroy: U.S. Geol. Survey Water-Supply Paper 1542–B, p. 35–55.

Johnson, C. G., 1970, A proposed streamflow data program for central New England: U.S. Geol. Survey open-file rept., 38 p.

Matalas, N. C., and Gilroy, E. J., 1968, Some comments on regionalization in hydrologic studies: Water Resources Research, v. 4, no. 6, p. 1361–1369.

Riggs, H. C., 1965, Estimating probability distributions of drought flows: Water and Sewage Works, v. 112, no. 5, p. 153–157.

Jour. Research U.S. Geol. Survey
Vol. 3, No. 1, Jan.–Feb. 1975, p. 113–121

ADJUSTMENT OF LOGARITHMIC FLOOD-FREQUENCY STATISTICS FOR GAGED CALIFORNIA STREAMS TO MINIMIZE THE TIME SAMPLING ERROR

By S. E. RANTZ and J. R. CRIPPEN, Menlo Park, Calif.

Abstract.—Methods for adjusting logarithmic flood-frequency statistics for gaged streams to minimize the time sampling error that is inherent in short records are discussed. Statistical procedures for adjusting the mean and standard deviation of a short-term array of annual peak discharges are already well established; two standard sets of equations for utilizing the additional information contained in longer records of peak discharge observed at nearby gaging stations are given. A standard method for adjusting the coefficient of skew does not exist, and consequently a special technique for estimating the long-term value of that statistic was developed for this study. Regional equations were developed that relate the logarithmic skew coefficient to logarithmic transformations of mean annual basinwide precipitation and mean annual peak discharge per square mile. The technique appears to be satisfactory for use in the greater part of California, where over large areas the peak discharge in any year is usually associated with a single widespread general storm—or with a series of such storms where snowmelt runoff is involved—rather than with localized precipitation events.

On the recommendation of the Water Resources Council, a Federal interagency group, most government agencies have adopted a uniform procedure for flood-frequency analysis at sites where records of annual peak discharge are available. The basic method recommended in the report by the Water Resources Council (1967) involves the fitting of a Pearson type III distribution to the logarithms of the array of annual peak discharges at a gaged site. The mechanics of the method require that the mean (M), standard deviation (S), and coefficient of skew (g) of the logarithms be computed, after which the computed values are used to calculate logarithms of the peak discharges corresponding to various recurrence intervals. The equation used in the latter computation is

$$Q_T = M + K_{gT} S, \qquad (1)$$

where Q_T is the logarithm of the peak discharge corresponding to a recurrence interval of T years, and

K_{gT} is a characteristic of the Pearson type III distribution. For the purpose of this paper it may be defined as a coefficient corresponding to a recurrence interval of T years and a coefficient of skew equal to g. A table of values of K_{gT} is given by Harter (1969).

The discharges corresponding to values of Q_T, as computed by equation 1, are commonly correlated with various basin and climatic parameters to obtain regional relations for use in deriving flood-frequency curves for ungaged basins. This study, however, is concerned only with the elements involved in computing Q_T for streamgaging sites.

The record of annual peak discharges at a site is only a small sample of the parent population of annual peak discharges at that site, and therefore the distribution of recorded peak flows may not be representative of the distribution of the parent population. Consequently the three computed logarithmic statistics—mean, standard deviation, and coefficient of skew—are only estimates of the three statistical parameters of the parent population. It follows that those estimates are subject to a time sampling error whose magnitude is dependent on the degree of representativeness of the period of record. Generally speaking, the longer the period of years for which record is available the greater the likelihood of computing reliable estimates of the statistical parameters of the population, and the greater the likelihood of obtaining a reliable flood-frequency relation for the study site.

The fact is well documented that the use of differing periods of years extracted from the long-term record of annual peak discharge at a gaging station will result in differing flood-frequency relations for the station. It is obvious, for example, that a flood-frequency relation based on a short record that includes several years of intense flood activity will give greater discharges than one based on a short record that includes no years that had intense floods. Almost 40 years ago, in a report by Jarvis and others (1936), several of the authors discussed the effect of varying the period of record used for analysis. More recently, Victorov (1971) demonstrated large changes in the computed values of both the logarithmic coefficient of

skew and the discharge corresponding to various recurrence intervals when he divided the 68-yr record of annual peak discharge for the Minnesota River at Mankato, Minn., into many periods of various lengths. The method of analysis used by Victorov is the one that is discussed in this paper; that is, fitting a log-Pearson type III distribution to an array of annual flood peaks. Results similar to those of Victorov, with respect to the effect of varying the period of record, were obtained in this study. Because the more reliable estimates of the statistical parameters—mean, standard deviation, and coefficient of skew—are usually obtained from the longer records, it is evident that the data collected at short-term stations should be augmented, wherever possible, by the data collected at appropriate long-term stations.

The purpose of this study, therefore, is to show how the statistics for a short-term array of annual peak-discharge data may be adjusted to reflect the additional information contained in longer records of peak discharge at nearby gaged sites. The statistical procedures for adjusting the mean and standard deviation are well established and will be discussed only briefly. The authors, however, know of no standard adjustment for the coefficient of skew, and a special technique for estimating the long-term value of that statistic was developed for this study. The technique appears to be satisfactory for use in the greater part of California, where over large areas the peak discharge in any year is usually associated with a single widespread general storm—or with a series of such storms where snowmelt runoff is involved—rather than with localized precipitation events.

The data used in this study are flood-peak arrays for 87 long-term gaging stations in the four regions of California shown on the map in figure 1. The long-term stations used were those whose peak discharges were not seriously affected by artificial regulation or diversion. The regional boundaries, which are those currently being used in a Statewide flood-frequency study, reflect physiographic and climatic variation in California, and few of the boundaries follow drainage divides. For example, the north coast and central coast regions include drainage basins on both the east and west slopes of the Coast Ranges, and similarly the south coast region includes basins that drain in either direction from the crests of the Transverse and Peninsular Ranges. The three-way division of coastal California—north, central, and south—which is made along drainage divides, reflects not only the systematic decrease in annual precipitation from north to south, but also the lack of homogeneity in storm precipitation throughout the coastal regions. The peak discharges in

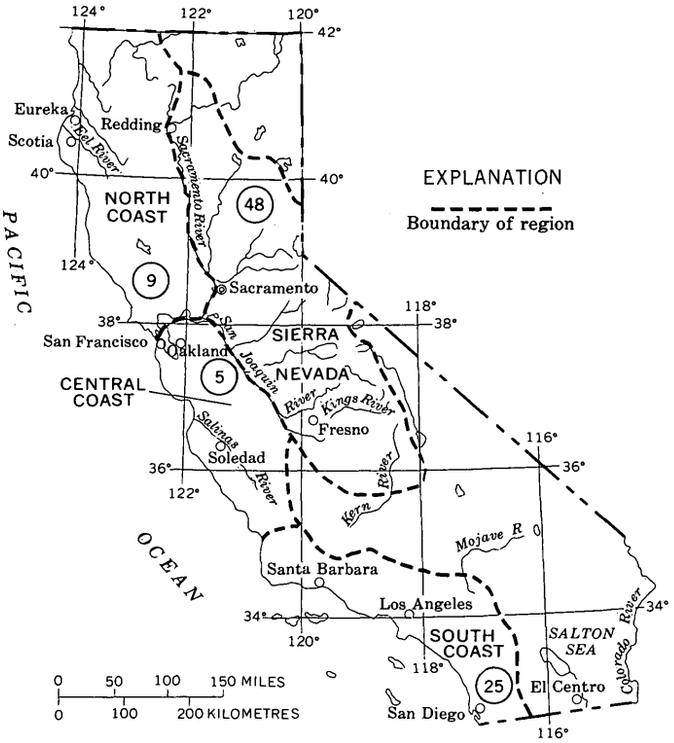

FIGURE 1.—Location of California regions used in this study. Circled figures indicate the number of long-term stations used in each region.

a given year in north coastal California usually result from a general storm that does not extend into south coastal California. Conversely, the peak discharges in a given year in south coastal California usually result from a general storm that does not extend into north coastal California. Annual peak discharges in central coastal California usually result from what might be referred to as "spillover" from either or both of the two storm systems. Snowmelt is seldom a significant factor in peak discharge in any of the coastal regions.

Snowmelt, however, is usually a factor in peak discharge in the Sierra Nevada region, and that region, as delineated in figure 1, includes basins on both sides of the Sierra crest. The Central Valley, or valley floor between the Coast Ranges and the Sierra Nevada, is a distinct hydrologic unit with respect to peak discharge, but records for Central Valley streams are too few and too short for the derivation of generalized relations concerning flood frequency in that valley area. Consequently the Central Valley was roughly bisected to provide a boundary between the coast regions and the Sierra Nevada region; the boundary used runs along the Sacramento and San Joaquin Rivers. There are also too few stations in the subhumid northeastern and arid southeastern parts of the State to permit generalizations concerning flood frequency in those areas.

The long-term stations used in this study were generally those that had 40 yr or more of peak-discharge record. Exceptions were made in the north and central coast regions, where records as short as 35 yr were used. The shorter records were included because only eight stations in the north coast region and two stations in the central coast region had 40 yr or more of record. Figure 1 shows the number of long-term stations available for use in each region.

Prior to analyzing the peak-discharge data used in this study, all discharge values were transformed to their logarithmic equivalents. Before the transformation, discharges were expressed in cubic feet per second (1 $ft^3/s=0.0283\ m^3/s$). Logarithmic values of drainage area size are also used in this study. Before transformation drainage area size was expressed in square miles (1 $mi^2=2.59\ km^2$). The values of mean annual basinwide precipitation used in this study were likewise transformed to logarithms. The original precipitation units were inches (1 in=25.4 mm).

ADJUSTMENT OF SHORT-TERM LOGARITHMIC VALUES OF THE MEAN

As mentioned earlier there are standard statistical procedures for adjusting the value of the mean of the logarithms of the array of annual peak discharges at a short-term station. A prerequisite of those procedures is the correlation of the logarithms of concurrent annual peak discharges for the short-term station and for a nearby long-term station. The procedures described in the following paragraphs give an adjusted value of the mean that reflects the additional information contained in the longer record for the nearby station.

Matalas-Jacobs procedure

A report by Matalas and Jacobs (1964) provides table 1 which gives critical minimum values of the correlation coefficient corresponding to various lengths of concurrent peak-discharge record for the short-term and nearby long-term stations. If, for a given number of years of concurrent record, the correlation coefficient exceeds the critical minimum value given in table 1 of their report, then the value of the mean of the logarithms for the concurrent years at the short-term station may be adjusted by the use of equation 34 of the Matalas-Jacobs report. Their equation 34 is

$$\bar{y}=\bar{y}_1+\frac{N_2}{(N_1+N_2)}b(\bar{x}_2-\bar{x}_1), \qquad (2)$$

where $\bar{y}$ is the adjusted value of the mean of the logarithmic array for the short-term station,

$\bar{y}_1$ is the mean of the logarithmic array for the short-term station for the years of concurrent record at the two stations,

N_1 is the number of years of concurrent record for the two stations,

N_2 is the additional number of years of record for the long-term station (thus (N_1+N_2) is the total number of years of record for the long-term station),

b is the slope (y_1/x_1) of the regression line given by the correlation of concurrent logarithmic peak discharge for the two stations,

$\bar{x}_1$ is the mean of the logarithmic array for the long-term station for the years of concurrent record at the two stations, and

$\bar{x}_2$ is the mean of the logarithmic array for the long-term station for the additional years of record (N_2).

Corps of Engineers procedure

A report by the U.S. Army Corps of Engineers (1962) presents an equation 8 of somewhat different form for adjusting the value of the mean of the logarithms of the array of annual peak discharges for a short-term station. Equation 8 in the Corps of Engineers report is

$$M'_1=M_1+(M'_2-M_2)R\frac{S_1}{S_2}, \qquad (3)$$

where M'_1 is the adjusted value of the mean of the logarithmic array for the short-term station,

M_1 is the mean of the logarithmic array for the short-term station for the years of concurrent record at the short- and long-term stations,

M'_2 is the mean of the logarithmic array for the long-term station for the entire period of record at the long-term station,

M_2 is the mean of the logarithmic array for the long-term station for the years of concurrent record at the short- and long-term stations,

R is the coefficient of correlation for concurrent logarithmic peak discharges for the short- and long-term stations,

S_1 is the standard deviation of the logarithmic array for the short-term station for the years of concurrent record at the short- and long-term stations, and

S_2 is the standard deviation for the logarithmic array for the long-term station for the years of concurrent record at the short- and long-term stations.

A comparison of the Matalas-Jacobs equation 2 in this report and the Corps of Engineers equation 3 in this report follows:

1. The Matalas-Jacobs procedure specifies a critical minimum value of the correlation coefficient, below which no adjustment to the short-term mean is to be made; the Corps of Engineers equation includes the correlation coefficient, and for low values of that coefficient the computed adjustment to the short-term mean will be small.
2. The two equations themselves can be shown to be virtually equivalent despite the difference in the terms used.

ADJUSTMENT OF SHORT-TERM LOGARITHMIC VALUES OF THE STANDARD DEVIATION

Standard statistical procedures for adjusting the value of the standard deviation of the logarithms of the array of annual peak discharges at a short-term station are also available. Again, a prerequisite of those procedures is the correlation of the logarithms of concurrent annual peak discharges for the short-term station and for a nearby long-term station. The procedures described in the following paragraphs give an adjusted value of the standard deviation that reflects the additional information contained in the longer record for the nearby station.

Matalas-Jacobs procedure

The report by Matalas and Jacobs (1964) provides tables 2 and 3 which give critical minimum values of the correlation coefficient corresponding to various combinations of the length of concurrent peak-discharge record for the two stations and the additional length of record for the long-term station. If, for a given combination of years, the correlation coefficient falls below the value given in their table 2, no adjustment of the short-term standard deviation is to be made. If, for a given combination of years, the correlation coefficient falls between the values given in their tables 2 and 3, the value of the standard deviation of the logarithms for the concurrent years at the short-term station may be adjusted by the use of equation 35 of their report. That equation includes a term for noise. (The term for noise is the third term in the brackets in the equation that follows—it is the term that includes the symbols α and θ). If, for a given combination of years, the correlation coefficient exceeds the value given in their table 3, the adjustment to the standard deviation is again made by using equation 35 of their report, but the term for noise in that equation may be dropped ($\theta=0$).

Equation 35 of the Matalas-Jacobs report is

$$s^2_y=\frac{1}{(N_1+N_2-1)}\left[(N_1-1)s^2_{y_1}+(N_2-1)b^2s^2_{x_2}\right.$$
$$\left.+(N_2-1)\alpha^2\theta^2(1-r^2)s^2_{y_1}+\frac{N_1N_2}{(N_1+N_2)}b^2(\overline{x}_2-\overline{x}_1)^2\right], \quad (4)$$

where s_y is the adjusted value of the standard deviation of the logarithmic array for the short-term station,

N_1 is the number of years of concurrent record for the two stations,

N_2 is the additional number of years of record for the long-term station,

s_{y_1} is the standard deviation of the logarithmic array for the short-term station for the years of concurrent record at the two stations,

b is the slope of (y_1/x_1) of the regression line given by the correlation of concurrent logarithmic peak discharges for the two stations,

s_{x_2} is the standard deviation of the logarithmic array for the long-term station for the additional years of record (N_2),

α^2 is equal to $\dfrac{N_2(N_1-4)(N_1-1)}{(N_2-1)(N_1-3)(N_1-2)}$,

θ is equal to 0 if noise is not to be included,

θ is equal to 1 if noise is to be included,

r is the coefficient of correlation for concurrent logarithmic peak discharges for the two stations,

$\overline{x}_1$ is the mean of the logarithmic array for the long-term station for the years of concurrent record at the two stations, and

$\overline{x}_2$ is the mean of the logarithmic array for the long-term station for the additional years of record (N_2).

Corps of Engineers procedure

The report by the U.S. Army Corps of Engineers (1962) presents an equation 18, which is an approximate but simple equation for adjusting the value of the standard deviation of the logarithms of the array of annual peak discharges for a short-term station. Equation 18 in the Corps of Engineers report is

$$S'_1-S_1=(S'_2-S_2)R^2\frac{S_1}{S_2}, \quad (5)$$

where S'_1 is the adjusted value of the standard devia-

tion of the logarithmic array for the short-term station,

S_1 is the standard deviation of the logarithmic array for the short-term station for the years of concurrent record at the short- and long-term stations,

S'_2 is the standard deviation of the logarithmic array for the long-term station for the entire period of record at the long-term station,

S_2 is the standard deviation of the logarithmic array for the long-term station for the years of concurrent record at the short- and long-term stations, and

R is the coefficient of correlation for concurrent logarithmic peak discharges for the short- and long-term stations.

ADJUSTMENT OF SHORT-TERM LOGARITHMIC VALUES OF THE COEFFICIENT OF SKEW

The coefficient of skew is the least conservative of the three statistics—mean, standard deviation, and coefficient of skew—of the station array of the logarithms of annual peak discharges. Not only is there wide variation in the long-term values of the skew coefficient between nearby gaging stations, but values of the coefficient for any long-term station vary widely with the period of record used in their computation. As mentioned earlier there is no standard method for adjusting the short-term value of the coefficient of skew to obtain an estimate that is more likely to be representative of the long-term value of that statistic.

The wide range in values of the skew coefficient between stations is illustrated in table 1, which summarizes information on the distribution of skew values at the 87 long-term stations used in this study. In that tabulation and in subsequent discussion, the maximum value of the skew coefficient is the largest numerical value bearing a positive sign, and the minimum value is the largest numerical value bearing a negative sign. (Although the coefficient of skew of an array of peak discharges is always, or nearly always, positive when untransformed values of discharge are used, the coefficient of skew may be either positive or negative when the logarithms of the peak discharges are arrayed, as was done on this study.) For reasons to be explained later, table 1 not only summarizes the data for the four individual regions, but it also presents a combined summary for the north and central coast regions.

TABLE 1.—*Summary of the distribution of values of the coefficient of skew of the arrayed logarithms of annual peak discharge at 87 long-term stations in 4 California regions*

	North coast	Central coast	North coast plus Central coast	South coast	Sierra Nevada
Number of stations	9	5	14	25	48
Range in length of record ___years	35–60	35–66	35–66	40–57	40–60
Coefficient of skew for period of record (log units):					
Median	−0.195	−0.533	−0.359	−0.019	0.065
Mean	−.459	−.479	−.466	−.083	.107
Standard deviation	.599	.439	.529	.438	.629
Maximum	.189	.248	.248	.929	1.362
Minimum	−1.401	−.834	−1.401	−.899	−1.689

The variation of the logarithmic coefficient of skew with period of record is illustrated in table 2, which presents logarithmic values of the skew coefficient for the Eel River at Scotia computed from peak discharge records for various periods of years between 1911 and 1971. The Eel River is in the north coast region.

TABLE 2.—*Logarithmic coefficient of skew for Eel River at Scotia, computed from peak-discharge records for various periods of years between 1911 and 1971*

Period	Coefficient of skew of logarithms of annual peak discharges for indicated length of period, in years					
	10	20	30	40	50	60
1911–21 [1]	−0.224	----	----	----	----	----
1911–31 [1]	----	−0.190	----	----	----	----
1911–41 [1]	----	----	−0.130	----	----	----
1911–51 [1]	----	----	----	−0.131	----	----
1911–61 [1]	----	----	----	----	−0.131	----
1911–71 [1]	----	----	----	----	----	−0.048
1922–31	−0.362	----	----	----	----	----
1922–41	----	−0.069	----	----	----	----
1922–51	----	----	−0.105	----	----	----
1922–61	----	----	----	−0.098	----	----
1922–71	----	----	----	----	−0.023	----
1932–41	−0.047	----	----	----	----	----
1932–51	----	−0.089	----	----	----	----
1932–61	----	----	−0.149	----	----	----
1932–71	----	----	----	−0.055	----	----
1942–51	−0.084	----	----	----	----	----
1942–61	----	−0.182	----	----	----	----
1942–71	----	----	+0.003	----	----	----
1952–61	−0.541	----	----	----	----	----
1952–71	----	−0.061	----	----	----	----
1962–71	+0.987	----	----	----	----	----
Maximum	+0.987	−0.061	+0.003	−0.055	−0.023	−0.048
Minimum	−.541	−.190	−.149	−.131	−.131	−.048

[1] Period is an even multiple of 10 yr; no record available for 1916.

The consistency of the logarithmic skew values for various periods of years at numerous stations was next examined. It will be recalled that the 87 long-term stations for use in this study had been grouped in

regions that were homogeneous with respect to the occurrence of major storms. Of those 87 stations, 55 had peak-discharge record for the 40-yr period 1931–70. That was the longest common period practical for use, and those 55 stations were therefore selected for examination. The central coast region could not be treated as a separate entity because only one station in that region—Arroyo Seco near Soledad—had complete record for the base period 1931–70. The Arroyo Seco station is in the northern part of the region, and it was therefore grouped with the seven stations in the north coast region that met the criterion with respect to the 40-yr period of record. The south coast region had 20 stations with record for the period 1931–70, and the Sierra Nevada region had 27 stations in that category. The logarithmic coefficient of skew was computed for each of the 55 stations for the following 10 periods:

Years	*Periods*
40	1931–70.
30	1931–60 and 1941–70.
20	1931–50, 1941–60, and 1951–70.
10	1931–40, 1941–50, 1951–60, and 1961–70.

The three regions (north-central coast, south coast, and Sierra Nevada) were treated separately in the study that followed. For each of the three regional groups of stations, nine individual correlations were performed. In each correlation the 40-yr value of the skew coefficient was the dependent variable, and each of the remaining nine values of the skew coefficient was, in turn, the independent variable in a correlation. In almost all of the 27 correlations (9 correlations for each 3 regional groups of stations) the coefficient of correlation was found to be significant, and, as expected the coefficient of correlation increased with the length of record of the independent variable.

The results of the 27 correlations suggested that for periods of record shorter than 40 yr the coefficient of skew for a short-term station could be adjusted to provide an estimate of its value for the 40-yr period 1931–70. For those records of 40 yr or longer the value of the skew coefficient computed for the entire period of record would be accepted. However, after further consideration it was decided that that course of action was not satisfactory because the sensitivity of the coefficient of skew to the actual period used is so extreme that skew values cannot be interpolated or extrapolated to fit standard time periods. For example, if one had a short-term station record for the 16-yr period 1943–58, how would it be used with one of the nine correlations discussed earlier? The answer is that it could not be so used, and one would require a separate correlation equation for each period of years that a short-term station had been operated.

Furthermore, the effect of offsetting even a single year in a fairly long record can make a significant change in the value of the coefficient of skew. For example, for the Eel River at Scotia the logarithmic coefficient of skew for the 40-yr period 1932–71 is −0.055 (table 2); the logarithmic coefficient of skew for the 40-yr period 1931–70 is +0.035. There was doubt, therefore, as to the reliability of the coefficient of skew for a given station obtained from a record even as long as 40 yr. As a matter of fact, a recent paper by Wallis, Matalas, and Slack (1974) concludes, in effect, that the uncertainty of values of the skew coefficient is great, even when computed for periods as long as 90 yr. It follows then that the computation of that statistic for shorter periods can give values that are misleading. A more satisfactory method was therefore sought for estimating long-term skew values from short-term records.

The method for adjusting skew coefficients that was finally decided on was one in which values of the logarithmic skew coefficient were related to climatic and basin parameters. The values of the coefficient of skew to be used in the relation would be restricted to those for long-term stations in California; in other words, those for the 87 stations that are summarized in table 1. The following assumptions underlie the method chosen.

1. Despite the wide fluctuations of the coefficient of skew with period of record, values of the skew coefficient for a sample tend to converge on the population value of skew as the size of the sample increases. Therefore the entire length of record at a station will be used for computing the sample value of the skew coefficient, rather than some shorter period of record that is common to a group of stations.
2. Because of the variation of the coefficient of skew with the period of record used, estimates of the "true" station values of the skew coefficient, as determined from the entire periods of observed discharge, will be subject to considerable error, but the error will tend to be random.
3. Because of the randomness of the error in computed station values of the coefficient of skew, use of those skew coefficients as the dependent variable in a relation with hydrologic parameters will probably have no serious effect on the actual equation defining the relation, although the standard error of estimate of the relation will undoubtedly be high.
4. Despite a large standard error of estimate for the relation of coefficient of skew to climatic and basin parameters, values of the skew coefficient

computed from the relation will probably be more reliable than the individual station values used in deriving the relation because of the probable error in the individual station values.

Because of the small number of stations in the north and central coast regions, those two regions were combined into a single entity for relating station values of the skew coefficient to hydrologic parameters. The five stations in the central coast region that were available for use are all in the northern half of that region. Separate relations were derived for the combined north and central coast region, the south coast region, and the Sierra Nevada region.

With regard to the above-mentioned regional relations, it was hypothesized that the relation of the logarithmic coefficient of skew to hydrologic parameters would take the form

$$g=K+a\log(CP)\pm b\log(BP), \qquad (6)$$

where g is the coefficient of skew of the logarithms of annual peak discharge,

CP is a climatic parameter for gaged basins,

BP is a basin parameter for gaged basins, and

K, a, and b are constants.

It was expected that CP and BP would interact; that is, the effect of any particular value of BP would be dependent on the simultaneous value of CP, and therefore use of the logarithms of those parameters was desirable. By using logarithms the joint relation of CP and BP could be retained in an equation whose linear form permitted a simple least-squares solution.

The obvious choice for a climatic parameter was mean annual basinwide precipitation. Mean annual precipitation is an excellent index of the relative magnitude of storms of any frequency in a region because the bulk of the annual precipitation occurs there during several general storms each year and the same number of general storms occur at all stations in any given year. (As explained on page 114, that statement is not quite true for the central coast region.) Furthermore, it had become evident in the course of this study that the logarithmic skew coefficients tended to vary directly with value of mean annual basinwide precipitation as determined from an isohyetal map of California.

A basin parameter was sought that would integrate the effects of the many physical elements that influence peak discharge; in other words, a parameter was desired that would serve as an index of the efficiency of the basin in converting precipitation to peak discharge. Such an index is the mean annual peak discharge per square mile per inch of mean annual precipitation. Furthermore, it was noticed in the course of this study that, for a given value of mean annual precipitation, the logarithmic skew coefficients tended to vary inversely with mean annual peak discharge per square mile.

By substituting the selected climatic and basin parameters in equation 6 we have

$$g=K+a\log P-b\log[Q_m/DA/P], \qquad (7)$$

where P is mean annual basinwide precipitation, in inches,

Q_m is mean annual peak discharge, in cubic feet per second, and

DA is drainage area, in square miles.

If we expand equation 7 we have

$$g=K+a\log P-b(\log Q_m-\log DA-\log P),$$

or

$$g=K+(a+b)\log P-b(\log Q_m-\log DA). \qquad (8)$$

If we let constant c equal $(a+b)$ and let q_m represent $(\log Q_m-\log DA)$, equation 8 becomes

$$g=K+c\log P-bq_m. \qquad (9)$$

In the interest of expediency, q_m was computed for each gaging station by subtracting the logarithm of its drainage area from the previously determined mean of the logarithms of annual peak discharge. That is not precisely the same as subtracting the logarithm of the drainage area from the logarithm of the mean annual peak discharge, but q_m, when computed as described above, serves equally well as an index of basin efficiency and at the same time offers an opportunity for the use of an adjusted logarithmic mean when dealing with short-term records. (Adjustment of the logarithmic mean was discussed in an earlier section of this paper.)

Table 3 summarizes the station data for the several regions with respect to P and q_m. A similar summation of logarithmic skew values (g) was given in table 1.

Table 4 summarizes the results of the correlations for the several regions; the regression equations all have the predicted form. To give some perspective to the values of the standard error of estimate associated with the regressions in table 4, the tabulation below shows the standard errors of the coefficient of skew for an individual station for records of various lengths. (The shortest record used in this study was 35 yr; the mean length of record was 48 yr; the longest record was 66 yr.)

Number of years	*Standard error of coefficient of skew*
35	0.398
48	.343
66	.295

The poorest of the three correlations was that for the subhumid south coast region. That result was expected because of the lesser degree of climatologic homogeneity in the south coast region, it being almost axiomatic that climatologic homogeneity decreases as one progresses from a humid region (north coast) to a subhumid region (south coast).

TABLE 3.—*Summary of the distribution of values of mean annual precipitation* (P) *and logarithmic values of mean annual peak discharge per square mile* (q_m) *at 87 long-term stations in 4 California regions*

	North coast	Central coast	North coast plus central coast	South coast	Sierra Nevada
Number of stations	9	5	14	25	48
Range in length of record years	35–60	35–66	35–66	40–57	40–60
Mean annual precipitation (P) in inches:					
Median	52	34	46	26	42
Mean	55.7	32.8	47.5	25.7	43.0
Standard deviation	19.77	14.17	20.78	6.55	13.02
Maximum	101	48	101	35	63
Minimum	35	16	16	15	18
Mean of logarithms of annual peak discharge for period of record minus logarithm of drainage area (q_m):					
Median	1.559	1.443	1.530	1.290	1.160
Mean	1.615	1.344	1.518	1.158	1.158
Standard deviation	.340	.367	.362	.387	.325
Maximum	2.105	1.707	2.105	1.706	1.752
Minimum	1.066	.949	.949	.340	.454

TABLE 4.—*Summary of regional correlations for determining coefficient of skew*

Region	Number of stations used in correlation	Regression equation	Standard error of estimate (log units)	Coefficient of correlation
Combined north and central coast.	14	$g=-3.060+2.49(\log P)-0.976q_m$	0.446	[1]0.632
South coast	25	$g=-2.857+2.33(\log P)-0.417q_m$	.417	[2].408
Sierra Nevada.	48	$g=-4.113+3.27(\log P)-0.905q_m$	.527	[3].573

[1] Significant at 3-percent confidence level.
[2] Significant at 5-percent confidence level.
[3] Significant at 1-percent confidence level.

Note:
g=coefficient of skew of logarithms of annual peak discharge,
P=mean annual basinwide precipitation, in inches, and
q_m=mean of logarithms of annual peak discharge minus logarithm of drainage area.

In using the regional equations in table 4, the station values of q_m to be applied would be those based on adjusted values of the mean of the logarithmic annual peak discharges for the station. The adjustment of short-term mean, described earlier, involves the use of either equation 2 or equation 3.

The application of the equation given in table 4 for the combined north and central coast region requires some discussion. It will be recalled that the five central coast stations used in deriving that equation were all in the northern part of the central coast region. To compute the long-term coefficient of skew for any station in the central coast region, it is recommended that the skew coefficient be computed by use of the equations for both the combined north and central coast region and for the south coast region. Personal judgment should then be used in weighting the two computed values of the skew coefficient, giving consideration to the location of the basin with respect to the north and south boundaries of the central coast region.

SUMMARY

This report discusses methods for adjusting logarithmic flood-frequency statistics for gaged streams to minimize the time sampling error that is inherent in short records. The statistical procedures for adjusting the mean and standard deviation of a short-term logarithmic array of annual peak discharges are well established; the adjustments made by those procedures reflect the additional information contained in longer records of peak discharge observed at nearby sites. There is no standard method, however, for adjusting the short-term value of the coefficient of skew to obtain an estimate that is more likely to be representative of the long-term value of that statistic. Consequently, a special technique for estimating the long-term value of the skew coefficient was developed for this study. The technique appears to be satisfactory for use in the greater part of California, where over large areas the peak discharge in any year is usually associated with a single widespread general storm—or with a series of such storms where snowmelt runoff is involved—rather than with localized precipitation events. A brief summary of the methods for adjusting short-term values of the mean, standard deviation, and coefficient of skew follows.

Mean.—Correlate logarithms of annual peak discharges for the short-term station with concurrent values for a nearby long-term stations. Use the results of the correlation in equation 2 or equation 3 to obtain the adjusted logarithmic value of the mean. (The adjusted value of the mean is not only used directly in equation 1 to compute the discharge for various recurrence intervals, but it is also used as a factor in estimating the long-term coefficient of skew, as discussed below.)

Standard deviation.—Obtain the adjusted logarithmic value of the standard deviation by using, in equation 4 or equation 5, the results of the correlation of the logarithms of concurrent annual peak discharges for the short- and long-term stations.

Coefficient of skew.—Compute the logarithmic coefficient of skew by use of the regional equations in table 4. Those equations relate the logarithmic skew coefficient to logarithmic transformations of mean annual basinwide precipitation and mean annual peak discharge per square mile.

REFERENCES CITED

Harter, H. L., 1969, A new table of percentage points of the Pearson Type III distribution: Technometrics, v. 11, no. 1, p. 177–187.

Jarvis, C. S., and others, 1936, Floods in the United States—magnitude and frequency: U.S. Geol. Survey Water-Supply Paper 771, 497 p.

Matalas, N. C., and Jacobs, Barbara, 1964, A correlation procedure for augmenting hydrologic data: U.S. Geol. Survey Prof. Paper 434–E, 7 p.

U.S. Army Corps of Engineers, 1962, Adjustment of frequency statistics: Sacramento, Calif., U.S. Army Corps of Engineers 5, 4 p.

Victorov, Peter, 1971, Effect of period of record on flood prediction: Am. Soc. Civil Engineers, Hydraulics Div. Jour., v. 97, no. HY 11, p. 1853–1866.

Wallis, J. R., Matalas, N. C., and Slack, J. R., 1974, Just a moment!: Water Resources Research, v. 10, no. 2, p. 211–219.

Water Resources Council, 1967, A uniform technique for determining flood-flow frequencies: Washington, D.C., Hydrol. Comm. Bull. 15, 15 p.

Jour. Research U.S. Geol. Survey
Vol. 3, No. 1, Jan.–Feb. 1975, p. 123–126

PYRROLIDONE–A NEW SOLVENT FOR THE METHYLATION OF HUMIC ACID

By R. L. WERSHAW, D. J. PINCKNEY, and S. E. BOOKER, Denver, Colo.

Abstract.—In the past, humic acid has been methylated by suspending it in a solution of diazomethane in diethyl ether, and degrading the partly methylated humic acid to release those parts of the molecule that were methylated. Only small fragments of the molecule have been identified by this technique. In the procedure described here the humic acid is dissolved in 2-pyrrolidone and methylated by the addition of diazomethane in diethyl ether and ethanol to the solution. Because the humic acid is completely dissolved in the reaction medium, disaggregation of the humic acid particles takes place and much more complete methylation is obtained. The methylated products may be fractionated by countercurrent distribution and analyzed by mass spectrometry.

Several workers have attempted to methylate humic acids with the conventional methylating reagents (Kononova, 1966, Schnitzer and others, 1973). The most popular of these reagents is diazomethane which is particularly attractive because the only reaction products are the desired methyl esters and nitrogen. Typically the humic acid is suspended in a methanol and diethyl ether solution of diazomethane for the reaction (Riffaldi and Schnitzer, 1973). In general, however, very poor exposure of the reactants to each other will be obtained in a suspension, especially where one of the reactants (humic acid) forms aggregates in which the groups that are susceptible to methylation are the very ones that bond in the aggregation reactions (Wershaw and Pinckney, 1973a).

Schnitzer and Ortiz de Serra (1973) in their work on the degradation and methylation of humic acids obtained low yields of guaiacyl and syringl monomers; one biphenyl compound was also isolated but no larger molecules were identified. In order to elucidate the structure of humic acid, however, larger fragments of the molecules must be obtained. We reasoned that the only way to obtain methylation of all the sites on a humic acid molecule would be to dissolve the humic acid in the methylating solvent. In this way more complete methylation would be obtained because of increased exposure of the humic acid functional groups to the diazomethane. Extensive experimentation with a wide variety of different solvents resulted in our discovering that 2-pyrrolidone is exceptionally well suited as a solvent for the methylation of humic acids.

The presence of apparent monomeric humic acid particles in 2-pyrrolidone has been detected by small angle X-ray scattering measurements where we found particles as small as any we have seen in water solutions (Wershaw and Pinckney, 1973a, b). In addition to the monomeric species, larger particles were also detected. The monomers should provide better exposure of the acid groups to methylation than the aggregates.

An equilibrium apparently exists between the humic acid monomers and the aggregates. If the methylated molecules do not participate in the aggregation reaction, then (1) as the monomers react, they will cease to participate in the reaction, (2) the equilibrium will be shifted in favor of the production of more monomers, and (3) all the material will react after a period of time.

Preliminary studies have been conducted on the fractionation of the methylated humic acids by countercurrent distribution (King and Craig, 1962) and on the analysis of fractions obtained by mass spectrometry. The results of this work which should provide new insight into the chemical structure of humic acids will be reported later.

Acknowledgments.—The authors wish to acknowledge the many useful discussions they had with Mr. J. P. Copes and Dr. E. M. Smolin of the GAF Corp., and Dr. J. S. Meek of the University of Colorado.

EXPERIMENTAL PROCEDURE

The sodium humate which was obtained by extracting soil with 0.1 *N* NaOH was fractionated by column chromatography on Sephadex columns as described previously (Wershaw and Pinckney, 1973a). To prepare the humic acid fractions used in this work, hydrochloric acid was added to the sodium humate fractions. After precipitation the suspensions were centrifuged and the supernatant liquid discarded. The precipitates were washed with water and recentrifuged; the humic

acids were then air dried. Solutions of approximately 1 percent (w/v) of the humic acid fractions were prepared in 2-pyrrolidone (GAF 2-pyrol); normally, gentle heating was necessary to completely dissolve the sample. The humic acids in solution were then methylated with a solution of ether and ethanol generated from N-methyl-N-nitroso-*p*-toluenesulfonamide (Aldrich Diazold). A solution of 2 g of Diazold dissolved in 20 ml of anhydrous diethyl ether was intermittently added as needed to a solution of 0.5 g of KOH in 0.8 ml of water and 2.5 ml of ethanol. (See fig. 1 for diagram of apparatus.) The generation flask was heated to about 50°C and the diazomethane in the ether and ethanol solution was distilled and allowed to run into the 2-pyrrolidone solution which was stirred with a Teflon-covered magnetic stirring bar. This was continued until nitrogen generation ceased (generally about 45 min).

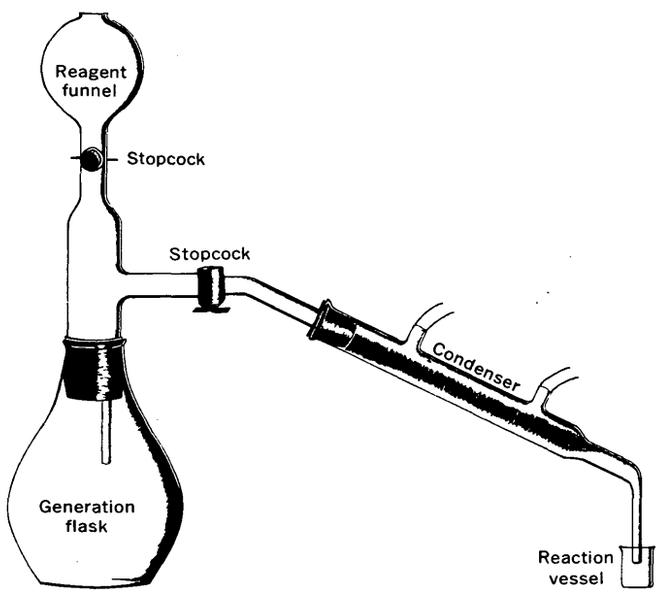

FIGURE 1.—Methylation apparatus.

After methylation, a sufficient amount of 2-butanol saturated with water was added to the reaction mixture to yield a 3-percent solution with respect to the 2-pyrrolidone. Approximately 75 ml of the 2-butanol solution was repetitively extracted in a 250-ml separatory funnel with an equal volume of 0.1 *N* NaCl solution in water which had been previously saturated with 2-butanol. The funnel was gently agitated for approximately 5 s and the solvent mixture was then allowed to separate into two phases; the water layer was drawn off and discarded, and a fresh aliquot of 0.1 *N* NaCl solution was added to the funnel. This procedure was repeated until 2-pyrrolidone could no longer be detected in the 2-butanol phase (normally 10–15 extractions).

Analyses for 2-pyrrolidone were made using a modification of Bergmann's method (1952). In this procedure, 1 ml of 2 *N* hydroxylamine hydrochloride, 1 ml of 3.5 *N* NaOH, and 1 ml of sample were mixed and heated in a boiling water bath for 15 min. The solution was rapidly cooled and 1 ml of 3.5 *N* HCl and 1 ml of 0.15 *M* $FeCl_3$ were added. The presence of 2-pyrrolidone was indicated by the purple color which developed immediately and was measured at 500 nm on a Cary Model 118 spectrophotometer, or was estimated visually.

The methylated humic acid was recovered from the 2-butanol by evaporation in a boiling water bath or flash evaporator. In some experiments the dried product was only partly soluble in the benzene and methanol solvent mixture and in others it was completely soluble. The part that was not soluble in benzene and methanol was redissolved in 2-pyrrolidone and remethylated. After the second methylation the entire sample was generally soluble in a 1:1 mixture of benzene and methanol.

DISCUSSION OF RESULTS

The success that we have attained in achieving methylation of the humic acid fraction and complete solution in organic solvents appears to be due to the stepwise breaking of both intermolecular and intramolecular weak bonds (for example, hydrogen bonds) leading to disaggregation and unfolding of the molecules. This process apparently begins with the initial fractionation of the crude sodium humate sample by Sephadex gel-permeation chromatography (see Wershaw and Pinckney 1973a, b) and continues through the methylation reaction, solution of part of the sample in benzene and methanol mixture, the final methylation, and the subsequent solution in benzene and methanol mixture.

The rate of methylation of the acid and phenol groups of humic acid will be dependent on the amount of steric hindrance present in the molecules. This steric hindrance may be of two types: (1) that due to the presence of bulky groups in the molecules which block the approach of the methylating reagent to the hydroxyl or carboxyl group and (2) that due to aggregation of molecules. Both types of hindrance probably occur during the methylation of humic acids, although at the present time our results only suggest that aggregation causes a reduction in methylation rate.

The rate of methylation taking place in systems containing diazomethane may be readily monitored by the rate of nitrogen evolution in the system. We have tried

to methylate both fractionated and unfractionated humic acids. Only fractionated materials gave rapid evolution of nitrogen. In fact, in some of the unfractionated samples practically no nitrogen evolution was observed. The absence of nitrogen production in the unfractionated humic acids is probably due to steric hindrance of the reactive groups. As we have shown previously (Wershaw and Pinckney 1973a, b) our fractionation procedure causes partial disaggregation of the humic acid particles with the separation of chemically different molecules, so that phenolic hydroxyl and carboxyl fractional groups which, in the aggregated state, participated in intermolecular and intramolecular hydrogen bonding will be exposed to the diazomethane molecules.

In addition to the disaggregation of chemically dissimilar molecules which takes place during fractionation of humic acid salts on Sephadex, disassociation of the particles of a humic acid fraction will also occur in solution. We have shown (Wershaw and Pinckney, 1973b) that the degree of association of some sodium humate fractions in water solutions is a function of pH. It appears from our data that, in these solutions, monomers are in equilibrium with a range of different-size aggregates.

Some preliminary conclusions about the reasons for the unique ability of pyrrolidone to dissolve humic acid may be reached by considering what is known about the physical and chemical properties of humic acid and pyrrolidone. Konova (1966), Felbeck (1965, 1971), Scheffer and Ulrich (1960), Steelink (1963) and Flaig (1970) have reviewed the literature on the structural chemistry of humic acids. It is generally agreed that humic acids contain phenolic, quinonic, polycarboxylic, aromatic acid, fused ring aromatic, alcoholic, amino acid, peptide, heterocyclic, and aliphatic groups. It appears that in most humic acids the aromatic groups dominate (Jackson and others 1972). Practically nothing is known of the detailed structure of humic acid; however, small-angle X-ray scattering studies have shown that most of the humic acid fractions consist of aggregates which are composed of molecules with molecular weights of a few thousand (Wershaw and Pinckney, 1973b).

In solvent-solute systems three types of association can take place: (1) bonding between solute molecules, (2) bonding between solvent molecules, and (3) bonding between solvent and solute molecules. The relative strengths of these interactions determine the size of the solute aggregates in solution. The strength of interaction of a solvent with solute molecules is determined both by the size and shape of the solute and solvent molecules and by the functional groups on these molecules. The 2-pyrrolidone molecule has a very nearly planar conformation (Warshel and others, 1970) so that it is able to form stacked complexes with planar solutes. Charge-transfer complexing and hydrogen bonding may occur between the carbonyl and peptide groups of the lactam and other groups in the solute molecules.

Although very little work has been done on elucidation of the mechanism of solvent-solute interactions in systems where lactams are the solvent phase, several general conclusions may be reached from the available data, Randall, Smolin, and Copes (1973) have studied the formation of complexes of phenols and lactams. They have proposed that the lactams form plane-to-plane charge-transfer complexes with planar phenolic compounds, coupled with hydrogen bonding. Rothschild (1972) has made a very careful study of the binding of hydrogen donors by poly (1-vinyl-2-pyrrolidone) and its monomeric analog 1-ethyl-2-pyrrolidone. He found that binding takes place both at the carbonyl bond of the lactams and at the C-N bond, which results in a decrease in the conjugation of the peptide linkage and a loss of the partially double-bond character of the C-N bond. The monomer 1-ethyl-2-pyrrolidone forms a number of different lactam-water species; hydrogen-donor bonding by the polymer is weaker than by the monomer. Rothschild's studies were all done on compounds with tertiary nitrogen atoms; however, in 2-pyrrolidone a hydrogen atom is bonded to the nitrogen atom and, therefore, direct intermolecular and intramolecular hydrogen bonding can take place in the 2-pyrrolidone systems but will be absent in the tertiary nitrogen systems.

Many amides are good waterlike solvents whose relatively high dielectric constants (Paul, 1968) make them good solvents for ionic solutes The relatively high dielectric constant of 2-pyrrolidone (see table 1) promotes the ionization of humic acid. Although the delectric constant of N-methyl-2-pyrrolidone is some-

TABLE 1.—*Physical properties of 2-pyrrolidone and N-methyl-2-pyrrolidone*

	2-Pyrrolidone	N-methyl-2-pyrrolidone
Melting point °C	25.67	−24.4
Boiling point (at 1 atm) °C	245	202
Density	1.1068(26°C)	1.027(25°C)
Viscosity cP	12.75(26°C)	1.65(25°C)
Dipole moment [1]	3.76 D(30°C)	4.09 D
Dielectric constant	27.46(26°C)	32.2(25°C)
Index of refraction	1.4848(26°C)	1.469(25°C)

[1] 1 D (debye unit)$=10^{-18}$ statcoulomb-centimetre$=3.3\times10^{-30}$ coulomb-metre.

Note.—All data for 2-pyrrolidone except boiling point and dipole moment are from Blumenshine and Sears (1966). The boiling point is from the GAF Corp., Chemical Division (1972), and the dipole moment is from Lee and Kumler (1961). All the N-methyl-2-pyrrolidone data are from the GAF Corp., Chemical Division (1972).

what higher than that of 2-pyrrolidone, we found that it is a much poorer solvent for humic acid than 2-pyrrolidone. The slight basicity of 2-pyrrolidone (Huisgen and others, 1957) no doubt contributes somewhat to the increased solubility of humic acid, but probably a more important factor is the ability of 2-pyrrolidone to form complexes with phenolic and other aromatic groups and to act as both a proton donor and accepter in hydrogen bonding.

CONCLUSIONS

The procedure reported here renders an entire humic acid fraction soluble in organic solvents with a minimum of alteration to the skeletons of molecules. In this regard, this procedure is unique and should allow a new approach to be tried in the elucidation of the structure of humic acids.

REFERENCES CITED

Bergmann, Felix, 1952, Colorimetric determination of amides as hydroxamic acids: Anal. Chemistry, v. 24, p. 1367–1369.

Blumenshine, R. L., and Sears, P. G., 1966, Several properties of the 2-pyrrolidone–water system as functions of composition and temperature: Jour. Chem. and Eng. Data, v. 11, no. 2, p. 141–143.

Felbeck, G. T., Jr., 1965, Structural chemistry of soil humic substances: Advances in Agronomy, v. 17, p. 327–368.

——— 1971, Structural hypotheses of soil humic acids: Soil Sci., v. 111, p. 42–48.

Flaig, Wolfgang, 1970, Contribution à la connaissance de la constitution et de la synthèse des acides humiques, *in* Science du sol: Assoc. Française Étude Sol Bull 2, supp., p. 39–72.

GAF Corp., Chemical Division, 1972, *M*-pyrol, *N*-methyl-2-pyrrolidone handbook: New York, GAF Corp., 367 p.

Huisgen, Rolf, Brade, Heinz, Walz, Helmut and Glogger, Irmgard, 1957, Die Eigenschaften aliphatischer Lactame und die *cis-trans*-Isomerie der Säureamidgruppe: Chemische Ber., v. 90., p. 1437–1447.

Jackson, M. P., Swift, R. S., Posner, A. M., and Knox, J. R., 1972, Phenolic degradation of humic acid: Soil Sci., v. 114, p. 75–78.

King, T. P., and Craig, L. C., 1962, Countercurrent distribution, *in* Glick, David, ed., Methods of biochemical analysis: New York, Interscience Publishers, v. 10, p. 201–228.

Kononova, M. M., 1966, Soil organic matter, its nature, its role in soil formation and in soil fertility: London, Pergamon Press, 544 p.

Lee, C. M., and Kumler, W. D., 1961, The dipole moment and structure of five- and six-membered lactams: Am. Chem. Soc. Jour., v. 83, p. 4593–4596.

Paul, R. C., 1968, Amides as non-aqueous solvents, *in* Ebsworth, E. A. D., Maddock, A. E., Sharpe, A. G., eds., New pathways in inorganic chemistry: London, Cambridge Univ. Press, p. 233–261.

Randall, D. I., Smolin, E. M., and Copes, J. P., 1973, New complexes of phenols and lactams: Nature, v. 244, p. 369–370.

Riffaldi, R., and Schnitzer, Morris, 1973, Effects of 6N HCl hydrolysis on the analytical characteristics and chemical structure of humic acids: Soil Sci., v. 115, no. 5, p. 349–356.

Rothschild, W. G., 1972, Binding of hydrogen donors by peptide groups of lactams.—identity of the interaction sites: Am. Chem. Soc. Jour., v. 24, p. 8676–8683.

Scheffer, Fritz, and Ulrich, Bernhard, 1960, Morphologie, Biologie, Chemie und Dynamik des Humus, *in* Part 3, Humus und Humusdüngung *of* Lehrbuch der Agrikulturchemie und Bodenkunde: Stuttgart, Ferdinand Enke, 266 p.

Schnitzer, Morris, and Ortiz de Serra, M. I., 1973, The chemical degradation of a humic acid: Canadian Jour. Chemistry, v. 51, p. 1554–1566.

Schnitzer, Morris, Ortiz de Serra, M. L., and Ivarson, K. C., 1973, The chemistry of fungal humic acid-like polymers and of soil humic acids: Soil Sci. Soc. American Proc., v. 37, p. 229–236.

Steelink, Cornelius, 1963, What is humic acid? Jour. Chem. Education, v. 40, p. 379–384.

Warshel, A., Levitt, M., Lifson, S., 1970, Consistent force field for calculation of vibrational spectra and conformations of some amides and lactams rings: Jour. Molecular Spectroscopy v. 33, p. 84–99.

Wershaw, R. L., and Pinckney, D. J., 1973a, Determination of the association and dissociation of humic acid fractions by small angle X-ray scattering: U.S. Geol. Survey Jour. Research, v. 1, no. 6, p. 701–707.

——— 1973b, The fractionation of humic acids from natural water systems: U.S. Geol. Survey Jour. Research, v. 1, no. 3, p. 361–366.

☆ U.S. GOVERNMENT PRINTING OFFICE 1974: 585-404/3

RECENT PUBLICATIONS OF THE U.S. GEOLOGICAL SURVEY

(The following books may be ordered from the Superintendent of Documents, Government Printing Office, Washington, DC 20402, to whom remittances should be sent by check or money order. Give series number, title, stock number shown in parentheses in this list, and catalog number shown in brackets. Prices of Government publications are subject to change. Increases in costs make it necessary for the Superintendent of Documents to increase the selling prices of many publications offered. As it is not feasible for the Superintendent of Documents to correct the prices manually in all the publications stocked, the prices charged on your order may differ from the prices printed in the publications and in this list)

Professional Papers

352–J. Chemical weathering, soil development, and geochemical fractionation in a part of the White Mountains, Mono and Inyo Counties, Calif., by D. E. Marchand. 1974. p. 379–424. $1.35. (2401–02484) [I 19:16:352–J]

794. Large-magnitude Late Tertiary strike-slip faulting north of Lake Mead, Nev., by R. E. Anderson. 1973 (1974). 18 p.; plate in pocket. $1.65. (2401–02285) [I 19:16:794]

811. Geology of salars in northern Chile, by G. E. Stoertz and G. E. Ericksen. 1974. 65 p. $1.65. (2401–02455) [I 19:16:811]

828. Fuller's earth and other industrial mineral resources of the Meigs-Attapulgus-Quincy district, Georgia and Florida, by S. H. Patterson. 1974. 45 p.; plates in pocket. $2.40. (2401–02503) [I 19:16:828]

831–B. General geology of the Harold D. Roberts Tunnel, Colo., by C. S. Robinson, L. A. Warner, and E. E. Wahlstrom. 1974. p B1–B48; plate in pocket. $2.25. (2401–02469) [I 19:16:831–B]

Bulletins

1308. Geology and placer-gold deposits of the Jicarilla Mountains, Lincoln County. N. Mex., by Kenneth Segerstrom and G. E. Ryberg. 1974. 25 p.; plate in pocket. 45¢. (2401–02502) [I 19:3:1308]

1368–A. Surficial deposits of the Iliamna quadrangle, Alaska, by R. L. Detterman and B. L. Reed. 1973 (1974). p. A1–A64; plate in pocket. $2. (2401–02421) [I 19:3:1368–A]

1382–C. Argentian cryptomelane and bromargyrite in volcanic rocks near Silver Cliff, Colo., by F. A. Hildebrand and E. L. Mosier. 1974. 23 p. 40¢. (2401–02509) [I 19:3:1383–C]

Water-Supply Papers

1850–D. Floods of June 1965 in Arkansas River basin, Colorado, Kansas, and New Mexico, by R. J. Snipes and others. 1974. p. D1–D97; plates in pocket. $2.35. (2401–02483) [I 19:13:1850–D]

2001–D. Appraisal of operating efficiency of recharge basins on Long Island, N.Y., in 1969, by D. A. Aronson and G. E. Seaburn. 1974. p. D1–D22; plate in pocket. $1.45. (2401–02445) [I 19:13:2001–D]

2031. Influence of recharge basins on the hydrology of Nassau and Suffolk Counties, Long Island, N.Y., by G. E. Seaburn and D. A. Aronson. 1974. 66 p.; plate in pocket. $1.75. (2401–02492) [I 19:13:2031]

Techniques of Water-Resources Investigations

TWI 2–D1. Application of surface geophysics to ground-water investigations, Chapter D1, by A. A. R. Zohdy, G. P. Eaton, and D. R. Mabey. 1974. 116 p. $1.90. (2401–02543) [I 19:15/5:Bk. 2/chap. D1]

U.S. GOVERNMENT
PRINTING OFFICE
PUBLIC DOCUMENTS DEPARTMENT
WASHINGTON, D.C. 20402

OFFICIAL BUSINESS
PENALTY FOR PRIVATE USE $300

POSTAGE AND FEES PAID
U.S. GOVERNMENT
PRINTING OFFICE
375

U.S. MAIL